Supramolecular chemistry of some naphthoquinone derivatives

A Dissertation submitted to the
Indian Institute of Technology Guwahati as
partial fulfillment for the Degree of
Doctor of Philosophy in Chemistry

Submitted by

Bigyan Ranjan Jali

Department of Chemistry

Indian Institute of Technology Guwahati

May 2014

TH-1303_09612216

Dedicated to My Family
and
Friends….

TH-1303_09612216

TH-1303_09612216

Statement

I hereby declare that this thesis entitled "**Supramolecular chemistry of some naphthoquinone derivatives**" is the outcome of research work carried out by me under the supervision of Prof. Jubaraj B. Baruah, at the Department of Chemistry, Indian Institute of Technology Guwahati, India.

In keeping with the general practice of reporting scientific observations, due acknowledgement has been made whenever work described here has been based on the findings of other investigators.

IIT Guwahati
May, 2014

Bigyan Ranjan Jali

TH-1303_09612216

TH-1303_09612216

Certificate

This is to certify that Bigyan Ranjan Jali has been working under my supervision since August, 2009 as a regular registered Ph. D. student. I am forwarding his thesis entitled "**Supramolecular chemistry of some naphthoquinone derivatives**" being submitted for the Ph. D. (Science) Degree of this Institute.

I certify that he has fulfilled all the requirements according to the rules of this institute regarding the investigations embodied in his thesis and this work has not been submitted elsewhere for a degree.

IIT Guwahati
May, 2014

Prof. Jubaraj B. Baruah

TH-1303_09612216

TH-1303_09612216

Acknowledgements

This thesis might not have seen through its completion unless I had the support and encouragement of numerous people around me. Today, when I bring it to an end, I would like to express few words of appreciation to the people who actually made this thesis a reality and an unforgettable experience for me.

To begin with, I would like to thank my supervisor, Prof. Jubaraj B. Baruah. The enlightening experience of doing science under his guidance can hardly be described in words. The numerous discussions and interactions I had with him expanded my horizons to hitherto unknown frontiers of science and knowledge. I am indebt to this wonderful person for all that he has given me and above all for motivating me towards scientific research.

I would like to thank Prof. Nouri Neamati and Ms. Yuting Kuang of University of Michigan for their help in cytotoxicity data and discussion portion of this writing. I would like to take this opportuity to convey my sincere gratitude to Dr. Rupam Jyoti sarma Gauwahati University for his valuable contribution during the 2D-NMR measurements.I would like to take this opportuity to convey my sincere gratitude to Mr. Anil kumar Verma Department of Biotechnology, IIT Guwahati for his valuable contribution during docking analysis.

I would like to acknowledge my sincere gratitude to all my doctoral committee members for their insightful advices and valuable suggestions. I am also grateful to the entire faculty and staff in the Department of Chemistry, Indian Institute of Technology Guwahati for providing a wonderful work atmosphere throughout this period.

I would like to thank my lab mates Dr. W. Marjit Singh, Dr. Rupam sarma, Dr. Devendra Singh, Dr. Dipjyoti Kalita, Dr.Babulal Das, Bhaskar, Prithviraj, Jayant, Tapan, Nithi, Kripasankar, Arup, Sovam, Anvita, Ananta, Indra whom I had an opportunity to work with and other group members Narshima, Kishore, Kiran, Renjith, Laxman, Sidhick, Rajendra, Samir, Nibedita, Karuna, Richa, Hari, santosh, Nityananda, Kanhu, Saroj and Balaram for their timely help, support and for the wonderful time we shared during this period. No words can express my thankfulness for giving me their time and companionship, which made the time spent in the laboratory and outside pleasant and memorable. I would like to give my

TH-1303_09612216

special thanks to my lab senior Dr. Rupam Sarma and Dr. Marjit Singh for their support and valuable suggestions throughout my research career and also extend my thanks to Dr. Himashu Sekhar Jena and Dr. Subash Sahoo for their valuable suggestion throughout my research career.

This thesis wouldn't have seen the light of this day without the care and encouragement of my chemistry teachers Dr. Satyaban Jena, Dr. Prakash Mohanty, Dr. Prafulla Sahoo, Dr. Guru Charan Pradhan and Dr.Santosini Patra. I would like to furnish my sincere gratitude to these wonderful people of my life for their excellent teaching and constant motivation which made me reach this point.

Finally, I would like to thank my family for their understanding, encouragement, patience, unending support and blessings in my every endeavor without which my Ph.D. could not be completed. They are the main soul and inspiration for each and every step that I achieve in my life.

TH-1303_09612216

Preview

Quinones and their derivatives form self-assemblies which are guided by various weak interactions such O-H···O, C-H···O, C-H···π and O-H···π interactions. Strong directional hydrogen bonds are generally characteristics of quinoidal compounds to form linear chain, dimer and cyclic assemblies or host-guest complexes. Thus, quinone derivatives are useful to construct various supramolecular architectures. There is a necessity to systematically study and identify the role of weak interactions in various host-guest systems of quinone derivatives. The thesis entitled as "**Supramolecular chemistry of some naphthoquinone derivatives**" deals with the synthesis, characterization and supramolecular aspects of quinone derivatives. The structural aspects are investigated with objectives to understand their self-assembly processes. Apart from these, protein binding properties and anti-cancer activities of a series of naphthoquinone derivatives are presented in the last part of this thesis.

The contents of the thesis are divided into five chapters based on the results on the analysis of the experimental observations obtained during the research period are described below.

Chapter 1: Introduction

A general introduction to the quinone derivatives is brought forward in this chapter with their structural features and spectroscopic properties. The role of weak intermolecular interactions in the construction of supramolecular architecture of various quinone derivatives is presented. Importance of various quinone derivatives in the field of supramolecular chemistry, anion and cation sensing, coordination chemistry, biochemicals and medicinal chemistry is also described. Various applications related to optical properties and biological applications of quinone and thier derivatives are elaborated.

Chapter 2: Supramolecular chemistry of thiocarboxylic acid tethered 1,4-naphthoquinones

In this chapter the self-assemblies of 2-(1,4-dihydro-2-methyl-1,4-dioxonaphthalen-3-ylthio) benzoic acid (**2.1**), 2-(1,4-dihydro-2-hydroxy-1,4-dioxo-naphthalen-2,3-diylthio)benzoic

TH-1303_09612216

acid (**2.2**) and 2-(1,4-dihydro-2-methyl-1,4-dioxonaphthalen-3-ylthio)phenyl)acetic acid (**2.3**) leading to different polymorphs and solvate are discussed.

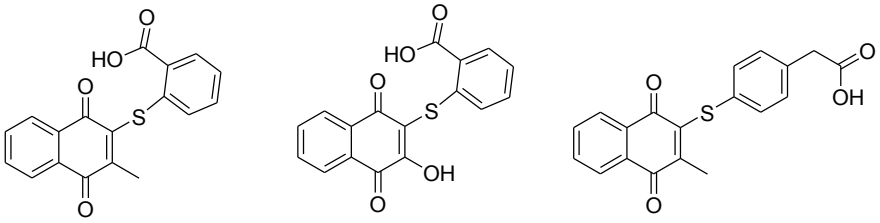

Figure 1: The thiocarboxylic acid tethered 1,4-naphthoquinones **2.1-2.3**.

when the compound **2.1** was crystallized from different solvents namely, tetrahydofuran/acetone (1:1 v/v) or methanol or chloroform three different types of crystals were obtained. The analysis of these crystals have shown them to have similar composition, however they belonged to different space groups.

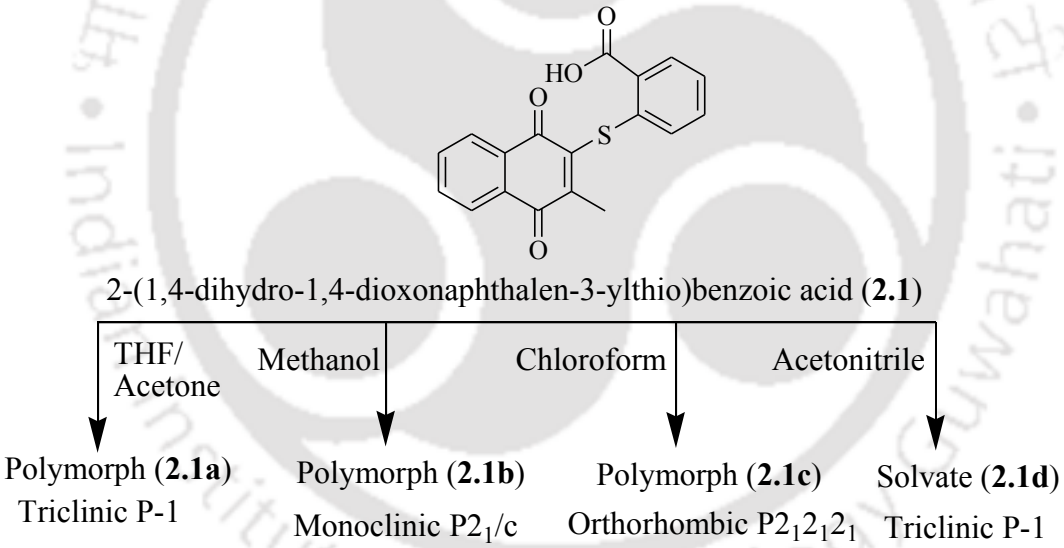

Scheme 1: Formation of different polymorphs and solvate of **2.1**.

The crystals obtained from tetrahydrofuran/acetone mixture belong triclinic space group P-1 is designated as polymorph **I** (**2.1a**), the crystal obtained from a solution of **2.1** in methanol belongs to space group monoclinic $P2_1/c$ this set of crystals are designated as polymorph **II** (**2.1b**); similarly the crystals obtained from solution of the chloroform belong orthorhombic space group $P2_12_12_1$ is designated as polymorph **III** (**2.1c**). On the other hand, the compound **2.1** forms 3: 1 acetonitrile solvate (solvate **IV**) when it was crystallize from acetonitrile. From the crystal structure of polymorph **I (2.1a)** and

TH-1303_09612216

polymorph **II** (**2.1b**), it was observed that the sulfur atom bearing 2-methyl-1,4-naphthoquinone groups are *trans* to each other across a $R_2^2(8)$ type of hydrogen bond motif (Figure 2a and 2b). Whereas, the polymorph **III (2.1c)** has two symmetry independent molecules (designated as X and Y-sets) in the crystallographic asymmetric unit. From the crystal structure, it is observed that sulfur atom bearing 2-methyl 1,4-naphthoquinone groups are *cis* to each other across $R_2^2(8)$ types of hydrogen bond motif as shown in figure 2c.

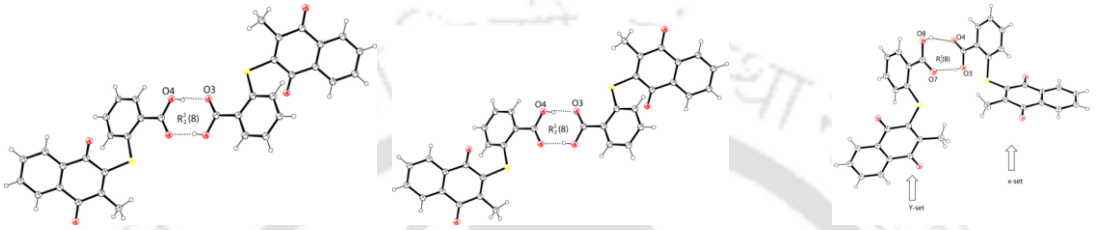

(a) (b) (c)

Figure 2: Dimeric self-assemblies of (a) Polymorph **I** (**2.1a**), (b) Polymorph **II** (**2.1b**) and (c) Polymorph **III** (**2.1c**).

The main distinctions between the three polymorphs arise in their dihedral angles and packing patterns. The packing diagram of polymorph **III** (Figure 3c) indicates that there are pair of molecules of one type of symmetry which is embraced by six molecules that have another type of symmetry (**2.1d**).

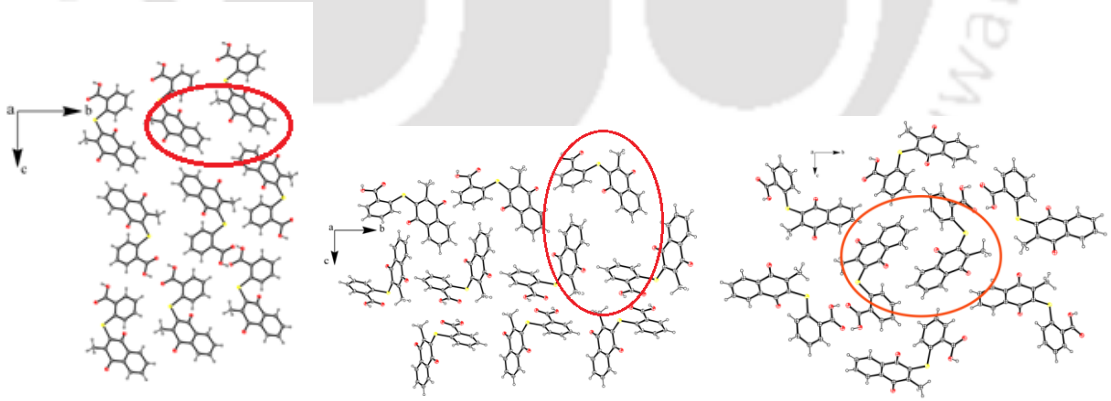

(a) (b) (c)

Figure 3: (a) Packing pattern of polymorph **I** (**2.1a**), (b) Polymorph **II** (**2.1b**) and (c) Polymorph **III** (**2.1c**).

In case of polymorph **I** (**2.1a**) 2-methyl-1,4-naphthoquinone parts are in a *head-head manner (*consider naphthoquinone moiety as head and thiocarboxylic acid part is tail*)*, on the other hand polymorph **II** (**2.1b**), 2-methyl-1,4-naphthoquinone parts are in *head-tail* arrangements. These arrangements make the lattice of these three polymorphs clearly

TH-1303_09612216

distinguishable. The structure of the acetonitrile solvate **IV** (**2.1d**) has three symmetry independent molecules (designated as X, Y and Z-set) in crystallographic asymmetric unit. Among three independent molecules, the two sets designated as X and Y-set of molecules are engaged in an $R^2_2(8)$ type of hydrogen bond motif whereas remaining set is designated as Z-set of molecules leads to formation of a cyclic hydrogen bonded assembly among themselves as shown in figure 4.

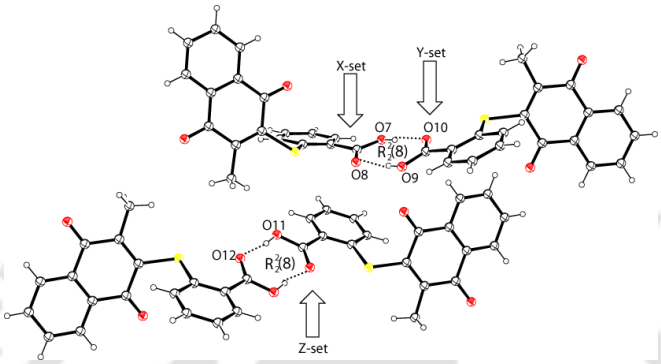

Figure 4: The self-assemblies of molecules in acetonitrile solvate.

But in case of compound **2.2** and **2.3** we were not able to get any polymorphs from different solvents. However, we were able to crystallize the DMF solvate of **2.2** and unsolvated from of **2.3** from methanol.

Chapter 3: Anion binding properties of 2-methyl-1,4-naphthoquinone functionalized imidazole derivatives

This chapter deals with synthesis, characterization and the anion recognition of imidazole tethered 2-methyl-1,4-naphthoquinone derivatives. The synthesis and characterization of imidazole tethered 2-methyl-1,4-naphthoquinone derivatives (**3.2-3.3**) and their anion recognition properties in solution as well as in the solid state are presented in this chapter.

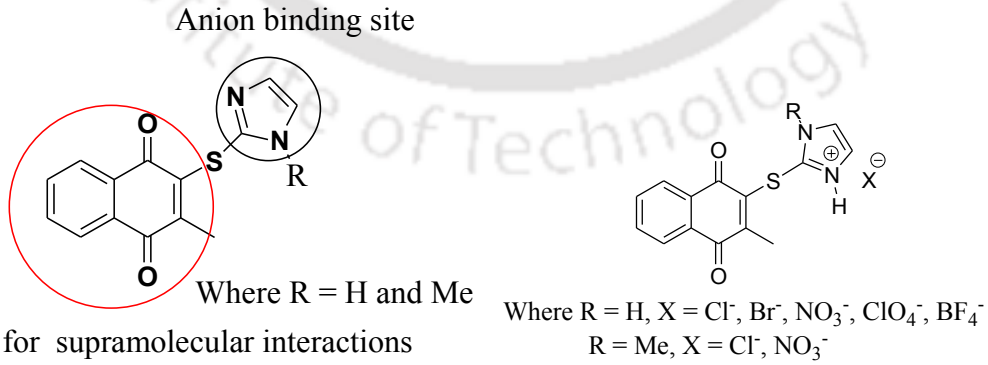

Figure 5: (a) Structure of **3.2** (abbreviation as *imd*) and **3.3** (abbreviation as *mmd*) and (b) Different salts **3.2** and **3.3**.

Both compounds form crystalline salts on treatment with different acids. The salt of **3.2** (*imd*) with acids such as hydrochloric, hydrobromic, nitric, perchloric, and

TH-1303_09612216

tetrafluoroboric acid easily crystallizes with the general composition [Himd][X] (in which X = Cl^- (**3.2a**), Br^- (**3.2b**), NO_3^- (**3.2c**), ClO_4^- (**3.2d**), and BF_4^- (**3.2e**)). The salt of **3.3** (*mmd*) with acids such as hydrochloric, hydrobromic, nitric acid easily crystallizes with the general composition [Hmmd][X] (X = Cl^- (**3.3a**), Br^- (**3.3a**), NO_3^- (**3.3b**). The structures of each salt were determined.

Each of the salts was structurally characterized by single crystal X-rays diffractions. The structural details provided the insight coordination environment of the anions in these salts. Salt **3.2a** (chloride salt) and **3.2b** (bromide salt) are isostructural. The hydrogen-bond distances involving bromide atom in the bromide salt are slightly greater than those of the chloride salts. This is due to the larger ionic radii of the bromide ion compared to chloride.

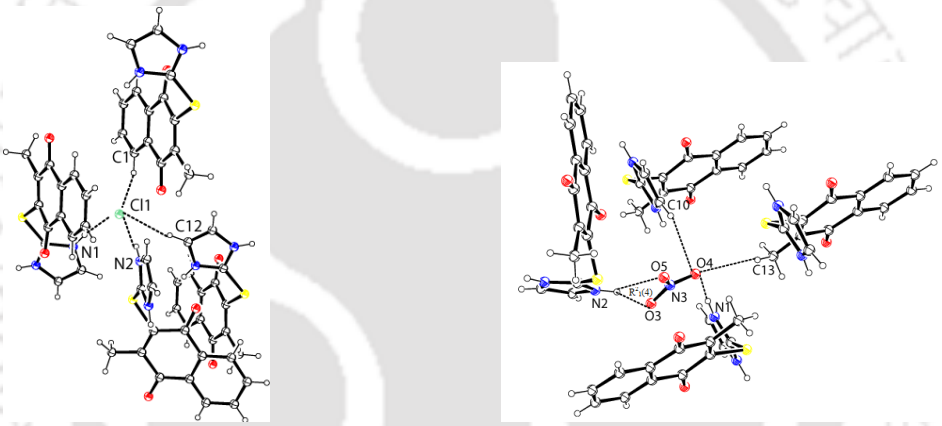

(a) (b)

Figure 6: (a) Environment of a chloride ion in the lattice of **3.2a.** (b) Bifurcated hydrogen bond in nitrate salt **3.2c**.

Nitrate salts of the **3.2** (**3.2c**) and **3.3** (**3.3b**) are isostructural. From the crystal lattice it is obtained that nitrate anions are associated with a bifurcated N^+-H···O interaction between the hydrogen of the protonated imidazole and the nitrate oxygen atoms O3 and O5 respectively. Such hydrogen bond interactions lead to formation of a cyclic $R^2_1(4)$ hydrogen bond architecture as shown in figure 6b.

The UV-visible spectrum of compound **3.2** shows absorption maximum at 329 nm as a result of an n–π* transition. A solution of **3.2** in methanol shows an emission at 418 nm on excitation at 350 nm. Taking advantage of this emission, a series of fluorometric titrations of **3.2** were performed by adding different acids, such as hydrochloric, hydrobromic, nitric, perchlorate, and tetrahydrofluoroboric acid. A general

TH-1303_09612216

trend in the enhancement of fluorescence emission of **3.2** by these acids is observed. Upon addition of hydrochloric acid, the intensity of the fluorescence emission of a solution of **L** was enhanced and a new emission at 433 nm occurred as shown in figure 7a. The profile of emission obtained from the interaction of a solution of **3.2** in methanol with hydrogen bromide was different from the emission profiles of solutions of **3.2** interacting with other acids. In the case of hydrogen bromide, initially a sharp enhancement in fluorescence emission at 418 nm was observed; this emission was shifted to 452 nm upon gradual addition to reach a maximum emission. Upon adding hydrogen bromide beyond this concentration, another new sharp emission appears at 480 nm appeared. Thus, a new emission peak at 480 nm appeared which grew as the concentration of hydrogen bromide was increased as shown in figure 7b. On the other hand, when nitric acid was added the enhancement of the fluorescence emission intensity was 4-times higher than the intensity of fluorescence of **3.2**.

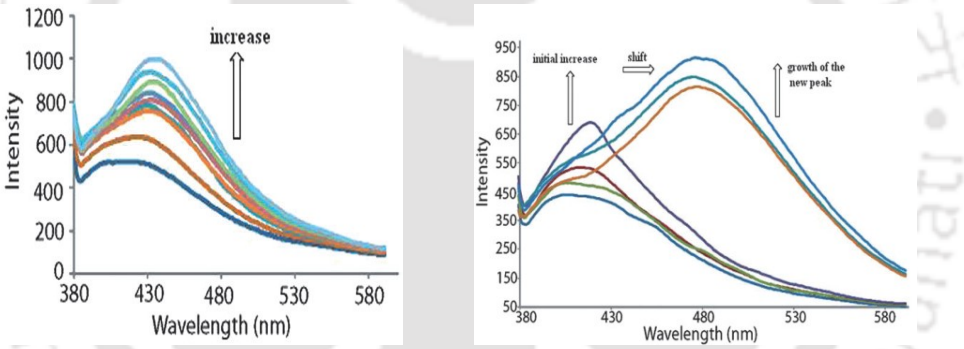

(a) (b)

Figure 7: Fluorescence emission of **3.2** (10^{-5} M in methanol) on addition of (a) hydrochloric acid, and (b) hydrobromic acid (5 µL of 10^{-5} M in methanol solution in each aliquot).

Fluorescence intensity of **3.2** by addition of perchloric or tetrafluoroboric acid showed a similar trend to that of hydrogen chloride. On the other hand, **3.3** did not show significant fluorescence changes with different mineral acids. The binding constants of the acids with **3.2** were determined and the order of magnitude was HNO_3 < HBF_4 < HCl < $HClO_4$ < HBr. However, there were two binding constants for hydrogen bromide of 11.66×10^6 and 1.43×10^5 M^{-1}, respectively. The reaction of phosphoric acid was found to be an exception; while such study we observed the C-S bond cleavage by phosphoric acid in 2-methyl-1,4-naphthoquinone derivatives leading to S-S bond formation and also leading to

dimer of parent naphthoquinone which is equivalent to a 2+2 cycloadduct of the parent naphthoquinone compound.

Chapter 4: Structural studies of polymorphs and solvates of different aromatic thiol substituted naphthalene-1,2-dione and their photophysical properties

This chapter deals with synthesis, characterization of different aromatic thiolato tethered 1,2-naphthoquinone derivatives (**4.1-4.7**, figure 8) and study of their polymorphs, solvates and photophysical properties. This chapter delineates two aspects namely polymorphism of the compounds from the self-assembly of the 1,2-naphthoquinone derivatives, and the role of intermolecular interactions to form bifurcated hydrogen bonds.

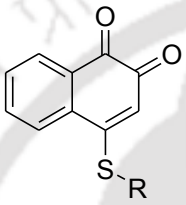

Where R = -C_6H_5 (4.1), 4-$CH_3C_6H_4$- (4.2), 4-Cl-C_6H_4-(4.3), 4-Br-C_6H_4- (4.4), 2-OHC_6H_4-(4.5), 3-OHC_6H_4-(4.6) and 4-OHC_6H_4-(4.7).

Figure 8: The structure of 1,2-napthoquinone derivatives.

When the compound **4.1** was crystallized methanol or ethanol two different types of crystals were obtained. From the spectroscopic and crystallographic analysis they are found to be two different polymorphs. Which are designated as polymorph **I** (**4.1a**) and polymorph **II** (**4.1b**) as shown in Scheme 2.

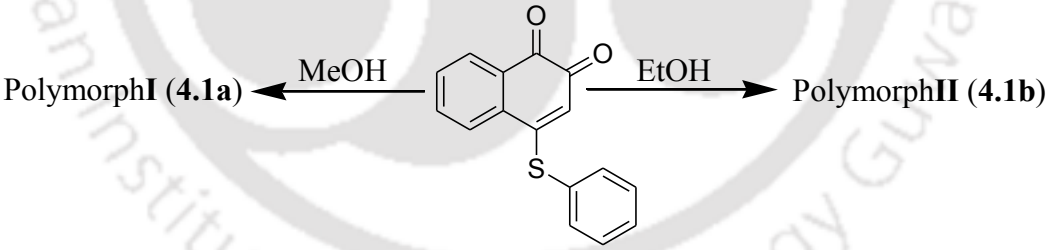

4.1

Scheme 2: Schematic diagram of polymorphs of **4.1**.

In the crystal structure of **4.1a**, it is observed that molecules occur in pairs formed by intermolecular cyclic hydrogen bonded motif (Figure 9a), whereas thio phenolate groups are *cis* to each other whereas in **4.1b**, the thio phenolate groups are *trans* to each other (Figure 9b). The main distinctions between the two polymorphs arise in their dihedral angles and packing patterns. The torsion angle of C5-C10-S1-C11 and C9-C10-S1-C11 of polymorph **II** (**4.1b**) are 178.25°, -1.98° (Figure 9d), whereas in polymorph **I** (**4.1a**) the torsion angles of C5-C10-S1-C11 and C9-C10-S1-C11 are -179.84° and 0.36° (Figure 9b)

TH-1303_09612216

respectively, which shows the difference between the conformation of the polymorphs **I** (**4.1a**) and **II** (**4.1b**).

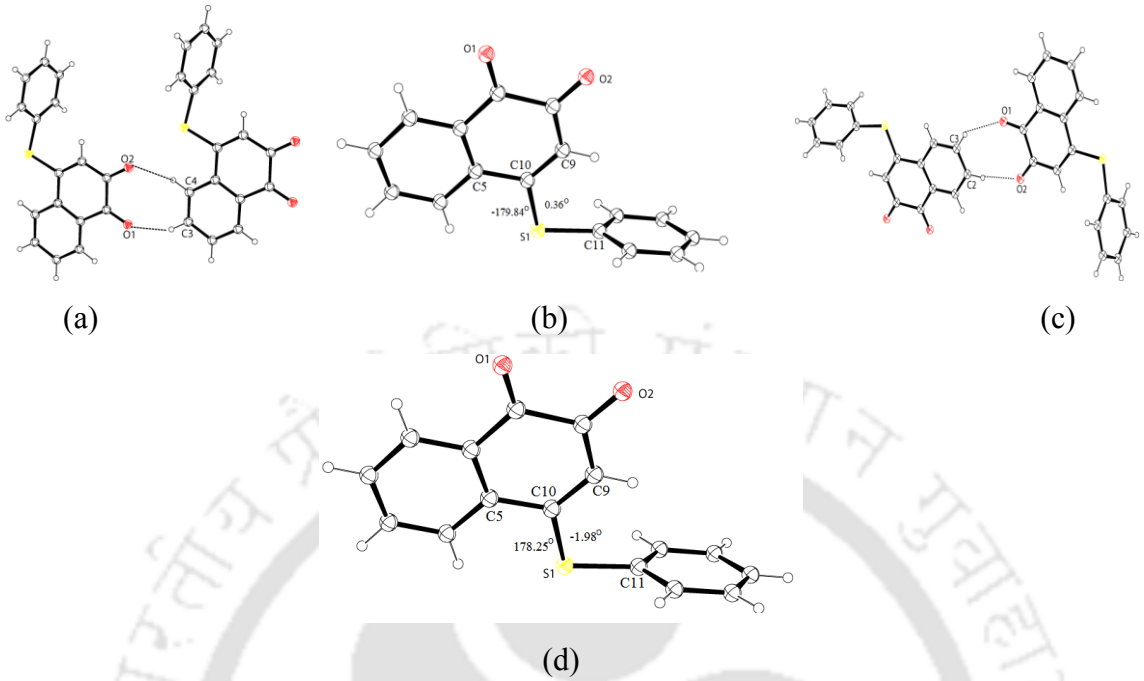

Figure 9: (a) Cyclic H-bonding motif observed in polymorph **I** (**4.1a**), (b) Torsion angle of polymorph **I** (**4.1a**), (c) Cyclic H-bonding motif observed in polymorph **II** (**4.1b**) (d) Torsion angle of polymorph **II** (**4.1b**).

Compounds **4.2-4.7** resulted in the formation anhydrous crystals. Interestingly; when the compound **4.7** was crystallized in different solvent different types of crystal were obtained. The anhydrous form **4.7a** of **4.7** was obtained from dimethylformide (DMF) solvent. The crystal obtained from the methanol solution was isolated as its methanol solvate **4.7b**, similarly; crystal obtained from the dimethylacetamide (DMA) solution was isolated as its DMA solvate **4.7c** and

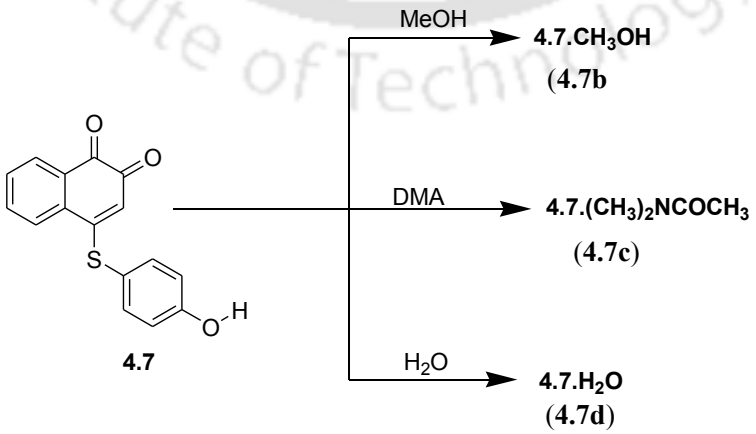

Scheme 3: Schematic diagram of anhydrous and solvates of **4.7**

crystal of **4.7** from water/ methanol mixture was its mono-hydrated solvate **4.7d** as shown in Scheme 3. From the crystal lattice of anhydrous form (**4.7**), it is observed that the sulfur atom bearing 1,2-naphthoquinone groups are *trans* to each other across a $R_2^2(10)$ hydrogen bond motif (Figure 10a).

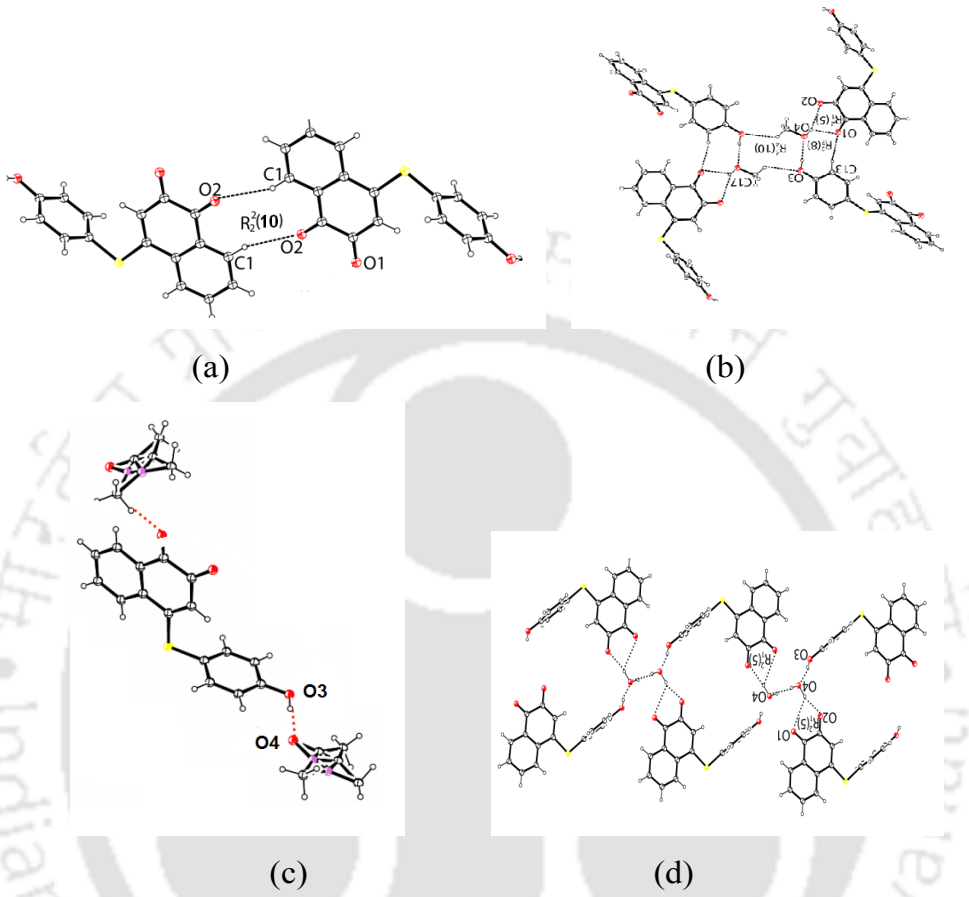

(a) (b) (c) (d)

Figure 10: (a) Dimeric assembly of **4.7a**, (b) Assembly of methanol solvate of **4.7**, (c) Assembly to form chain like structure in DMA solvate of **4.7** and (d) Assembling of **4.7** through bifurcated hydrogen bonds with water.

In the crystal lattice of methanol solvate **4.7b**, the host molecules are bridged by methanol molecules through strong O-H···O and weak C-H···O interactions. These hydrogen bonds make $R_4^4(10)$ types of cyclic hydrogen bonded motifs (Figure 10b). On the other hand, the packing pattern of the DMA solvate **4.7c** has strong O-H···O interactions between carbonyl of DMA with the OH-group of phenol (Figure 10c). In the case of hydrate crystal **4.7d**, the carbonyl group of 1,2-naphthoquinone participating in $R_1^5(5)$ cyclic hydrogen bond with the water molecules as shown in figure 10d. Compounds **4.5-4.7** in methanol and dimethylacetamide show UV-absorptions are due to n→π* transition around 317 nm. Interestingly, compound **4.7** shows solvate-emissive

TH-1303_09612216

property upon excitation at 320 nm, whereas similar excitation of compounds **4.5** and **4.6** did not show significant changes. The solution of compound **4.7** in DMA showed dual fluorescence emission at 421 nm and 567 nm on excitation at 320 nm. Whereas, under similar conditions the compound **4.5** shows emission peak at 416 nm. These results are further supported by carrying out fluorescence titration of a solution of **4.7** in DMA by adding different aliquots of methanol. During such titration dual fluorescence observed in DMA solution changes and the higher wavelength emission got quenched whereas the emission at lower wavelength enhanced as shown in figure 11. Finally addition of more amount of methanol to the solution of **4.7** in DMA led to single emission peak resembling the emission spectra.

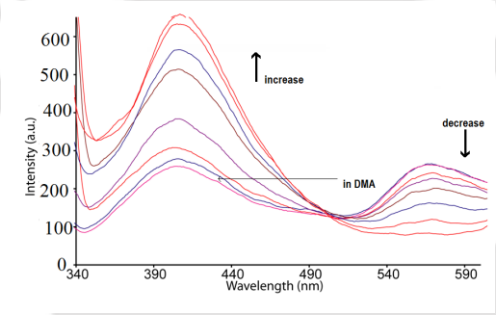

Figure 11: Fluorescence spectra of **4.7** (10^{-5} M in 3 mL DMA; λ_{ex} = 320 nm) on addition of different aliquot methanol (10 µL in each aliquot).

Chapter 5: Cytotoxicity and protein binding studies of naphthoquinone derivatives

This chapter deals with synthesis, characterization of different naphthoquinone derivatives (**5.1**-**5.12**) and study of their protein binding and cytotoxicity.

*Interactions of bovine serum albumin and human serum albumin proteins with compounds **5.1**-**5.12***

Bovine serum albumin (BSA) a common protein has a strong emission maximum at 352 nm, when excited at 295 nm at pH 7.4. Gradual addition of **5.1**-**5.12** to solution of BSA led to significant changes in fluorescence emission. The fluorescence intensity decreased with increase in concentration of all compounds, with a blue shift. The quenching with blue shifts is indicative of the binding of the compounds to BSA. From the changes in fluorescence binding constants were determined; the compound **5.8** was identified to have highest binding than then rest of compounds. The binding constant order towards BSA has following trends: compound **5.8** > **5.6** > **5.11** > **5.9** > **5.3** > **5.12** > **5.7** > **5.1** > **5.10** > **5.2** > **5.4** > **5.5**.

TH-1303_09612216

The binding constants with human serum albumin also were determined and the fluorescence anisotropies were determined to ascertain the possible denaturisation of proteins. HSA has a strong emission maximum at λ_{332} nm, when excited at λ_{295} nm at

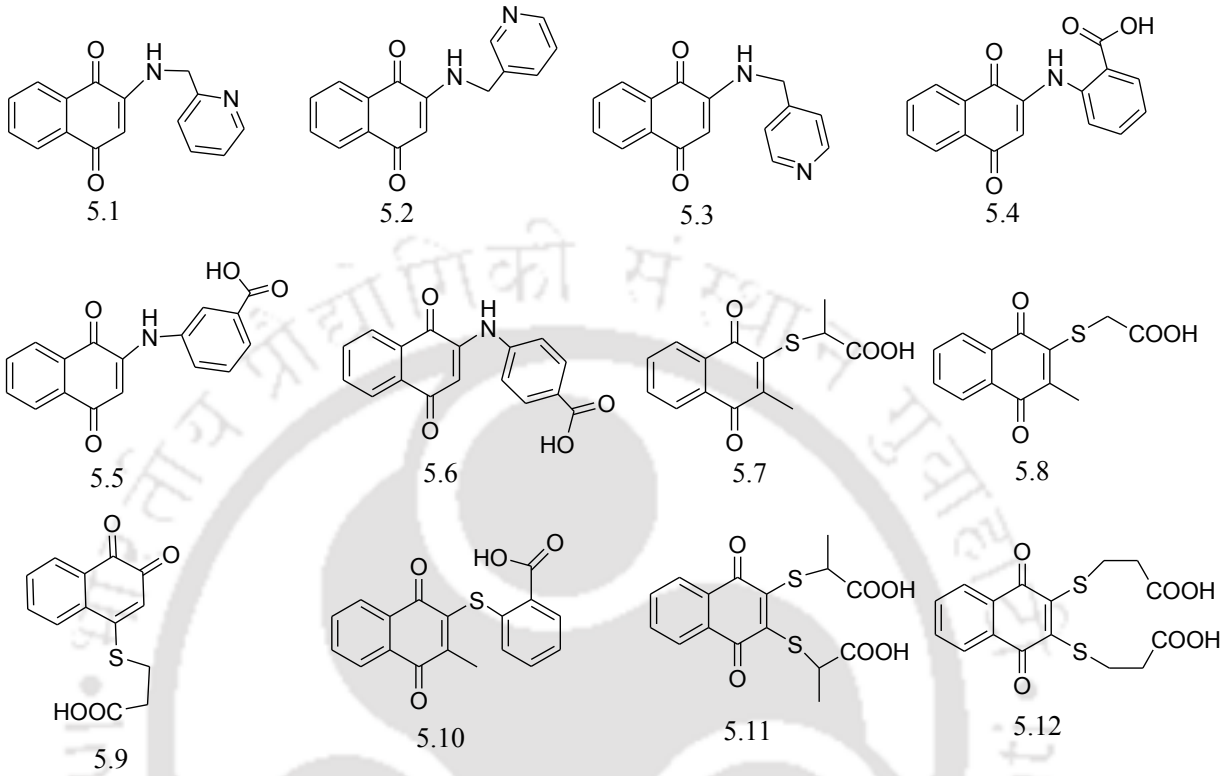

Figure 12: Structures of naphthoquinone derivatives.

pH 7.4. Gradual addition of **5.1-5.12** to a solution of HSA led to significant changes in fluorescence emission. The fluorescence intensity decreased with increase in concentration of all compounds, with a blue shift. The quenching with blue shifts are indicative of the binding of the compounds to HSA.

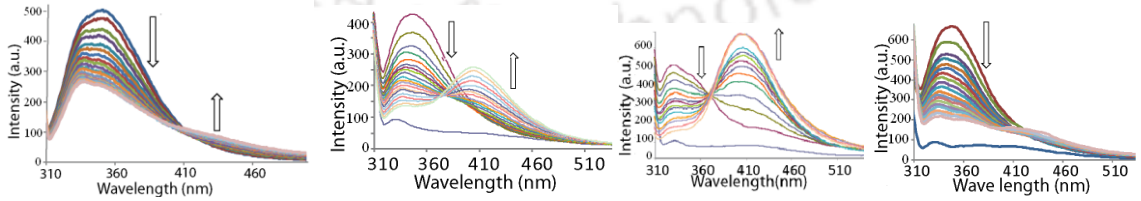

(a) (b) (c) (d)

Figure 13: Changes in fluorescence spectra of BSA with (a) compound **5.1**, (b) compound **5.6** (2 µL BSA, in tris buffer pH 7.4) and changes of fluorescence emission spectra of HSA with (c) compound **5.4** and (d) compound **5.7** (2 µL HSA , in tris buffer pH 7.4)

TH-1303_09612216

Table 1: Cytotoxicity of compounds **5.1-5.12**

Compound No.	Mia Paca-2	BxPC-3	Panc-1	HCT116
5.1	19.3 ± 1.7[b]	32.0 ± 1.2	16.1 ± 0.8	14.4 ± 1.6
5.2	21.6 ± 2.2	12.6 ± 1.4	14.7 ± 1.3	24.3 ± 2.3
5.3	26.6 ± 2.4	24.2 ± 1.5	16.5 ± 1.7	36.3 ± 2.1
5.4	26.6 ± 0.9	24.1 ± 2.1	25.8 ± 0.4	13.1 ± 1.0
5.5	23.0 ± 2.1	15.5 ± 2.4	25.5 ± 1.5	13.5 ± 1.9
5.6	12.0 ± 1.6	14.0 ± 1.8	18.1 ± 0.6	12.0 ± 0.9
5.7	9.4 ± 1.1	17.9 ± 1.5	11.6 ± 1.0	16.5 ± 1.1
5.8	16.5 ± 1.7	23.4 ± 1.7	13.5 ± 1.2	19.5 ± 3.4
5.9	2.7 ± 0.6	7.6 ± 1.0	3.0 ± 0.1	4.9 ± 0.1
510	32.0 ± 2.7	34.4 ± 3.2	21.6 ± 0.7	27.8 ± 2.5
5.11	26.9 ± 0.6	68.9 ± 3.4	17.4 ± 0.4	43.2 ± 2.5
5.12	28.7 ± 0.8	55.7 ± 4.2	25.8 ± 2.7	35.6 ± 2.1

[a] IC_{50} is defined as drug concentration causing a 50% decrease in cell population. [b] Mean ± Sd were calculated from three independent experimenents.

From the binding constant, we concluded that compound **5.10** has shown better binding with HSA, where as compounds **5.4**, **5.8**, **5.12**, **5.9**, **5.7**, **5.6**, **5.11** has moderate binding but compounds **5.1-5.3** and **5.5** does not shown any significance changes. The binding constant order towards HSA has following trends: compound **5.10** > **5.4** > **5.8** > **5.12** > **5.9** > **5.7** > **5.6**. The cytotoxicity of compounds **5.1-5.12** were determined in four cancer cell lines (Table 1) representing pancreatic ductal adenocarcinoma (Mia Paca-2, BxPC-3, Panc-1) and colorectal carcinoma (HCT 116). The cytotoxicity of the compounds varied in different cell lines. In the Mia paca-2 cell line the cytotoxicity sequence was **5.9** > **5.7** > **5.6** > **5.8** > **5.1** > **5.2** > **5.5**> **5.3** ≈ **5.4** ≈ **5.11** > **5.12** > **5.10**.

Each chapter has the spectroscopic details of the compounds along with synthetic methodology. Pertaining literature are included at the end of the each chapter. The crystallographic data for all the structures that have discuss in this work, except those, which are used as references are tabulated in the appendix section towards the end of the thesis. Details of the instruments used are given at the appendix section. A brief summary on the finding of the presented work have been discussed is this at the end of the thesis. The CIF of the crystal structures are presented in terms of electronic data in a CD.

TH-1303_09612216

TH-1303_09612216

Contents

TH-1303_09612216

Chapter 1

Introduction

1.1: General features of Quinones

Quinones are conjugated organic cyclic dicarbonyl compounds derived from aromatic hydrocarbons in which carbonyl groups are either 1,2- or 1,4- disposed.[1a-c] The main quinone structural skeleton on which different quinone derivatives are built is referred to as quinoidal. Some common quinoidal back-bones are shown in figure 1.1. They are biologically important compounds [2-3] and have relevance in electron-transfer and photochemical processes.[4-6] Quinoidal unit in the Vitamin K1 (**1.7**) and Vitamin K2 (**1.8**) are primarily responsible for anti-inflammatory, anticancer and toxicities.[7-12] Quinone derivatives such as lapachol,[13] plumbagin,[14] dichloroallyl lawsone[15] show anticancer activity.[16] From an organic chemistry point of view, quinones are commonly used as catalysts, substrates for cycloadditions and precursors for nucleophilic substitution reactions.[17-23]

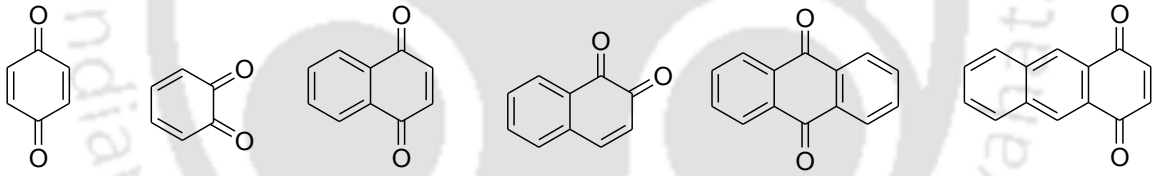

1.1 **1.2** **1.3** **1.4** **1.5** **1.6**

Figure 1.1: Some examples of quinones.

Quinones are useful to generate redox active metal-organic frameworks.[24-25] The molecular recognition properties of quinones are well studied and quinones are extensively used for anion and cation binding.[26-27] Due to biological relevance supramolecular interactions of quinones are of great interest.[28]

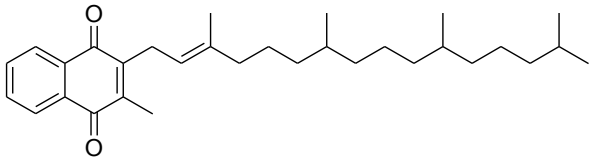

Vitamin K1 (1.7)

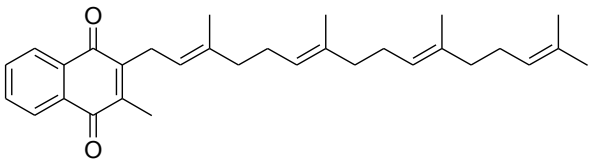

Vitamin K2 (1.8)

TH-1303_09612216

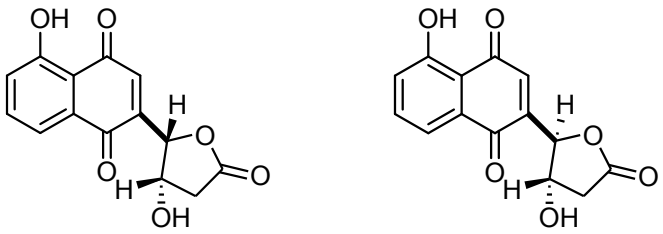

Juglomycin A (1.9a) **Juglomycin B (1.9b)**

Figure 1.2: Structures of Vitamin K1 (**1.7**), Vitamin K2 (**1.8**), Juglomycins (**1.9a**) and **1.9b**).

Juglomycin A (**1.9a**) and juglomycin B (**1.9b**) are quinoidal compounds. They show inhibitory action against a variety of microorganisms.[29] Quinone derivatives such as anthracyclines, mitoxantrones and saintopin are used as anticancer drugs. [26,30-31]

1.2 Quinones and its derivatives in catalysis

Reaction of *E*-isomer of compound **1.10** with catalytic amount of Li_2PdCl_4 in the presence of *p*-benzoquinone and LiCl in acetone-acetic acid gives a mixture of two isomeric allylic chlorides **1.11a** and **1.11b** (Scheme 1.1). Under the same reaction condition *Z*-isomer of compound **1.10** reacts to give the same product with different ratios.[31b] In this nucleophilic addition reaction the quinone replaces chloride attached to the palladium and facilitates attack of chloride on (η^3-allyl) palladium complex.

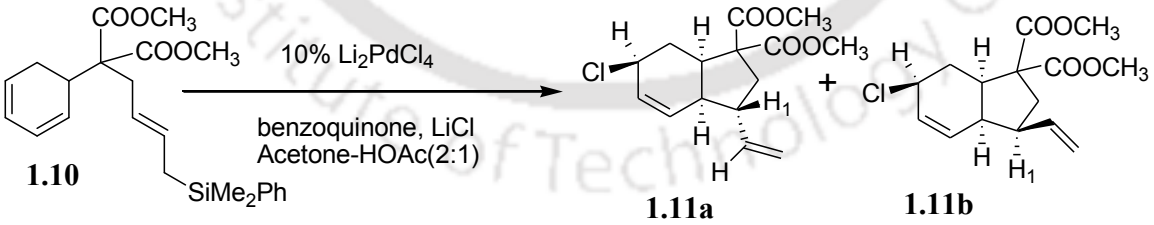

Scheme 1.1

The 1,4-oxidation reactions of 1,3-cyclohexadiene is catalyzed by zerovalent palladium in the presence of *p*-benzoquinone **1.12** (5 mol%) to give 1,4-diacetoxy-2-cyclohexene **1.13**[31c] (Scheme 1.2). In this reaction benzene is formed as a side product. In this palladium-catalyzed 1,4-oxidation reactions, *p*-benzoquinone causes reoxidation of Pd (0)

TH-1303_09612216

to palladium(II) for making the reversible catalytic cycle. The quinone induces the nucleophilic attack on the (η^3-allyl) palladium complex as well as it mediates the reoxidation of the Pd(0).

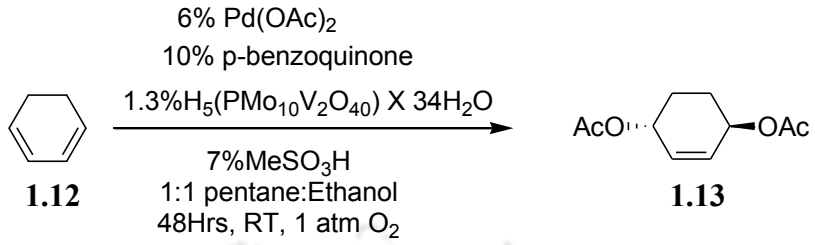

Scheme 1.2

Hydroxy group containing naphthoquinone derivatives **1.18** were prepared from 2-allyl or 2-methylallyl-1-naphthol[31e-f]**1.14**. The reaction starts with hydroboration of **1.14** to form **1.15** followed by two successive oxidation reactions using Fremy's salt {$Na_2NO(SO_3)_2$} to form **1.16** and by 2,6-dichloro-3,5-dicyano-1,4-benzoquinone (DDQ, **1.19**). Hydrolysis of **1.17** in basic medium gives naphthoquinone alcohols **1.20**. Naphthoquinone esters were obtained by esterification of naphthoquinone alcohols with 2-naphthoic acid (**1.19**) in the presence of 1,1′-carbodiimidazole (CDI) in tetrahydrofuran[31d] (THF) as shown in Scheme 1.3. The corresponding diester was formed in moderate yield.

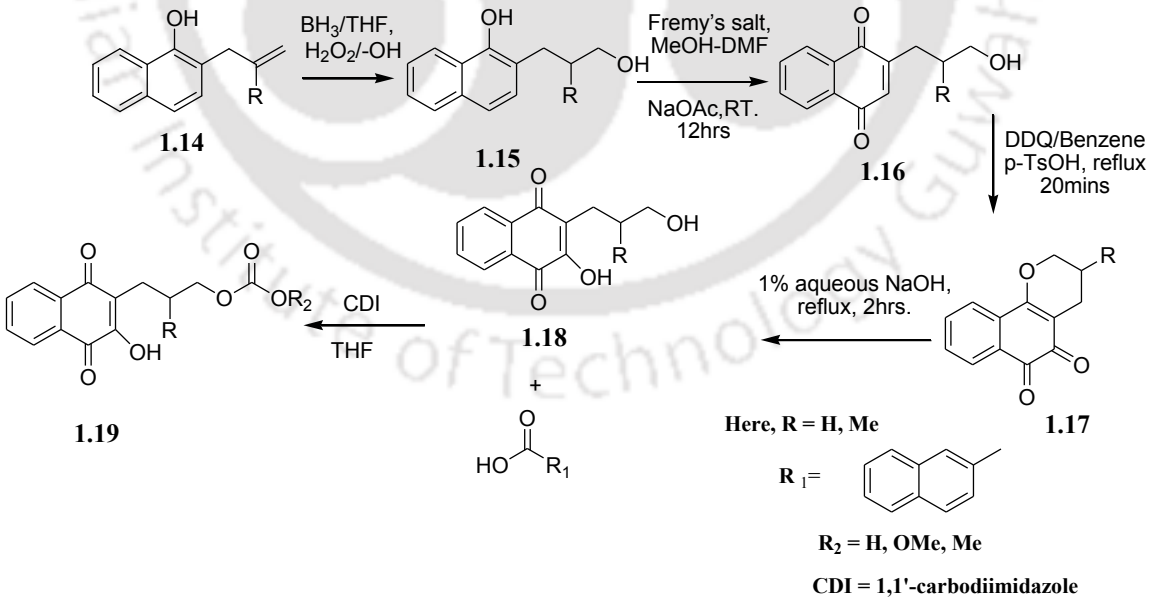

Scheme 1.3

TH-1303_09612216

1.3: Supramolecular and host-guest chemistry of quinone derivatives

Quinones and derivatives form self-assemblies guided by various weak interactions such as O-H···O, C-H···O, C-H···π and O-H···π interactions.[32-33] Presence of strong directional hydrogen bonds in quinoidal compounds form hydrogen bonded assemblies which may be in the form of linear or cyclic assemblies. There are several characteristic supramolecular features associated with substituted quinones. Some of the weak interactions in *p*-benzoquinone are shown in figure 1.3a.

(a) (b)

Figure 1.3: (a) Sites for supramolecular interactions in the *p*-benzoquinone and (b) *p*-benzoquinone as a guest in a host-guest complex.

One example of host-guest complex formed by cyclic amide with *p*-benzoquinone is illustrated in figure 1.3b. In this compound the carbonyl groups of *p*-benzoquinone forms hydrogen bonds with N-H bond of amides and *p*-benzoquinone molecule is associated with π···π interactions with the aromatic part of host.[34] The adduct formed in 1:1 stoichiometry between *p*-benzoquinone with 1,4-hydroquinone is known as quinhydrone. Quinhydrone forms a 1D hydrogen bonded chain-like structure in solid state.[35-36] Hydrogen bonds between the carbonyl groups of *p*-benzoquinone and hydroxy groups of 1,4-hydroquinone are shown in figure 1.4.

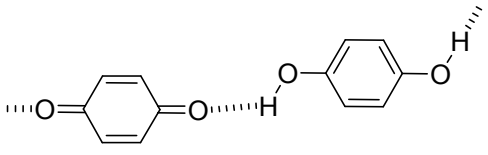

1.20

Figure 1.4: O-H···O interactions in quinohydrone.

TH-1303_09612216

2,5-Dichloro-3,6-dihydroxy-1,4-benzoquinone is commercially known as chloranilic acid. It forms salts and elsewhere co-crystals with different organic bases.[37] In such salts or co-crystals chloranilic acid acts as a proton donor whereas organic bases act as proton acceptors (Scheme 1.4). Co-crystals in these cases can be considered as host-guest complexes of chloroanilic acid with corresponding amine; they are formed by hydrogen bonds between the acid and amines without proton transfer from the acid to the base. In salts the proton-transfer from chloroanilic acid to the base takes place and their self-assemblies are guided by hydrogen-bonds as well as electrostatic interactions.

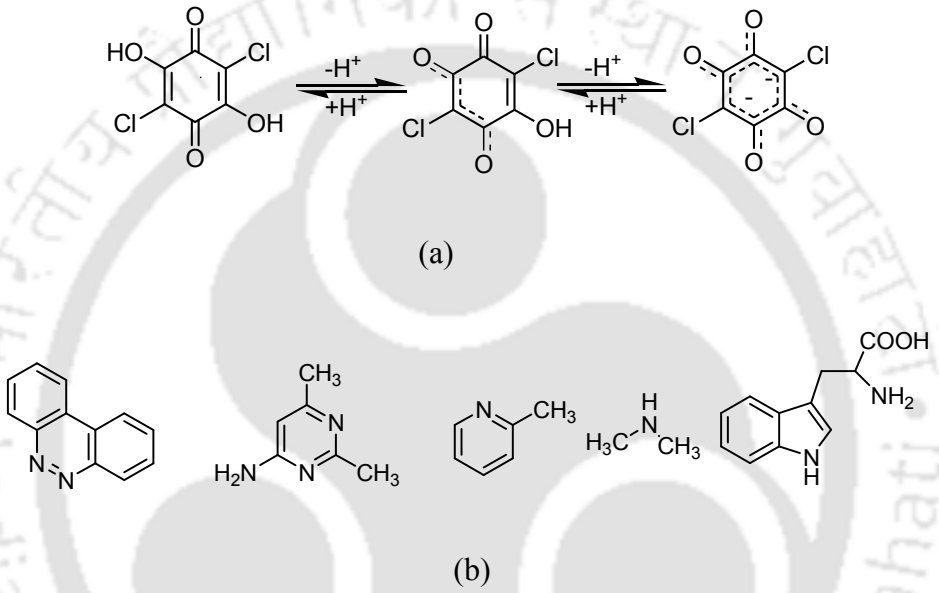

Scheme 1.4: (a) Different acid-base equilibria of chloranilic acid at different pH and (b) Nitrogen containing bases used for co-crystals and salts formation with chloroanilic acid.

These co-crystals and salts are important in understanding proton-transfer process between quinoidal part and amine. Depending on pH the chloranilic acid remains as delocalized monoanion or dianion as shown in two equilibrium of Scheme 1.4a. Hence the stoichiometry and type of salt or co-crystal formed are influenced by basicity and hydrogen bond forming ability of the amines.

Similar derivative 2,5-dibromo-3,6-dihydroxy-1,4-benzoquinone, which is also known as bromanilic acid forms co-crystals with pyrazine derivatives (Scheme 1.5).[38] Self-assemblies of these co-crystals are governed by hydrogen bonds between the hydroxy

TH-1303_09612216

groups of host molecules with nitrogen atom of the protonated base. Such interactions result in formation of one dimensional zig-zag chains.

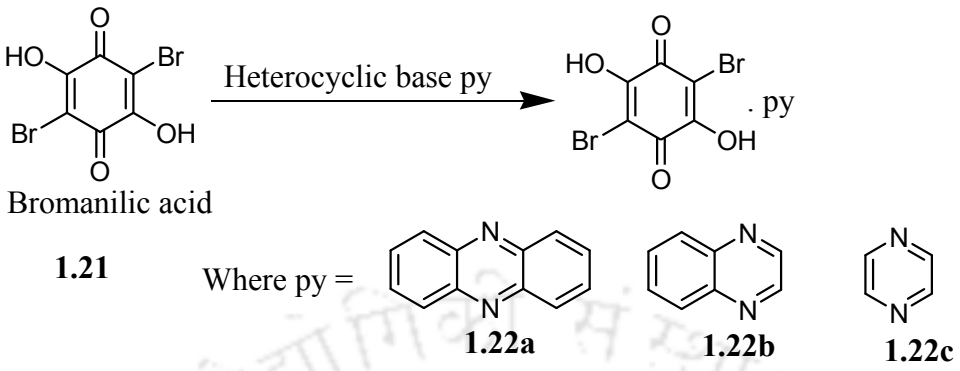

Scheme 1.5: Cocrystals of bromanilic acid with different pyrazine derivatives.

The co-crystals of substituted benzoquinones (**1.25**) with substituted *bis*-phenols (**1.23a-c** and **1.24**) are well known. [39-40] As different *bis*-phenols give different colour with *p*-benzoquinone in solid state, *p*-benzoquinone is used as visible indicator for *bis*-phenol derivatives. *Bis*-phenol A **(1.25a)**, 2,2′-bis(4-hydroxyphenyl)hexafluoropropane (**1.15b**) and 4,4′-methylenediphenol (**1.24**) forms charge-transfer complexes with *p*-benzoquinone

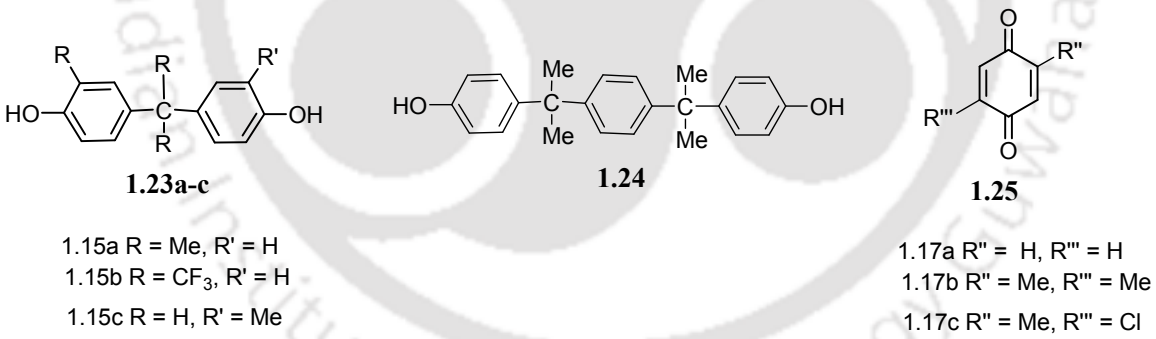

Scheme 1.6: Examples of *bis*-phenol hosts and quinone guests.

Self-assemblies of these co-crystals are formed by assistance of different weak interactions. For example, co-crystal of **1.23a** with **1.25a** has one dimensional zig-zag hydrogen bonded chain-like structure. The zig-zag structures are held together by C-H···π interactions in the form of a two dimensional layered structure along crystallographic *a* and *c*-axes (Figure 1.5).

TH-1303_09612216

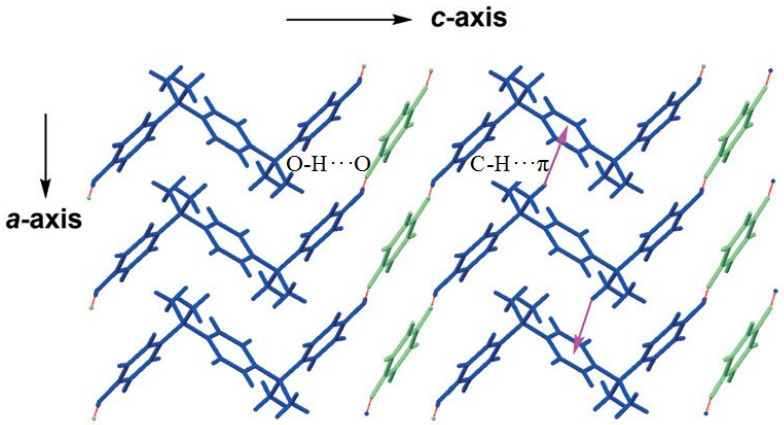

Figure 1.5: The O-H···O and C-H···π interaction of cocrystal of **1.23a** with **1.25a**.

On the other hand, a three dimensional hydrogen bonded structure was observed in co-crystals of **1.23b** with **1.25b**. Three dimensional layered structure possesses charge transfer interactions between the π-aromatic rings and C-H···π interactions. The packing pattern in the structure along bc-plane is shown in figure 1.6.

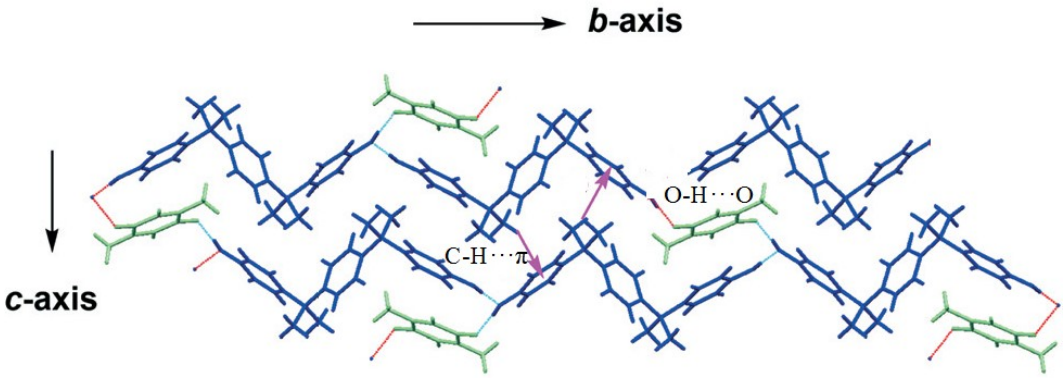

Figure 1.6: O-H···O and C-H···π interactions of cocrystal of **1.23b** with **1.25b**.

These examples suggest possibilities to bring out large numbers of structural variations by varying substituents and adding functional groups to quinoidal compounds to create numbers of different types of self-assemblies.

1.4: **Polymorphism in quinone derivatives**

Polymorphism is a phenomenon of a single substance having several different crystal forms or modifications.[41-46] Polymorphs are formed as a consequence of differences in crystal structures. They are chemically identical but differ in their physical properties, such as solubility, thermal stability, density. They also show different vibrational spectra and diffraction patterns. Study on polymorphs provide opportunity to understand

TH-1303_09612216

structure-property relationships. In recent years, many polymorphs of active drugs such as barbiturates, sulfa-drugs and steroids have been discovered.[47-48] The conformational polymorphism in quinone derivatives can arise due to *syn* and *anti* conformation across directly bonded atoms or groups on a quinone ring.[49-54] Alkyl or arylthio quinones show conformational polymorphism.[55-56] This is due to ease of formation of different conformations across two directly bonded sulfur atoms or two sulfur atoms separated by intervening carbon atoms.[57-64] Pictorial descriptions of the different conformations of two sulfur atoms separated by intervening carbon atoms attached to a rigid unit are shown in figure. 1.7.

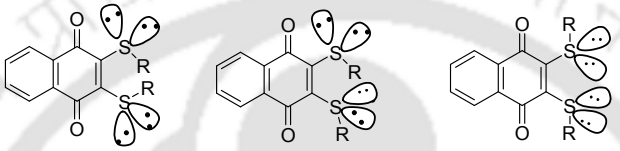

Figure 1.7: Different orientations of two thio-alkyl groups across 1,4-naphthoquinone.

Structures of two conformational polymorphs of 2,3-*bis*-*p*-methylphenylsulfanyl-1,4-naphthoquinone were shown.[65] Polymorph **1.26a** was obtained by fast oxidation of 2,3-*bis*-*p*-methylphenylsulfanyl-1,4-naphthalenediol with copper(II) acetate catalyst; while the polymorph **1.26b** was obtained by slow aerial oxidation of the 2,3-*bis*-*p*-methylphenylsulfanyl-1,4-naphthalenediol in methanol. Polymorphs of 2,3-*bis*-*p*-methylphenylsulfanyl-1,4-naphthoquinone occur due to relative orientations of *p*-methylphenylsulfanyl groups attached to the 1,4-naphthquinone ring as shown in figure 1.8. In polymorphs **1.26a** and **1.26b** thiolate groups are not in the plane of the quinone plane. Two polymorphs differ in their packing patterns, and the packing patterns have also differences in weak interactions.

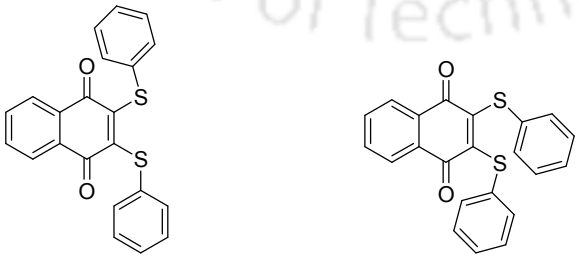

Polymorph 1.26a **Polymorph 1.26b**

Figure 1.8: Two conformational polymorphs **1.26a** and **1.26b**.

TH-1303_09612216

3,3'-(4,4'-Biphenyldiylbisthio)bis-2-methyl-1,4-naphthoquinone shows conformational polymorphs. Three polymorphs designated as **1.27a**, **1.27b** and **1.27c** posses distinguishable

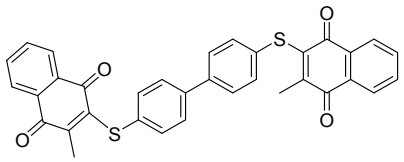

3,3'-(4,4'-biphenyldiylbisthio)bis-2-methyl-1,4-naphthoquinone.

Colors.[66] They show the different packing patterns shown in figure 1.9. The packing pattern of polymorph **1.27a** shows that there are two naphthoquinone rings inclined in

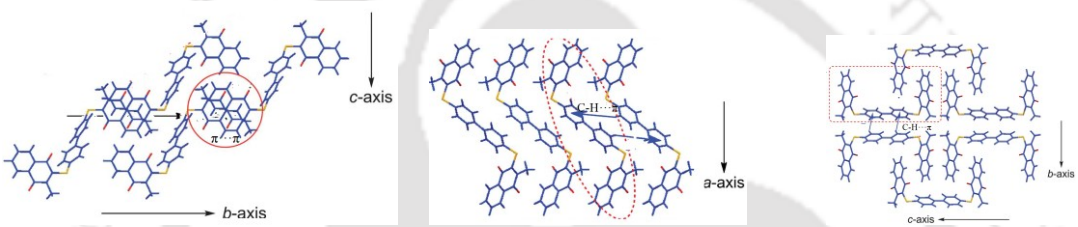

(a) (b) (c)

Figure 1.9: Weak interactions in the packing patterns of different conformational polymorphs (**1.27a-c**).

opposite directions with respect to the biphenyl backbone adopting *anti* form. Besides this, it forms a two dimensional layered structure along *a* and *b*-crystallographic axes and has π···π interactions as shown in figure 1.9a. Whereas polymorph **1.27b** has a similar orientation of methyl groups to polymorph **1.27a** but it forms a one dimensional zig-zag layered structure. One dimensional layered structures of polymorph assembles themselves with interlayer aryl-aryl edge-to-face interactions along the crystallographic *c*-axis, this results in the formation of a two dimensional layered structure as shown in figure 1.9b. On the other hand, in structure of polymorph **1.27c**, two naphthoquinone rings are inclined in the same direction with respect to biphenyl backbone. X-ray crystallographic analysis revealed that it has a one-dimensional layered structure along the crystallographic *a*-axis. This one dimensional layered structure is formed by intracolumnar C-H···S hydrogen bonds. The assembly of these layers with intercolumnar

TH-1303_09612216

aryl-aryl edge-to-face interactions along the crystallographic *b*-axis results in formation of arrangement of molecules as shown in figure 1.9c.

Fuchsones belong to a class of molecules having structural similarity to *p*-benzoquinone. Fuchsones such as, 4-(α,α′-diphenylmethylene)1,4-benzoquinones **1.28a-d** show conformational polymorphism.[67-68] The chloro and isopropyl derivatives are dimorphic means shows two polymrphs; while methyl and *t*-butyl derivatives are found to be trimorphic (**1.28a-d**). Present examples of polymorphs are formed due to differences in conformation in crystalline forms. Conformational changes take place due to difference in orientations of the phenyl rings of exo-diphenylmethylene group present at the 4-position of benzoquinone ring.

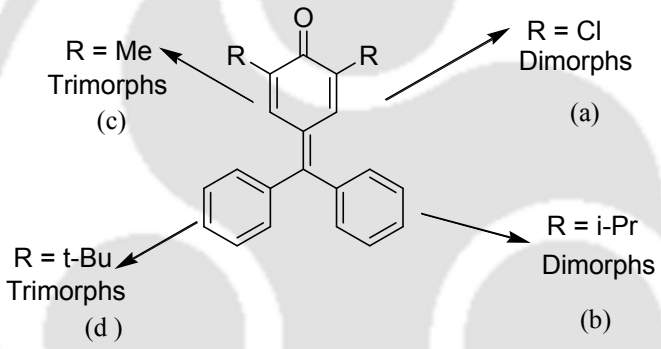

Figure 1.10: Conformational polymorphs in fuchsone (**1.28a-d**).

Covalently linked to benzoquinone to zinc-porphyrin complexes *via* a cyclohexanediyl bridge can adopt different conformations. Such conformational differences in solid state resulted in isolation of polymorphs having equatorial-equatorial and equatorial-axial arrangement across 1,4 position of a cyclohexyl ring.[69] Two porphyrin quinone polymorphs undergo electron transfer from porphyrin to quinone at comparable rates. A similar concept has been extended to prepare conformational polymorphs of porphyrin-quinone cyclophanes with one or two quinones covalently attached above or below the porphyrin plane.[70-72] These examples point out that the quinoidal compounds have wide ranges of variation on packing patterns leaving a wide opening to for understand physical properties.

TH-1303_09612216

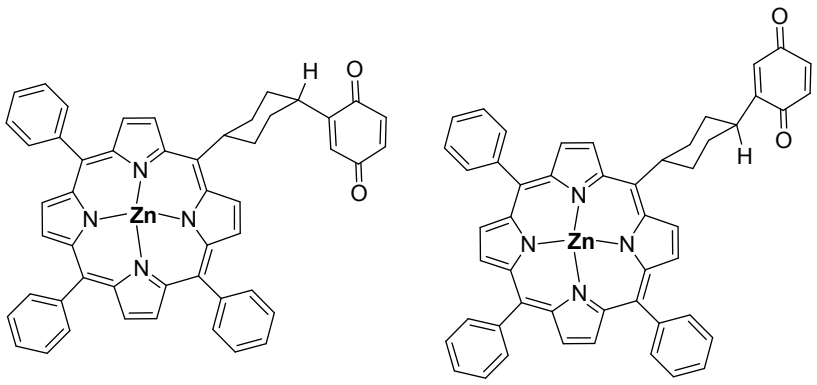

Polymorph 1.29a **Polymorph 1.29b**

Figure 1.11: Conformational polymorphs **1.29a** and **1.29b**.

1.5 Quinone and their derivatives as sensors for anions and cations

Photophysical and electrochemical response of quinone and their derivatives are of interest in anion binding.[73-74] Hydrogen-bonded receptors, as well as charged assisted anion receptors have been extensively used in the field of anion recognition and sensing. Various photophysical properties of quinone derivatives are easily tuned through well thought-out structural design. Synthetic modifications are readily accommodated on either the quinone moiety itself, among them various amines and thiols derived compounds can be easily prepared. The easy synthetic procedures involved in such reactions allow incorporation of varieties of functional groups and structural motifs to quinone backbones. Some quinoidal compounds are ions receptors, representative examples are discussed in the subsection to follow.

1.5.1: Quinone and their derivatives in anion sensing

Anthraquinone-based anion receptors (**1.30a-c**) were used as both colorimetric and fluorescent chemosensors. These compounds show selective detection of fluoride ions in the presence of other halides. Color change by fluoride to solutions of the receptors.[75] Pale red color of solutions of **1.30a-c** became dark red in the case of **1.30a** and **1.30b** on addition of fluoride ions, whereas it turned reddish brown in the case of **1.30c** in acetonitrile. Solvent plays a role in change in color; as yellow solutions of **1.30a-c** turned pink in case of **1.30a** and reddish brown in case of **1.30b** and **1.30c** in chloroform. Color changes takes place due to the formation of hydrogen bond between the OH group and

TH-1303_09612216

fluoride ion. Such hydrogen bond formation had affected the electronic properties of the chromophores, resulting in a charge-transfer transition.[76-77] Fluoride ions interacted with the receptors more strongly than other halides due to its higher electronegativity and smaller size.[78-79]

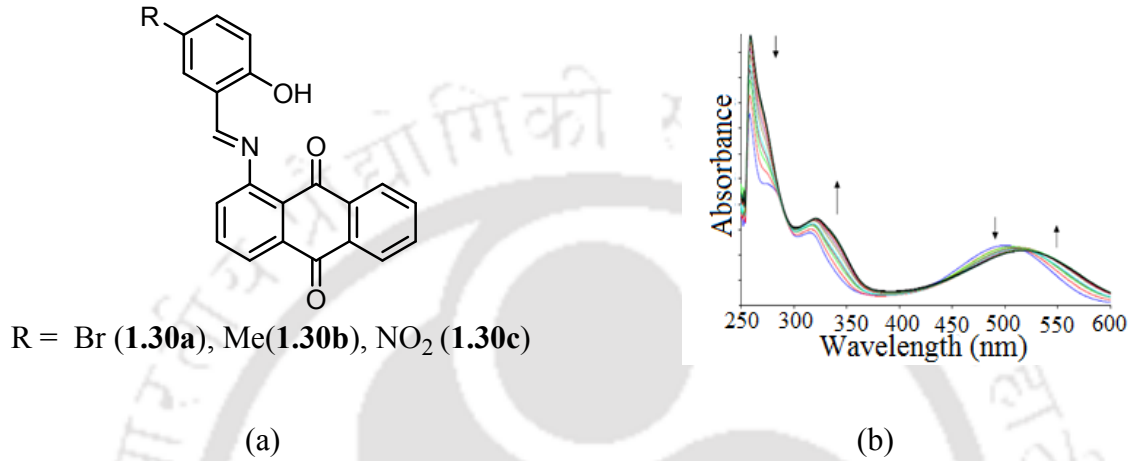

Figure 1.12: (a) Anthraquinone based receptor and (b) Change in absorption of receptor **1.30a** on addition of 0-10 equiv. of tetrabutylammonium fluoride in dimethylsulphoxide.

There are other also examples on related anthracene-9,10-dione derived quaternary ammonium salt-based chromogenic and fluorescent chemosensors for fluoride ions.[80-82] For example, chemosensors **1.31** and **1.32** possesses quaternary ammonium cation and N-H group. They exhibit absorption and emission changes with fluoride ions.

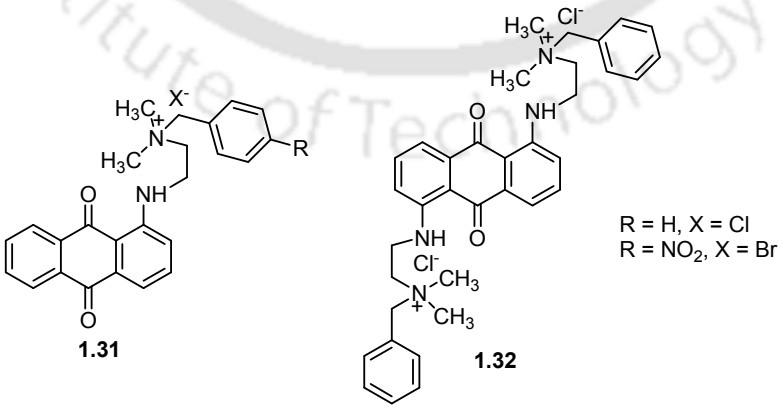

Figure 1.13: Anthraquinone based receptors.

TH-1303_09612216

Chemosensor **1.31** on excitation at 450 nm emits at 580 nm. No significant response to other anions such as chloride, bromide, iodide, nitrate, acetate, sulphate, phosphate and perchlorate were observed with the receptor **1.31**. The changes in the fluorescence emission of the **1.31** and **1.32** on addition of fluoride ions are shown in figure 1.14b.

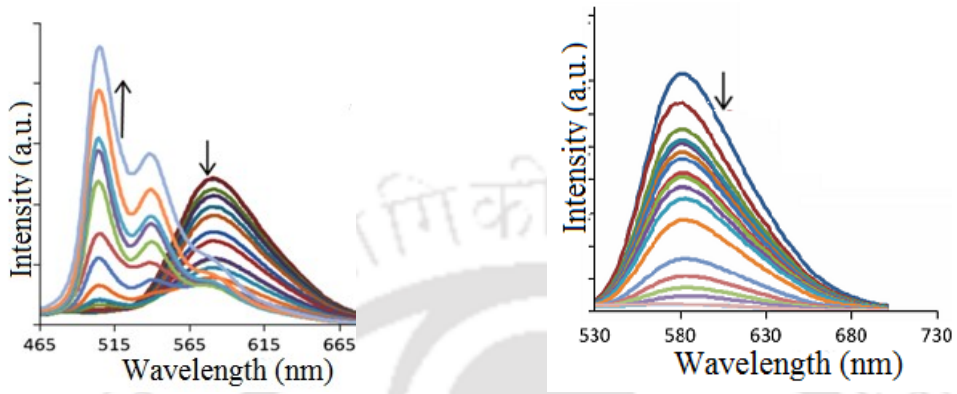

(a) (b)

Figure 1.14: (a) Fluorescence emission of compounds (a) **1.31** and (b) **1.32** on addition of fluoride ions.

Addition of fluoride ions the fluorescence intensity at 580 nm was gradually decreased and a new blue shifted fluorescence emission at two new emission bands at 505 and 540 nm appeared. But compound **1.32** on addition of fluoride ions shows quenching of emission at 580 nm.

6-(4-Ethylphenoxy)-5,12-naphthacenequinone (**1.33**) is photochromic.[83-84] UV-visible absorption spectra of compound **1.33** in acetonitrile changes on irradiation by 365 nm radiation. The spectral changes show characteristic peaks in 400-550 nm region, which corresponds to quinoidal form of phenoxynaphthacenequinone. Peak intensities increase with increase of irradiation time. Gradual addition of cyanide ions to a solution of **1.33** while UV irradiation is in operation, brings about significant change in the absorption spectra in a selective as well as sensitive manner over the other anions. The color of acetonitrile solution of **1.33** was changed from yellow to pale brown. This spectral change helps to detect cyanide anion at a concentration as low as 18.7 µM.

TH-1303_09612216

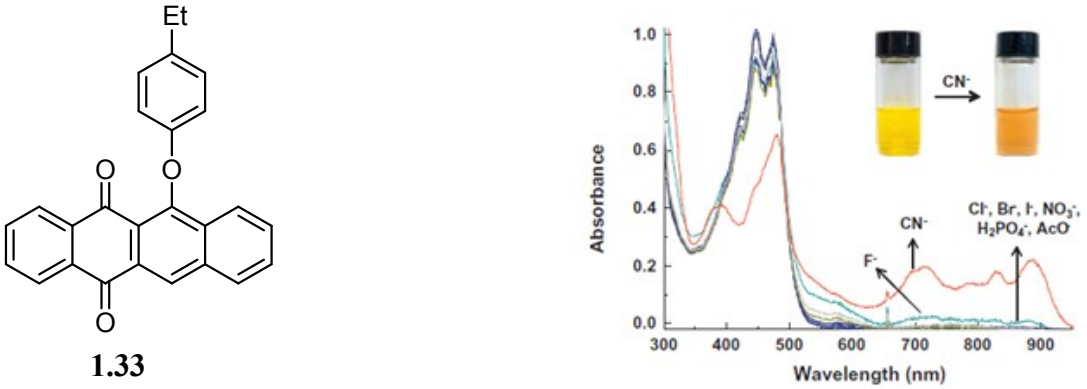

(a) (b)

Figure 1.15: (a) UV-vis spectra of **1.33** and (b) Changes in absorption of **1.33** when irradiated by 365 nm in the presence of different anions.

A film of poly-(2-hydroxyethylmethacrylate) doped with 1,2-diaminoanthraquinone is used as colorimetric sensing material for detection of nitric oxide and nitrite ion.[85-86] In this colorimetric sensing process chemical transformation on the diamine groups takes place to form heterocyclic compound shown in figure 1.16. The heterocyclic compound formation is very specific by nitric acid in presence of oxygen or with nitrite ions and an acid in aqeous medium.

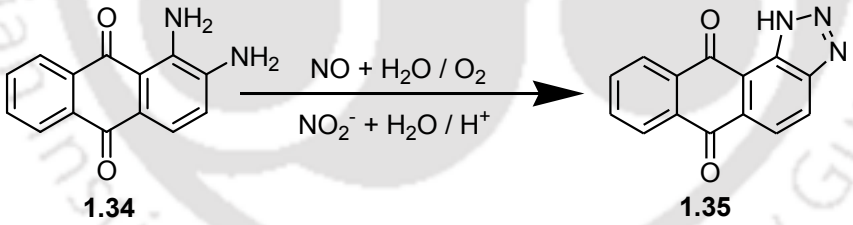

Figure 1.16: Reaction in colorimetric detections of nitric oxide and nitrate anion.

1,4-Di-(2-aminoethylamino)anthraquinone urea or thiourea are used todistinguish isomers of dicarboxylate anions.[87] Selective colour changes of receptors (**1.36a-b**) in presence of maleate and fumarate anions in dimethylsulphoxide/water were observed by naked eye.

TH-1303_09612216

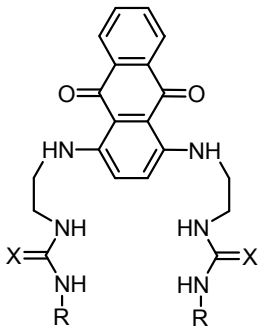

X = S, R = p-NO_2-naphthyl **(1.36a)**
X = O, R = P-NO_2-phenyl **(1.36b)**

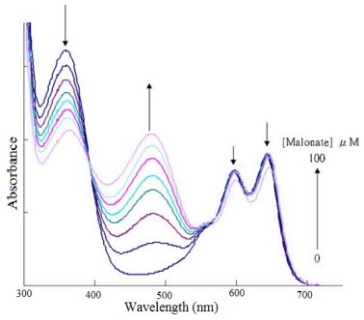

(a) (b)

Figure 1.17: (a) Urea/thiourea based anthraquinone receptors for dicarboxylic acids and (b) Changes of UV-visible absorptions of **1.36a** in dimethylsulphoxide on the addition of malonate anion.

When concentration of maleate was increased, a new absorption band at 480 nm was formed, whose intensity was substantially enhanced on increase in concentration of maleate anions. In contrast, a similar experiment with fumarate salt showed no significant change in UV-visible spectra. Different colors observed with maleate and fumarate was related regiochemistry of the receptor. Maleate anion has a *cis* configuration perfectly fit between the thiourea parts of receptor inducing a conformation change in the receptor as shown in figure 1.18.

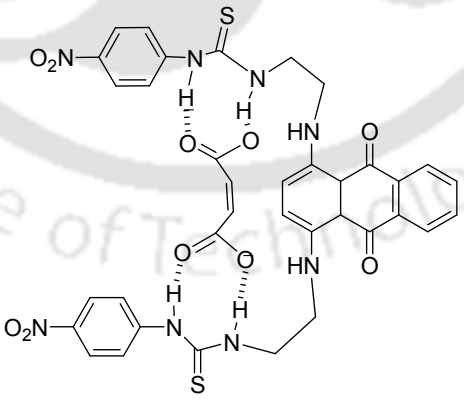

Figure 1.18: Binding of **1.36a** with maleate anion.

In contrast, fumarate anion has a *trans* geometry which cannot form 1:1 host-guest complex to hold two thiourea units from same host molecule. Receptor **1.36b** is a urea

TH-1303_09612216

based molecule changes color from blue to green with maleate and blue to pink color with fumarate respectively. Hydrogen bond host-guest complex affects electronic properties of the chromophore of parent host molecule which results in the observed color changes.

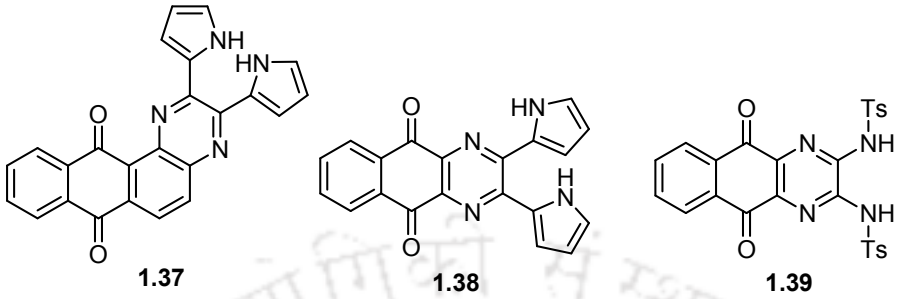

Figure 1.19: Anthraquinone based and diazaanthraquinone based anion receptors.

To make efficient receptors for ions anthraquinone derivatives are modified by connecting additional heterocyclic rings or by incorporating hetero atoms to anthraquinone skeleton. Examples of such anion receptors are shown in figure 1.19. UV-visible spectroscopy and visual inspection of solutions of **1.37-1.39** after addition of an anion such as fluoride, cyanide, acetate or pyrophosphate ions show dramatic changes in color.[88] Based on the redox properties of such compounds coupled with fluorescence properties of the oxidized and reduced states reversible switch is developed. Fluorescence emission study indicated that *N*-dansylcarbazoloquinone shows highly reversible increase and decrease in emission relating a molecular switching property. By adding sodium borohydride to a solution of compound **1.40** emissions can be generated and allowing aerial oxidation of compound **1.41** the quenching of emission can be achieved as illustrated in Scheme 1.7.[89]

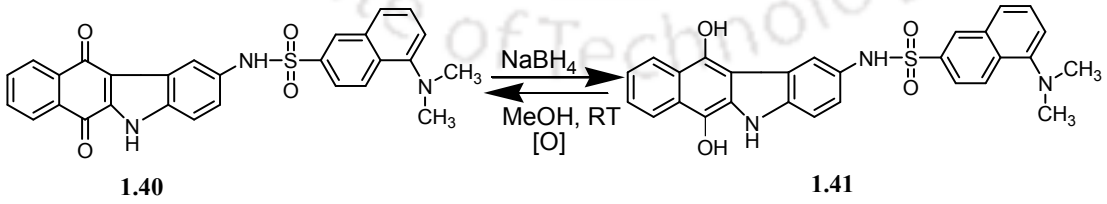

1.40 **1.41**

Fluorescence *OFF* Fluorescence *ON*

Scheme 1.7: Fluorescence switch off by redox reaction.

TH-1303_09612216

In this example it was shown that the fluorescence emission of **1.40** on excitation at 336 nm of the dansyl group was totally quenched but could be instantly generated after reduction of the quinone to dihydroxy compound by chemical reduction of the quinone **1.41** with sodium borohydride. These are some of the examples of quinonic derivates which act as receptors for anions. They behave differently in different pH, redox conditions as well as photochemical condition. Thus there is a large scope to develop new quinoidal scaffolds for detections of anions and also understand their selectivity towards anion binding.

1.5.2: **Quinone and their derivatives in cation sensing**

2-Methyl-1,4-naphthoquinone based chemosensors selectively detect copper (II) ions in the presence of other metal salts.This is attributed to the binding of copper (II) ions to the amine which induces deprotonation of N-H to cause the observed color change.

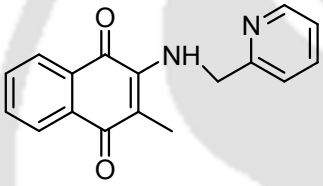

1.42

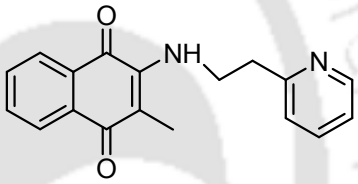

1.43

Figure 1.20: Chemosensors for copper (II) ions.

Chemosensors **1.42** and **1.43** underwent color change from orange to dark blue with a 168 nm red shift in the presence of copper (II) ions. In the case of other divalent metal ions, such as calcium, cadmium, cobalt, iron, mercury, magnesium, manganese, nickel and zinc ions insignificant color changes were observed. Similarly, 9,10-anthraquinone based 2-aminothiophenol derived compounds **1.44a** and **1.44b** were found to be selective copper (II) ions .[91]

TH-1303_09612216

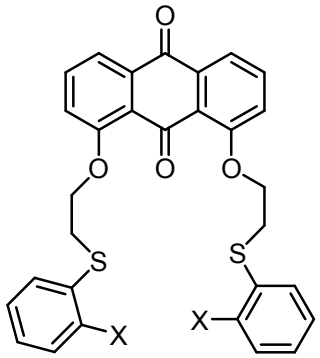

1.44a X = NH_2
1.44b X = H

Figure 1.21: 9,10-Anthraquinone based chemosensors.

Gradual addition of divalent copper ions to a solution of **1.44** shows a new absorption in the region 520 - 800 nm. Color change from light yellow for **1.44b** to brown was observed. Addition of divalent cations of nickel, cadmium, zinc, silver, lead and mercury do not affect the absorption spectrum of **1.44b**. The chromophores **1.44a** lacks the NH_2 group, hence it does not show change in its absorption spectrum on addition of different metal salts. This clears indicates that the role of NH_2, it presence is a requirement to form chelated complex to show the change in color by this series of receptor. Anthraquinonoidalcalix[4]arene (figure 1.22a) preferentially recognizes zinc (II) ions.[92] Its ability to recognize zinc (II) ion was studied by using UV-Vis absorbance, fluorescence and ^{1}H-NMR spectroscopy. The receptor **1.45** showed excellent selectivity for zinc (II) ions over other transition metal ions to quench fluorescence emission as illustrated in figure 1.22b.

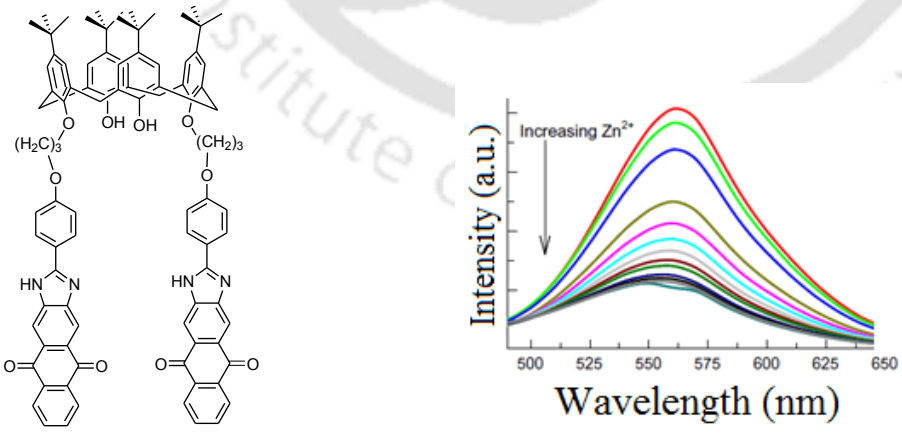

(a) (b)

Figure 1.22: (a) Receptor **1.45**. (b) Quenching of fluorescence of **1.45** by zinc (II) ions.

TH-1303_09612216

From these examples it is clear that the quinone connected to functional units are capable of selectively binding to different cations, enable them to cause drastic change in the inherent optical or related properties of the quinoidal part. Such changes make them useful analyte.

1.6: Quinones in supramolecular metal complexes

Highly organized structures of quinones with and without metal ions can be built partially or completely involving supramolecular interactions.[93] Quinones are capable of engaging in charge-transfer complexes and intermolecular interactions through the formation of hydrogen bonds.[94-95] Complexation of a metal to quinoidal π-system significantly influence the proton and electron transfer, and results in the formation of semiquinone and other oxidation products.[96] The ability of a quiniodal system to coordinate a metal through the π-system such as in hydroquinone and catechol constitutes a basis to develop organometallic coordination networks.[97-103] A large numbers of examples of quinone metal complexes with metal-carbon bonds are available. The η^4-type of metal carbonyl complexes such as **1.48** and **1.51** are often encountered in organometallic chemistry. Such complexes are formed form the corresponding η^6-types of complexes of parent hydroquinone derivatives.

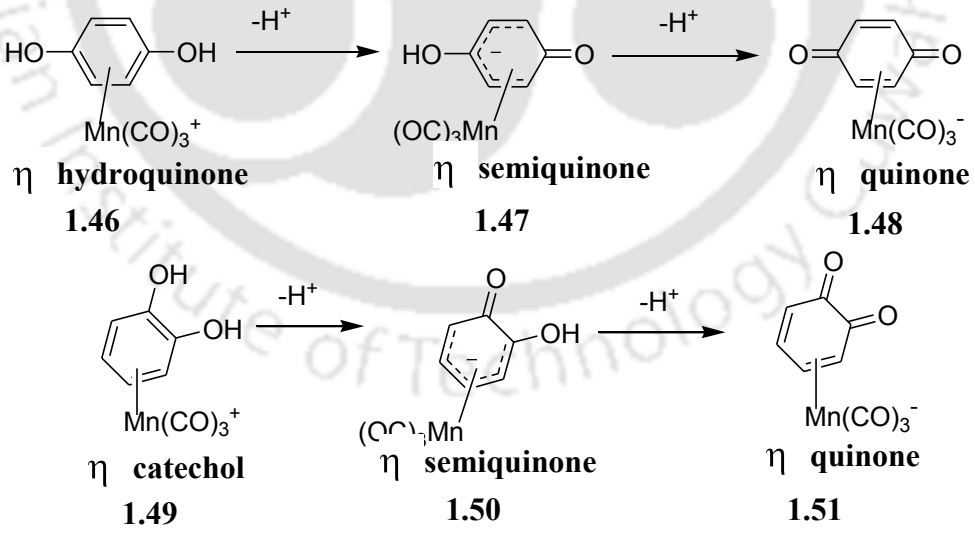

Scheme 1.8: Metal-carbon bonded quinone complexes.

Hydroquinone derivatives readily transform to semiquinone derivatives and further transform to quinone complexes. Two representative cases are shown in Scheme 1.8. In

TH-1303_09612216

the case of the neutral η^5-semiquinone complex **1.47** has a linear polymeric array-like structure dictated by strong intermolecular hydrogen bonds. Similar catechol analogue **1.50** exists as discrete hydrogen-bonded dimer. X-ray structural studies on the semiquinone derivatives have shown that the semiquinone complexes possess strong hydrogen-bond interactions as shown in figure1.23.

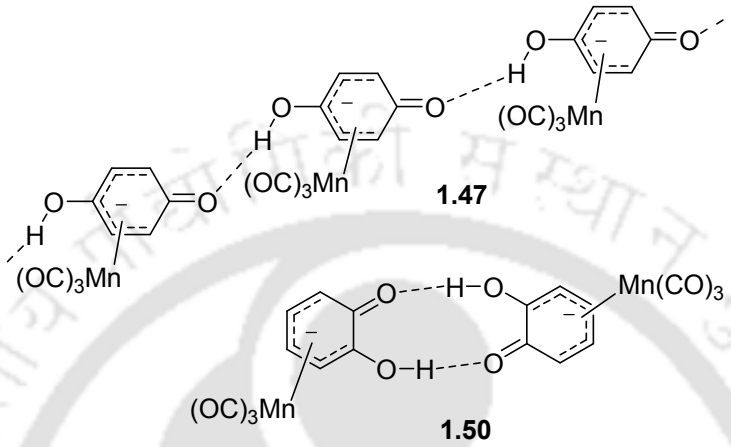

Figure 1.23: Hydrogen-bonds in organometallic semi-quinone complexes **1.47** and **1.50**.

On the other hand, there are many examples of metal complexes in which quinone act as bridge by coordinating through the carbonyl oxygen atoms. For example, a *p*-benzoquinone complex **1.52**serves as a bifunctional ligand with appropriate metal ions by *σ*-bonding through both the oxygen atoms of carbonyls[105] resulting in formation of neutral coordination networks **1.52** as shown in figure 1.24.

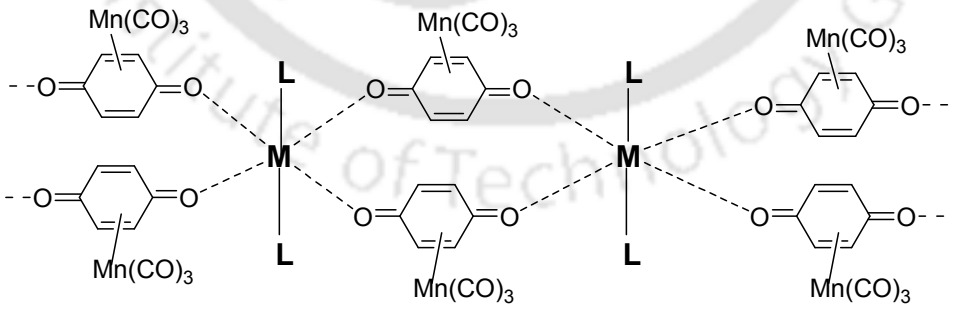

1.52 (M = Mn, Co, Cd; L = DMSO, Py)

Figure 1.24: Metal complexes with bridging quinones.

Ligands are prepared by introducing functional legating sites to bind metal ions. Such ligands are of interest as they are useful to understand electron transfer reactions. For

TH-1303_09612216

examples, 1-(1-((2,6-diisopropylphenyl)imino)ethyl)-1*H*-benzo[*f*]indazole-4,9-dione (**La**) and 2-(1-((2,6-diisopropylphenyl)imino)ethyl)-2*H*-benzo[*f*]indazole-4,9-dione (**Lb**), and tforms copper(I) complexes $[Cu^{I}(Lb)_2](ClO_4)$ (**1.53a**) and $[Cu^{I}(Lb)(PPh_3)_2](ClO_4)$ (**1.53b**)[106] whose structures are shown in figure 1.25.

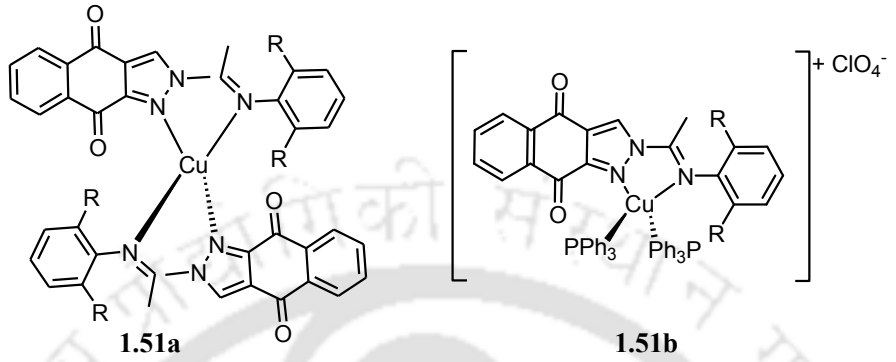

Figure 1.25: Copper (I) complex of **La**.

The crystal structures of the complexes correspond to mononuclear complexes in each case with the quinone ligands coordinated to the copper(I) in a distorted tetrahedral geometry. The coordination spheres of the complex **1.53a** are completed by four N atoms whereas in case of complex **1.53b** there are two N and two P atoms.

Platinum(II) complexes of 3-(aminomethyl)naphthaquinone abriviatted as amq were synthesized and characterized by determining crystal structure and cytotoxic activities of the complexes was studied.[107] The complexes *cis*-$[Pt(amq)(NH_3)_2]NO_3$ (**1.54a**) the deprotonated form of the ligand which coordinates *via* the nitrogen atoms, and the other two positions around the platinum (II) ion are completed with NH_3 ligands.

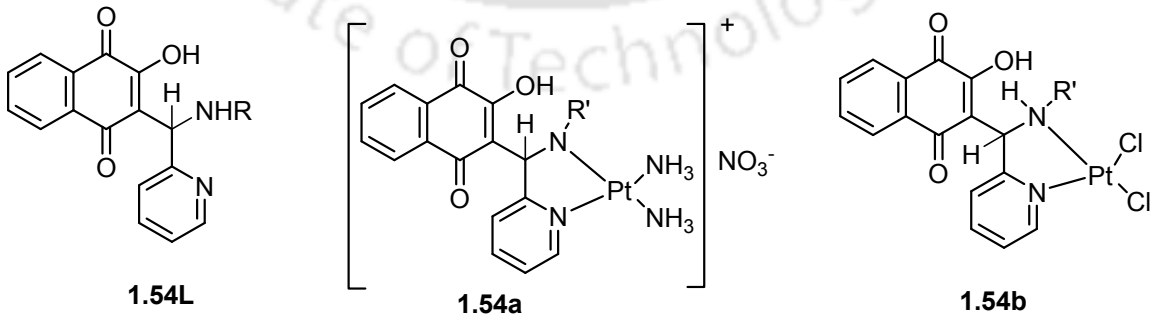

Figure 1.26: The ligand **1.54L** and platinum (II) complexes of **1.54b** and **1.54c**.

TH-1303_09612216

Mixed ligands complexes containing quinoidal ligand as one of the constituent have been studied. Metal complexes with 4,4',7,7'-tetra-tertbutyl-2,2'-bi-1,3-benzodithiole-5,5',6,6'-tetrone ligand (tet) are examples of such mixed ligands complexes.[108] For example, the reaction of $M(hfac)_3.2H_2O$ (M = dysprosium (III) and gadolinium (III) ions, $hfac^-$ = 1,1,1,5,5,5-hexafluoroacetylacetonate anion) with tet yielded two dinuclear complexes $[M_2(hfac)_6(H_2O)_2(tet)]$ (**1.55a**) and $[M_2(hfac)_6(H_2O)_2(tet)]$ (**1.55b**). The structures of these complexes are shown in figure 1.27.

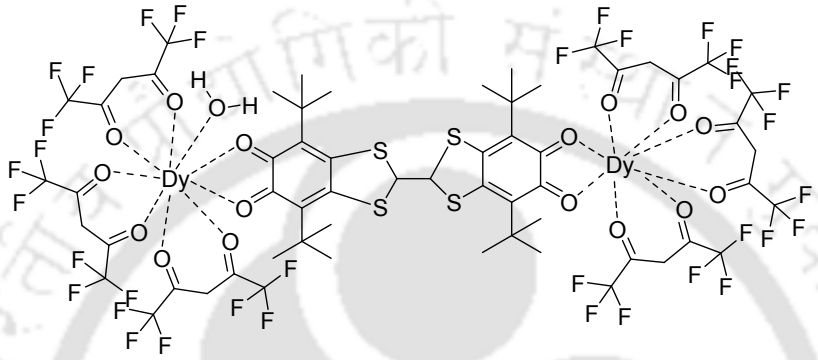

Figure 1.27: Structure of complex of **1.55a**.

1,2-Benzoquinone forms chelates with metal ions, which adopt three different forms namely, quinolate, semiquinolate and catecholate[109] (Scheme 1.9). Such complexes replicate the redox activity of the quinone ligands and their electronic configuration and delocalization of electron/s on the metal ions make them unique. They adopt different forms, which complicates their spectroscopic and magnetic properties.[110-112]

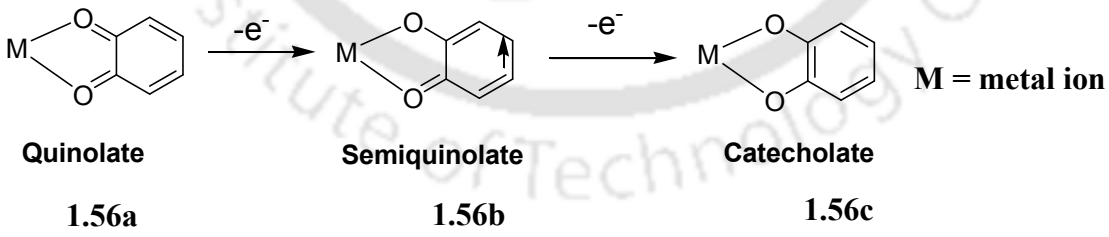

Scheme 1.9: Different types of interactions of o-quinone with metal ions.

Reaction of 3,5-di-*tert*-butyl-1,2-benzoquinone with $Co_2(CO)_8$ and with 2,2′-bipyridine (bpy) leads to a semi-quinone complex. This reaction gives $[Co^{3+}$(bpy)(3,5-DBSQ)(3,5-DBCat)],[113] **1.57b** (where 3,5-DBSQ = 3,5-di-*tert*-butyl-semiquinolate, 3,5-DBCat = 3,5-di-*tert*-butyl-catecholate). The structure of this complex is characterized by single X-ray

TH-1303_09612216

crystallography. From the electronic, electron paramagnetic resonance, ^{1}H-NMR spectra and magnetic characterization redox equilibrium between cobalt (III) and cobalt (II) was shown. This type of equillibrium is called as valence tautomerism[114] which is shown in Scheme 1.10.

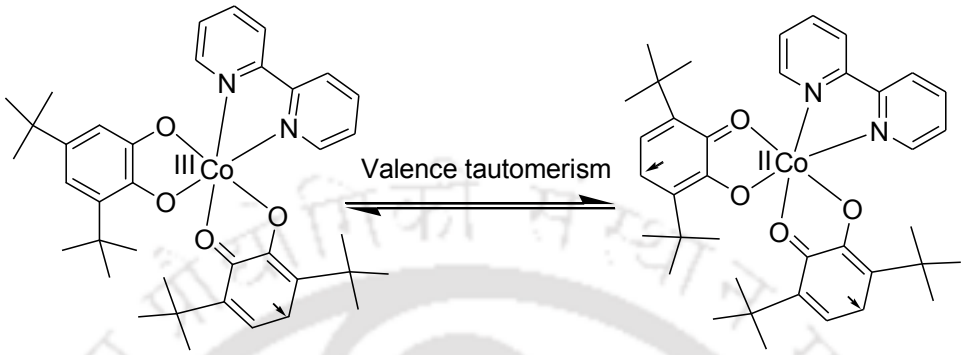

1.57a **1.57b**

Scheme 1.10: Valence tautomerism in cobalt quinone complex.

The valence tautomerism was observed in similar cobalt complexe (**1.58**)[115] with 2-methyl-3-hydroxy-1,4-naphthoquinone. The structure of a 2,2'-bipyridine containing the hydroxyquinone is shown in figure 1.28.

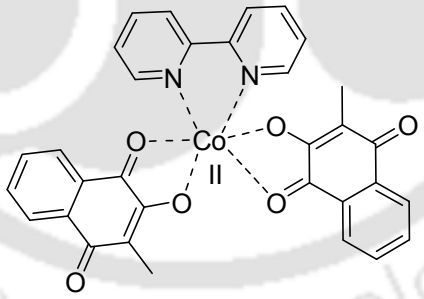

Figure 1.28: Complex **1.58** which shows valence tautomerism.

A series of novel mononuclear copper (II) complexes of chloranilic acid also having 2,2'-bipyridine ligand/s were prepared and structurally characterized.[116] The complex **1.59** has square-planar geometry, **1.60** has square-pyramidal geometry whereas the complex **1.61** has an octahedral geometry around the respective copper ion.

TH-1303_09612216

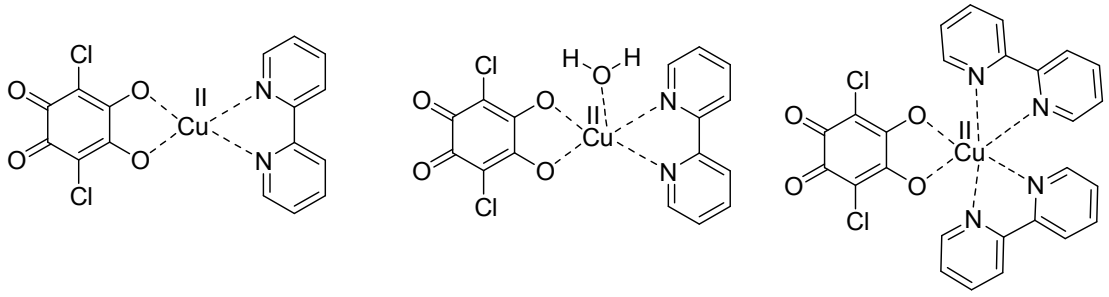

1.59 **1.60** **1.61**

Figure 1.29: Copper (II) complexes of chloranilic acid.

From these descriptions it is clear that the quinone metal complexes formed by direct interactions of metal ion with carbon skeleton form metal-olefinic complexes and through carbonyl group coordinating to a metal ion forms M-O bonded metal complexes. On the other hand, the attachment of ligating sites to the quinone units also helps to develop large numbers of metal quinone complexes with wide range of variations of environments around metal ions.

1.7: Pharmaceutical application of quinone derivatives

As mentioned earlier quinone derivatives are well known for their pharmacological and therapeutic uses,[117] which includes the antifungal,[118-119] antibacterial,[120-123] antivirial,[124] anticancer[13-16,125-135]activities. For example, annthracycline antibiotics are highly functionalized glycosides containing quinoidal chromophores. These compounds currently constitute the second largest class of anticancer drugs in clinical application.[136-137] Natural hydoxyquinones have large structural diversities. Lawsone (**1.62**) is a simple hydroxynaphthoquinone. There are also naturally occurring compounds such as conocurvone (**1.63**) which is a potential anti-HIV agent. It has three hydroxynaphthoquinone units conncted each other,thus possessing a relatively complicated structure. [138-139]

TH-1303_09612216

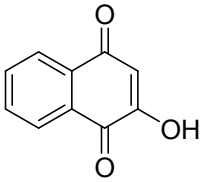

1.62

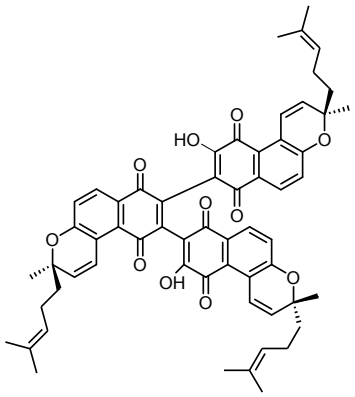

1.63

Some natural quinones, such as kinamycins A, B, C, D, (**1.64a-d**) and streptonigrin (**1.65**) are used as antibiotic and antitumor agents. Recently, during screening of natural products

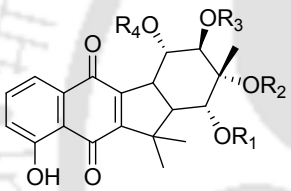

1.64a-d

R_1 = H, R_2 = Ac, R_3 = Ac, R_4 = Ac (**1.64a**)
R_1 = H, R_2 = Ac, R_3 = H, R_4 = H (**1.64b**)
R_1 = Ac, R_2 = H, R_3 = Ac, R_4 = Ac (**1.64c**)
R_1 = Ac, R_2 =H, R_3 = Ac, R_4 = H (**1.64d**)

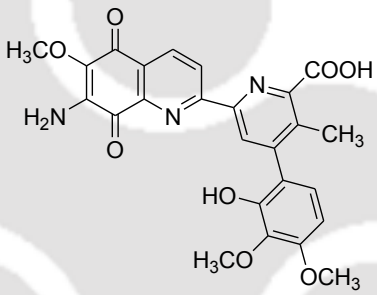

1.65

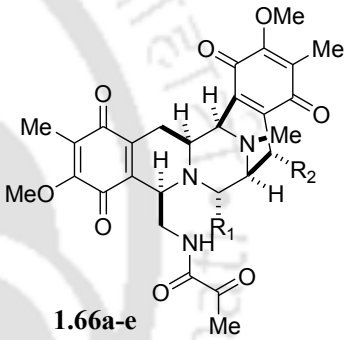

1.66a-e

R_1 = CN, R_2 = H (**1.66a**)
R_1 = H, R_2 = H (**1.66b**)
R_1 = H, R_2 = OMe (**1.66c**)
R_1 = CN R_2 =OH (**1.66d**)
R_1 = OH, R_2 =H (**1.66e**)

for inhibition against the HIV virus, streptonigrin tested positive as an inhibitor towards the reverse transcriptase of HIV.[140] Saframycins A, B, C, D and E (**1.66a-e**) are isolated from *Strepto-myces lavendulae*[141] display antitumor activities.[142] In the following two sub sections, we are discussing about biological importance of two quinone derivatives namely anthracyclines and calphostins.

1.7a: **Anthracyclines and its synthetic analogues**

Anthracylines are naturally occurring compounds having anthraquinone part embedded in their structures (Figure 1.30). Anthracyclines are the most effective chemotherapeutic agents. They bind to the C1 domain of activates Protein kinase C (PKC). Protein kinase C

TH-1303_09612216

(PKC) is a family of serine/threonine kinases which are the major cellular receptor for diacylglycerol (DAG) and phorbolesters. DAG dependent PKC activation controls several cellular pathways including tumor promotion, apoptosis, differentiation and cell growth. Disregulations of these cellular pathways cause several diseases including cancer, diabetes, stroke, heart failure and Alzheimer's disease. Therefore, PKC is an attractive drug target for the treatment of cancer and other diseases.

Anthracyclines are isolated from pigment-producing *Streptomyces peucetiusand* known as doxorubicin (DOX, **1.67**) and daunorubicin (DNR, **1.68**).[143] It is well documented that, doxorubicin (DOX) induces antitumor effect through DNA interaction and topoisomerase II inhibition.[144-145] DOX and DNR contains a glyconic and sugar moieties. Only difference between the DOX and DNR is side chain of DOX ends with a primary alcohol, whereas DNR ends are with methyl groups. This minor difference has important consequences on the biological activity of DOX and DNR. DOX is an essential component for treatment of breast cancer, childhood solid tumors, soft tissue sarcomas, and aggressive lymphomas, whereas, DNR shows activity in acute lymphoblastic or myeloblasticleukemias. Doxorubicin (**1.67**) does not effectively bind to PKC because of its localized hydrophilicity in the nucleus.[145] When 3-amino group of daunosamine aminoglycoside is substituted with a benzyl group and C14 hydroxy group at C14 is acylated, forms new hydrophobic derivatives of doxorubicin (**1.67**). Compound **1.67** shows strong binding with PKC but weak binding with DNA. This controls resistance power of cancer cells to DOX and doxorubicin-induced cardiotoxicity. A semisynthetic *N*-benzyladriamycin-14-valerate (**1.69**, Figure 1.30)[146] showed weak interactions with DNA and showed minor inhibitor activity on topoisomerase II. Additionally, it showed a weak interaction with C1 domain of PKC but AD198 (**1.69**) is effective *in vitro* against several cancer cell lines and its antitumor activity is superior to DOX (**1.67**).[147] The binding orientation of AD198 (**1.68**) was explained by proposing theoretical models based on the crystal structure of the PKCδ C1b domain. It revealed that, AD198 (**1.69**) has different orientations compared to phorbol ester.[168]

TH-1303_09612216

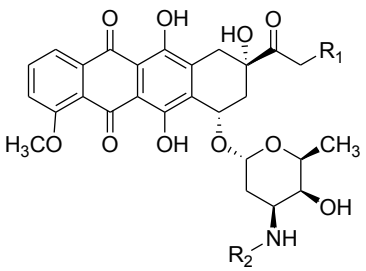

R_1 = OH, R_2 = H (Doxorubicin/DOX, **1.67**)
R_1 = H, R_2 = H (Daunorubicin/-mycin, **1.68**)

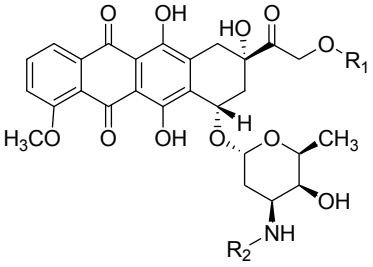

R_1 = $CO(CH_2)_3CH_3$, R_2 = Bn (AD 198,**1.69**)
R_1 = $CO(CH_2)_2CH_3$, R_2 = Bn (AD 444, **1.70**)
R_1 = CO*t*-Bu, R_2 = Bn (AD 445, **1.71**)
R_1 = H, R_2 = Bn (AD 288, **1.72**)
R_1 = $CO(CH_2)_3CH_3$, R_2 = $COCF_3$ (Valrubicin, AD 32, (**1.73**)
R_1 = H, R_2 = $COCF_3$ (AD 41, **1.74**)

Figure 1.30: Structures of natural anthracyclines (**1.67** and **1.68**) and synthetic anthracyclines (**1.69-1.674**).

Several semisynthetic anthracycline derivatives were prepared including AD 444 (**1.71**), AD 445 (**1.72**), *N*-benzyladriamycin (AD 288, **1.71**), *N*-trifluoroacetyladriamycin-14-valerate (AD 32, **1.73**) and *N*-trifluoroacetyladriamycin (AD 41, **1.74**) as shown in the figure 1.30. These compounds were targeted for PKC by interacting with C1 domain.[145] Among these valrubicin (AD 32, **1.74**) showed similar PKC inhibitory properties to AD 198 (**1.69**).[149] Valrubicin (**1.74**) is in the final phase trial for blood cancer.[150]

1.7b: **Calphostins and its synthetic analogues**

The calphostins are perylenequinone natural products which is isolated from the phytoparasitic mold *Cladosporiumcladosporioides* (Figure 1.31).[151] The calphostins are potent and specific inhibitors of PKC and exhibit strong cytotoxic activity, but do not show antifungal or antibiotic activities.[152-153] Calphostin C **1.75** selectively binds the C1 regulatory domain of PKC and exhibits > 10^3-fold selectivity in inhibition of PKC (IC_{50} = 0.05µg/mL) in compared with AMP-dependent kinase or tyrosine kinase.[154] It was suggested that calphostins C **1.75** bind with C1 domain of PKC in a similar way that of anthracyclines.[155]

TH-1303_09612216

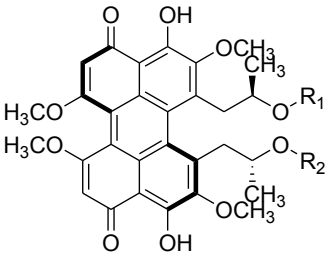

R_1 = Bz, R_2 = COO(4-OH-Ph) (Calphostin C, **1.75**)
R_1 = H, R_2 = H (Calphostin D, **1.76**)

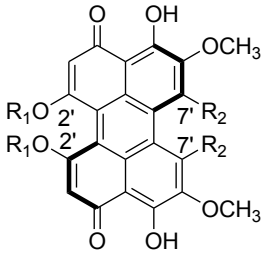

R_1 = Me, R_2 = (2*R*-OH)propyl (ent-pleicrome,**1.77**)
R_1 = isopropyl, R_2 = (2*R*-OH)propyl (**1.78**)
R_1 = *n*-propyl, R_2 = (2*R*-OH)propyl (**1.79**)
R_1 = Me, R_2 = *n*-propyl (**1.80**)

Figure 1.31: Structures of natural calphostins (**1.75** and **1.76**) and synthetic analogues (**1.77-1.80**).

Calphostin C **1.75** was reported to show proapoptotic effects in numerous cancer cell lines and it is a useful candidate for photodynamic cancer therapy.[156] In order to study the binding affinity and biding orientation of calphostin derivatives with PKC C1 domain, *ent*-pleichrome an atropisomer of calphostin D (**1.76**) were designed and synthesised.[157] The *bis*-iso-propyl and *bis*-n-propyl derivatives of Calphostin **1.78** and **1.79** and these two compounds gave better binding affinities with rat brain PKC isozymes (IC_{50} = 0.8, and 1.5 μM) than the **1.77** (IC_{50} = 3.5 μM). The substitution on 2-hydroxypropyl groups at C7 and C7' (R_2 in **1.78**) with *n*-propyl group resulted calphostin derivative **1.79** shows better binding affinity (IC_{50} = 0.4 μM) compared to natural calphostins.[158] From this discussion it is clear that the modification of the structural analogues of anticancer medicines changes their activities, hence there are scopes to develop new molecules as functional models for drug-substrate interactions.

1.7: **Electron transfer in quinones and their derivatives**

Biological photosynthesis process is characterized by a series of electron transfer events in the reaction center which produces long-lived charge-separated states.[159] The initial step in this series of electron transfer processes is transfer of an electron from one photoexcited chlorophyll to an adjacent quinone.[160] A large numbers of porphyrin-quinone systems are developed for understanding photo-induced charge separation in photosynthetic reaction centers. Most of the model compounds consist of porphyrin molecules covalently linked to electron acceptor quinones.[161-163] Spectroscopic study on these materials have revealed the electron-transfer rates depends on donor-acceptor coupling, solvent and temperature.

TH-1303_09612216

Electron transfer in non-covalently bound quinone system has been explored in zinc porphyrin complexes. For example, a calix[4]arene substituted zinc (II) metalloporphyrin (**1.81**) binds benzoquinone through hydrogen bonds of two phenolic O-H groups serving as a tweezer with carbonyl of quinone was studied.[164] In this case spectroscopic evidences on through space electron transfer were observed.

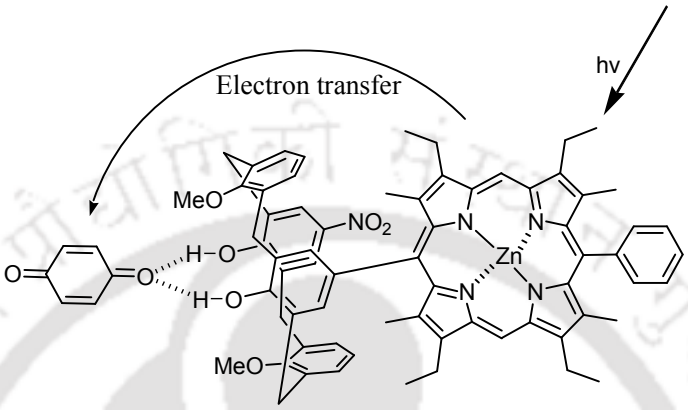

Figure 1.32: Calix[4]arene substituted zinc (II) metalloporphyrin bound to benzoquinone receptor (**1.81**).

The electron transfer in the quinone-linked zinc porphyrin with a flexible peptide spacer (**1.82**) was studied by ^{1}H-NMR and fluorescence spectroscopy.[165] Such study indicated that the flexibility of peptide group contributes to the electron transfer process.

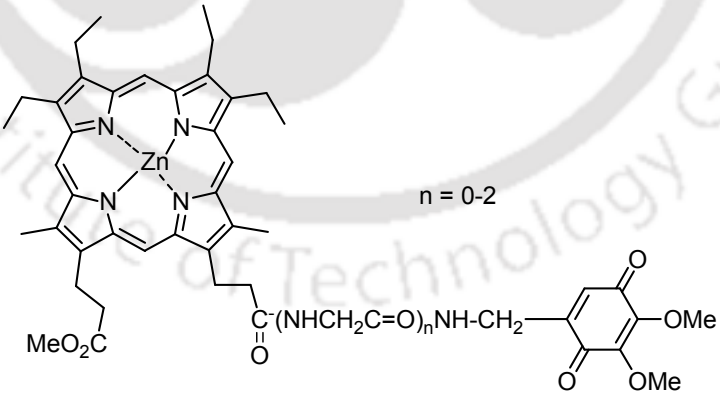

Figure 1.33: Quinone-linked zinc-porphyrin with flexible peptide spacer (**1.82**).

Covalently linked quinone to porphyrin exhibited enhanced fluorescence on interaction with hydroquinone (**1.83**).[166] This occurs due to the unfavorable condition for an electron transfer process between the singlets excited porphyrin and quinone-hydroquinone entity.

TH-1303_09612216

Addition of 1,4-hydroquinone to a solution of **1.83** showed a drastic enhancement of the fluorescence intensity at 652 nm and 720 nm.

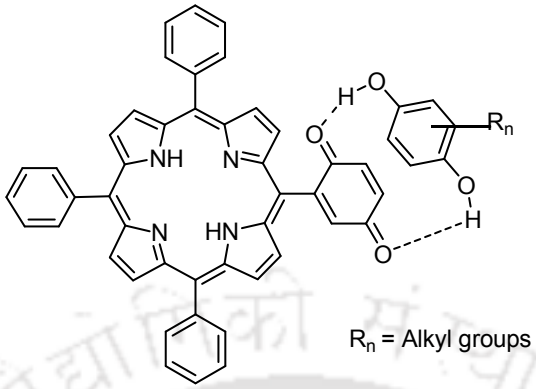

Figure 1.34: Adduct of porphyrin linked quinone receptor with hydroquinone (**1.83**).

1.7.1: **Quinone and their derivatives in photosynthesis**

Quinone derivatives play important role in biological systems such as respiration and photosynthesis.[167-170] The functional and structural protein units participating in photosynthesis is called photosystems. Their function is to absorb light and transfer energy and electron. The reaction centers in the photosystem are enzymes that use light to reduce molecules. Two families of reaction centers are present in the photosystems namely, photosystem I (PS I) and photosystem II (PS II). There are differentiated by the response to light by which they are reactive namely; photosystem I (PS I) 700 nm and photosystem II (PS II) 680 nm in chloroplasts. Photosynthesis is initiated by a series of photochemical reactions in which light energy absorbed by chlorophylls is converted to redox energy that is used to power a series of metabolic reactions.[171-178] The reactions by light absorption in photosynthetic organisms can be divided into two separate processes. In the first step, light is absorbed by antennae, which are proteins that bind several chlorophyll molecules. In many cases, a large numbers of such proteins are available to trap light energy. Chlorophylls absorb light and pass on this energy to other adjacent pigments in a process called exciton transfer or resonance energy transfer. Structural and organization of antennae proteins reveal that these proteins are ligated to chlorophylls in highly organized manner. The photosynthetic reaction centers of photosystem I and II of oxygenic organisms such as cyanobacteria, red and green algae, higher plants and in photosynthetic bacteria, contain a single photosystem. There are multi-subunit membrane

TH-1303_09612216

protein complexes that function as photochemical devices. Photosystem II contains two quinones, one function as one-electron acceptor and other functions as two-electron and two-proton accumulator. In photosystem II, plastoquinone-9 (PQ-9) serves the role of mobile quinone, which shuttles electrons to Photosystem I *via* the cytochrome complex.

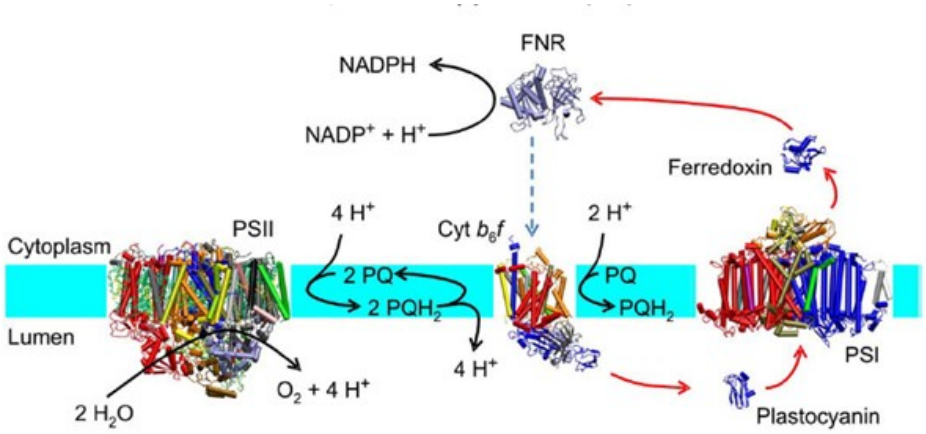

Scheme 1.8: Role of quinone systems in photosynthesis process.

The reaction centers of photosystem I of cyanobacteria and green plants, contain two bound phylloquinone (**1.7**). Thus, phylloquinone (**1.7**) is a focus of structure function relationships due to its central role in electron transfer.[179-188] In this context, the light-induced[189-193] reduction of quinoidal units in photosystem II is shown in Scheme 1.8. The core of photosystem II has water and plastoquinone oxidoreductase. The photosystem II catalyzes the light-induced electron transfer from water to plastoquinone. These are accompanied by net transport of protons from the cytoplasm to the lumen and accompany the production of molecular oxygen and also release of the plastoquinol into the membrane phase.

1.8.2: **Quinone derivatives in environment**

Quinones interact with biological systems to promote inflammatory, anticancer actions and also induce toxicities.[194-195] Naphthoquinone derivatives are of a particular interest for environmental science because of their prevalence as natural products and their presence in the atmosphere as by-products of fuel and tobacco combustion.[196-197] For example, 1,2- and 1,4-naphthoquinones (**1.3** and **1.4**) are toxic metabolites of naphthalene and these are also major polynuclear aromatic hydrocarbons present in ambient air. Quinones are formed by direct and indirect ozone-based processes in which polynuclear aromatic hydrocarbons are adsorbed on particle surfaces. They are oxidized by ozone or

TH-1303_09612216

by ozone-based oxidized alkenes derivative.[198-201] There are differences in reactivities between particle bound and vapour phase quinones each of which could also cause toxicity in different ways. Quinones in vapour phase have ready access to the lung components, whereas particle exposure varies with size and content. Studies with radiolabeled benzo[a]pyrene-7-8-dione (**1.76**) have shown that when it is in the particle bound state to diesel exhaust particles, this poly aromatic hydrocarbon (PAH) persists for protracted periods relative to free vapour phase PAH.[202-204] Quinone and their derivatives can easily get distributed to cellular components by dissociation from the particles in accordance with their partition characteristics,

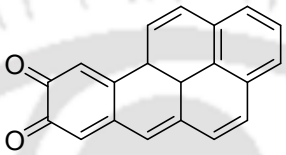

Figure 1.35: Benzo[*a*]pyrene-7-8-dione (**1.84**).

1.9: **Scope of the present work**

From foregoing discussion it is clear that quinone derivatives are extensively studied for various applications. Various quinone derivatives undergo photochemical reactions or photoinduced single electron transfer to show varieties of electron transfer properties.[205-207] Metal complexes of 1,4-naphthoquinone-SALEN[205]derivatives shown in figure 1.36 are used for multiple electron/proton transfer reactions.

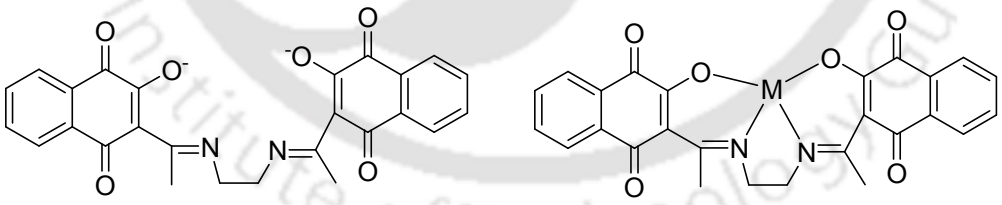

Figure 1.36: A salene-based quinoidal ligand and its nickel and copper (II) complexes.

Metal complexes[208] of flexible hinge-like ligand 2,2′-bi-(3-hydroxy-1,4-naphthoquinone) **1.86** (**1.86** is abbreviated as H_2bhnq) adopt various structures depending on metal ions and ancillary ligands. Ligand H_2bhnq has two hydroxy-naphthoquinones linked by a single bond which allows rotation about this single bond. Thus, ligand shows conformational flexibility. There are at least four possible architectures with skewed

TH-1303_09612216

conformations which would lead zigzag, helix, square and dimer structures. All these architectures are accessible in different metal complexes. In the case of copper (II) complex with $bhnq^{2-}$ the chelating $bhnq^{2-}$ ions bridge copper (II) to form one-dimensional zigzag chain **1.86a**. Cobalt (II) and zinc (II) ions in aqeous tetrahdrofuran (THF) form one dimensional helical chain **1.86b-c**. Nickel (II) ions form cyclic tetramers **1.86d**; whereas dimer **1.86e** is formed by the reaction of zinc (II) ions and bhnq in methanol.

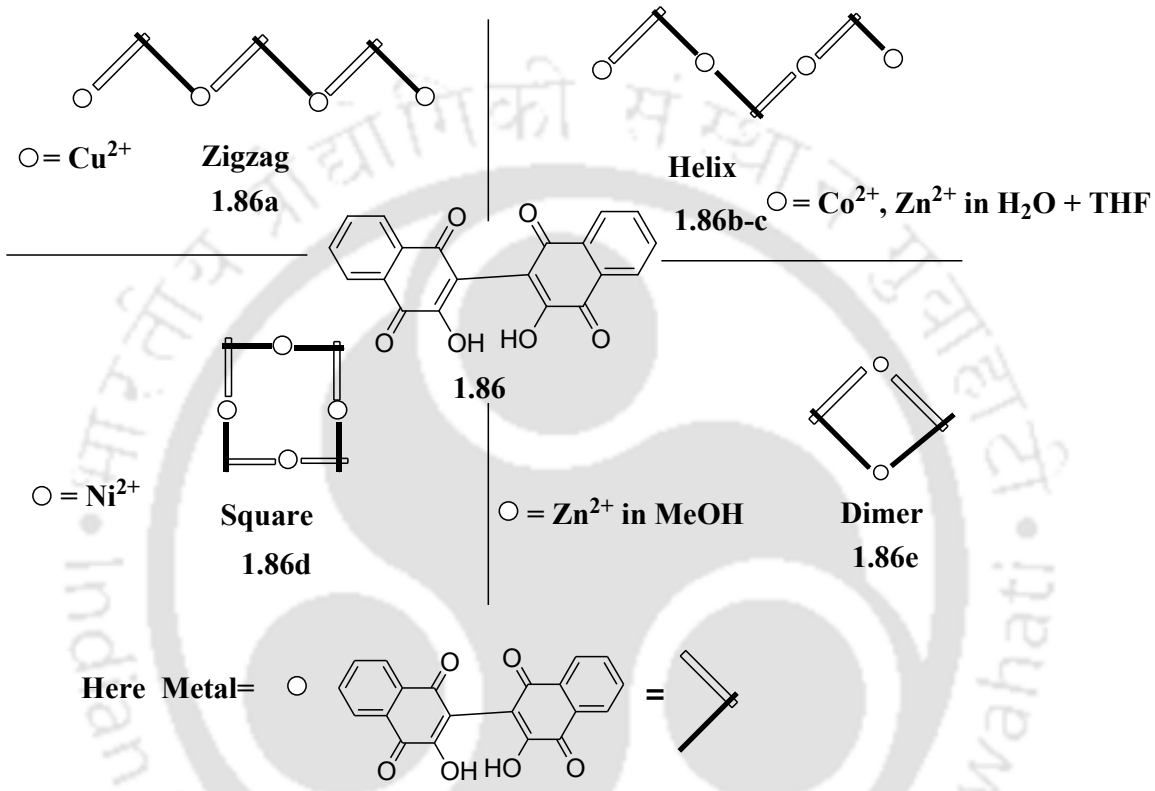

Scheme 1.9: Various metal metal complexes of 2,2′-bi-(3-hydroxy-1,4-naphthoquinone).

The metal-organic frameworks of quinone and their derivatives are recognized as photoluminescent material and selective gas adsorbent. Besides there are many structurally simple quinone derivatives such as Thymoquinone, Mansonone B and Rolyleanone used in pharmaceutical applications.[209] Thus, there is a definite scope to explore their analogous system to utilize as drugs.

TH-1303_09612216

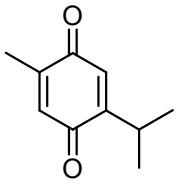

1.87

Thymoquinone

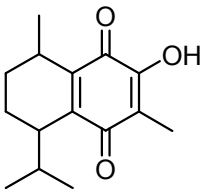

1.88

Mansonone B

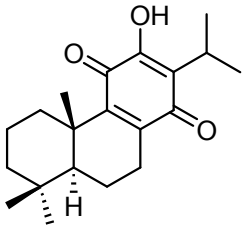

1.89

Royleanone

Supramolecular features of quinone derivatives for molecular recognition and host-guest chemistry is well sought after. Looking at the potential of the quinone derivatives as prospect for substrate binding with interesting photochemical and photophysical properties, there is need to develop new materials and self-assemblies with novel properties. The ease of synthetic modification on quinones make them amenable to built for receptors for anion and cation sensing, molecular recognition and host-guest chemistry and coordination chemistry. Hence, ample scopes to synthesize and understand properties of C-N and C-S bonded compounds such as **1.90-1.94** exists.

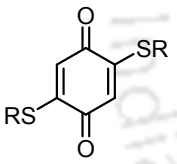

1.90

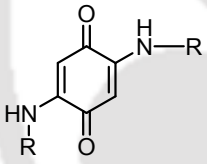

1.91

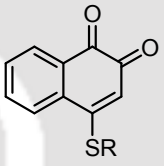

1.92

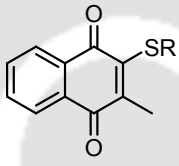

1.93

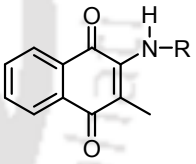

1.94

In the present work, we have synthesized and characterised various quinone derivatives through a synthetic method which maintains atom economy. In each reaction two components are reacted together without additional reagents. A variety of aspects of quinoidal chemistry including host-guest compounds, self-assemblies, polymorphism, molecular recognition as well as their photophysical properties and protein binding properties of different quinone derivatives are taken up in the course of work described in the subsequent chapters of the thesis.

References:

1. (a) A. D. McNaught and A. Wilkinson, IUPAC. *Compendium of Chemical Terminology, 2nd ed.* (the "Gold Book"), *Blackwell Scientific Publications*, Oxford, UK, **1997**. (b) S. Patai, *The chemistry of the Quinonoid Compounds*, *John*

TH-1303_09612216

Wiley and Sons, New York, **1974**. (c) R. H. Thomson, *Naturally Occurring Quinones*, 2nd *ed*. *Academic press*, London, **1971**.

2. F. Löbermann, L. Weisheit, and D. Trauner, *Org. Lett.*, **2013**, 15, 4324.
3. M. Mure, *Acc. Chem. Res.*, **2004**, 37,131.
4. R. Hielscher, M. Yegres, M. Voicescu, E. Gnandt, T. Friedrich, and P. Hellwig, *Biochemistry*, **2013**, 52, 8993.
5. L. M. Utschig, M. C. Thurnauer, D. M. Tiede and O. G. Poluektov, *Biochemistry,* **2005**, 44, 14131.
6. X. Lu, A. Altharawi, J. Gut, P. J. Rosenthal, and T. E. Long, *Med. Chem. Lett.*, **2012**, 3, 1029.
7. H. R. Nasiri, M. G. Madej, R. Panisch, M. Lafontaine, J. W. Bats, C. R. D. Lancaster, and H. Schwalbe, *J. Med. Chem.*, **2013**, 56, 9530.
8. S. Banerjee, S. Padhye, A. Azmi, Z. Wang, P. A. Phillp, O. Kucuk, F. H. Sarkar and R.M. Mohammad, *Nutr. Cancer*, **2010**, 62, 938.
9. K. Ngampong, P. R. Narathip, H. A. Komkrit and K. Boonsong, *Biosci. Biotechnol. Biochem.*, **2010**, 74, 1205.
10. V. Kuete, H. K. Wabo, K.O. Eyong, M. T. Feussi, B. Krusche, P. Tane, G. N. Folefoc and T. Efferth, *PLOSone*, **2011**, 6, e21762.
11. P. Pandya, Md. M. Islam, G. Sureshkumar, B. Jayaram and S. Kumar, *J. Chem. Sci*., **2010**, 122, 247.
12. N. J. Lajkiewicz, A. B. Cognetta, III, M. J. Niphakis, B. F. Cravatt, and J. A. Porco, Jr. *J. Am. Chem. Soc.*, **2014**, 136, 2659.
13. B. -S. Park, J. -R. Kim, S. -E. Lee, K. S. Kim, G. R. Takeoka, Y. -J. Ahn, and J. -H. Kim *J. Agric. Food Chem.*, **2005**, 53, 1152.
14. W. Knecht and M. Loffler, *FEBS Lett*., **2000**, 467, 27.
15. A. J. Kemp, S. D. Lyons and R. I. Christopherson, *J. Biol. Chem*., **1986**, 261, 14891.
16. Y. L. Hsu, C. Y. Cho, P. L. Kuo, Y. T. Huang and C. C. Lin, *J. Pharmacol. Exp. Ther*., **2006**, 318, 484.
17. G. Yin, T. Ren, Y. Rao, Y. Zhou, Z. Li, W. Shu, and A. Wu, *J. Org. Chem.*, **2013**, 78, 3132.
18. P. Kasaplar, C. R. -Escrich, and M. A. Pericàs *Org. Lett.*, **2013**, 15, 3498.

TH-1303_09612216

19. Ł. Albrecht, C. V. Gómez, C. B. Jacobsen and K. A. Jørgensen *Org. Lett.*, **2013**, 15, 3010.
20. B. J. D. Wright, J. Hartung, F. Peng, R. V. de Water, H. Liu, Q.-H. Tan, T.-C. Chou and S. J. Danishefsky, *J. Am. Chem. Soc.,* **2008**, 130, 16786.
21. A. Kuboki, C. Maeda, T. Arishige, K. Kuyama, M. Hamabata and S. Ohira, *Tetrahedron Lett.,* **2008**, 49, 4516.
22. R. D. Adams and S. Miao, *J. Am. Chem. Soc.,* **2004**, 126, 5056.
23. S. B. Colbran, S. T. Lee, D. G. Lonnon, F. J. D. Maharaj, A. M. McDonagh, K. A. Walker and R. D. Young, *Organometallics,* **2006**, 25, 2216.
24. N. Deibel, D. Schweinfurth, S. Hohloch, M. Delor, I. V. Sazanovich, M. Towrie, J. A. Weinstein and B. Sarkar, *Inorg. Chem.*, **2014**, 53, 1021.
25. M. K. Kabir, H. Tobita, H. Matsuo, K. Nagayoshi, K. Yamada, K. Adachi, Y. Sugiyama, S. Kitagawa and S. Kawata, *Cryst. Growth Des*. **2003**, 3, 791.
26. M. Kivala, C. Boudon, J.-P Gisselbrecht, P. Seiler, M. Gross and F, Diederich, *Chem. Commun.,* **2007**, 4731.
27. Z. Zhang, L. Huang, V. M. Shulmeister, Young-Inchi, K. K. Kim, L.- W. Hung, A. R. Crofts, E. A. Berry and S.- H. Kim, *Nature,* **1998**, 392, 677.
28. J.-M. Lu, S. V. Rosokha, I. S. Neretin and J. K. Kochi, *J. Am. Chem. Soc.,* **2006**, 128, 16708.
29. K. U. Baldenius, L. von dem Bussche-Hu¨nnefeld, E. Hilgemann, P. Hoppe and R. Sturmer, In *Ullmann's Encyclopedia of Industrial Chemistry*; VCH: Weinheim, Germany, **1996**, Vol. A27.
30. H. W. Moore and R. Czemiak, *Med. Res. Rev.,* **1981**, 1, 249.
31. (a) M. Das Sarma, R. Ghosh, A. Patra, R. Chowdhury, K. Chaudhuri and B. Hazra, *Org. Biomol. Chem.,* **2007**, 5, 3115. (b) A. M. Castano and J.- E. Ba¨ckvall, *J. Am. Chem. Soc.,* **1995**, 117, 560. (c) K. Bergstad, H. Grennberg and J.-E. Ba¨ckvall, *Organometallics,* 1998, 17, 45 (d) K. Krohn and S. Bernhard, *Synthesis,* **1996**, 699. (e) I. K. Boddy, R. C. Cambie, G. Dixon, P. S. Rutledge and P. D. Woodgate, *Aust. J. Chem.,* **1983**, 36, 803. (f). Reich, S. H.; Melnick, M.; Pino, M. J.; Fuhry, M. A. M.; Trippe, A. J. K. Appelt, J. F. Davies, Wu, B. W. II and L. Musick, *J. Med. Chem*., **1996**, 39, 2781.
32. T. S. Wu, H. C. Hsu, P. L. Wu, C. M. Teng and Y. C. Wu, *Phytochemistry* **1998**, 49, 2001.

TH-1303_09612216

33. K. M. Aubart and C. H. Heathcock, *J. Org. Chem.,* **1999,** 64, 16.

34. C. Allott, H. Adams, P. L. Bernad, C. A. Hunter, C. Rotger and J. A. Thomas, *Chem. Commun*., **1998**, 2449.

35. F. Wohler, *Annalen Chem. Pharm.* **1844**, 51, 145.

36. G. P. Stahly, *Cryst. Growth Des.* **2009**, 9, 4212.

37. K. Molcanov and B. KojicProdi, *CrystEngComm*, **2010**, 12, 925.

38. M.Tomura and Y.Yamashita, *CrystEngComm*, **2000**, 2, 92.

39. N. Iwase, Y. Kobayashi, T. Kinuta, T.Sato, N. Tajima, R. Kuroda, Y.Matsubaraa and Y. Imai, *CrystEngComm*, **2012**, 14, 8599.

40. N. Iwase, Y. Shigeno, T. Wakabayashi, T.Sato, N. Tajima, R. Kuroda and Y. Imai, *CrystEngComm*, **2014**, 16, 159.

41. J. D. Dunitz, *Pure Appl. Chem.* **1991**, 63, 177.

42. J. D. Dunitz and J. Bernstein, *Acc. Chem. Res.* **1995**, 28, 193.

43. J. D. Dunitz, *Acta Crystallogr., Sect. B.,* **1995**, 51, 619.

44. J. Bernstein, R. J. Davey and J.-O. Henck, *Angew. Chem. Int. Ed.,* **1999**, 38, 3441.

45. J. Bernstein, *Polymorphism in Molecular Crystals*; Oxford University Press: Oxford, **2002**.

46. R. J. Davey, *Chem. Commun.,* **2003**, 1463.

47. J. Bernstein, *Chem. Commun.,* **2005**, 5007.

48. S. R. Bryn, R. R. Pfeiffer and J. G. Stowell, *Solid-State Chemistry of Drugs*, SSCI: West Lafayette, IN, **1999**.

49. M. L. Peterson, S. L. Morissette, C. McNulty, A. Goldsweig, P. Shaw, M. LeQuesne, J. Monagle, N. Encina, J. Marchionna, A. Johnson, J. Gonzalez-Zugasti, A. V. Lemmo, S. J. Ellis, M. J. Cima and O. Almarsson, *J. Am. Chem. Soc.,* **2002**, 124, 10958.

50. C. P. Price, A. L. Grzesiak and A. J. Matzger, *J. Am. Chem. Soc.,* **2005**, 127, 5512.

51. S. Roy, R. Banerjee, A. Nangia and G. J. Kruger, *Chem. Eur. J.,* **2006**, 12, 3777.

52. J. Bernstein, R. J. Davey and J.-Ol Henck, *Angew. Chem. Int. Ed.,* **1999**, 38, 3440.

TH-1303_09612216

53. R. P. Kashyap, D. Sun and W. H. Watson, *J. Chem. Cryst.,* **1995**, 25, 339.

54. G. R. Desiraju, *J. Chem. Soc. Perkin Trans.,* **1983**, 2, 1025.

55. T. W. Lewis, D. Y. Curtin and I. C. Paul, *J. Am. Chem. Soc.* **1979**, 101, 5717.

56. H.-D. Becker, *J. Org. Chem.* **1967**, 32, 2943.

57. V. N. Nesterov and V. V. Nesterov, *Acta Cryst. C*, **2004**, 60, 781.

58. J. Pacifico and H. Stoeckli-Evans, *Acta Cryst. C*, **2004**, 60, 152.

59. K. Kobayashi, R. Shimaoka, M. Kawahata, M. Yamanaka and K. Yamaguchi, *Org. Lett*., **2006**, 8, 2385.

60. W. M. Wolf, *Acta Cryst. B*, **2001**, 7, 806.

61. G. Hogararth and I. Richards, *Inorg. Chem. Commun*., **2007**, 10, 66

62. L. Ma, S. Liu, H. Zhu and J. Zubieta, *Polyhedron*, **1989**, 8, 669.

63. R. S. Morgan and J. M. Mcadon, *Int. J. Peptide and Protein Res*., **1980**, 15, 177.

64. F. I. Adam, G. Hogarth, I. Richards and B. E. Sanchez, *J. Chem. Soc. Dalton Trans*., **2007**, 2495.

65. W. M. Singh and J. B. Baruah, *J. mol. Struct,* **2009**, 931, 82.

66. T. Kinuta, T. Sato, N. Tajima, Y.Matsubara, M. Miyazawaa and Y. Imai, *CrystEngComm*, **2012**, 14, 1016.

67. S. K. Chandran, N. K. Nath, S. Roy, and A. Nangia, *Cryst. Growth. Des,* **2008,** 8, 140.

68. A. Nangia, *Acc. Chem. Res*. **2008**, 41, 595.

69. J. Fajer, K. M. Barkigia, D. Melamed, R. M. Sweet, H. Kurreck, J. Von Gersdorff, M. Plato, H.-C. Rohland, G. Elger and K. Mo1bius, *J. Phys. Chem.,* **1996**, 100, 14236.

70. H. A. Staab, M. Tercel, R. Fischer and C. Krieger, *Angew. Chem., Int. Ed. Engl.,* **1994**, 33, 1463.

TH-1303_09612216

71. C. Krieger, J. Weiser and H. A. Staab, *Tetrahedron Lett.,* **1985**, 26, 6055.

72. J. L. Sessler, M. R. Johnson, S. E. Creager, J. C. Fettinger and J. A. Ibers, *J. Am. Chem. Soc.,* **1990**, 112, 9310.

73. J.-M. Lehn, *Angew. Chem., Int. Ed.* **1988**, *27*, 89.

74. Y. Yuan, G. Gao, Z.-L. Jiang, J.-S. You, Z.-Y. Zhou, D.-Q. Yuana and R.-G. Xiea, *Tetrahedron* **2002**, 58, 8993.

75. S. Devaraj, D. Saravanakumar and M. Kandaswamy, *Tetrahedron Lett.,* **2007**, 48, 3077.

76. C. Bargossi, M. C. Fiorini, M. Montalti, L. Prodi and N. Zaccheroni, *Coord. Chem. Rev.* **2000**, 208, 17.

77. A. B. Descalzo, D. Jimenez, M. D. Marcos, R. Martinez- Manez, J. Soto, J. El Haskouri, C. Guillem, D. Beltran, P. Amoros and M. V. Borrachero, *Adv. Mater*. **2002**,14, 966.

78. C. B. Black, B. Andrioletti, A. C. Try, C. Ruiperez and J. L. Sessler, *J. Am. Chem. Soc.* **1999**, 121, 10438.

79. H. Miyaji, W. Sato and J. L. Sessler, *Angew. Chem. Int. Ed*. **2001**, 40, 154.

80. V.Luxami, N. Sharma and S. Kumar, *Tetrahedron Lett.,* **2008**, 49, 4265.

81. N. Kaur and S. Kumar, *Chem. Commun*. **2007**, 3069.

82. S. Kumar and N. Kaur, *Supramol. Chem*. **2006**, 18, 137.

83. N. Kaur and S. Kumar, *Dalton Trans.* **2006**, 3766.

84. N. Kaur and S. Kumar, *Tetrahedron Lett.,* **2006**, 47, 4109.

85. I.- S. Park and E.-J. Heo and J.-M. Kim, *Tetrahedron Lett.,* **2011**, 52, 2454.

86. M. Bru, M. I. Burguete, F. Galindo, S. V. Luis, M. J. Marıin and L. Vigara, *Tetrahedron Lett.,* **2006**, 47, 1787.

87. Y.-P. Yen and K.-W. Ho, *Tetrahedron Lett.,* **2006**, 47, 7357.

TH-1303_09612216

88. P. Anzenbacher, Jr., M. A. Palacios, K. Jursıkova and M. Marquez, *Org. Lett.* **2005**, 7, 5027.

89. P. Rothemund and A. R. Mennotti, *J. Am. Chem. Soc*. **1941**, 63, 267.

90. S.-P. Wu, R.-Y. Huang and K.-J. Du, *Dalton Trans.* **2009**, 4735.

91. S. Kumar, Pramila and S. Kaur, *Tetrahedron Lett.,* **2002**, 43, 1097.

92. H. M. Chawla, R. Shukla and S. Pandey, *Tetrahedron Lett.,* **2012**, 53, 2996.

93. J.-M. Lehn, *Angew. Chem., Int. Ed.* **1988**, *27*, 89.

94. Y. Aoyama, K. Endo, T. Anzai, Y. Yamaguchi, T. Sawaki, K. Kobayashi, N. Kanehisa and H. Hashimoto,Y. Kai and H. Masuda, *J. Am. Chem. Soc.,* **1996,** 118*,* 5562.

95. M. Bouvet, B. Malezieux, P. Herson and F. Villain, *Helvet. Chim. Acta,* **2009,** 92, 453.

96. A. Tsuda, C. Fukumoto and T. Oshima, *J. Am. Chem. Soc.,* **2003**, 125, 5811.

97. Y.-S. Huang, S. Sabo-Etienne, X.-D. He and B. Chaudret, *Organometallics,* **1992**, 11, 3031.

98. H. Amouri and J. Le Bras, *Acc. Chem. Res.,* **2002**, 35, 501.

99. M. Oh, G. B. Carpenter and D. A. Sweigart, *Angew. Chem. Int. Ed.,* **2002,** 41, 3650.

100. M. Oh, G. B. Carpenter and D. A. Sweigart, *Angew. Chem. Int. Ed.,* **2003**, 42, 2026.

101. M. Oh, G. B. Carpenter and D.A. Sweigart, *Chem. Commun.,* 2002, 2168.

102. M. Oh, G. B. Carpenter and D. A. Sweigart, *Organometallics,* 2003, 22, 2364.

103. H. Schumqnn, A. M. Arif and T.G. Richmond, Polyhedron **1990**, 9, 1677.

104. M. Oh, G. B. Carpenter and D. A Sweigart, *Organometallics,* **2002**, 21, 1290.

105. M. Oh, G. B. Carpenter and D. A. Sweigart, *Angew. Chem., Int. Ed.,* **2001**, 40, 3191.

TH-1303_09612216

106. M. A. Escobar, D. H. Jara, R. A. Tapia, L. Lemus, R. Fröhlich, J.Guerrero and R. S. Rojas, *Polyhedron,* **2013**, 62, 66.

107. A. P. Neves, G. B. da Silva, M. D. Vargas, C. B. Pinheiro, L. do C. Visentin, J. D. B. M. Filho, A. J. Ara´ujo, L.V. Costa-Lotufo, C. Pessoa and M. O. de Moraes, *Dalton Trans.*, **2010**, 39, 10203.

108. F. Pointillart, S. Klementieva, V. Kuropatov, Y. L. Gal, S. Golhen, O. Cador, V. Cherkasov and L. Ouahab, *Chem. Commun.,* **2012**, 48, 714.

109. C. G. Pierpont, *Coord. Chem. Rev.,* **2001,** 216, 99.

110. C. G. Pierpont and R. M. Buchanan, *Coord. Chem. Rev.,* **1981**, 38, 45.

111. C. G. Pierpont and C. W. Lange, *Prog. Inorg. Chem.,* **1994**, 41, 331.

112. F. Rohrscheid and A. L. Balch, R. H. Holm, *Inorg. Chem.,* **1966,** 5, 1542.

113. A. S. Attia and C. G. Pierpont, *Inorg. Chem.,* **1997**, 36, 6184.

114. S. Attia and C. G. Pierpont, *Inorg. Chem.* **1995**, 34, 1172.

115. M. A. Ribeiro, M. Lanznaster, M. M. P. Silva, J. A. L. C. Resende, M. V. B. Pinheiro, K. Krambrock, H.O. Stumpf and C. B. Pinheiro, *Dalton Trans.*, **2013**, 42, 5462.

116. K. Molčanov, M. Jurić and B. K. Prodić, *Dalton Trans.*, **2013**, 42, 15756.

117. J. D. Scott and R. M. Williams, *Chem. Rev.,* **2002**, 102, 1669.

118. V. K. Tandon, D. B. Yadav, R. V. Singh, M. Vaish, A. K. Chaturvedi and P. K. Shukla, *Bioorg. Med. Chem. Lett.,* **2005,** 15, 3463.

119. C.-K. Ryu, J.-Y. Shim, M. J. Chae, I. H.Choi, J.-Y. Han, O.-J. Jung, J.Y. Lee and S. H. Jeong, *Eur. J. Med. Chem.,* **2005**, 40, 438.

120. G. Errante, G. L. Motta, C.Lagana, V. Wittebolle, M.- E. Sarciron and R. Barret, *Eur. J. of Med. Chem.,* **2006,** 41, 773.

121. V. K. Tandon, H. K. Maurya, D. B. Yadav, A. Tripathi, M. Kumar and P. K. Shukla, *Bioorg. Med. Chem. Lett*., **2006,** 16, 5883.

TH-1303_09612216

122. V. K. Tandon, D. B. Yadav, A. K. Chaturvedi and P. K. Shukla, *Bioorg. Med. Chem. Lett*., **2005**, 15, 3288.

123. S. Y. Hung, K. H. Chung, H. J. You, I. H. Choi, M. J. Chae, J. Y. Han, O. J. Jung, S. J. Kang and C. K. Ryu, *Bioorg. Med. Chem. Lett.,* **2004**, 14, 3563.

124. K. Ushiyama, N. Tanaka, H. Ono and H. Ogato, *Jpn. J. Anribiot.,* **1971**, 24 , 197.

125. D. Barasch, O. Zipori, I. Ringel, I. Ginsberg, A. Samuni and J. Katzhendler, *Eur. J. Med. Chem.,* **1999,** 34, 597.

126. D. L. Boger and R. M. Garbaccio, *J. Org. Chem.,* **1999**, 64, 8350.

127. L. F. Tietze, K. M. Gericke, R. R. Singidi and I. Schuberth, *Org. Biomol. Chem.*, **2007**, 5, 1191.

128. E. Champeil, M. M. Paz, S. Ladwa, C. C. Clement, A. Zatorski and Maria Tomasz, *J. Am. Chem. Soc.*, **2008**, 130, 9556.

129. J. Yoo, H.- S. Choi, C.- H. Choi, Y. Chung, B. Hee Kim and H. Cho, *Arch. Pharm. Res.,* **2008,** 31, 142.

130. Y. Ikeda, Y. Shimada, K. Honjo, T. Okumoto and T. Munakata, *J. Antibiot.* **1983**, 36, 1290.

131. T. Okumoto, M. Kawana, I. Nakamura, Y. Ikeda and K. Isagai, *J. Antibiot.* **1985**, 38, 767.

132. Y. Fan, E. M. Schreiber, A. Giorgianni, J. C. Yalowich and B. W. Day, *Chem. Res. Toxicol.,* **2006,** 19, 937.

133. D. L. Boger and R. M. Garbaccio, *J. Org. Chem.* **1999,** 64, 8350.

134. N. M. Kogan and R. Rabinowitz, P. Levi, D. Gibson, P. Sandor, M. Schlesinger and R. Mechoulam, *J. Med. Chem.* **2004,** 47, 3800.

135. P. J. O'Brien, *Chem.-Biol. Interact.*, **1991**, 80, 1.

136. C. Asche, *Mini-Rev. Med. Chem.*, **2005,** 5, 449.

137. A.R. Mehendale and R.H. Thomson, *Phytochemistry* **1975**, 14, 801.

TH-1303_09612216

138. J. Yin and L. S. Liebeskind, *J. Org. Chem*. **1998,** *63*, 5726.

139. Y. Hafuri, E. Takemori, K. Oogose, Y. Inouye, S. Nakamura, Y. Kitahara, S. Nakahara and A. Kubo, *J. Antibiot*, **1988**, 41, 1470.

140. T. Arai, K. Takahashi and A. Kubo, *J. Antibiot.,* **1977**, 30, 1015.

141. J. D. Scott and R. M. Williams, *Chem. Rev.,* **2002,** 102, 1669.

142. V. Sundstrom, *Prog. Quantum Electron,* **2000**, 24, 187.

143. F. Arcamone, G. Cassinelli, G. Fantini, A. Grein, P. Orezzi, C. Pol, S. C. Adriamycin, *Biotechnol. Bioeng.* **1969**, 11, 1101.

144. C. A. Frederick, L. D. Williams, G. Ughetto, G. A. van der Marel, J. H. van Boom, A. Rich, A. H. Wang, *Biochemistry* **1990**, 29, 2538.

145. J. B. Roaten, M. G. Kazanietz, M. J. Caloca, P. J. Bertics, L. Lothstein, A. L. Parrill, M. Israel, T. W. Sweatman, *Mol. Cancer Ther.* **2002**, 1, 483.

146. G. Minotti, P. Menna, E. Salvatorelli, G. Cairo, L. Gianni, *Pharmacol. Rev*. **2004**, 56, 185.

147. M. Israel, R. Seshadri, J. M. Idriss, *Proc. Am. Assoc. Cancer Res*. **1985**, 26, 220.

148. C. M. Barrett, F. L. Lewis, J. B. Roaten, T. W. Sweatman, M. Israel, J. L. Cleveland, L. Lothstein, *Mol. Cancer Ther*. **2002**, 1, 469.

149. J. B. Roaten, M. G. Kazanietz, T. W. Sweatman, L. Lothstein, M. Israel, A. L. Parrill, *J. Med. Chem.* **2001**, 44, 1028.

150. A. Harstrick, U. Vanhoefer, N. Schleucher, J. Schroeder, J. Baumgart, M. E. Scheulen, H. Wilke, S. Seeber,. *Anti-cancer Drugs* **1995**, 6, 681.

151. E. Kobayashi, H. Nakano, M. Morimoto, T. Tamaoki, *Biochem. Biophys. Res. Commun.* **1989**, 159, 548.

152. T. Iida, E. Kobayashi, M. Yoshida, H. Sano, *J. Antibiot.* **1989**, 42, 1475.

153. E. Kobayashi, K. Ando, H. Nakano, T. Iida, H. Ohno, M. Morimoto, T. Tamaoki, *J. Antibiot.* **1989**, 42, 1470.

154. S. A. Rotenberg, M. H. Huang, J. Zhu, L. Su, H. Riedel, *Mol. Carcinog.* **1995**, 12, 42.

155. R. Gopalakrishna, Z. H. Chen, U. Gundimeda, *FEBS Lett*. **1992**, 314, 149.

TH-1303_09612216

156. R. F. Bruns, F. D. Miller, R. L. Merriman, J. J. Howbert, W. F. Heath, E. Kobayashi, I. Takahashi, T. Tamaoki, H. Nakano, *Biochem. Biophys. Res. Commun*. **1991**, 176, 288.

157. C. A. Merlic, C. C. Aldrich, J. A. Walker, A. Saghatelian, *J. Am. Chem .Soc.* **2000**, 122, 3224.

158. C. A. Merlic, C. C. Aldrich, J. A. Walker, A. Saghatelian, J. Mammen, *J. Org. Chem.* **2001**, 66, 1297.

159. N. P. Redmore, I. V. Rubtsov and M. J. Therien, *J. Am. Chem. Soc.,* **2003***,* 125, 8769.

160. A. Dreuw, G. A. Worth, L. S. Cederbaum and M. Head-Gordon, *J. Phys. Chem. B,* **2004**, 108*,* 19049.

161. J. Springer, G. Kodis, L. de la Garza, A. L. Moore, T. A. Moore and D. Gust, *J. Phys. Chem. A,* **2003**, 107, 3567.

162. F. DSouza and G. R. Deviprasad, *J. Org. Chem.,* **2001,** 66, 4601.

163. X. Shi, S. R. Amin and L. S. Liebeskind, *J. Org. Chem.,* **2000,** 65, 1650.

164. T. Arimura, S. Ide, H.Sugihara, S.Murata and J. L. Sessler, *New J. Chem.,* **1999**, 23, 977.

165. T. Hayashi, T. Takimura, Y. Hitomi, T. Ohara and H. Ogoshi, *J. Chem. Soc., Chem. Commun.,* **1995**, 545.

166. F. D'Souza and G. R. Deviprasad, Y.-Y. Hsieh, *Chem. Commun*., **1997**, 533.

167. K. Abdelmohsen, P. A. Gerber, C. vonMontfort, H. Sies and L. O. Klotz. *J. Biol. Chem.* **2003**, 278, 38360.

168. J. I. Beier, C. vonMontfort, H. Sies and L.O. Klotz, *FEBS Lett.* **2006**, 580, 1859.

169. 79. L. O. Klotz, P. Patak, N. Ale-Agha, D. P. Buchczyk and K. Abdelmohsen, *Cancer Res.* **2002**, 62, 4922.

170. S. Kikuno, K. Taguchi, N. Iwamoto, S. Yamano and A. K. Cho, *Toxicol. Appl. Pharmacol.* **2006**, 210, 47.

171. N. K. Tonks. *FEBS Lett.* **2003**, 546, 140.

172. R. Malkin, *FEBS Lett.* **1986**, 208, 343.

TH-1303_09612216

173. H.U. Schoeder and W. Lockau, *FEBS Lett.* **1986**, 199, 23.

174. Y. Takahashi, K. Hirota and S. Katoh, *Photosynth. Res.*, **1985**, 6, 183.

175. J. Biggins, and P. Mathis, *Biochemistry*, **1988**, 27, 1494.

176. F. Müh, C. Glöckner, J. Hellmich and A. Zouni, *Biochim. Biophys. Acta.* **2012**, 1817, 44.

177. S. S. Hasana, E. Yamashita, D. Baniulis, and W. A. Cramera, *PNSA*, 2012.

178. Z. Zhu and M. R. Gunner, *Biochemistry* **2005,** *44,* 82.

179. C. A. Wraight, *Front. Biosci*. **2004**, 9, 309.

180. M. L. Paddock, G. Feher, and M. Y. Okamura, *FEBS Lett.* **2003**, 555, 45.

181. A. W. Rutherford and P. Faller, *Trends Biochem. Sci.* **2001**, 26, 341.

182. P. Fromme, P. Jordan, and N. Krauss, *Biochim. Biophys. Acta.* **2001**, 1507, 5.

183. A. E. Fernandez, A. Miguel, E. D. Stefano, D. Schmitz and A. K. Cho, *Aerosol Sci. Technol.* **2008**, 42, 854.

184. M. Y. Chung, R. A. Lazaro, D. Lim, J. Jackson and J. Lyon *Environ. Sci. Technol.* **2006**, 40, 4880.

185. C. A. Jakober, S. G. Riddle, M. A. Robert, H, Destaillats and M. J. Charles, *Environ. Sci. Technol.* **2007**, 41, 4548.

186. M. Shinyashiki, A. E. Fernandez, D. A. Schmitz, E. D. Stefano and N. Li, *Environ. Res.* **2009**, 109, 239.

187. K. E. Kautzman, J. D. Surratt, M. N. Chan, A. W. H. Chan and S. P. Hersey, *J. Phys. Chem. A* **2010**, 114, 913.

188. S. N. Chu, S. Sands, M. R. Tomasik, P. S. Lee and V. F. McNeill. *J. Am. Chem. Soc.* **2010**, 132, 15968.

189. R. Murray and M. Singh, *Polycycl. Aromat. Compd.* **1997**, 12, 51.

190. N. Li, C. Sioutas, A. Cho, D. Schmitz and C. Misra, *Environ. Health Perspect.* **2003**,111,455.

191. M. Shiraiwa, R. Garland and U. Poeschl, *Atmos. Chem. Phys.* **2009**, 9, 9571.

192. J. D. Sun, R. K. Wolff, G. M. Kanapilly and R. O. McClellan, *Toxicol. Appl. Pharmacol.* **1984**, 73, 48.

193. P. G. Seybold and M. Gouterman, *J. Mol. Spectrosc.*, **1969**, 31, 1.

194. D. J. Quimby and F. R. Longo, *J. Am. Chem. Soc.* **1975**, 97, 5111.

TH-1303_09612216

195. J. L. Bolton, M. A. Trush, T. M. Penning, G. Dryhurst and T. J. Monks, *Chem. Res. Toxicol.* **2000**, 13, 135.

196. E, Cadenas, P, Hochstein and L, Ernster. *Adv. Enzymol. Relat. Areas Mol. Biol.* **1992**, 65, 97.

197. T. J. Monks and D. C. Jones. *Curr. Drug Metab.* **2002**, 3, 425.

198. P. J. O'Brien. *Chem. Biol. Interact.* **1991**, 80, 1.

199. T. M. Penning, M. E. Burczynski, C. F. Hung, K. D. McCoull, N. T. Palackal and L. S. Tsuruda, *Chem. Res. Toxicol.* **1999**, 12, 1.

200. A. V. Pinto and S. L. de Castro. *Molecules* **2009**, 14, 4570.

201. K. Abdelmohsen, P. Patak, C. von Montfort, I. Melchheier, H. Sies and L. O. Klotz. *Methods Enzymol.* **2004**, 378, 258.

202. M. J. Shearer and P. Newman, *Thromb. Haemost.* **2008**,100, 530.

203. S. Kar, I. M. Lefterov, M. Wang, J. S. Lazo and C. N. Scott, *Biochemistry* **2003**, 42, 10490.

204. J. M. Samet and T. L. Tal, *Annu. Rev. Pharmacol. Toxicol.* **2010**, 50, 215.

205. E. Katz and I. Willner, *Chem. Commun.,* **2005**, 5641.

206. S.-H. Luo, Y. Liu, J. Hua, X.-M. Niu, S.-X. Jing, X. Zhao, B. Schneider, J. Gershenzon and S.-H. Li, *Org. Lett.,* **2012**, 14, 4146.

207. E. Katz and H.-L. Schmidt, *J. Electroanal. Chem.,* **1993**, 360, 337.

208. E. Katz and I. Willner, *Chem. Commun.,* **2005**, 5641

209. T. C. Quinn, *Proc. Natl. Acad. Sci.* **1994**, 91, 2407.

TH-1303_09612216

Chapter 2

Supramolecular chemistry of thiocarboxylic acid tethered 1,4-naphthoquinones

Polymorphism has received immense practical importance in pharmaceuticals as each polymorph can exhibit different chemical and physical properties including dissolution rate, bioavailability, stability, melting point, solubility, optical and mechanical properties, vapor pressure, etc.[1-3] When different conformers of a molecule occur in different crystal forms, the phenomenon is termed as conformational polymorphism.[4-9] Polymorph stability is of special interest because their energy differences are relatively small and inter-conversion is very common. Conformational energy change or rotation about single bonds (torsion) of a molecule is within the range 1-3 kcal mol^{-1} and can go up to 7-8 kcal mol^{-1}; that may lead to conformational polymorphs. Energies of intramolecular torsions and intermolecular non-bonded interactions lie in the same range (0.5-10 kcal mol^{-1}).[10-16] So, a conformationally flexible system with provision of weak interactions could show polymorphism. Carboxylic acid group is one of the functional groups that have been extensively explored in the realm of supramolecular chemistry. In supramolecular assemblies, carboxylic acid group adopt *syn* and *anti* geometry as illustrated in figure 2.1.[17] Primarily, packing patterns of assemblies of carboxylic acids are centrosymmetric dimer and polymeric catemer motifs.[18-32] Schematic representations of different self-assemblies of carboxylic acids are shown in figure 2.1. In general, the dimeric motif is found in > 90% of acid structures where other functional groups potentially competing for hydrogen bond are absent. Catemers and other patterns including dimeric motifs expanded by solvents, tetramers, hexamer and a helical motif are observed in the remaining 10% of the structures.[33-48] Carboxylic acid serves as one hydrogen bond donor and one hydrogen bond acceptor in both dimeric as well as catemeric motifs. Thus, understanding the factors promoting formation of either dimeric or catemeric motif is important in the utilization of carboxyl groups in crystal engineering.

TH-1303_09612216

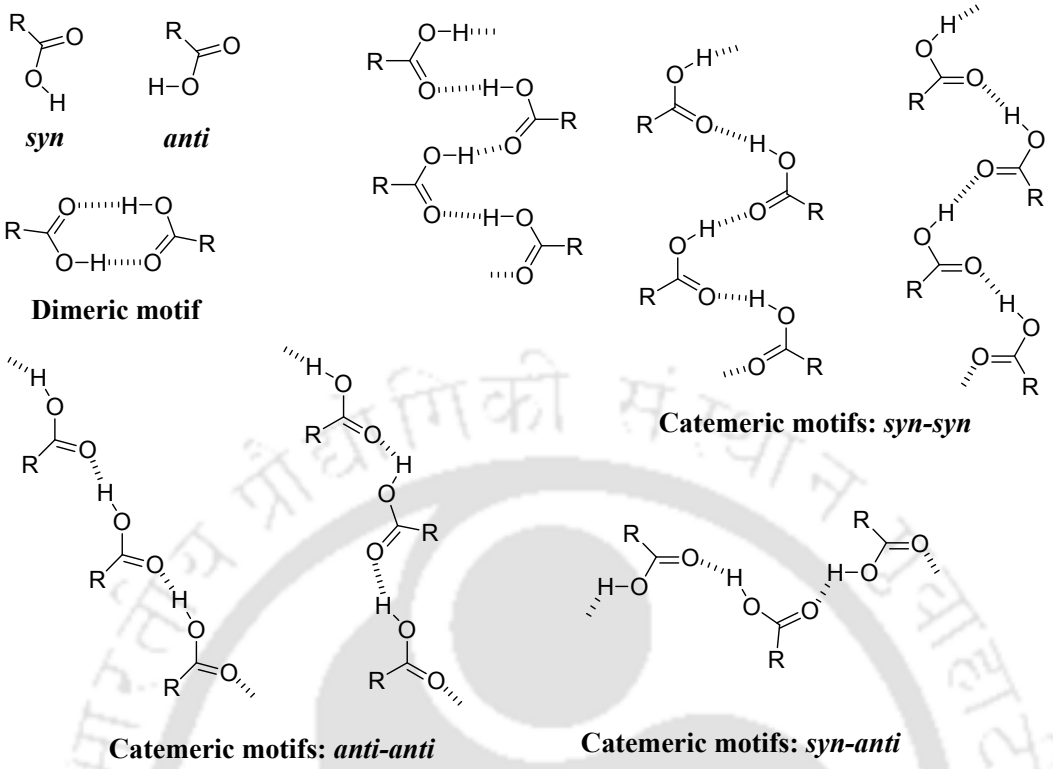

Figure 2.1: Various motifs found in self-assemblies of carboxylic acids.

Attaching carboxylic acid group to a quinone will provide additional supramolecular features and enable the generation new structural motifs. Introducing a quinone unit will also provide competition between the carbonyl group of the quinoidal part with carbonyl of carboxylate group to form hydrogen bond which would change the packing patterns. Further the stacking interactions of planar quinone units will play crucial role in the packing patterns of such a molecule. These changes would cause different orientations and would affect polymorphism in quinone compounds having COOH functional groups. Quinone derivatives with a thioaryl substituent show conformational polymorphs.[45] So, a naphthoquinone derivative having thiocarboxylic acid moiety would form self-assemblies guided by hydrogen bond interactions of carboxylic acid but influenced by the quinoidal carbonyl groups capable of acting as hydrogen bond acceptors. Hence the assembling of carboxylic acid group tethered to quinone by a S-atom will be guided by quinoidal part leading to different possibilities of self assembling as shown in figure 2.2.

TH-1303_09612216

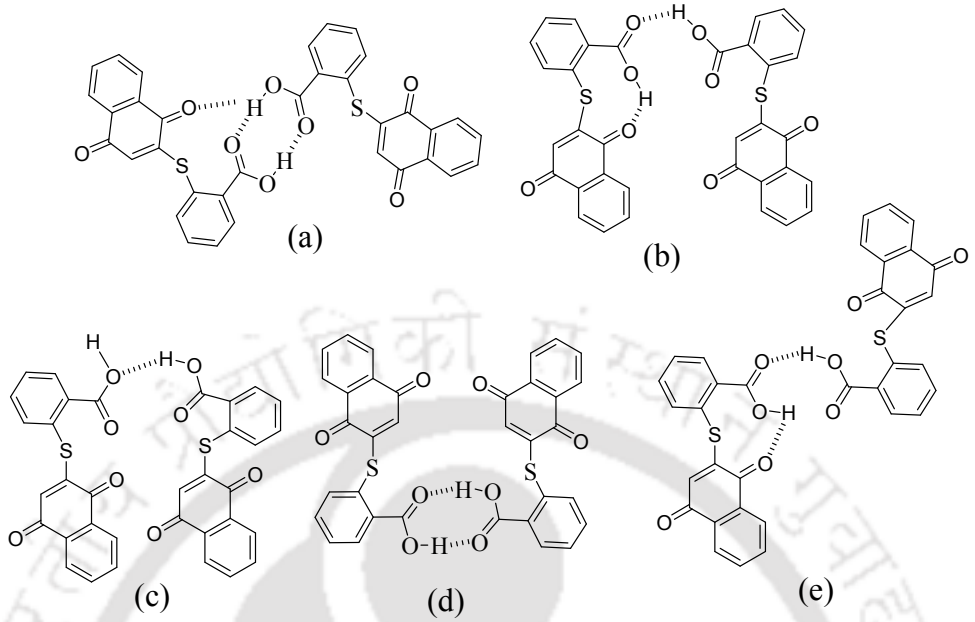

Figure 2.2: Some possible self-assemblies of thiocarboxylic acid containing naphthoquinone moiety.

With an anticipation to obtain new hydrogen bonded motifs shown in figure 2.2, we have chosen to study the structural and physical properties of three carboxylic acid tethered 1,4-naphthoquinone derivatives **2.1-2.3**. 2-(1,4-dihydro-2-methyl-1,4-dioxonaphthalen-3-ylthio) benzoic acid (**2.1**), 2-(1,4-dihydro-2-hydroxy-1,4-dioxonaphthalen-2,3-diylthio)benzoic acid (**2.2**) and 2-(1,4-dihydro-2-methyl-1,4-dioxonaphthalen-3-ylthio)phenyl)acetic acid (**2.3**). Structural study is complemented by other spectroscopic properties of these molecules.

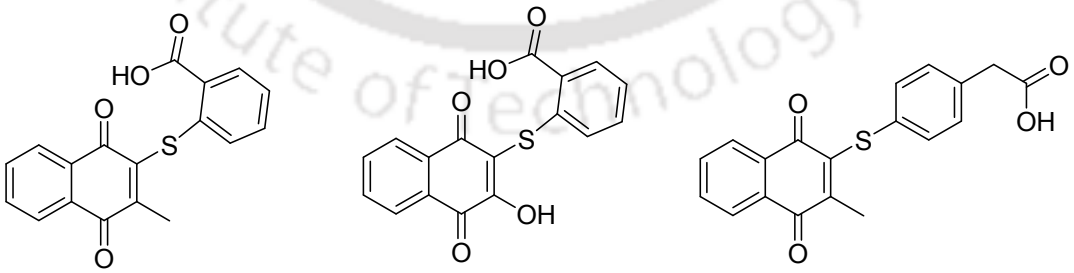

2.1 2.2 2.3

Figure 2.3: The thiocarboxylic acid tethered 1,4-naphthoquinones **2.1-2.3**.

TH-1303_09612216

*2.1: Synthesis and characterization of compounds **2.1**, **2.2** and **2.3***

2-(1,4-Dihydro-1,4-dioxonaphthalen-3-ylthio)benzoic acid (**2.1**) and 2-(1,4-dihydro-2-hydroxy-1,4-dioxo-naphthalen-2,3-diylthio)benzoic acid (**2.2**) were prepared by reacting 2-methyl-1,4-napthoquinone and 2-hydroxy-1,4-naphthoquinone with thiosalicylic acid under aerial conditions. 2-(1,4-Dihydro-2-methyl-1,4-dioxonaphthalen-3-ylthio)phenyl)acetic acid (**2.3**) was prepared by reacting 2-methyl-1,4-naphthoquinone with 2-(4-mercapto-phenyl)acetic acid. These reactions pass through formation of the corresponding 1,4-dihydroxynaphthalene derivatives which get quickly oxidized under ambient condition. This can be related to the fact that in reactions of arylthio compounds the second substitution reaction is relatively slower than the first substitution reaction.[49] Similar coupling reactions of naphthoquinone with arylthiols leading to substituted arylthiolato naphthoquinones are well documented in literature.[49] Compounds were characterized by ^{1}H-NMR, ^{13}C-NMR, infrared and mass spectroscopy. The ^{1}H-NMR of **2.1** is shown in figure 2.4a. We observed a doublet at 8.06 ppm for proton on carbon atom *a*, triplet at 7.92 ppm for *b*, doublet at 7.73 ppm for proton *c* of naphthoquinone moiety as shown in figure 2.4. In addition to these signals there are signals at doublet at 7.52 ppm for proton *g*, triplets at 7.29 and 7.23 ppm for protons *e* and *f* respectively. On the other hand, there is a singlet at 2.42 ppm from the proton of the methyl group. ^{13}C-NMR of compound **2.1** has signals for C-atom of carbonyl groups at 182.7, 180.0, 167.5 ppm; signals for C-atoms next to S-atom are at 152.8 ppm, 142.5 ppm and C-atom of methyl group appear at 16.0 ppm. The rest of the aromatic carbons for twelve carbon atoms are in the range of 138.4 ppm - 125.3 ppm. IR-spectra of the compound has a strong IR stretching at 1661 cm^{-1} due to carboxylic acid. The OH stretching of the carboxylic acid groups appear at 3434 cm^{-1}. ESI mass-spectra shows the m/z peak at 324.01 which corresponds to the $[M+H]^{+}$. Compound **2.2** and **2.3** are also characterized in similar way, a representative example of the ^{13}C-NMR spectra of the compound **2.2** is shown in figure 2.4b. The ^{13}C-NMR of **2.2** has three signals at 182.4, 179.9 and 172.4 for the C-atoms of the carbonyl groups of naphthoquinone and carboxylic acids. The signal at 149.9 ppm is due carbon attached to OH group and the signal at 143.0 ppm is due to C-atom flanked by carbonyl group and S-atom, rest of the carbon signals in the range of 134.6-126.2 ppm are from the other C-atoms of the rings.

TH-1303_09612216

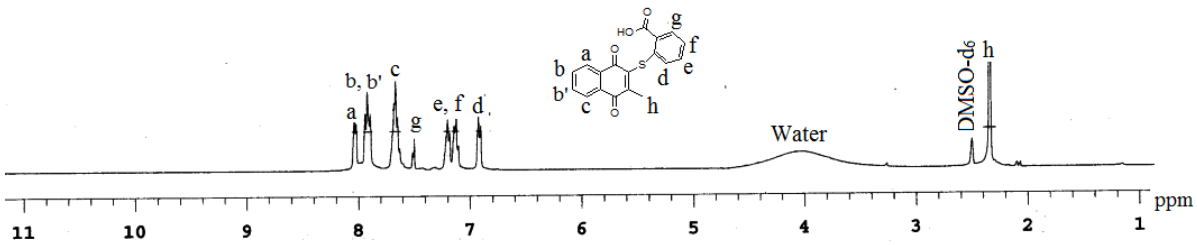

(a)

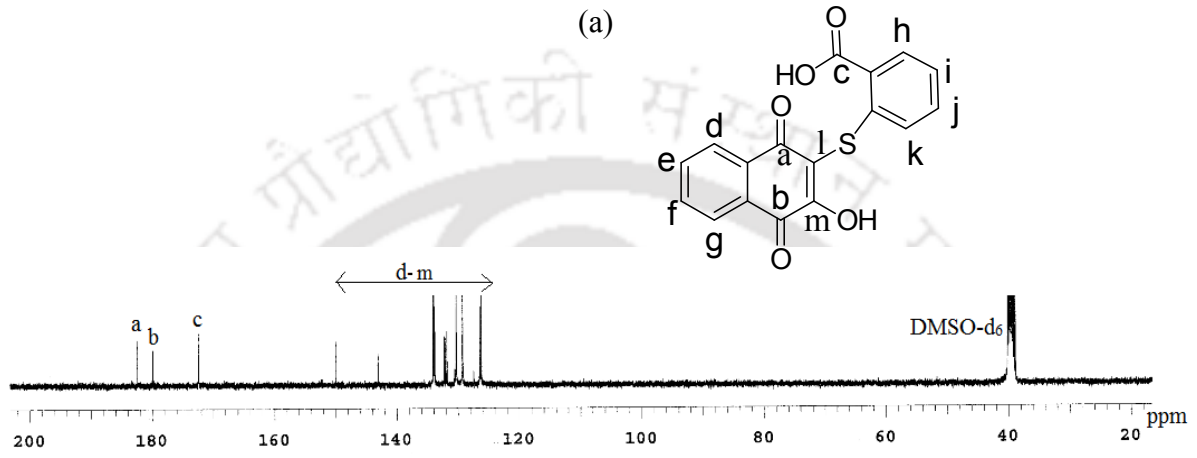

(b)

Figure 2.4: (a) The ^{1}H-NMR (400MHz, DMSO-d_6) spectra of the **2.1** and (b) ^{13}C-NMR (100MHz, DMSO-d_6) spectra of **2.2**.

The ^{1}H-NMR of the compound **2.3** has signals for aromatic proton similar to the other two compounds but the aliphatic region has clear distinction of showing a singlet at 3.90 corresponding to the methylene protons, it also shows a singlet at 2.40 ppm due to methyl protons. The ^{13}C-NMR of compound **2.3** also has three signals for C-atoms on the carbonyl groups of naphthoquinone and carboxylic acid part appearing at 182.3, 180.5, 167.0 ppm; and other peaks for aromatic carbons. In this case there are two ^{13}C-signals in aliphatic region one appearing at 42.05 ppm due to the C-atom of methylene group and another at 16.0 ppm due to C-atom of methyl group. IR of the compound shows O-H stretching at 3332 cm^{-1}, and carbonyl stretching at 1695 cm^{-1} and 1660 cm^{-1}.

*2.2: Polymorphs and solvate of **2.1***

As we anticipated wide variations of packing patterns in the carboxylic acid tethered naphthoquinone were observed. The unit cells of different crystals of **2.1** obtained by crystallization from different solvents were obtained. We have observed that solvents play a

TH-1303_09612216

crucial role in crystallization process. From trial and error type of crystallization experiments we could obtain four different types of crystals of which three were identified as polymorphs of **2.1,** whereas the fourth one was an acetonitrile solvate of **2.1**. Only experiment where crystals were isolated in a pure form are discussed here. When compound **2.1** was crystallized from different solvents, namely tetrahydrofuran/acetone (1:1 v/v) or methanol or chloroform, in each case different types of crystals were obtained. Analysis of these crystals have shown them to have similar composition, however the crystals belonged to different space groups. The crystals obtained from mixture solvent tetrahydrofuran/acetone belong to triclinic space group P-1, they are designated as crystal of polymorph **I** (**2.1a**). The crystals obtained from a solution of **2.1** in methanol belongs to space group monoclinic $P2_1/c$ this set of crystals are designated as crystals of polymorph **II** (**2.1b**); similarly crystals obtained from solution of chloroform belongs orthorhombic space group $P2_12_12_1$ is designated as polymorph **III** (**2.1c**). On the other hand a crystal of the 2.1 obtained from acetonitrile was a solvate of acetronitrile (**2.1d**). Types of crystals obtained from different solvents are described in Scheme 2.1.

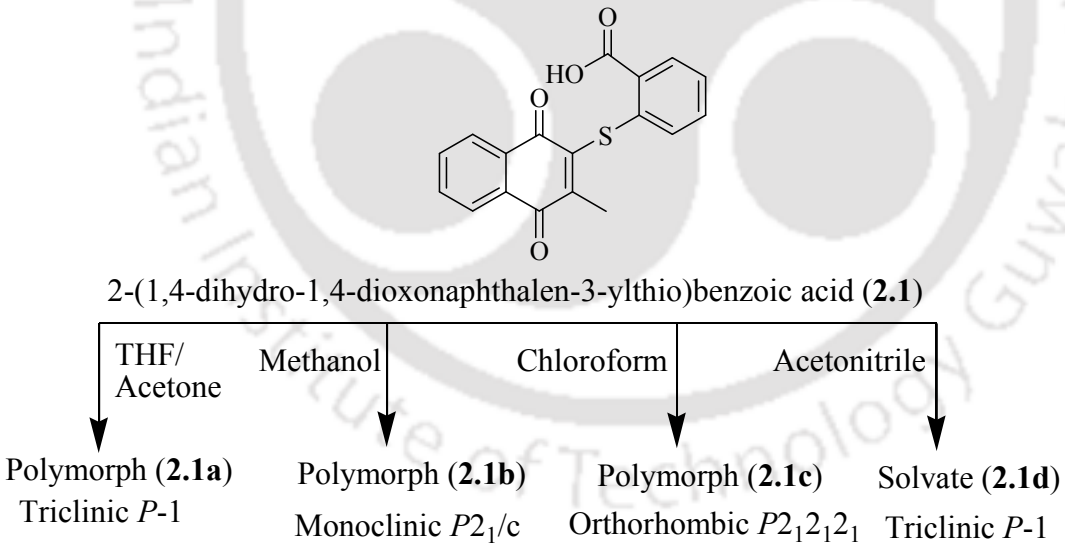

Scheme 2.1: Polymorphs and solvate of **2.1**.

The crystal structure of polymorph **I** is shown in figure 2.5a. Polymorph **I** has dimeric self-assembly through hydrogen bonds between two carboxylic acid groups. In dimeric assemblies sulfur atom bearing 2-methyl-1,4-naphthoquinone groups are *trans* to each other

TH-1303_09612216

across a $R_2^2(8)$ type of cyclic hydrogen bond motif (figure 2.5b). The carboxylic acid groups form strong O4-H4A···O3 interactions leading to a cyclic hydrogen bond architecture.

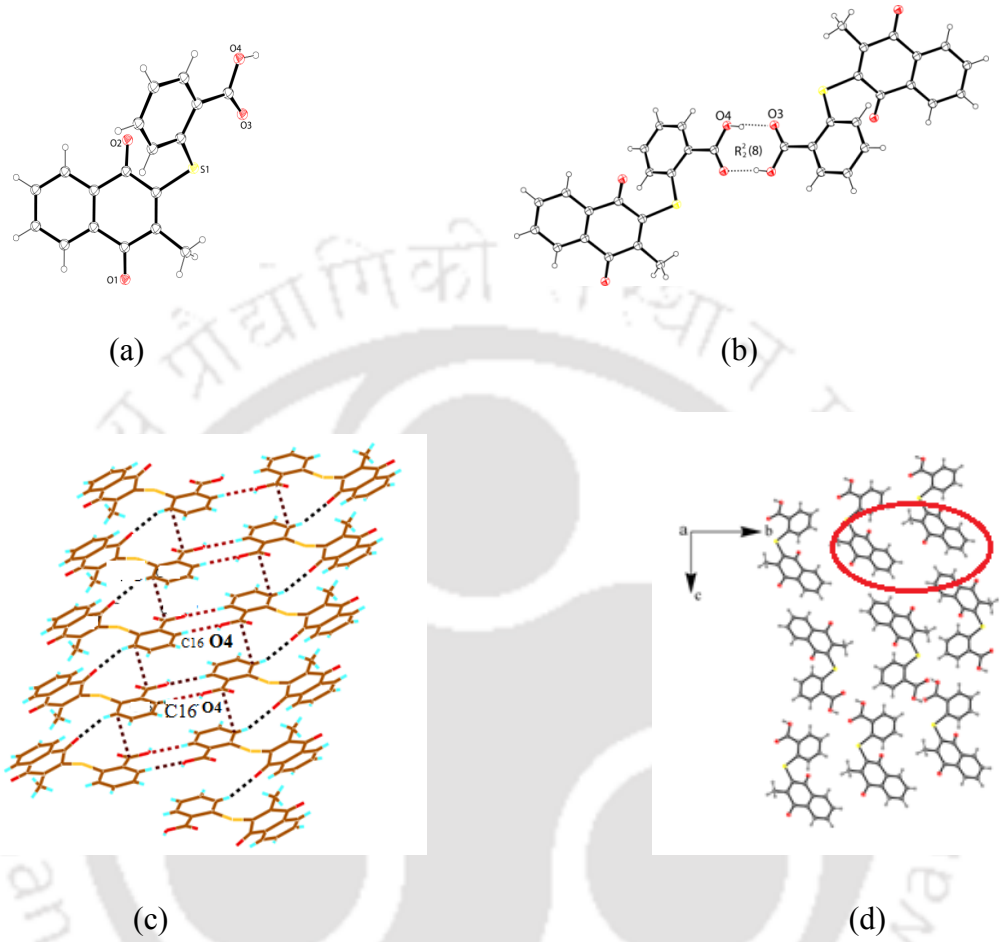

(a) (b)

(c) (d)

Figure 2.5: (a) ORTEP diagram of polymorph **I** (drawn with 30% thermal ellipsoids), (b) Cyclic H-bonding motif, (c) C-H···O and π-interactions in polymorph **I** and (d) Packing diagram of polymorph **I**.

C-H···O interactions are weak interactions generally found in organic molecules while adopting particular crystal packing and are highly directional in nature. Although the strength of such an interaction is very small they play important role in polymorphs and stabilization of particular conformation.[50] The polymorphs of the compounds **2.1** are no exception, they have extensive C-H···O interactions. In polymorph **I** there are C-H···O interactions between the carbonyl group of the naphthoquinone with of the C-H bond of the phenyl carboxylic acid group projecting in a suitable geometry to have such interactions.

TH-1303_09612216

Table 2.1: Hydrogen bond geometry (Å, °) of polymorph **I** and **II**

Compounds no.	D-H···A	d $_{D–H}$	d $_{H···A}$	d $_{D···A}$	∠D-H···A
Polymorph I	O4-H4A···O3 [3-x,2-y,-z]	0.82	1.84	2.66 (2)	173.38
	C13-H13···O2 [-1+x,y,z]	0.93	2.44	3.29 (3)	152.49
	C16-H16···O4	0.93	2.36	2.70 (3)	132.15
Polymorph II	O4-H4A···O3 [3-x,2-y,-z]	0.82	1.84	2.64(10)	168.02
	C16-H16···O1 [1+x,1+y,z]	0.93	2.48	3.13(12)	127.42
	C16-H16···O4	0.93	2.40	2.73(12)	101.00

Due to these interactions the polymorph **I** forms a layered one dimensional polymer-like structure in the lattice. Carboxylic acid groups and phenyl rings placed parallel in the crystal lattice of polymorph **I**, which shows stacking between the phenyl and carboxylic acid group. The $C13_{Phenyl}\cdots C18_{carboxy}$ distance is 3.4 Å is conducive for having π···π interactions. Generally for parallel arrangement of π-clouds within a range of 3-4 Å π-interactions takes place.[51] The hydrogen bond parameters of the prominent hydrogen bonds in self-assembly of polymorph **I** are listed in table 2.1.

ORTEP diagram of the polymorph **II** is shown in figure 2.6a. Crystal packing of the polymorph **II** shows that the carboxylic acids are engaged in strong O4-H4···O3 interactions. These interactions allow the neighboring molecules to form dimeric assemblies. The $R_2^2(8)$ motifs formed by the carboxylic acid part has comparable hydrogen bond parameters to the conventional $R_2^2(8)$ motifs observed.[52] The interactions resulting in the formation of cyclic hydrogen bond architectures is shown in figure 2.6b.

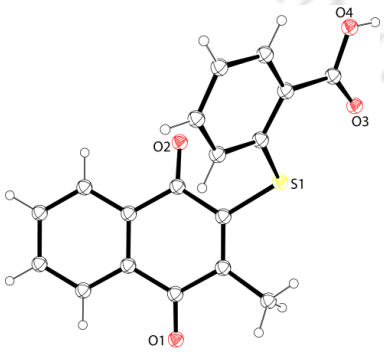

(a)

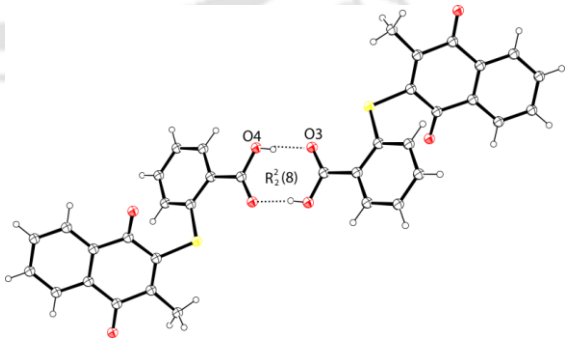

(b)

TH-1303_09612216

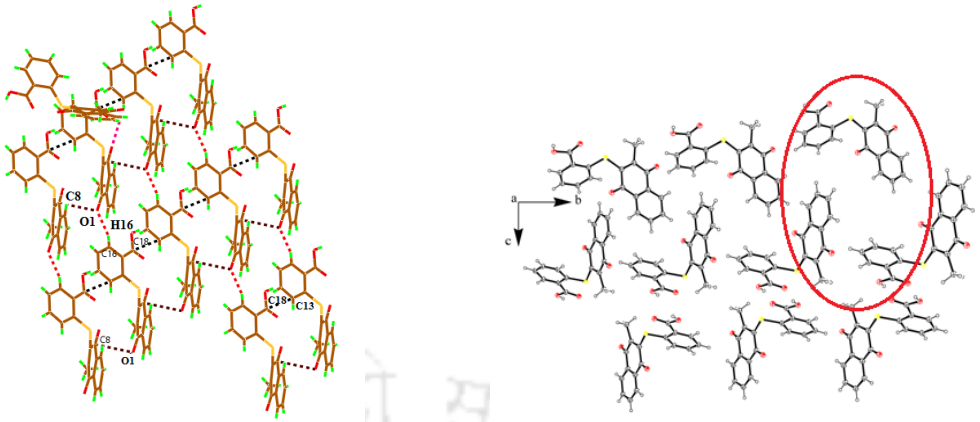

(c) (d)

Figure 2.6: (a) ORTEP diagram of polymorph **II** (**2.1b**) (drawn with 30% thermal ellipsoids), (b) Cyclic H-bonded motif. (c) C-H···O and π-interactions in polymorph **II**. (d) Packing diagram of polymorph **II** (The red circle indicates that; 2-methyl-1,4-naphthoquinone moiety is *head* whereas thiocarboxylic acid is *tail*).

Packing pattern of the polymorph **II** is guided by C16-H16···O1 and C2-H2···O2 interactions (Table 2.1). These weak interactions help to generate a 1D polymeric structure. Besides these, structure of polymorph **II** extends to a 1D zigzag architectures by parallel stacking between the phenyl units with carbon atom of the carboxylic acid group ($C13_{Phenyl}$···$C18_{carboxy}$ 3.34 Å) as shown in figure 2.6c.

Polymorph **III** has two symmetry independent molecules (X and Y) in the crystallographic asymmetric unit as shown in figure 2.7a. From the crystal packing, it is observed that in this case also dimeric hydrogen bonded assemblies are formed but the difference from the former two cases is that the partner molecules of the pairs are from two crystallographically symmetry independent molecules. The sulfur atom bearing 2-methyl-1,4-naphthoquinone groups in this case are *cis* to each other across $R_2^2(8)$ types hydrogen bond motif as shown in figure 2.7b.

TH-1303_09612216

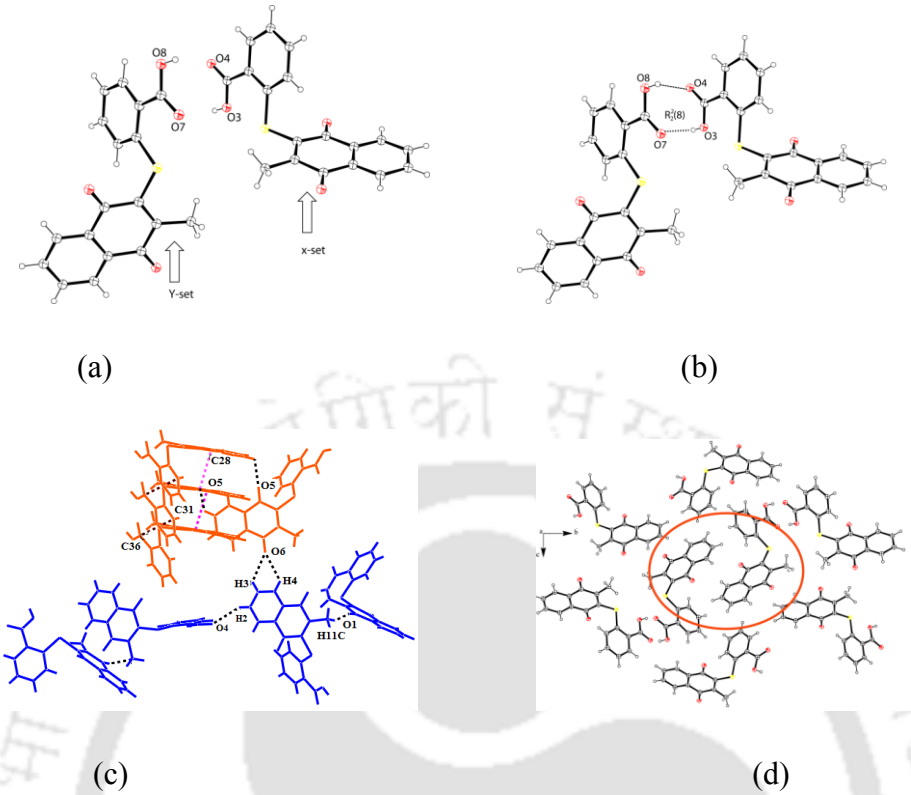

Figure 2.7: (a) ORTEP diagram of polymorph **III (**drawn with 30% thermal ellipsoids), (b) Cyclic H-bonded motif, (c) C-H···O and π-interactions in polymorph **III** and (d) Packing diagram of polymorph **III** (The red circle indicates that; 2-methyl-1,4-naphthoquinone moiety is *head* whereas thiocarboxylic acid is *tail*).

Due to symmetry non-equivalence the hydrogen bonded dimer formed is not symmetric. Hence two strong hydrogen bond, namely O3-H3A···O7 and O8-H8···O4 interactions are observed in this case (Table 2.2). It is observed that polymorph **III** assembles in the lattice through C20-H20···O5 bifurcated hydrogen bonds namely C3-H3···O6 and C4-H4···O6 bonds. As a result of these interactions a one dimensional linear architecture is formed (Figure 2.7c). There is also parallel stacking of the phenyl groups with carboxylic acid part of independent molecules with the phenyl ring to carboxylic acid. The packing diagram of the molecules (Figure 2.7d) indicates that there are pair of molecules of one type of symmetry which are embraced by six neighboring molecules of another type of symmetry. The packing pattern of polymorph **I** has *head* to *head* (Figure 2.5d). Whereas polymorph **II** has *head* to *tail* arrangements (Figure 2.6d). These make the lattice of three polymorphs distinguishable.

TH-1303_09612216

Table 2.2: Hydrogen bond geometry (Å, °) of polymorph **III (2.1c)**

D-H···A	d $_{D-H}$	d $_{H\cdots A}$	d $_{D\cdots A}$	∠D−H···A
O3-H3···O7[2-x,1/2+y,1/2-z]	0.82	1.82	2.63 (3)	175.43
O8-H8···O4[2-x,-1/2+y,1/2-z]	0.82	1.81	2.62 (3)	171.54
C2-H2···O4[1-x,-1/2+y,1/2-z]	0.93	2.58	3.30 (5)	134.93
C3-H3···O6[-1/2-x,-y,-1/2+z]	0.93	2.56	3.17 (5)	123.83
C11-H11B···O1	0.96	2.36	2.74 (5)	103.00
C11-H11C···O1[1/2+x,1/2-y,-z]	0.96	2.44	3.35 (5)	158.00
C13-H13···O2[-1+x,y,z]	0.93	2.58	3.37 (4)	143.83
C16-H16···O4	0.93	2.37	2.71 (4)	101.00
C29-H29B···O6	0.96	2.33	2.78 (4)	108.00

The conformational polymorphs in carboxylic acids are well-documented.[53-57] Some of the examples of carboxylic acid compounds which shows conformational polymorphs are shown in figure 2.8. We had earlier showed conformational polymorphs of a 1,4-naphthalenediol acid (**2.4**).[53] In that case polymorphs were guided by $R_2^2(8)$ cyclic hydrogen bond pattern but they had different packing patterns. Conformation polymorphism of mefenamic acid was observed due to the differences in orientation of aryl groups across the nitrogen atom.[54]

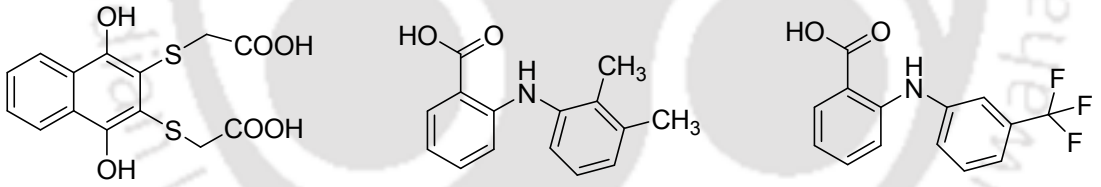

2.4 2.5 2.6

Figure 2.8: Example of carboxylic acids which showed conformational polymorphs.

An additive-induced method used to cause polymorphism in flufenamic acid.[55] Common feature of all these compounds in the orientation of substituents across a hetero atom. From these structures of the polymorphs, it is observed that the torsion angle of C8-C7-S1-C12 and C6-C7-S1-C12 of polymorph **II** (**2.1b**) are -62.88°, 126.56°, whereas in polymorph **I** (**2.1a**) the torsion angles of C8-C7-S1-C12 and C6-C7-S1-C12 are 57.82° and -129.38° respectively, which shows the difference between the conformation of the polymorphs **I** (**2.1a**) and **II** (**2.1b**). In the case of polymorph **III** the symmetry independent molecules of the polymorph X and Y show different torsion angles. The torsion angles for X-set, namely, C8-C7-S1-C12,

TH-1303_09612216

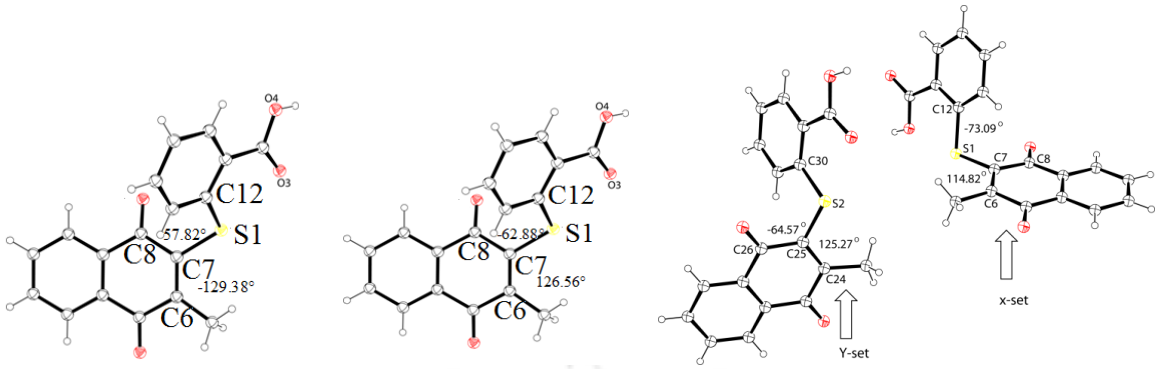

(a) (b) (c)

Figure 2.9: (a) Torsion angle of polymorph **I** (**2.1a**), (b) Torsion angle of polymorph **II** (**2.1b**) and (c) Torsion angle of polymorph **III** (**2.1c**) (drawn with 30% thermal ellipsoids).

C6-C7-S1-C12 are -73.09° and 114.82° (figure 2.9c) respectively. Whereas, torsion angles of C26-C25-S2-C30, C24-C25-S2-C30 for molecules designated as Y-set are -64.57° and 125.27°, respectively. The torsion angles are listed in table 2.3. Hence, the differences in the torsion angles establish that in each case different conformer are present.

Table 2.3: Torsion angles of polymorph **I-III (2.1a-2.1c)**

Polymorph	Dihedral angles (°)
Polymorph I	C6-C7-S1-C12,-129.38º; C8-C7-S1-C12, 57.82º
Polymorph II	C6-C7-S1-C12, 126.56º; C8-C7-S1-C12, -62.88º
Polymorph III	For X-set: C6-C7-S1-C12, 114.82 º; C8-C7-S1-C12, -73.09 º. For Y-set: C24-C25-S2-C30, 125.27 º; C26-C25-S2-C30, -64.57 º.

Conformational polymorphs of **2.1** occur due to different orientations of the carboxylate group across the sulfur atoms. Such differences cause packing patterns leading polymorphs. On the other hand, we have compared the phase purity of each polymorph by comparing the powder X-ray diffraction pattern of them with the simulated pattern from the structure determined by single crystal X-ray diffraction. The powder X-ray diffraction patterns of the three polymorphs are distinguishable which are shown in the figure 2.10. We observe that polymorph **I** has a crystal density of 1.432 g/cm^3, polymorph **II** has 1.411 g/cm^3 and polymorph **III** has a crystal density of 1.444 g/cm^3. In accordance with the Kitaigorodskii packing principle,[59] the polymorph with larger density should have loose molecular packing.

TH-1303_09612216

This is an indirect outcome of the Burger-Ramberger density rule,[60] which suggests that at absolute zero, lower density polymorph has less stability.

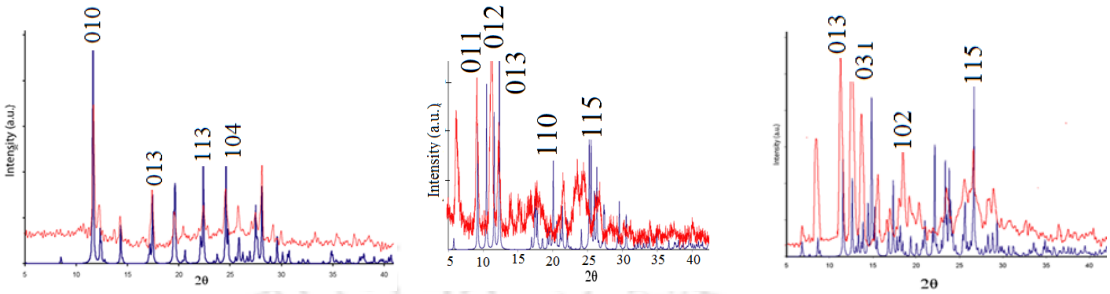

(a) (b) (c)

Figure 2.10: PXRD patterns of the (a) Polymorph **I** (**2.1a**), (b) Polymorph **II** (**2.1b**) and (c) Polymorph **III** (**2.1c**) (at heating rate 5°C per minute).

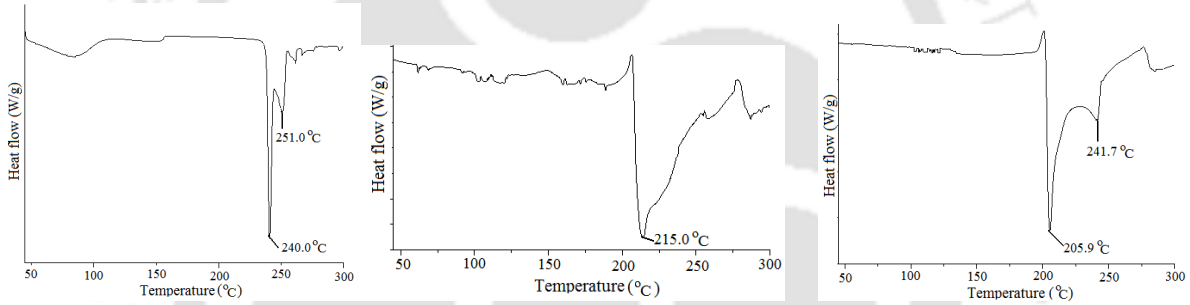

(a) (b) (c)

Figure 2.11: The differential scanning calorimetry of the (a) Polymorph **I** (**2.1a**), (b) Polymorph **II** (**2.1b**) and (c) Polymorph **III** (**2.1c**) (heating rate 5°C per minute).

On the other hand, differential scanning calorimetry (DSC) of the polymorph **II** shows it to melt at 215 °C (Figure 2.11b) and followed by this it decomposes (vide thermo gravimetric analysis). On the other hand in case of polymorph **III** has two endothermic peaks at 205 °C and 241 °C respectively, the latter corresponds to decomposition. From DSC with a heating rate of 5°C per minute, it is found that the polymorph **I** show two endothermic peaks at 240 °C and followed by decomposition of the compound at 251.8 °C. Decompositions of the compounds are confirmed from their corresponding thermograms. The results clearly show

TH-1303_09612216

that three polymorphs have distinguishable melting temperature and melting temperatures follows a trend **I > II > III**.

As mentioned earlier the compound **2.1** on crystallization from acetonitrile led to formation of an acetonitrile solvate. Solvate **IV** (**2.1d**) crystallizes in triclinic space group P-1 and its asymmetric unit contains three symmetry independent molecules of **2.1** (X, Y and Z) with a solvate molecule (acetonitrile) as shown in figure 2.12a. Among the three independent **2.1**, two X and Y-set molecules form $R^2_2(8)$ type hydrogen bond motifs. Whereas another set designated as Z-set of molecules forms also cyclic hydrogen bonded dimer among themselves (Figure 2.12b).

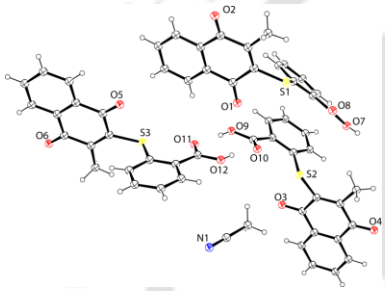

(a)

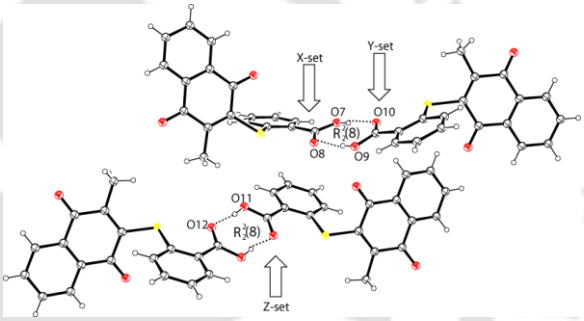

(b)

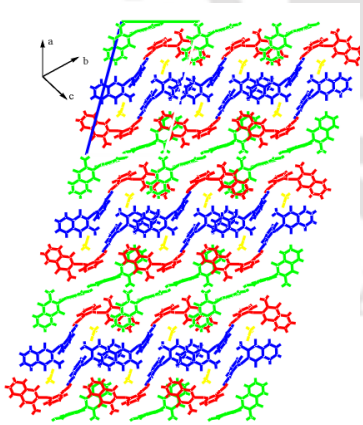

(c)

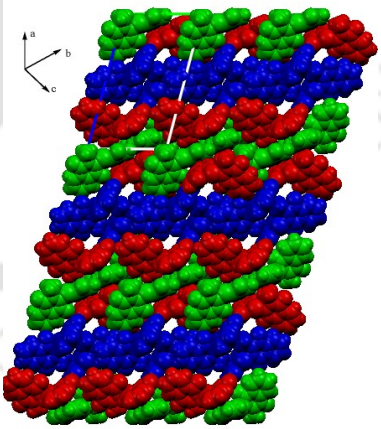

(d)

TH-1303_09612216

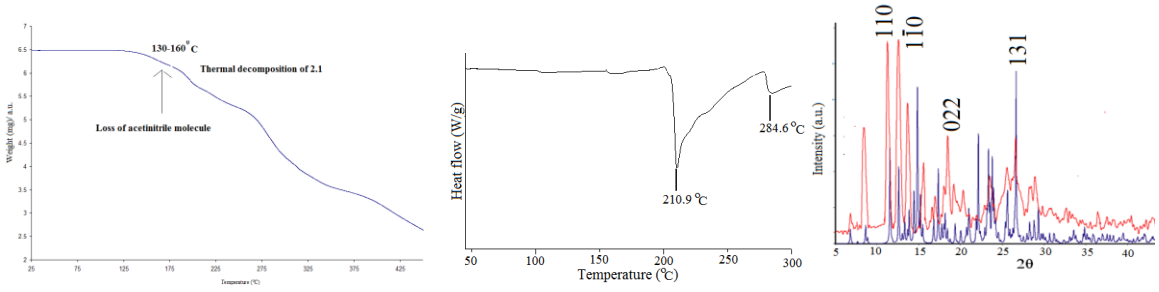

(e) (f) (g)

Figure 2.12: (a) ORTEP diagram of solvate **IV** (**2.1d**) (drawn with 30% thermal ellipsoids), (b) Cyclic hydrogen-bonded motif, (c) C-H···O and π-interactions in solvate **IV**, (d) Space filling model after removal of the acetonitrile molecules, (e) Thermogram of **IV** (heating rate 5ºC/minute), (f) DSC of solvate **IV** (heating rate 5ºC/minute) and (g) PXRD of solvate **IV**.

Although two sets of distinguishable dimeric assemblies are obtained, in both dimeric assemblies 2-methyl-1,4-naphthoquinone groups are *trans* across the hydrogen bond motif. From crystal lattice, it is observed that solvate **IV** assembles through C-H···O interactions (Table 2.4) between the quinoidal moieties as well as solvent molecules. This leads to the formation of a one-dimensional zigzag supramolecular polymeric structure. The IR spectra of the solvate **2.1d** differs from the polymorphs **I-III** significantly. In the case of solvate the carboxylic acid stretching frequency appears at 1643 cm^{-1}. Whereas IR stretching frequency at 1683 cm^{-1} is due to carboxylic acid of parent compound. The OH stretching of carboxylic acid groups appear at 3444 cm^{-1} of compounds, on the other hand OH stretching of carboxylic acid groups appear at 3410 cm^{-1} of acetonitrile solvate. The nitrile frequency appears at 2326 cm^{-1}. The thermogram from thermogrvimetric analysis (TGA) of the solvate **IV**, it is observed that the acetonitrile molecule are lost around 130-160 °C (Experimental weight loss 11.5 %, theoretical weight 12 %). However, there is a sharp weight loss in the region of 200-300 °C, which occurs due to decomposition of the compound. From the differential scanning calorimetry, it is observed that solvate **IV** has two endothermic peaks at 210 °C and 248 °C respectively. We have not observed any exo or endothermic peak for loss of acetonitrile at low temperature in DSC but show the weight loss in TGA, hence out of the two endothermic peaks of the solvate the lower temperature endothermic peak is due to the losses of acetonitrile and latter one is due to decomposition of the solvate.

TH-1303_09612216

Table 2.4: Hydrogen bond geometry (Å, °) of solvate **IV** (**2.1d**)

D-H···A	d $_{D–H}$	d $_{H···A}$	d $_{D···A}$	∠D-H···A
O7-H7···O10	0.82	1.86	2.68(3)	177.28
O9 -H9···O8	0.82	1.85	2.66(3)	172.94
O11-H11···O12 [-x,1-y,-z]	0.82	1.80	2.61(3)	173.95

The crystallization of compound **2.2** was attempted from different solvents, however good crystals could not be obtained from solvents such as methanol, ethanol, dimethylsulfoxide, tetrahydrofuran, acetone and dimethylacetamide. We could obtain crystals from dimethylformamide (DMF) solution which was found to be a DMF solvate of compound **2.2**. The dimethylformamide solvate **2.2** crystallizes in the monoclinic space group $P2_1$. The crystallographic asymmetric unit of **2.2** contains one host molecule and a DMF molecule. The DMF molecules interact with host molecules *via* both donor and acceptor types of interactions.

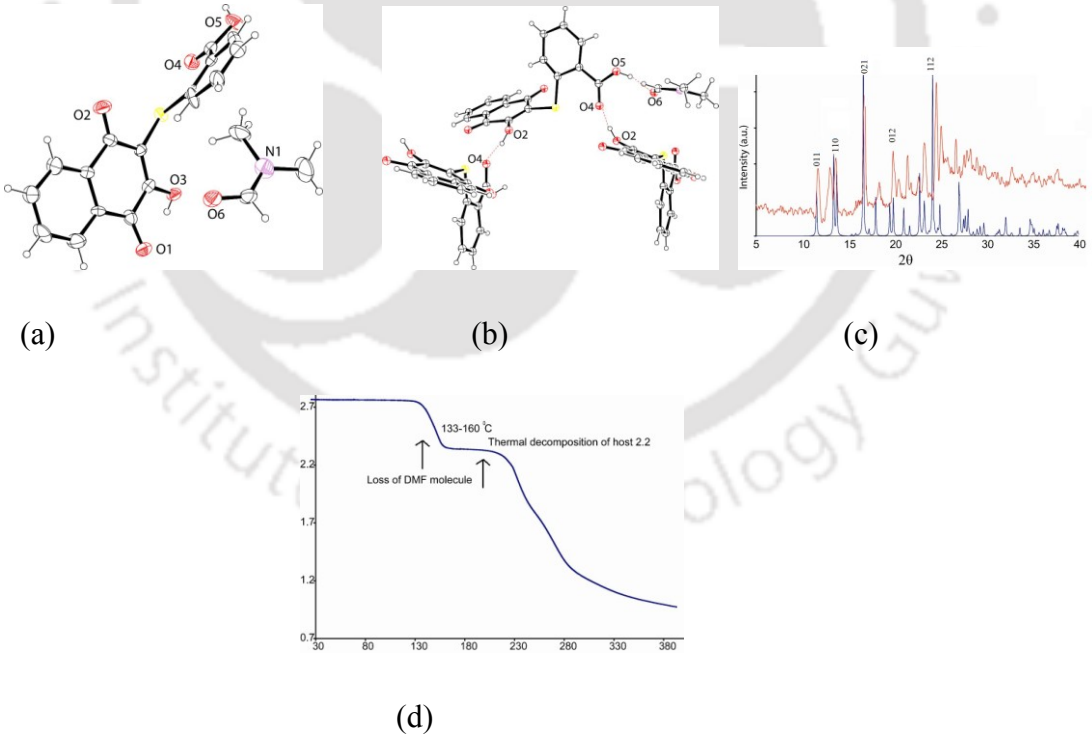

(a) (b) (c)

(d)

Figure 2.13: (a) Structure of **2.2**, (b) O-H···O interactions found in **2.2**, (c) PXRD of **2.2**. and (d) TGA of **2.3** (heating rate 5 ºC per minute).

TH-1303_09612216

The structure of compound **2.2** largely differs from the compound **2.1** as there is no dimer formation between the carboxylic acid groups. The hydroxy group of the compound interacts with the carbonyl of carboxylic acid group. The oxygen atom of the hydroxy part of carboxylic acid is involved in C-H···O interactions. The carbonyl oxygen of the DMF molecule acts as an acceptor and involves the O-H···O hydrogen bond with hydroxy group of host molecules, whereas the hydrogen atom of DMF present on carbonyl carbon acts as a donor and involves C-H···O interaction with one of carbonyl group of the quinone moieties (host molecule) as shown in figure 2.13b. The compound **2.2** are arranged in spiral manner in where DMF molecules are place in between the two host molecules. DMF solvates are well-documented in literature.[61] They interact with carboxylic acid as well as phenolic compounds through O-H···O and C-H···O interactions. In the structure of **2.2** carbonyl oxygen of DMF molecules are involved in C=O···π interaction with host molecules. The presence of DMF molecules as solvate of **2.2** is evident IR spectra of the solvate, in which stretching frequency of the carbonyl group of DMF molecule was observed at 1632 cm^{-1}. A strong IR stretching frequency at 1696 cm^{-1} due to carboxylic acid of parent compound was also observed. The OH stretching of carboxylic acid groups appeared at 3302 cm^{-1} of compound **2.2**. The thermogram (TGA analysis) of the solvate **2.2**, showed that the dimethylformide molecule was lost around 133-160 °C (Experimental weight loss 18.23 %,

Table 2.5: Hydrogen bond geometry (Å, °) of **2.2** and **2.3**

Compound no.	D-H···A	d_{D-H}	$d_{H\cdots A}$	$d_{D\cdots A}$	∠D-H···A
2.2	O2-H2A···O4 [-x,1/2+y,1-z]	0.82	2.08	2.79 (14)	146
	O6-H5···O6 [-x,1/2+y,2-z]	0.82	1.92	2.52 (15)	127
	C1-H1···O3	0.93	2.51	2.81 (18)	100
	C15-H15···O5	0.93	2.26	2.62 (18)	103
2.3	O3-H3···O4[-x,1-y,-z]	0.82	1.85	2.66 (5)	172
	C17-H17···O1	0.96	2.43	2.77 (5)	101

theoretical weight loss 18 %) (Figure 2.13d). There is sharp weight loss in the region of 200-300 °C, which occurs due to decomposition of the compound. The powder X-ray diffraction of the compound **2.2** was recorded (Figure 2.13c) to ascertain phase homogeneity. We have

TH-1303_09612216

found a good agreement of experimental and simulated PXRD data for this solvate, and it suggests the uniformity of the structural features of the bulk materials.

The compound **2.3** was crystallized from a solution of **2.3** in methanol; it crystallizes in monoclinic space group C2/c. We have tried crystallization of compound **2.3** from different solvents but in each case we obtained only one type of unsolvated crystals. From the crystal structure of **2.3**, it is observed that it forms dimeric assemblies as observed in earlier related compounds. The sulfur atom bearing 2-methyl-1,4-naphthoquinone groups are *trans* to each other across a $R_2^2(8)$ hydrogen bond motif as shown in figure 2.14b.

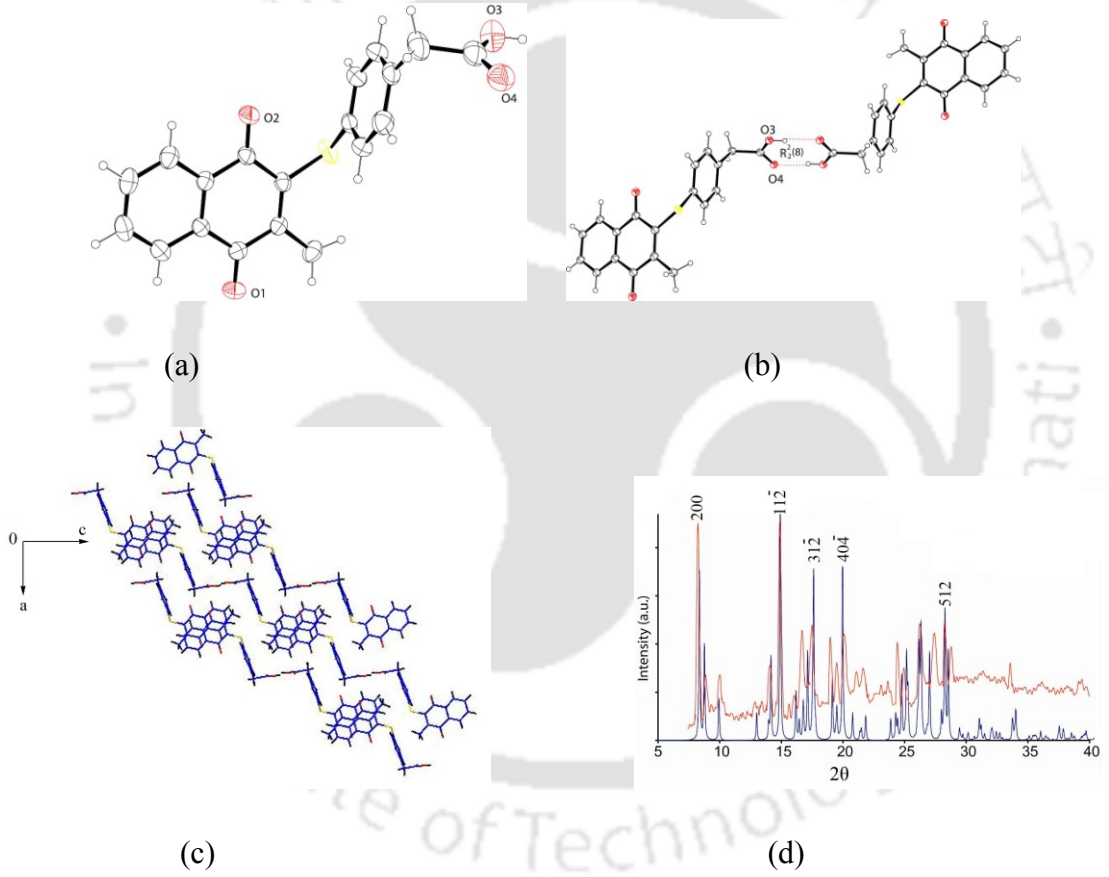

Figure 2.14: (a) ORTEP diagram of **2.3 (**drawn with 30% thermal ellipsoids), (b) O-H···O interactions found in **2.3**, (c) Packing pattern of **2.3** and (d) PXRD of **2.3**.

The carboxylic acid groups exhibit strong O3-H3···O4 interactions and form a cyclic hydrogen bond architecture as shown in figure 2.14b. Compound **2.3** forms a layered 1D polymeric structure in the lattice through C-H···O interactions as shown in table 2.4. The

TH-1303_09612216

compound **2.3** also shows π···π interactions between the carbonyl group of quinone moieties with carboxylic acid group as shown in the figure 2.14c. The powder X-ray diffraction of the compound **2.3** is recorded to ascertain their phase homogeneity. We have found a good agreement of experimental and simulated PXRD data suggesting phase uniformity of the bulk materials.

2.3: Conclusion

In conclusion, three conformational polymorphs of 2-(1,4-dihydro-1,4-dioxonaphthalen-3-ylthio) benzoic acid (**2.1**) are structurally characterized. There are dimeric assembly carboxylic acids in each polymorph but the arrangement and partner molecules makes distinctions among the polymorphs. The carbonyl groups of naphthoquinone participate in weak interactions scheme but it is not able to disrupt the formation of self assemblies between the carboxylic acid part. The acetonitrile solvates have multiple numbers of molecules in different orientations suggesting that during crystallization the solvent molecules guide certain orientations. Different polymorphs in pure form could be obtained from different solvents. In compound **2.2** the hydroxy group competes in hydrogen bonding and does not allow the formation of dimeric assemblies, on the other hand the compound **2.3** has structural similarity to compound **2.1** and retains the dimeric hydrogen bonded assemblies between the carboxylic acids.

2.4: Experimental section

2.4.1: Materials

All chemicals are obtained from commercial sources and used without further purification. Solvents (HPLC grade) are purchased from commercial sources and used without further purification or dried according to standard procedures. Melting point are recorded in open capillary tubes and are uncorrected.

2.4.2: Physical Measurement

X-ray diffraction data were collected on Bruker 3-circle diffractometers with CCD area detectors ProteumM APEX or SMART 6000 or Bruker Nonius Apex 2. The diffraction data for all the crystals were collected using Bruker SMART software. This software was also

TH-1303_09612216

used for indexing and determination of the unit cell parameters. The structures were solved by direct methods and refined by full-matrix least squares against F^2 of all data, using SHELXTL software. The IR spectra were recorded on Perkin-Elmer spectrum one spectrometer using KBr pellets. UV-visible absorption spectra were recorded using Perkin-Elmer Lambda 75 spectrophotometer equipped with double cell compartments. Melting points were recorded with a Büchi B-540 melting point apparatus. NMR spectra were recorded in DMSO-d_6 with tetramethylsilane as the internal standard for ^{1}H-NMR (400 MHz), DMSO-d_6 solvent as the internal standard for ^{13}C-NMR (100 MHz). The thermogravimetric studies were performed using a Mettler Toledo TGA/ STDA 851^e and Mettler Toledo DSC^e thermal analyzer. Typically about 4-6 mg of the samples were mounted on platinum crucibles and the TG/ DSC profiles recorded at the heating rate of 5 ºC/min and under nitrogen atmosphere (Other details of the instruments are given in Appendix).

2.4.3: General procedure for the synthesis of compounds ***2.1-2.3***

2-(1,4-Dihydro-2-methyl-1,4-dioxonaphthalen-3-ylthio)benzoic acid **(2.1)**

A solution of 2-methyl-1,4-naphthoquinone (0.34 g, 2 mmol), thiosalicylic acid (0.30 g, 2 mmol) in methanol (20 mL) was stirred for 3 h at room temperature. The color of the reaction mixture slowly turned yellow followed by formation of yellow precipitate. The precipitate was collected by filtration and dried in open air. Yield: 95%. ^{1}H-NMR (400 MHz, DMSO-d_6): 8.06 (d, J = 7.2 Hz, 1H), 7.92 (t, J = 6.0 Hz, 2H), 7.73 (d, J = 7.2 Hz, 1H,), 7.52 (d, J = 6.0 Hz, 1H), 7.29 (t, J = 7.2 Hz, 1H), 7.23 (t, J = 6.0 Hz, 1H), 6.92 (d, J = 6.0 Hz, 1H), 2.42 (s, 3H). ^{13}C-NMR (DMSO-d_6): 182.7, 180.0, 167.5, 152.8, 142.5, 138.4, 134.1, 134.0, 132.4, 132.1, 132.0, 130.9, 128.9, 128.3, 126.5, 126.3, 125.3, 16.0. IR (KBr, cm^{-1}): 3444 (m), 2922 (w), 2846 (w), 1661 (s), 1589 (m), 1459 (w), 1417 (s), 1300 (m), 1283 (s), 1179 (w), 1035 (m), 955 (m), 842 (w), 787 (w), 741 (w), 710 (w), 650 (w). MS (ESI) m/z: 324.01 $[M+H]^+$, m. p. 192 ºC.

Polymorph **I (2.1a)**: The polymorph **I (2.1a)** was obtained from a solution of **2.1** in THF/acetone (1:1 v/v) after 7 days (yield > 90%). IR (KBr, cm^{-1}): 3444 (m), 2922 (w), 2846 (w), 1683 (m), 1661 (s), 1589 (m), 1459 (w), 1417 (s), 1300 (m), 1283 (s), 1179 (w), 1035 (m), 955 (m), 842 (w), 787 (w), 741 (w), 710 (w), 650 (w).

TH-1303_09612216

Polymorph **II (2.1b)**: The polymorph **II** (**2.1b**) was crystallized as a red block from a solution of **2.1** in methanol after 3 days (yield > 40%).

Polymorph **III (2.1c)**: The polymorph **III** (**2.1c**) was obtained from a solution of **2.1** in chloroform after 4 h (yield > 70%).

Acetonitrile solvate **IV (2.1d)**: The solvate **IV** (**2.1d**) was obtained as yellow crystals from a solution of **2.1** in acetonitrile after one week (yield > 65%). IR (KBr, cm^{-1}): 3410 (m), 2937 (w), 2911 (w), 2816 (w), 2326 (m), 1643 (s), 1596 (m), 1554 (m), 1471 (w), 1432 (w) 1417 (s), 1296 (m), 1256(m), 1181 (m) 1143 (w), 1022 (m), 943 (w), 856 (w), 832 (w), 778 (w), 732 (w), 702 (w), 646 (w).

2-(1,4-Dihydro-2hydroxy1,4-dioxo-naphthalen-2,3-diylthio) benzoic acid **(2.2)**

A solution of 2-hydroxy-1,4-naphthoquinone (0.35 g, 2 mmol), thiosalicylic acid (0.30 g, 2 mmol) in methanol (20 mL) was stirred for 12 h at room temperature. The color of the reaction mixture slowly turned light yellow followed by formation of light yellow precipitate. The precipitate was collected by filtration and dried in open air. Yield: 89%. ^{1}H-NMR (400 MHz, DMSO-d_6): 8.07 (d, J = 7.2 Hz, 1H), 7.99 (d, J = 6.0 Hz, 1H), 7.94 (d, J = 7.0 Hz, 1H), 7.88 (d, J = 7.2 Hz, 1H,), 7.84 (t, J = 6.0 Hz,2H), 7.31 (t, J = 7.2 Hz, 1H), 7.17 (t, J = 6.0 Hz, 1H). ^{13}C-NMR (DMSO-d_6): 182.4, 179.9, 172.4, 149.9, 143.0, 134.6, 133.9, 133.7, 132.2, 132.0, 131.8, 130.5, 130.2, 129.2, 127.4, 126.4, 126.2. IR (KBr, cm^{-1}): 3302 (m), 3132 (w), 2857 (w), 2802 (w), 1696 (s), 1591(m), 1432 (w), 1408 (s), 1289 (m), 1223 (s), 1181 (w), 1032 (m), 941 (m), 878 (w), 753 (w), 723 (w), 701 (w), 645 (w). MS (ESI) m/z: 326.013 $[M+H]^+$, m. p. 186 ºC.

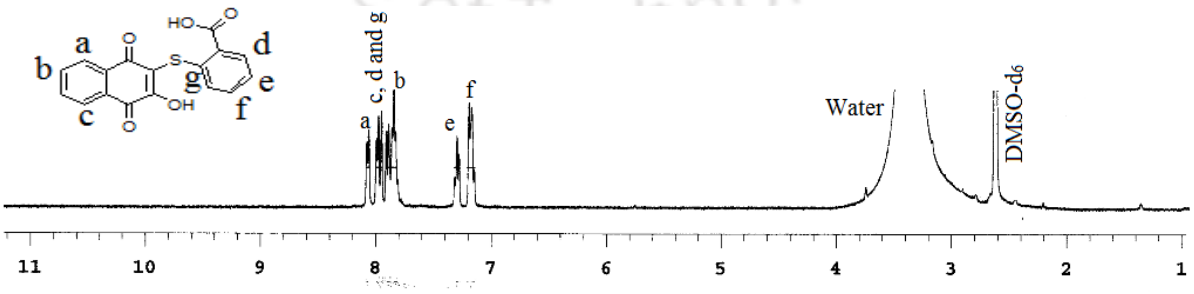

Figure 2.15: The ^{1}H-NMR (400MHz, DMSO-d_6) spectra of the **2.2**.

TH-1303_09612216

Dimethylformamide solvate **2.2:** The dimethylformamide solvate **2.2** was obtained as red crystals from a solution of **2.2** in dimethylformamide after two week (yield > 56%). IR (KBr, cm^{-1}): 3241(m), 3105 (w), 2912 (w), 2856 (w), 2817 (w), 1632 (s), 1589 (m), 1572 (m), 1521 (w), 1427 (w), 1401 (w), 1347 (m), 1211 (m), 1166 (m) 1117 (w), 1029 (m), 927 (w), 856 (w), 841 (w), 805 (w), 737 (w), 702 (w), 576 (w), 501 (w).

2-(1,4-Dihydro-2-methyl-1,4-dioxonaphthalen-3-ylthio)phenyl)acetic acid **(2.3)**

A solution of 2-methyl-1,4-naphthoquinone (0.34 g, 2 mmol), 2(4-mercaptophenyl) acetic acid (0.33 g, 2 mmol) in methanol (20 mL) was stirred for 6 h at room temperature. The color of the reaction mixture slowly turned yellow followed by formation of red precipitate. The precipitate was collected by filtration and dried in open air. Yield: 86 %. ^{1}H-NMR (400 MHz, DMSO-d_6): 12.06 (s, 1H), 8.29 (d, J = 7.2 Hz, 1H), 8.19 (d, J = 6.0 Hz, 1H), 8.10 (t, J = 7.6 Hz, 2H), 7.56 (d, J = 7.6 Hz, 2H,), 7.42 (d, J = 6.0 Hz, 2H), 3.90 (s, 2H) 2.40 (s, 3H). ^{13}C-NMR (DMSO-d_6): 182.3, 180.5, 167.0, 162.8, 140.2, 139.7, 138.6 135.6, 135.1, 134.0, 132.4, 132.1, 132.0, 130.9, 128.9, 128.3, 126.9, 42.05, 16.0. IR (KBr, cm^{-1}): 3332 (m), 2956 (w), 2872 (w), 1695 (s), 1660 (s), 1567 (m), 1432 (w), 1411 (s), 1296 (m), 1272 (s), 1164 (w), 1021 (m), 927 (m), 837 (w), 781 (w), 721 (w), 711 (w), 640 (w). MS (ESI) m/z: 338.02 $[M+H]^+$, m. p. 196 ºC.

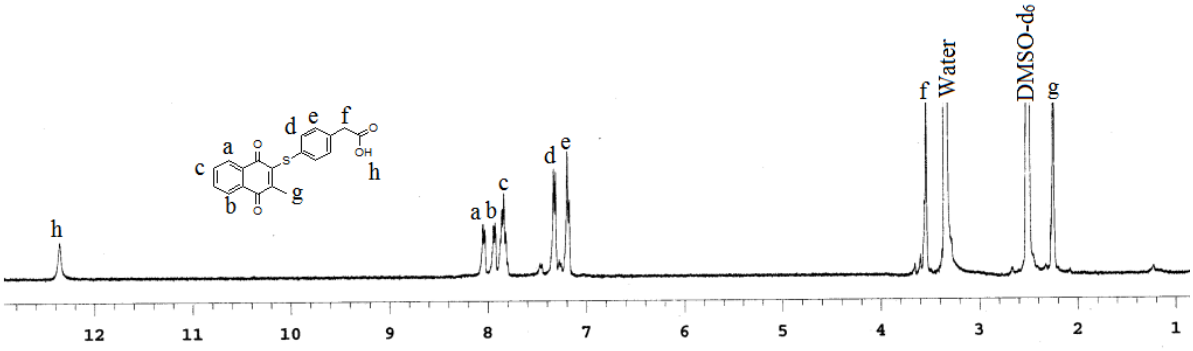

Figure 2.16: The ^{1}H-NMR (400MHz, DMSO-d_6) spectra of the **2.3**.

References:

1. S. R. Byrn, R. R. Pfeiffer and J. G. Stowell, *Solid-State Chemistry of Drugs*; SSCI: West Lafayette, IN, **1999**.

2. J. Bernstein, R. J. Davey and J. -O. Henck. *Angew. Chem. Int. Ed.* **1999**, 38, 3440.

TH-1303_09612216

3. A. Nangia, *Acc. Chem. Res.* **2008,** 41, 595.

4. B. Sarma, S. Roy and A. Nangia, *Chem. Commun.* **2006**, 4918.

5. R. Hilfiker, *Polymorphism in the Pharmaceutical Industry*, Wiley-VCH, Weinheim, Weinheim, **2006**.

6. H. G. Brittan, *Polymorphism in PharmaceuticalSolids*, Marcel Dekker, New York, **1999**.

7. T. L. Threlfall, *Analyst* **1995**, 120, 2435

8. B. R. -Spong, C. P. Price, A. Jayashankar, A. J. Matzger and N. Rodríguez-Hornedo, *Adv. Drug. Del. Rev.* **2004**, 56, 241

9. I. S. Lee, A. Y. Lee and A. S. Myerson, *Pharma. Res.* **2008**, 25, 4.

10. M. D. Prasanna and T. N. Guru Row, *CrystEngComm*, **2000**, 3, 134.

11. K. Reichenbacher, H. I. Suss and J. Hulliger, *Chem. Soc. Rev.*; **2005**, 34, 22.

12. D. Chopra and T. N. Guru Row, *CrystEngComm*, **2011**, 13, 2175.

13. R. Berger, G. Resnati, P. Metrangolo, E. Weber and J. Hulliger, *Chem. Soc. Rev.*, **2011**, 40, 3496.

14. A. G. Dikundwar, R. Sathishkumar, T. N. Guru Row and G. R. Desiraju, *Cryst. Growth Des.*, **2011**, 11, 3954.

15. D. Chopra, *Cryst. Growth Des.*, **2012**, 12, 541.

16. G. Kaur, P. Panini, D. Chopra and A. R. Choudhury, *Cryst. Growth Des.*, **2012**, 12, 5096.

17. L. Leiserowitz, *Acta Crystallogr.* B **1976**, 32, 775.

18. S.V. Kolotuchin, E.E. Felon, S.R. Wilson, C.J. Loweth and S.C. Zimmerman, *Anew. Chem., Int. Ed.* **1995**, 34, 2654.

19. T. Steiner, *Acta Crystallogr*. B **2001**, 57, 103.

20. D. Das and G.R. Desiraju, *Chem. Asian J.* **2006**, 1, 231.

TH-1303_09612216

21. S.S. Kuduva, D.C. Craig, A. Nangia, G.R. Desiraju, *J. Am. Chem. Soc.* **1999**, 121, 1936.

22. G. R. Desiraju, *Nat. Mater.* **2002**, 1, 77.

23. A. Nangia and G. R. Desiraju, *Chem. Commun*. **1999**, 605.

24. T. Laird, *Org. Process Res. Dev*. **2000**, 4, 371.

25. R. D. Rogers*, Cryst. Growth Des***. 2003**, 3, 867.

26. G. R. Desiraju, *Angew. Chem., Int. Ed*. **2007**, 46, 8342.

27. G. R. Desiraju, *CrystEngComm* **2007**, 9, 91.

28. J. Xu, J. Wang, J. C. Luft, S. Tian, G. Owens, A. A. Pandya, P. Berglund, P. Pohlhaus, B. W. Maynor, J. Smith, B. Hubby, M. E. Napier and J. M. DeSimone, *J. Am. Chem. Soc*., **2012**, 134, 8774.

29. G. R. Desiraju, *Angew. Chem., Int. Ed*. **1995**, 34, 2311.

30. A. M. Bittner, P. Behrens and E. Baeuerlein, *Handbook of Biomineralization: Biomimetic and Bioinspired Chemistry,* **2007***,* 335.

31. C. Bilton, J. A. K. Howard, N. N. L. Madhavi, A. Nangia, G. R. Desiraju, F. H. Allen and C. C. Wilson, *Chem. Commun*. **1999**, 1675.

32. V. S. S. Kumar, A. Addlagatta, A. Nangia, A. Robinson, W. T. Broder, C. K. Mondal, I. R. Evans, J. A. K. Howard and F. H. Allen, *Angew. Chem., Int. Ed*. **2002**, 41, 3848.

33. S. Chen, I. A. Guzei and L. Yu, *J. Am. Chem. Soc*. **2005**, 127, 9881.

34. P. Vishweshwar, J. A. McMahon, M. Oliveira, M. L. Peterson and M. J. Zaworotko, *J. Am. Chem. Soc*. **2005**, 127, 16802.

35. F. P. A. Fabbiania, D. R. Allan, S. Parsons and C. R. Pulham, *CrystEngComm* **2005**, 7, 179.

36. R. J. Davey, *Chem. Commun*. **2003**, 1463.

TH-1303_09612216

37. N. Blagden and R. J. Davey, *Cryst. Growth Des.* **2003**, 3, 873.

38. J. Bernstein, *Chem. Commun*. **2005**, 5007.

39. S. Long, S. Parkin, M. A. Siegler, A. Cammers and T. Li, *Cryst. Growth Des.* **2008**, 8, 4006.

40. T. Laird, *Org. Process Res. Dev*. **2000**, 4, 371.

41. R. D. Rogers*, Cryst. Growth Des*. **2003**, 3, 867.

42. L. Jiang and L. Lai, *J. Biol. Chem.,* **2002**, 277, 37732.

43. S. Scheiner, T. Kar and Y. Gu, *J. Biol. Chem.,* **2001**, 276, 9832.

44. Y. Gu and T Kar, *J. Am. Chem. Soc*. **1999**, 121, 9411.

45. R. P. Kashyap, D. Sun, W. H. Watson, *J. Chem. Crystallogr*. **1995**, 25, 339.

46. C. P. Price, A. L. Grzesiak and A. J. Matzger, *J. Am. Chem. Soc.,* **2005**, 127, 5512.

47. A. Burger and R. Ramberger, *Mikrochim. Acta* **1979**, 2, 259.

48. K. Kawakami, *J. Pharm. Sci.* 2007, **96**, 982.

49. W. M. Singh and J. B. Baruah, *Syn. Commun*. **2009**, 39, 1433.

50. T. Steiner, *Chem. Commun.* **1997**, 727.

51. F. Cozzi, M. Cinquini, R. Annunziata, T. Dwyer and J. S. Siegel, *J. Am. Chem. Soc.* **1992**, 114, 5729.

52. M. C. Etter, Acc. Chem. Res., **1990**, 23, 120.

53. W. M. Singh and J. B. Baruah, *J. mol. Struct,* **2009**, 931, 82.

54. S. Seethalekshmi and T. N. Gururow, *Cryst. Growth.Des* , **2012**, 12, 4283.

55. E. H. Lee, S. X. M. Boerrigter, A. C. F. Rumondor, S. P. Chamarthy and S. R. Byrn, *Cryst. Growth.Des* , **2008**, 8, 93.

56. P. Sanphui, B. Sarma, A. Nangia, *J. Pharm. Sci.* **2011**, 100, 2287.

TH-1303_09612216

57. G. M. Day, T. G. Cooper, A. J. Cruz-Cabeza, K. E. Hejczyk, H. L. Ammon, S. X. M. Boerrigter, J. S. Tan, R. G. Della Valle, E. Venuti, J. Jose, S. R. Gadre, G. R. Desiraju, T. S. Thakur, B. P. van Eijck, J. C. Facelli, V. E. Bazterra, M. B. Ferraro, D. W. M. Hofmann, M. A. Eumann, F. J. J. Leusen, J. Kendrick, S. L. Price, A. J. Misquitta, P. G. Karamertzanis, G. W. A. Welch, H. A. Scheraga, Y. A. Arnautova, M. U. Schmidt, J. van de Streek, A. K. Wolf, B. Schweizer, *Acta Crystallogr*. **2009**, B65, 107.

58. E. Lee, S. R. Byrn and M. T. Carvajal, *Pharm. Res.* **2006**, 23, 2375.

59. A. I. Kitaigordoskii, *Molecular Crystals*; Nauka: Moscow, **1971**.

60. A. Burger, R. Ramberger, *Microchim. Acta*, **1979**, II, 259.

61. V. Suitchmezian, I. Jess, and C. Näther, *Cryst. Growth.Des* , **2009**, 9, 774.

TH-1303_09612216

Chapter 3

Anion binding properties of 2-methyl-1, 4-naphthoquinone functionalized imidazole derivatives

Supramolecular chemistry of anions has received wide attention because of their relevance in biology and the environment.[1] It is difficult to pre-decide selective binding of anions with a receptor through weak interactions.[2-8] Anion recognition properties vary with substiuents and functional groups present on a receptor.[9-14] Anions are generally larger than neutral molecules, they can be polarized easily and have a tendency to associate through electrostatic interactions.[15] Generally anion receptors are designed from molecules having site/s for hydrogen bond formation as neutral hosts or have binding sites to exercise hydrogen bonds and electrostatic interactions.[16-18] Anion-directed assemblies of coordination polymers provide motivation to study them in recognition, separation, guest inclusion and catalysis.[19-35] The majority of hydrogen bonded anion receptors utilize *N*-H···anion or *O*-H···anion hydrogen bonds. Although C-H···anion interactions are present in biological systems, they are less utilized in general.[36-40] Selective binding of an anion by a host molecule depends on size and geometry of the anion as well as of the host molecule. Imidazole is a biologically relevant molecule. Imidazole can be functionalized to make either organic or inorganic scaffolds. Nitrogen atom of the imidazole ring can be easily protonated to form its corresponding salt and such hosts are used as cationic receptors for anions. There are numerous examples of host molecules containing imidazolium moieties.[41-42] Imidazolium functionalized complexes capable of binding anions through C-H···X^- hydrogen bonds.[43] Anion binding by imidazole derivatives [44] are also of interest as they occur as amino acid residues of natural proteins. Highly selective receptors (**3.1a-c**) based on an acridine-imidazolium functionalized cholestane[45] are used for various anion detection. For example compound **3.1c** showed the highest selectivity toward hydrogen pyrophosphate as shown in figure 3.1.

TH-1303_09612216

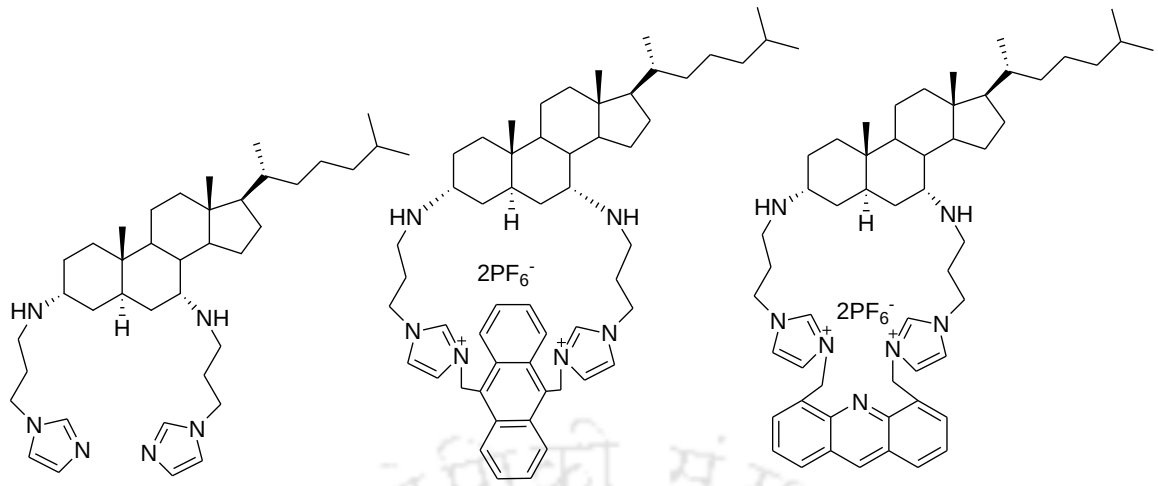

3.1a 3.1b 3.1c

Figure 3.1: Some examples of imidazole based anion receptors.

Most of the imidazole based receptor a signaling part is to be attached to generate signals. The signaling part can be in the form of a compound in which its characteristic signal can be tuned by external stimuli shows. Among such molecules attachment of a fluorescent unit to such binding molecules are commonly used as sensors. In this regard, quinones are weakly fluorescence compound but bio-compatible molecules. They also are electroactive, hence changes electrochemical properties can be monitored by electrochemical techniques. Quinones are fluorescent molecules and they are indispensible in nature. Thus, we have taken up synthesis and character, isolation of imidazole based naphthoquinone derivatives to study their anion binding properties. This chapter deals with synthesis, characterization and studies on acid-binding abilities of 2-(1*H*-imidazole-2-ylthio)-3-methylnaphthalene-1,4-dione (imd, **3.2**) and 2-(1-methyl-1*H*-imidazole-2-ylthio)-3-methylnaphthalene-1,4-dione (mmd, **3.3**) shown in figure 3.2.

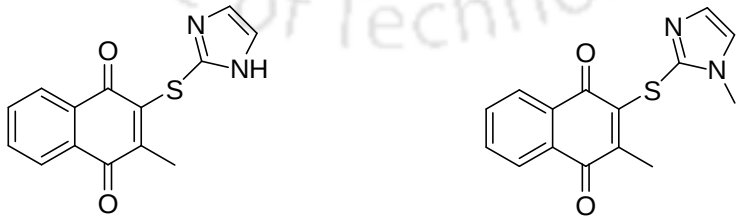

3.2 3.3

Figure 3.2: 2-(1*H*-imidazole-2-ylthio)-3-methylnaphthalene-1,4-dione (imd, **3.2**) and 2-(1-methyl-1*H*-imidazole-2-ylthio)-3-methylnaphthalene-1,4-dione (mmd, **3.3**)

TH-1303_09612216

3.1: Synthesis and characterization of imd and mmd

2-(1*H*-imidazole-2-ylthio)-3-methylnaphthalene-1,4-dione (imd; **3.2**) and 2-(1methyl-1*H*-imidazole-2-ylthio)-3-methylnaphthalene-1,4-dione (mmd; **3.3**) were synthesized by independently treating 2-methyl-1,4-naphthoquinone with 2-mercaptoimidazole and 2-mercapto-1-methyl-imidazole by adopting a procedure reported for analogous compounds.[46] Single product was formed in each case and they were characterized by IR, ^{1}H-NMR, ^{13}C-NMR and ESI mass. The ^{1}H-NMR spectra of imd is shown in figure 3.3. In the ^{1}H-NMR of imd, singlet at 2.09 ppm is for the protons of methyl group of 2-methyl-1,4-naphthoquinone, singlet at 7.35 ppm and 7.28 ppm are for imidazole protons; whereas singlet at 12.35 ppm is for -NH protons of imidazole. The ^{13}C-NMR signals at 184.9 and 184.5 ppm are attributed to the carbon attached to the two carbonyl of methyl naphthoquinone, whereas signals of the carbons appear in the range of 147.9-133.9 ppm and signals for three carbons of imidazole appear at 131.6, 126.0, 125.5 ppm. The methyl group attached to the naphthoquinone ring is observed at 15.9 ppm. In IR spectra of imd the N-H stretch appear at 3451 cm^{-1}. The ESI mass spectra m/z peaks at 271.05 and 541.10 which corresponds to the $[M+H]^{+}$ and $[2M+H]^{+}$ for compound imd. The ESI mass spectra m/z peak at 285.08 which corresponds to the $[M+H]^{+}$.

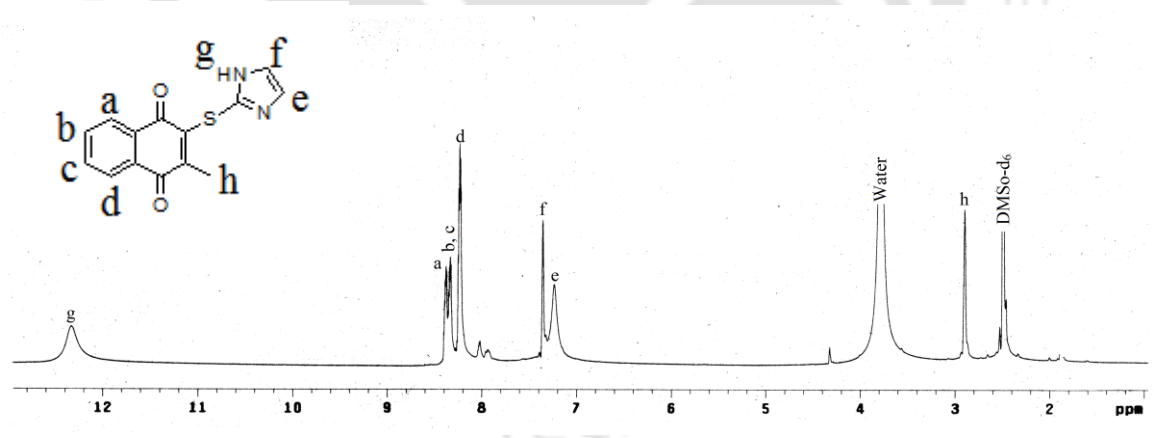

Figure 3.3: ^{1}H-NMR (400MHz, DMSO-d_6) spectra of the imd (**3.2**).

Naphthoquinone signals in ^{1}H-NMR of the mmd has similarity to the corresponding signals in the spectra of imd, but it has difference in the imidazole signals. Imidazole protons in this ring show a signal at 7.29 ppm and the signals for N-methyl group and C-methyl group appears at 3.60 ppm and 2.34 ppm respectively. In ^{13}C-NMR carbon-atom of the N-methyl and C-methyl groups appear at 28.3 ppm and 18.2 ppm respectively.

TH-1303_09612216

3.2: Structural study of products of imd and mmd on reactions with various acids

Compounds imd and mmd form various crystalline salts on reaction with different acids. The salts of imd with acids such as hydrochloric, hydrobromic, nitric, perchloric and tetrafluoroboric acid crystallize with the general composition [Himd]X ([Himd]Cl (**3.2a**), [Himd]Br (**3.2b**), [Himd]NO_3 **3.2c**), [Himd]ClO_4 (**3.2d**), and [Himd]BF_4 (**3.2e**)). Whereas in the case of mmd only corresponding chloride and nitrate salts with a general composition [Hmmd]X (In which [Hmmd]Cl (**3.3a**) and [Hmmd]NO_3 (**3.3b**)) were obtained (equation 3.1.a). Structures of all these salts were determined and their fluorescence properties were studied.

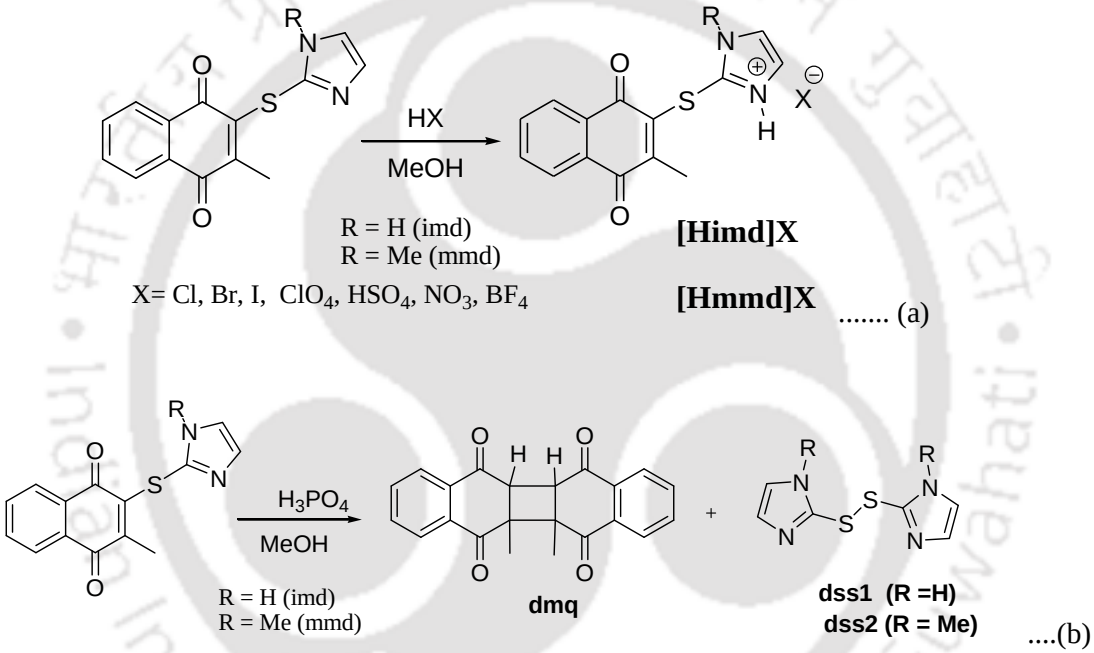

Scheme 3.1: Reactions of imd and mmd with acids.

Among various acids used for preparation of salts, phosphoric acid was found to be an exception, which caused dimerisation by loss of thioimidazole group. The reactions led to S-S bonded compounds dss1 and dss2 from thioimidazole part (equation 3.1b) from respective reactions phosphoric acid with imd and mmd. In case of imd, dss1 was formed and in case of mmd, dss2 was formed. Since these S-S bonded compounds dss1 and dss2 were reported earlier in literature,[46b-e] their physical properties were compared with authentic samples and confirmed. The dimeric product[46f] abbreviated as dmq obtained from such reactions of 2-methyl-1,4-naphthoquinone **3.4**, was characterized by IR, ^{1}H-NMR, ^{13}C-NMR spectroscopy and ESI mass spectrometry. From the ^{1}H-NMR spectra we

TH-1303_09612216

observed that product was formed in *cis* conformation and we could not find any *trans* product.

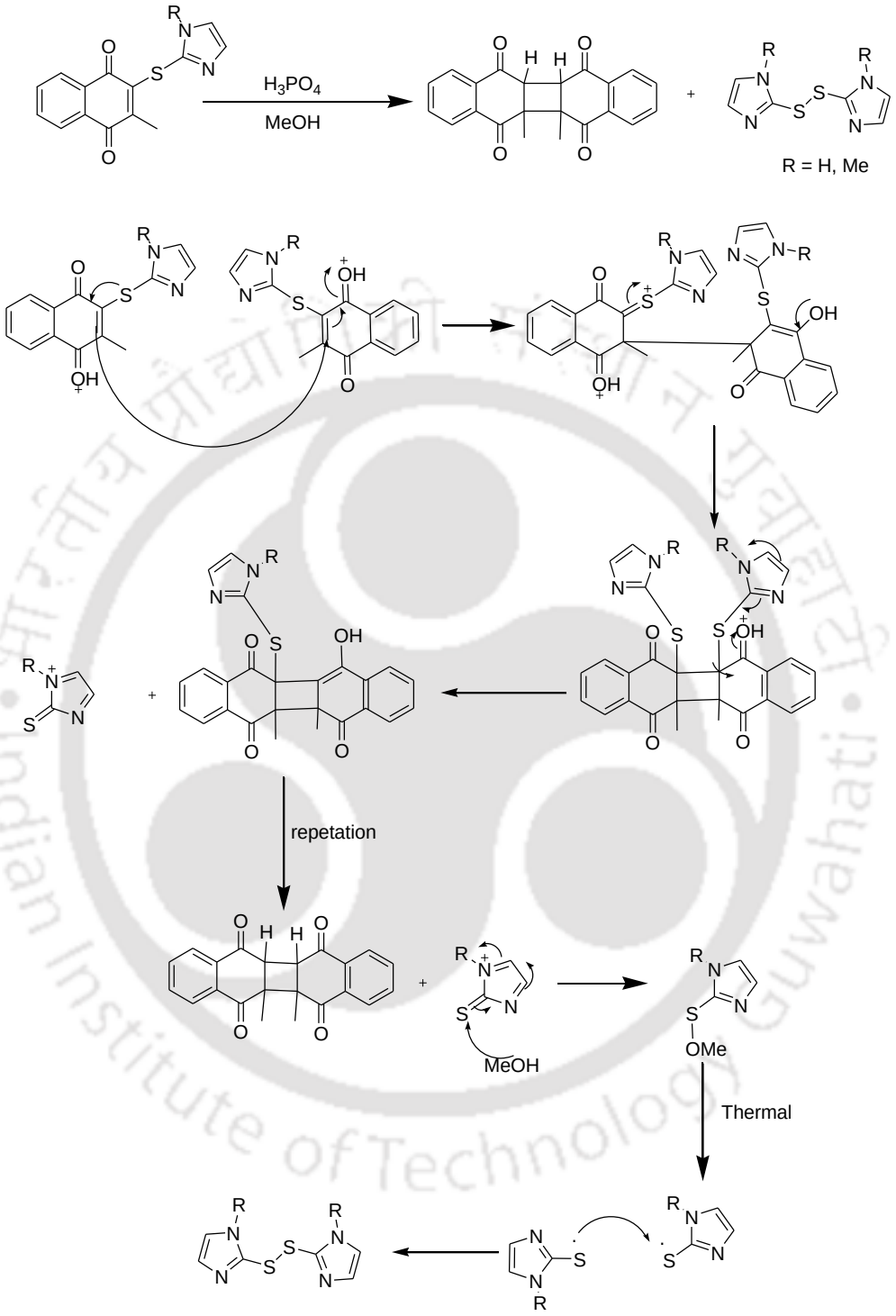

Scheme 3.2: The plausible mechanism for conversion of dmq.

In the ^{1}H-NMR we observed a triplet in the aromatic region at 7.63 ppm for proton b and c whereas two doublet peaks at 7.56 ppm and 7.53 ppm in aromatic region respectively. In addition, one sharp singlet peak was observed at 3.92 ppm for quaternary protons, on

TH-1303_09612216

the other hand one sharp singlet at 1.48 ppm for methyl protons as shown in the figure 3.4.

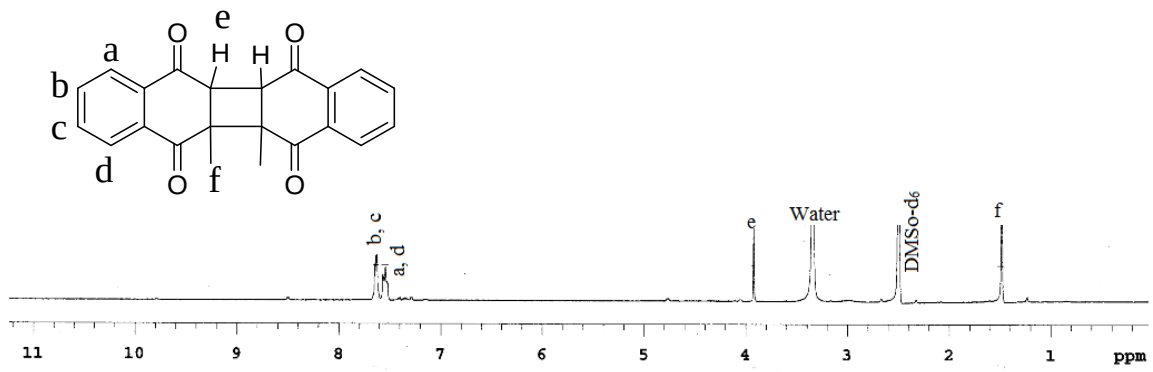

Figure 3.4: ^{1}H-NMR (400 MHz, DMSO-d_6) spectra dmq (**3.4**).

In ^{13}C-NMR spectra carbonyl peaks were observed at 196.5 and 193.6 ppm, whereas two quaternary carbon peaks at 53.8 and 51.6 ppm and methyl carbon at 19.3 ppm. Further, the stereochemistry of dmq was confirmed by determining structure by X-ray single crystal diffraction. Various salts and formation of dmq from reactions of imd and mmd with acids are listed in table 3.1.

Table 3.1: Formation of different salts

Sl. No.	Substrate	Acid	Product	Yield (%)
1	imd	H_3PO_4	dmq + dss1	86
2	imd	H_3PO_4	dmq + dss2	92
3	imd	$HClO_4$	[Himd]ClO_4	83
4	imd	HBr	[Himd]Br	79
5	imd	HCl	[Himd]Cl	76
6	mmd	HCl	[Hmmd]Cl	80
7	imd	HNO_3	[Himd]NO_3	65
8	mmd	HCl	[Hmmd]NO_3	72
9	imd	HBF_4	[Himd]BF_4	77

The single crystal structure of compound dmq (**3.4**) is shown in figure 3.5a. In crystal packing naphthoquinone moieties form cyclic hydrogen bonded assembly through weak C-H···O interactions (figure 3.5b). The hydrogen bond parameters for the C-H···O interactions are listed in table 3.2.

TH-1303_09612216

Table 3.2: Hydrogen bond geometries (Å, °) of bmq (**3.4**)

D-H···A	d $_{D-H}$	d $_{H\cdots A}$	d$_{D\cdots A}$	∠D-H···A
C4- H4···O1 [1-x,y,1/2-z]	0.93	2.57	3.34 (5)	142.00
C22-H22C···O2[1/2+x,-1/2+y,z]	0.96	2.47	3.37 (6)	157.00

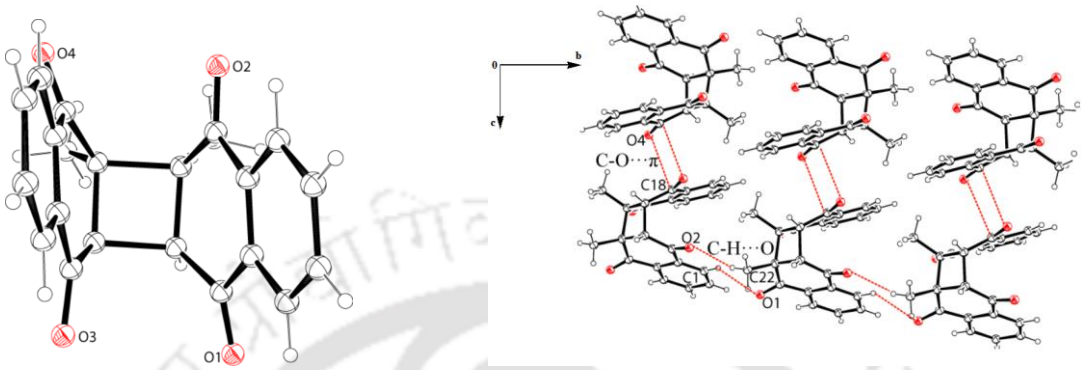

(a) (b)

Figure 3.5: (a) ORTEP diagram of dmq (**3.4**) (drawn with 30 % thermal ellipsoids). (b) Self-assemblies of dmq.

3.2a: Structural study on salts of imd

As mentioned the imidazole bearing compounds imd as well as mmd form salts of various acids, it is interesting to analyse their self assemblies. Such interest stems from understanding the role of anions on the emission properties of quinoidal compounds and their possibility to selectively recognise of anion. Imidazole has ambidentate characteristics; it can interact with an anion without getting protonated or after getting protonated as illustrated in scheme 3.3. It may be expected that the self assembly formed in the protonated imd and mmd will be guided by the directional properties associated with various anions.

TH-1303_09612216

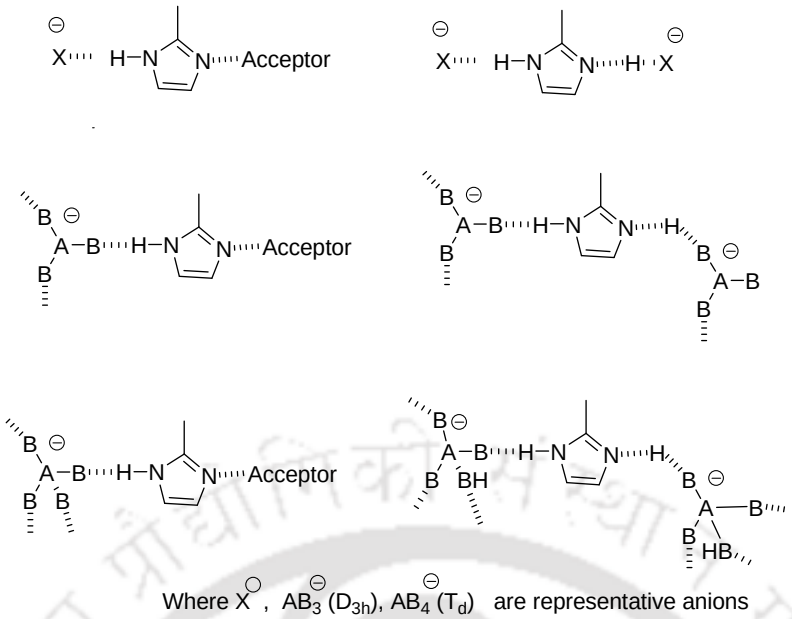

Scheme 3.3: Some ways to form anion assisted assemblies of protonated imidazole

Salt [Himd]Cl crystallizes in monoclinic space group $P2_1/c$, and it's asymmetric unit contains one protonated receptor and chloride anion. In [Himd]Cl the cationic part of the imidazolium salt is held by electrostatic interactions with the chloride ion. It forms a hydrogen-bonded self-assembly in which imidazolium unit acts as a hydrogen-bond donor, namely, N^+-H hydrogen bonds to chloride ions form an anion-assisted assembly as shown in figure 3.6a. The anions are in tetrahedral hydrogen-bonded environments as shown in figure 3.6b.

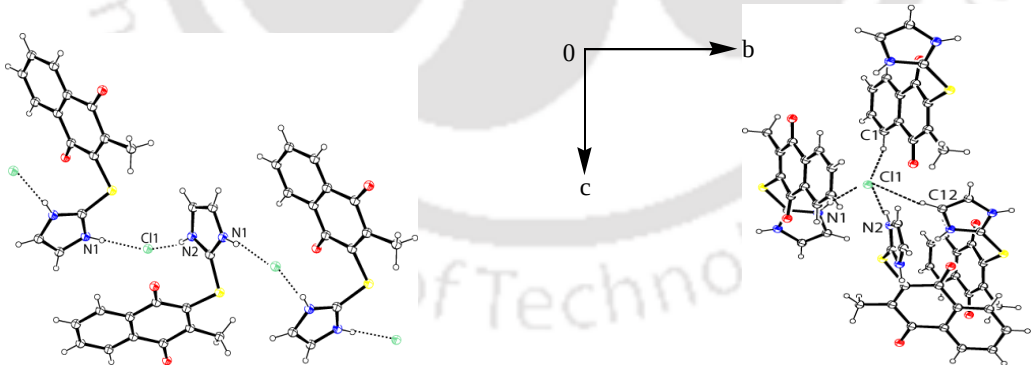

(a) (b)

Figure 3.6: (a) One dimensional hydrogen bond motif in [Himd]Cl. (b) Anion assisted assembly of [Himd]Cl.

Similar hydrogen-bonded environments are observed in halide-anion-assisted assemblies of amide or pyrrole-based hosts.[47-57] The cationic part of salt [Himd]Cl also contributes to the assembly by forming weak C4-H4···O2 and C13-H13···O1 hydrogen bonds in table 3.3.

TH-1303_09612216

Table 3.3: Hydrogen bond geometry (Å, °) for salt [Himd]Cl

D-H···A	d (D-H)	d (H···A)	d (D···A)	<D-H···A
N1-H1A···Cl	0.86	2.24	3.08 (4)	167.57
N2- H2A···Cl1[-x,-1/2+y,1/2-z]	0.86	2.26	3.11 (3)	169.79
C4- H4···O2 [-x,1-y,1-z]	0.93	2.52	3.43 (6)	170.26
C12- H12···Cl1 [-x,1-y,-z]	0.93	2.83	3.71 (4)	160.50
C13-H13···O1 [-1+x,1/2-y,-1/2+z]	0.93	2.40	3.23 (6)	149.07
C14- H14B···O1	0.96	2.43	2.76 (5)	100.43

Salt [Himd]Br crystallizes in monoclinic $P2_1/c$ space group, and the asymmetric unit of [Himd]Br contains one protonated receptor and one bromide anion as shown in figure 3.7a. It is isostructural with [Himd]Cl; so only the supramolecular coordination environment of bromide ion is shown. The N-H···Br and C-H···Br interactions parameters are listed in table 3.4.

Table 3.4: Hydrogen bond geometry (Å, °) of salt [Himd]Br

D-H···A	d_{D-H}	$d_{H\cdots A}$	$d_{D\cdots A}$	∠D-H···A
N1-H1A···Br1 [x,1/2-y,-1/2+z]	0.86	2.39	3.23 (4)	168.24
N2- H2A···Br1 [1-x,-y,1-z]	0.86	2.41	3.26 (5)	171.21
C4- H4···O1 [1-x,1-y,1-z]	0.93	2.46	3.35 (7)	160.93
C13-H13···Br1 [1-x,1/2+y,1/2-z]	0.93	2.90	3.81 (5)	166.26
C14-H14···O2 [-1+x,1/2-y,-1/2+z]	0.93	2.36	3.23 (6)	155.54

Hydrogen-bond distances of the bromide salt are slightly greater than those of the chloride salt (Table 3.4). This is due to the larger ionic radii and lower basicity of the bromide ion as compared to chloride ion.

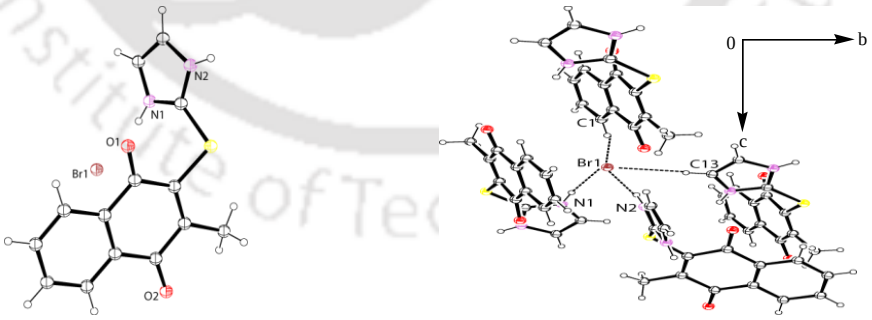

(a) (b)

Figure 3.7: (a) ORTEP diagram of [Himd]Br (drawn with thermal ellipsoid 30%) and (b) Hydrogen bond environment of bromide ion in [Himd]Br.

Nitrate salt [Himd]NO_3 obtained from the reaction of nitric acid with imd crystallizes in monoclinic space group $P2_1/c$, the asymmetric unit contains an anion and protonated receptor (Figure 3.8a). The nitrate anions are associated with bifurcated hydrogen bond

TH-1303_09612216

interactions between the hydrogen of the protonated imidazole and the nitrate oxygen atoms O3 and O5 with an N···O distance 2.76 Å, 3.13 Å and N-H···O bond angles are 157.70º and 129.44º respectively. Such hydrogen bond interactions form a $R^2_1(4)$ hydrogen bond cyclic architecture as shown in figure 3.8b. The environment around the nitrate shows that each anion is involved in a five point attachment from four $Himd^+$ units with four N-H···O contacts (including bifurcated interactions) and one C-H··O contact.

The imdazole moiety is involved in C13-H13···O4 interactions and the methyl group of 2-methyl-1,4-naphthoquinone ring shows C10-H10A···O4 interactions (Table 3.5). Both N-H and the N^+-H groups of the imidazole moiety act as H-bond donor, which engages in hydrogen bond with the nitrate ion forming a 1D linear H-bond architecture. The other weak interactions contributing to the lattice are C14-H14···O2, face to face π···π interactions, C-H···N and C-H···π interaction leads to a tight packed structure. The C-H···π interactions in biological molecules are involved in a wide variety of functions such

Table **3.5**: Hydrogen bond geometry (Å, °) of salt [Himd]NO_3

D-H···A	d $_{D–H}$	d $_{H···A}$	d $_{D···A}$	∠D-H···A
N1-H1A···O4 [x, 1/2-y, -1/2+z]	0.86	1.93	2.76 (19)	161.94
N2-H2A···O3	0.86	1.95	2.76 (2)	157.70
N2-H2A···O5	0.86	2.51	3.13 (2)	129.44
C2-H2···O2 [-x,1/2+y,-1/2-z]	0.93	2.58	3.47 (2)	161.08
C10-H10A···O4 [-x,-1/2+y,1/2-z]	0.96	2.59	3.25(3)	126.41
C14-H14···O2 [1+x,1/2-y,1/2+z]	0.96	2.47	3.08(2)	123.58

as stabilization secondary structure,[58] drug recognition,[59] DNA recognition[60] and enzyme action.[61] Indole-3-acetic acid shows C-H···π and N-H···π interactions while participating in biological functions such as cell division and protein synthesis.[62] Imidazole being an important part of amino acid residue understanding such C-H···O interaction enrich occurrence in biological related molecules.

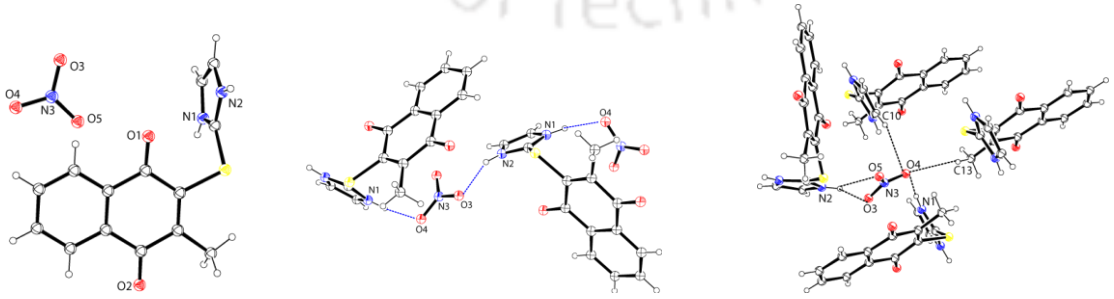

(a) (b) (c)

TH-1303_09612216

Figure 3.8: (a) ORTEP diagram of [Himd]NO_3 (drawn with thermal ellipsoid 30%), (b) 1D linear hydrogen bonding architecture found in nitrate salt and (c) Weak interactions found in [Himd]NO_3.

The crystals of salt [Himd]ClO_4 belong to the monoclinic space group C2/c, and an anion and protonated receptor constituted the asymmetric unit of the salt (Figure 3.9a). Salt [Himd]ClO_4 shows the packing constructed by hydrogen bond bridge between N^+-H of imidazolinium cation and two oxygen atoms O4 and O5 of perchlorate anion to form a chain-like structure. There are also C-H···O interactions between the naphthoquinone ring hydrogen (C2-H) with the oxygen O4 atom of the perchlorate anion (Table 3.6). $Himd^+$ interacts with the perchlorate anion in a similar fashion to that of the chloride/bromide anion shown in figure 3.9b. There are two types of intermolecular C-H···O interactions; the first interaction is between one of the oxygen atoms of perchlorate

Table 3.6: Hydrogen bond geometry (Å, °) of [Himd]ClO_4

D-H···A	d $_{D–H}$	d $_{H···A}$	d $_{D···A}$	∠D-H···A
N1-H1A···O4	0.86	2.10	2.84 (11)	144.18
N2-H2A···O5 [1/2+x,1/2+y,z]	0.86	2.10	2.85 (10)	147.34
C1-H1···O1 [1-x,y,1/2-z]	0.93	2.60	3.27 (12)	130.35
C14-H14···O2[1/2+x,1/2-y,1/2+z]	0.93	2.48	3.11 (10)	126.02

with the C2-H of the naphthoquinone ring; second interaction is between another oxygen atom of the perchlorate with the C13-H of the imidazolium ion (Table 3.6). It is observed that both N-H and N^+-H groups of the imidazolium part act as hydrogen-bond donors.

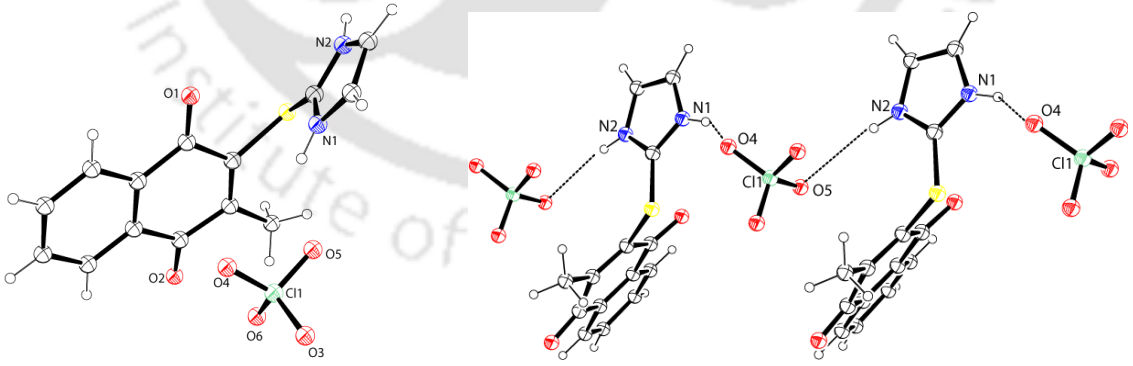

(a) (b)

TH-1303_09612216

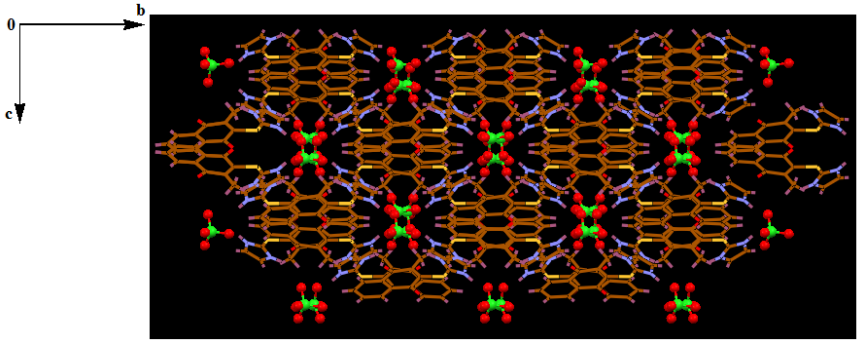

(c)

Figure 3.9: (a) ORTEP diagram of [Himd]ClO_4 (30% thermal ellipsoid). (b) One-dimensional assembly of [Himd]ClO_4 and (c) Channel-like structure of [Himd]ClO_4 to include perchlorate anions.

Salt [Himd]BF_4 crystallizes in monoclinic space group C2/c. It has one $Himd^+$ and one tetrafluoroborate in asymmetric unit. Structure of the salt is shown by ORTEP diagram given in figure 3.10a. The tetrafluoroborate anion posses two different N-H···F interactions in the lattice of salt [Himd]BF_4, namely, N1-H1A···F2 and N2-H2A···F1. There is also a C13-H13···F4 interaction as illustrated in figure 3.10b, this interaction contributes to the form anion assisted hydrogen-bonded assembly with the host cations.

Table 3.7: Hydrogen bond geometry (Å, °) of [Himd]BF_4

D-H···A	d_{D-H}	$d_{H\cdots A}$	$d_{D\cdots A}$	∠D-H···A
N1-H1A···F2 [-x,+y,-z+1/2]	0.86	1.93	2.74 (8)	153.07
N2-H2A···F1 [x+1/2,+y-1/2,+z]	0.86	2.01	2.81 (7)	151.83
C4-H4···O2 [-x,y,1/2-z]	0.93	2.59	3.29 (7)	132.25
C11-H11B···O1	0.96	2.66	2.75	85.62

In addition to these interactions, there are two other intermolecular C-H···O interactions between one of the oxygen atoms of naphthoquinone with C14-H of the imidazolium ion. Beside that the tetrafluoroburate ions are encapsulated by the receptor molecule through weak interactions such as C-H···O, C-H···π and π···π interactions.

TH-1303_09612216

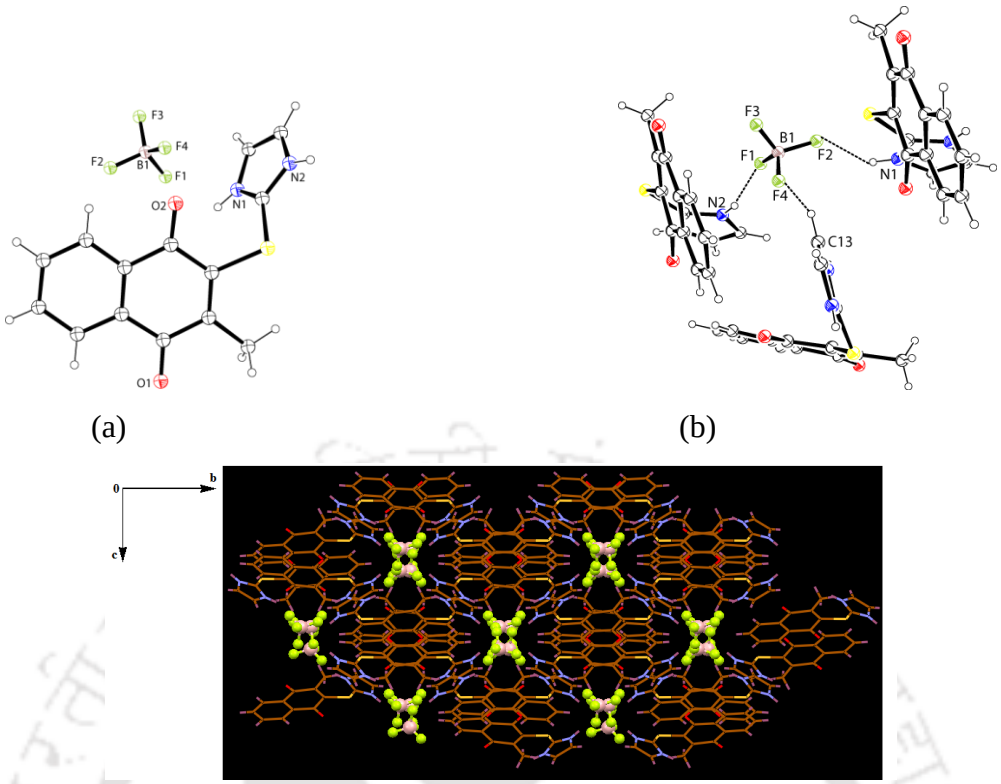

Figure 3.10: (a) ORTEP diagram of [Himd]BF_4 (drawn with 30% thermal ellipsoid), (b) The coordination environment of the chloride ion in [Himd]BF_4 and (c) Channel like structure where perchlorate anions are included.

*3.2b: Structural study on the salts of mmd (**3.3a-b**)*

The chloride salt [Hmmd]Cl crystallizes in the monoclinic space group C2/c, and the asymmetric unit contains an anion and protonated receptor (Figure 3.11a). The cationic part of the methyl-imidazolium salt is held by electrostatic interactions with chloride ion. It forms a hydrogen-bonded self-assembly. The methyl-imidazolium unit acts as a hydrogen-bond donor, namely, N^+-H hydrogen bonds to chloride ions to form an anion-assisted assembly (Table 3.8). The anions are in tetrahedral hydrogen-bonded environments as shown in figure 3.11b. Methyl group has definite impact in anion assisted assembly of mmd salt, it takes part in weak C11- H11B···O1 bond scheme, there is also C-H···O interaction between C-H of imidazole ring with chloride anion. Whereas such interactions in the case of chloride salt of imd take place through one of the C-H bond of imidazole ring and one from the C-H of naphthoquinone ring. The chloride ions in the anion assisted assembly of [Hmmd]Cl are in a distorted tetrahedral environment. Such environment is created by three C-H···Cl and one N-H···Cl interactions.

TH-1303_09612216

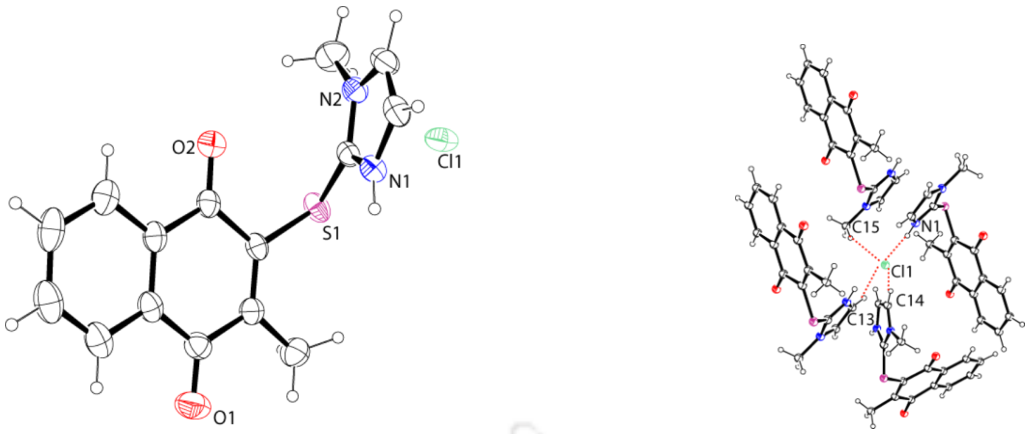

(a) (b)

Figure 3.11: (a) ORTEP diagram of chloride salt [Hmmd]Cl (drawn with 30% thermal ellipsoids) and (b) Self-assembly of chloride salt.

Table 3.8: Hydrogen bond geometry (Å, °) of chloride salt [Hmmd]Cl

D-H···A	d $_{D–H}$	d $_{H···A}$	d$_{D···A}$	∠D-H···A
N1-H1···Cl1[x,1/2-y,z]	0.86	2.13	2.98(16)	175.00
C11- H11B···O1	0.96	2.35	2.76 (3)	106.00
C13-H13···Cl1 [1-x,1/2+y,1/2-z]	0.93	2.65	3.55 (19)	164.00
C14-H14···O2	0.93	2.58	3.43 (2)	153.00

The asymmetric unit and which possesses a nitrate salt [Hmmd]NO_3 which are $P2_1/_C$ space group comprised of mmd cation and a nitrate ion. From the crystal lattice it is observed that the nitrate anions are associated with a bifurcated N^+-H···O interaction between the hydrogen atom of protonated imidazole with oxygen atoms O3 and O4 of the nitrate ion ($d_{N···O}$ distances of 2.72 and 3.25 Å and N-H···O bond angles of 169.89 and 127.03, as shown in table 3.9, respectively). Such hydrogen bonds lead to the formation of a cyclic $R^2_1(4)$ hydrogen-bond architecture. Each nitrate ion is involved in five-points of contacts provided by four $Himd^+$ units with one N-H···O interactions (including bifurcated interactions) and three C-H···O interaction as shown in figure 3.12b. It may be noted that nitrate salts can self-assemble and occur as dimeric assemblies[63] in organic salts and we have not observed such assembling and the anions occur as discrete units held by three host cations. N-methyl groups participates in C-H···O interactions with nitrate ion.

TH-1303_09612216

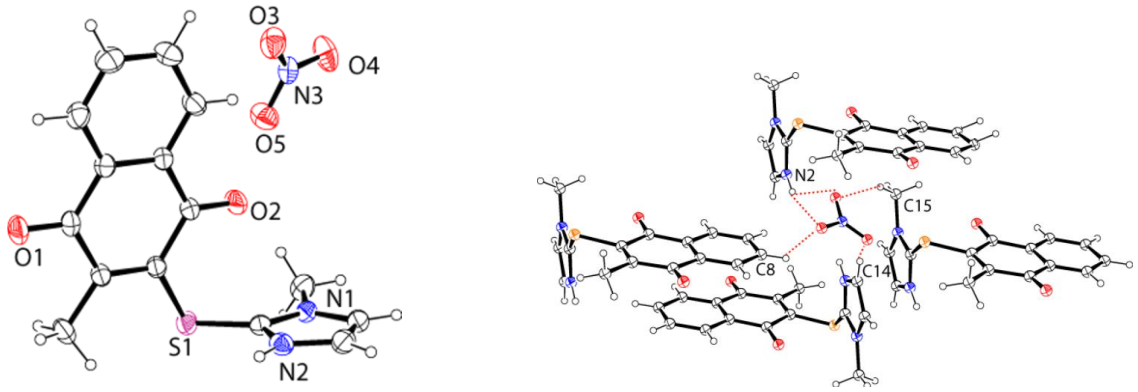

(a) (b)

Figure 3.12: (a) ORTEP diagram of nitrate salt (drawn with 30% thermal ellipsoids) and (b) The coordination environment of nitrate salts [Hmmd]NO_3 .

Table 3.9: Hydrogen bond geometry (Å, °) of nitrate salt [Hmmd]NO_3

D-H···A	d $_{D–H}$	d $_{H···A}$	d$_{D···A}$	∠D-H···A
N2-H2···O4[1+x,y,z]	0.86	1.87	2.72 (3)	169.89
C5- H5···O1 [-1+x,y,z]	0.93	2.49	3.31 (3)	149.00
C13- H13···O3 [1-x,1-y,1-z]	0.93	2.59	3.28 (4)	132.00
C14-H14···O5 [1-x,-y,-z]	0.93	2.44	3.12 (4)	130.00
C15-H15B···O3 [-x,1-y,-z]	0.96	2.49	3.21 (3)	133.00

3.3: Study on the interaction of imd and mmd with mineral acids

The UV-visible spectra of compound imd shows an absorption maximum at 329 nm due to n→ π* transition. A solution of imd in methanol shows an emission at 418 nm upon excitation at λ 350 nm. Taking advantage of this emission of the parent compound, we performed a series of fluorometric titrations of imd by adding different acids, such as hydrochloric, hydrobromic, nitric, perchloric, and fluoroboric acid. A general trend in the enhancement of fluorescence emission of imd at 418 nm by these acids was observed. The relative enhancement of emission positions and intensities caused by adding acids are listed in table 3.10. There is small change in the position but the intensities are largely affected. These changes are indicative of photo-induced energy transfer (PET) mechanism operative in each case. The Stokes shifts were calculated and are listed in table 3.9. The Stokes shifts are dependent on the anions and are of the order of hundreds of nm, which is also called a mega-shift and it is a unique property of these salts. The Stokes shifts are dependent on the acid used. Since the shifts are different, the anions

TH-1303_09612216

must have a role in such shifts. Upon addition of hydrochloric acid, the intensity of the fluorescence emission of a solution of imd was enhanced and emission shifted to 433 nm as shown in figure 3.14a. Profile of emission changes obtained from the interaction of a solution of imd with hydrogen bromide was different from the emission profiles of solutions of imd interacting with other acids. In the case of hydrogen bromide, initially a sharp enhancement in fluorescence emission at 418 nm was observed; shifted to 452 nm [Hmmd]Br upon gradual addition to reach a maximum emission. Upon adding hydrogen bromide beyond this concentration, another new sharp emission appeared at 480 nm.

Table 3.10: Fluorescence properties of imd and corresponding salts[#]

Compound	λ_{abs}(nm)	λ_{ems} (nm)	Stoke-shift (nm)	Relative ratio of change in intensity
imd		418	89	1.1
[Himd]Cl		433	104	1.6
[Himd]Br[$]		480	151	1.5
[Himd]NO_3	329	418	89	1.5
[Himd]ClO_4		431	102	1.5
[Himd]BF_4		430	102	1.3

In all cases excitation was at λ = 350 nm and relative ratio of the change is compared to 2-methyl-1,4-naphthoquinone. $ New peak appears.

Thus, single emission peak of imd was replaced by a new peak at 480 nm, which grew as the concentration of hydrogen bromide increased (figure 3.13b). During this process of interaction of acid, the anions played an important role to distinguish the protonated species. Thus it may be suggested as an effect of the anion on the protonated host, similar to anion recognition. Examples of imidazole based ligands are shown in figure 3.13. These imidazole containing compounds were extensively used for the detection of various anions,[35-46] having two steps emission change in hydrogen bromide recognition was not observed earlier. An imidazole-tethered cyclophanes derivative was shown to be selective to bind bromide ions (Figure 3.5d).[47] Such study was performed with the aid of ^{1}H-NMR titration. It was shown that bromide ions from 1:1 complex with the host molecule.[47] However, there are no examples on bromide selectivity shown with the imidazole derivatives with the aid of fluorescence as a tool. Fluorescence being a very sensitive tool

TH-1303_09612216

our system provides a better method for bromide ion selectivity study. Imidazole tethered anthraquinone selectively detects cyanide ions.[64-65] Besides this, imidazole tethered anthraquinone[64] selectively binds with fluoride and cyanide ions *via* intramolecular charge transfer. In our case we have seen a similar trend in emission change of imd with fluoride ions as that of the chloride, nitrate, perchlorate ions.

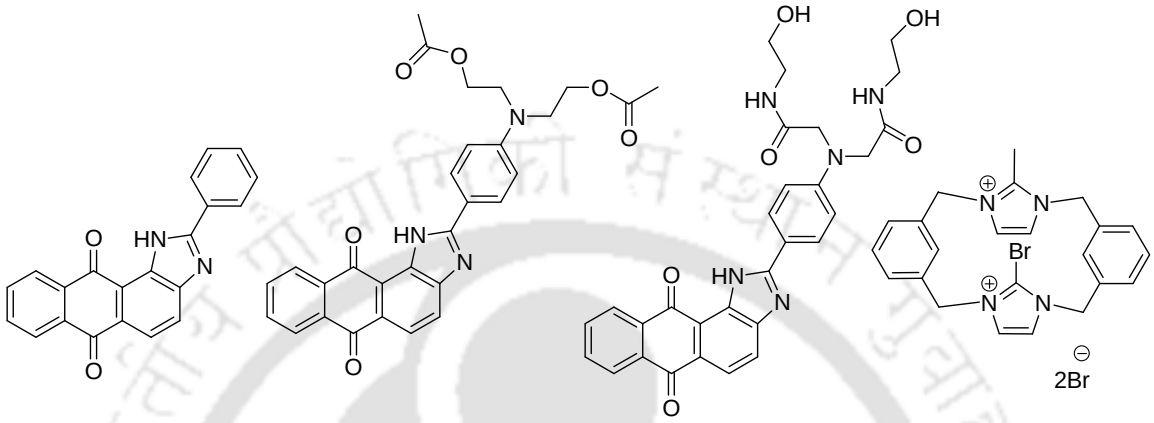

3.5a 3.5b 3.5c 3.5d

Figure 3.13: Some examples of quinone based receptors for anion recognition.

2-Methyl-1,4-naphthoquinone emits at 401 nm upon excitation at 350 nm, so the fluorescence emissions in case of its derivative, imd, and salts originate from the 1,4-naphthoquinone part. As imd forms imidazolium salt of corresponding acid, changes in the fluorescence emission in each case are brought about by protonation of the lone-pair electrons on the nitrogen atom of the imidazole ring. Thus, acid affects the intervening electron pair on the nitrogen atom, which becomes unavailable and causes a sharp increase in the fluorescence emission. However, this explanation is only partial in the case of hydrogen bromide interacting with imd because it shows an entirely new emission after a particular concentration. We do not observe an isoemissive point in this fluorescence titration; this is attributed to the formation of tautomeric species A (emitting at 452 nm) and B (emitting at 480 nm) as illustrated in Scheme 3.4 with different fluorescence emission intensities. Furthermore, species A is generated from protonated imd and undergoes a transformation to form B. Compound imd transforms to B at higher hydrogen bromide concentration, leading to the formation of multiple species. This deterred the formation of an isoemissive point and also supports the proposition of the tautomeric species shown in Scheme 3.4.

TH-1303_09612216

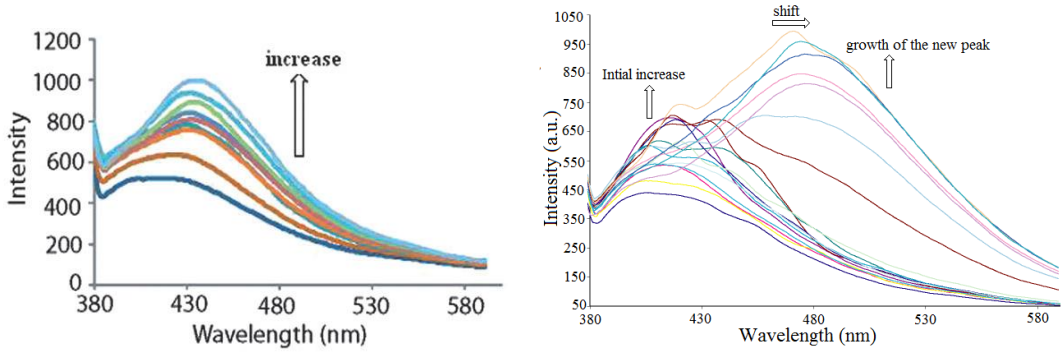

(a) (b)

Figure 3.14: Fluorescence emission of imd (a) hydrochloric acid and (b) hydrobromic acid in methanol. (In both caese 3 mL, 10^{-5} M imd in methanol on addition 5 µL of acid in each aliquot)

We have also tested relative recognition ability of imd towards hydrochloric acid over hydrogen bromide and found that hydrogen bromide was recognized in a competitive environment. This was seen in the formation of a new emission by hydrogen bromide in the presence of hydrochloric acid. There is a critical concentration, beyond which the *enol*

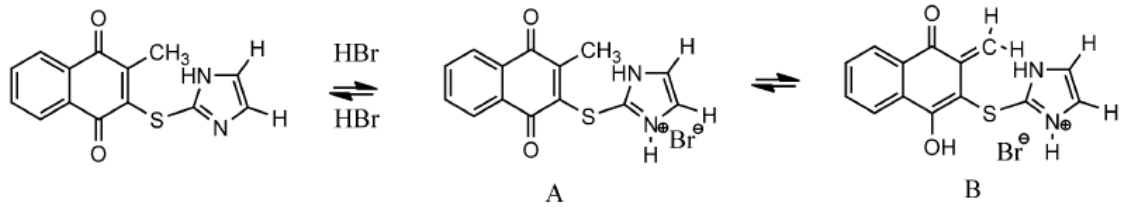

Scheme 3.4: Equilibria of imd with HBr.

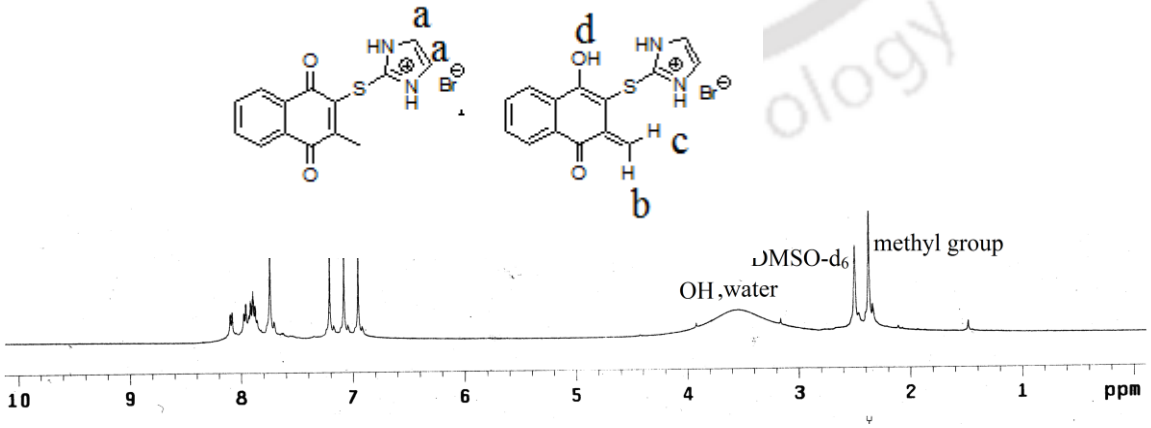

Figure 3.15: ^{1}H-NMR spectra (400 MHz, DMSO-d_6) of [Himd]Br.

form of the bromide salt coexists. There is also a critical concentration; below which hydrogen bromide behaves like other acids and above this concentration of hydrogen

TH-1303_09612216

bromide, specifically protonated imd, shows a new emission. The differences between the chloride and bromide salts are reflected in their ^{1}H-NMR spectra. The signals in the ^{1}H-NMR spectra of the chloride salt [Himd]Cl and bromide salts; [Himd]ClO_4 in DMSO-d_6 are similar, but the bromide salt [Himd]Br has three singlet peaks at 7.21, 7.08 and 6.95 ppm as shown in figure 3.15. Among these signals, two are exchangeable with D_2O, which suggests that they are attached to electronegative atoms. The occurrence of these three signals also distinguishes the bromide salt from the other salts. The ^{1}H-NMR spectra of the chloride, tetrafluoroborate and perchlorate salts of imd are also identical as shown in figure 3.16, except in the case of nitrate, for which additional three signals are observed and resemble the three additional signals observed in the case of the bromide salt [Himd]Br. The nitrate salt also shows such peaks but they are with very low integration values hence are not prominent.

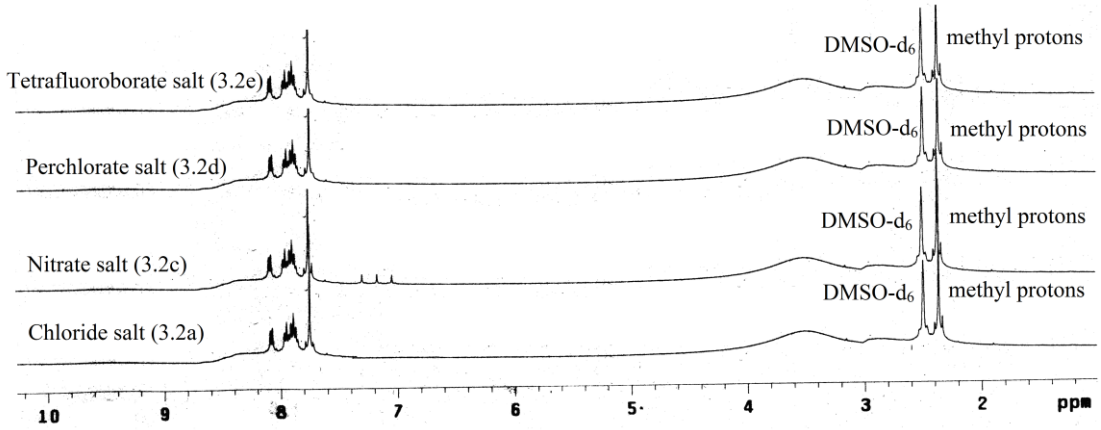

Figure 3.16: ^{1}H-NMR spectra (400MHz, DMSO-d_6) of [Himd]BF_4, [Himd]ClO_4, [Himd]NO_3 and [Himd]Cl.

The additional three signals observed for the bromide salt arise from an *enol* form, as illustrated in Scheme 3.4. Because these three signals exclusively arise from the *enol* form, the integration of these within the group of three does not change, but integration with respect to other aromatic signals differs. For example, integrations of these signals in the nitrate salt are relatively low with respect to the protons in the aromatic region. The presence of such minor signals shows a trace amount of the *enol* form in the case of nitrate. The HOMO-COSY spectrum of the aromatic region of the bromide salt is shown in figure 3.17. This also clearly depicts the three singlet peaks at 7.21, 7.08, 6.95 ppm. The natures of these protons are revealed in the HSQC spectrum in which it is evident that out of these three singlets, only the signal at 7.21 ppm is connected to a carbon atom (Figure 3.17). From these data, the signal in figure 3.16 corresponds to CH- of the

TH-1303_09612216

imidazole ring, whereas the signal for olefinic CH_2= (b and c) of *enol* form B appears at δ = 7.21 ppm, as confirmed by HSQC. The signal for the phenolic O-H of B merges with the water signal and could not be observed. Compound [Himd]Br in solution slowly decomposes; thus while recording the HSQC spectrum, we observed degradation signals, as indicated by the asterisks in figure 3.17b. The protonation of imidazole makes the two CH groups attached to the imidazole ring magnetically equivalent. Signal a in both forms appears at δ = 7.74 ppm. The methyl signal appears at δ = 2.37 ppm.

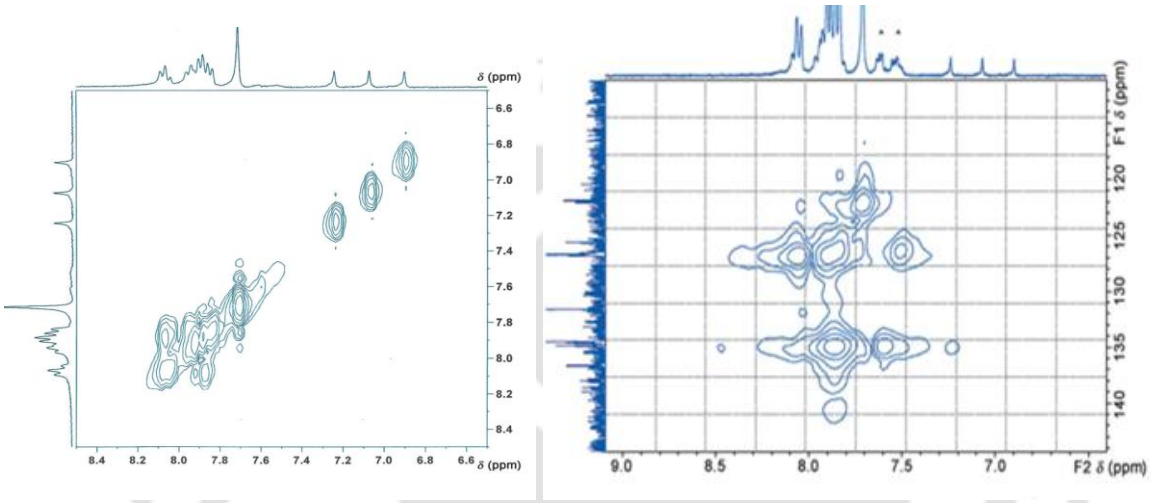

(a) (b)

Figure 3.17: ^{1}H-HOMO-COSY spectrum of [Himd]Br (aromatic region only) and (b) Aromatic region of the HSQC spectrum of [Himd]Br .

From integration, about 33% of the enol form is present (by comparing the relative integration of the $=CH_2$ and CH_3 protons). Thus, these data clearly indicate that the bromide salt remains in the *keto* and *enol* forms. The *enol* form (B in Scheme 3.3) Initial

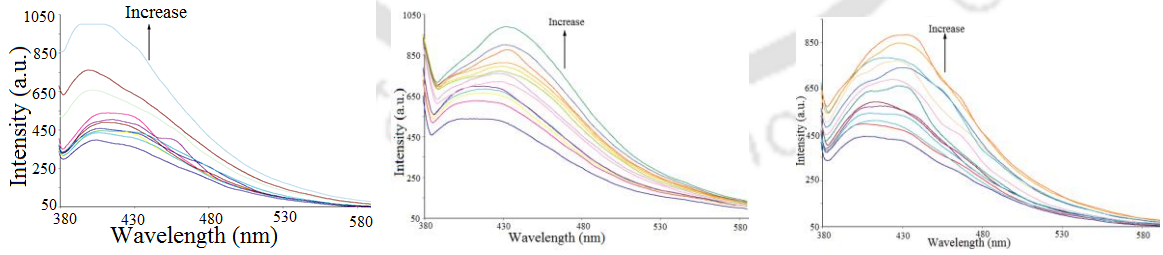

(a) (b) (c)

Figure 3.18 : Changes in fluorescence emission of imd on addition of (a) Nitric acid, (b) Perchloric acid, (c) Fluoroboroic acid. (In each case 3 mL, 10^{-5} M of imd in methanol on addition of 5 µL of acid in each aliquot).

increase in the emission at 418 nm, with a shift to 452 nm, is attributed to the formation of salt A in solution. The difference in the stabilization of the *enol* form by hydrogen

TH-1303_09612216

bromide may be attributed to the higher covalent nature of the bromide. In case of nitric acid enhancement of fluorescence emission intensity with respect to imd is 14-fold; **3.2c** (Figure 3.18a), fluorescence intensity of imd by perchloric (Figure 3.18b) and tetrafluoroboric acid (Figure 3.18c) revealed that they have also similar trend to hydrogen chloride. From the changes in the fluorescence emissions due to interactions of receptor with different acids the binding constants for all the salts were determined using the Benesi-Hildebrand equation and data are listed in table 3.11.

Table 3.11: Binding constant of salts

Salts	Binding constant (M^{-1})
[Himd]Cl	$K_1 = 1.307 \times 10^6$
[Himd]Br	$K_1 = 1.166 \times 10^7$
	$K_2 = 1.432 \times 10^5$
[Himd]ClO_4	$K_1 = 4 \times 10^4$
[Himd]NO_3	$K_1 = 1.644 \times 10^6$
[Himd]BF_4	$K_1 = 9.238 \times 10^5$

The binding constants of the acids with imd were determined and the first binding constants were in the order of $HNO_3 < HBF_4 < HCl < HClO_4 < HBr$; however, there were two binding constants for hydrogen bromide of 1.166×10^7 and 1.432×10^5 M^{-1}, respectively.

Compound mmd displayed UV absorbance maximium at 245 nm. This peak is from $\pi \rightarrow \pi^*$ transition. Addition of phosphoric acid cahnges the UV-emission to shorter wavelength, which corresponds to the absorption maxima of bmq (Figure 3.19a). This shows that the transforamtion of mmd to the bmq. Support for this processs also comes from the fluorescence emission of mmd on addition of phosphoric acid. The compound dmq emits at 335nm on excitaion at 250 nm. The flluorescence titration of a solution of mmd on with continous addition shows growth of the emission at 335 nm(Figure 31.9 b). This suggests that as phosphoric acid was added to mmd, dmq was formed. A series of fluorometric titrations of mmd by adding other acids also showed the phenomenon. From the fluorescence titration it is observed that mmd does not show changed emission with acids such as hydrochloric, nitric, prchloric, sulfuric acid.

TH-1303_09612216

(a) (b)

Figure 3.19: (a) UV-visible titration of mmd with phosphoric acid. (b) Similar fluorescence titration of mmd (mmd 10^{-5} M in 3 mL methanol and phosphoric acid in 10 μL in each aliquot).

Thus, it is clear that the the presence of the N-methyl group has significantly changes the fluorescence properties. The lack of acidic hydrogen in the the parent form of this imidazole derivative has resulted in a change in the anion binding. This compound can recognise phosphoric acid through a bond cleavage process as it changes the fluorescence significantly at an independent wavelength from the parent compound. On the other hand insensitivity of the mmd to other acids could help in distinguishing phosporic acid from the other acids.

3.4: Conclusions

Among the two imidizole functionalised naphthoquinones imd and mmd presence of methyl group in mmd changes the packing of anion assisted assemblies from imd and also greatly influence their fluorescence emission properties. Compound imd forms wide ranges of crystalline salts in which the quinoidal part plays important role to form anion assisted assemblies. Among several mineral acids hydrogen bromide is recognized by imd and it is evident from the spectroscopic properties that there exist a keto-enol tautomerism in [Himd]Br, which helps in distinguishing hydrobromic acid from other acids. The binding constants of the acids with imd follows a trend $HNO_3 < HBF_4 < HCl < HClO_4 < HBr$. Two binding constants for hydrogen bromide were ascertained. Despite the poor fluorescence emission changes mmd by mineral acids, a dramatic fluorescence change by phosphoric acid due to rupture of C-S bond of mmd was observed. This helps it to distinguish from other acid by mmd,

3.5: Experimental section

Matrials and physical measurement are as described in Chapter 2, Section 2.4.1 and Section 2.4.2.

TH-1303_09612216

3.5.1: Physical measurement

The UV-Vis spectra data were recorded using Perkin-Elmer Lambda 750 UV-Vis spectrophotometer. Fluorescence measurements were carried out with a Carry eclipse spectrofluorometer using 20 mm pathlength quartz cuvette with the slit width 5 nm. Fluorescence emission spectra of the compounds (10^{-5} M) in methanol were recorded by exciting at wavelegths mentioned in the text. The fluorescence titrations were carried out by taking 3 mL solution of compound (10^{-5} M imd or mmd) in methanol and adding definite aliquot of acid solution (10^{-5} M).

3.5.2: Calculation of binding constants

Binding constants of compounds with various acids were determined using the Benesi-Hildebrand equation by the fluorescence method.

$$\frac{1}{[I - I_0]} = \frac{1}{[I_1 - I_0]} + \frac{1}{[I_1 - I_0]K[compound]}$$

where I_0, I and I_1 are the emission intensities in absence of compounds, in presence of compounds and when the molecule is completely solubilized in compounds respectively.

*3.5.3: General procedure for the synthesis of compounds **3.2-3.3***

2-(1*H*-imidazole-2-ylthio)-3-methylnaphthalene-1,4-dione (imd, **3.2**)

A solution of 2-methyl-1,4-naphthoquinone (0.34 g, 2 mmol) and 2-mercaptoimidazole (0.20 g, 2 mmol) in methanol (20 mL) was stirred for 8 h at room temperature. Color of the reaction mixture slowly turned yellow and a yellow precipitate of imd was formed; which was collected by filtration and dried in air. Yield: 98%. ^{1}H NMR (400 MHz, DMSO-d_6): 12.33 (s, 1H), 8.40 (d, J = 3.2 Hz, 1 H), 8.37 (dd, J = 2.8 Hz, 1H), 8.34 (dd, J = 2.8 Hz, 1H), 8.23 (d, J = 3.2 Hz, 1 H,), 7.35 (d, J = 7.2 Hz, 1H), 7.28 (dd, J = 7.2 Hz, 1H), 2.09 (s, 3H); ^{13}C NMR (100 MHz, DMSO-d_6): 184.9, 184.5, 147.9, 135.2, 133.9, 133.9, 131.6, 126.0, 125.5, 15.9; IR (KBr, cm^{-1}): 3431 (bw), 3152 (w), 3113 (m), 3018 (w), 2936 (m), 2754 (m), 2654 (m), 1662 (s), 1589 (s), 1428 (w), 1284(s), 1261 (m), 1183 (w), 1088 (m), 1032 (m), 881 (m), 843 (w), 783 (s), 708 (m), 708 (m); MS (ESI) m/z: 271.015 $[M+H]^+$, 541.108 $[2M+H]^+$. Melting point, 173 ºC

Chloride salt [Himd]Cl (**3.2a**)

TH-1303_09612216

Compound imd (0.27 g, 1 mmol) in methanol (10 mL) was treated with concentrated hydrochloric acid in a 1:1 molar ratio at room temperature. After one week yellow crystals of [Himd]Cl were obtained. Yield: 76%. IR (KBr, cm^{-1}) 3431(bw), 3152 (w), 3113 (m), 3018 (w), 2936 (m), 2754 (m), 2654 (m), 1662 (s), 1589 (s), 1428 (w), 1284 (s), 1261 (m), 1183 (w), 1088 (m), 1032 (m), 881 (m), 843 (w), 783 (s), 708 (m), 708 (m).

Bromide salt [Himd]Br (**3.2b**)

Yellow block-shaped crystals of [Himd]Br were obtained upon slow evaporation of a solution of imd in methanol in the presence of hydrogen bromide (1:1 molar ratio). Yield: 79%. IR (KBr, cm^{-1}): 3436 (bw), 3146 (w), 3107 (w), 3014 (w), 2954 (w), 2896 (w), 2804 (m), 1662 (s), 1587 (s), 1458 (w), 1285 (s), 1262 (w), 1183 (w), 1087 (w), 1031 (w), 785 (s), 707 (m).

Nitrate salt [Himd]NO_3 (**3.2c**)

Salt [Himd]NO_3 was crystallized from a solution of imd and nitric acid in methanol in a 1:1 molar ratio. After one week yellow crystals were obtained. Yield: 65. IR (KBr, cm^{-1}): 3445 (b), 3149 (w), 3107 (w), 2952 (w), 2809 (w), 2662 (w), 1666 (s), 1589 (s), 1384 (s), 1337 (m), 1285 (m), 1183 (m), 1108 (w), 1031 (w), 784 (m), 771 (m), 707 (m).

Perchlorate salt [Himd]ClO_4 (**3.2d**)

Yellow block-shaped crystals of [Himd]ClO_4 were obtained upon slow evaporation of a solution of imd and perchloric acid in methanol in a 1:1 molar ratio. Yield: 83%. IR (KBr, cm^{-1}): 3146 (w), 2961 (w), 2822 (w), 2661 (w), 1664 (s), 1588 (s), 1458 (w), 1285 (s), 1245 (w), 1113 (s), 1083 (s), 844 (w), 785 (m), 706 (m), 668 (m), 626 (m).

Tetrafluoroborate salt [Himd]BF_4 (**3.2e**)

Salt [Himd]BF_4 was crystallized from a solution of imd and fluoroboric acid in methanol in a 1:1 molar ratio. Yellow crystals were obtained after a week. Yield: 77%. IR (KBr, cm^{-1}): 3237 (w), 3147 (w), 3015 (w), 2821 (w), 1664 (s), 1589 (s), 1422 (w), 1285 (s), 1251 (w), 1083 (s), 1032 (s), 915 (w), 787 (m), 764 (m), 708 (m), 670 (w).

2-(1-Methyl-1*H*-imidazol-2-ylthio)-3-methylnaphthalene-1,4-dione (mmd, **3.3**)

A solution of 2-methyl-1,4-naphthoquinone (0.34 g, 2 mmol) and 2-mercapto-1-methylimidazole (0.23 g, 2 mmol) in methanol (20 mL) was stirred for 8 h at room temperature. Color of the reaction mixture slowly turned yellow and a yellow precipitate of imd formed was collected by filtration and dried in air. Yield: 95%. ^{1}H-NMR (400 MHz, DMSO-d_6): 8.13 (t, J = 7.2 Hz, 1H), 7.94 (t, J = 6.4 Hz, 1H), 7.92 (d, J = 6.8 Hz, 2H), 7.36 (d, J = 6.0 Hz, 1H), 7.29 (d, J = 7.2 Hz, 1H), 3.60 (s, 3H), 2.34 (s, 3H). ^{13}C-NMR (DMSO-d_6): 182.6, 180.1, 148.5, 141.5, 137.4, 134.6, 134.2, 133.7, 132.1, 130.6,

TH-1303_09612216

28.3, 18.2. IR (KBr, cm^{-1}): 3429 (bw), 3132 (w), 3101 (m), 2998 (w), 2926 (m), 2753 (m), 2647 (m), 1676 (s), 1580 (s), 1436 (w), 1282 (s), 1257 (m), 1189 (w), 1086 (m), 1029 (m), 878 (m), 846 (w), 781 (s), 706 (m), 692 (w). MS (ESI) m/z: 285.08 $[M+H]^+$,m. p. 182 ºC.

Chloride salt [Hmmd]Cl (**3.3a**)

Compound mmd (0.45 g, 1 mmol) in methanol (10 mL) was treated with concentrated hydrochloric acid in a 1:1 molar ratio at room temperature. After 2 days yellow crystals of chloride salt were obtained. Yield: 80%. IR (KBr, cm^{-1}): 3436(bw), 3148 (w), 3117 (m), 2994 (w), 2931 (m), 2762 (m), 2656 (m), 1661 (s), 1583 (s), 1442 (w), 1281 (s), 1263 (m), 1176 (w), 1082 (m), 1027 (m), 878 (m), 823 (w), 776 (s), 696 (w), 624 (w).

Nitrate salt [Hmmd]NO_3 (**3.3b**)

Nitrate salt was crystallized from a solution of mmd and nitric acid in methanol in a 1:1 molar ratio. After 4 days yellow crystals were obtained. Yield: 72%. IR (KBr, cm^{-1}): 3439 (b), 3137 (w), 2990 (w), 2948 (w), 2799 (w), 2675 (w), 1669 (s), 1579 (s), 1384 (s), 1336 (m), 1283 (m), 1176 (m), 1089(w), 1021 (w), 781 (m), 756 (m), 699 (w), 613 (w).

Reaction of mmd with phosphoric acid

Compound mmd (0.90 g, 1 mmol) in methanol (10 mL) was treated with concentrated phosphoric acid in a 1:1 molar ratio at room temperature. After one day colourless crystals of dmq was obtained which was filtered and characterised. Yield: 92%. ^{1}HNMR (400 MHz, DMSO-d_6): 7.64 (t, J = 7.2 Hz, 2H), 7.54 (dd, J = 7.2 Hz, 2H), 3.92 (s, 2H), 1.48 (s, 6H). ^{13}C NMR (DMSO-d_6): 196.5, 193.6, 135.0, 134.6, 134.5, 1.34.3, 126.4, 125.6, 97.9, 53.8, 51.6, 19.3. IR (KBr, cm^{-1}): 3422 (bw), 2925 (w), 1686 (s), 1590 (s), 1462 (w), 1440 (w), 1390 (w), 1370 (w), 1300 (m), 1269 (m), 1230 (w), 1195 (w), 1160 (w), 1089 (w), 945 (w), 925 (w), 896 (w), 757 (m), 719 (w), 687(w). MS (ESI) m/z: 345.11 $[M+H]^+$. m. p. 205 ºC. On concentration and purification by preparative TLC yielded dss2. The compound dss2 was characterised by comparing its NMR and IR with authentic sample.

References:

1. J.-M. Lehn, *Supramolecular chemistry: concepts and Perspectives;* VCH: Weinheim, Germany, **1995**.
2. A. Bianchi, K. Bowman-James and E. Garcia-España, Eds. *Supramolecular Chemistry of Anions;* Wiley-VCH: New York, **1997**.
3. D. M. P. Mingos and V. Ramon, *Structure and Bonding, Recognition of Anions;* Springer-Verlag: Berlin, **2008**.

TH-1303_09612216

4. P. A. Gale, *Coord. Chem. Rev.* **2000**, 199, 181.
5. P. A. Gale, *Coord. Chem. Rev.* **2001,** 213, 79.
6. P. D. Beer and P. A. Gale, *Angew. Chem., Int. Ed.* **2001**, 40, 487.
7. P. A. Gale, *Chem. Soc. Rev.***2010**, 39, 3746.
8. S. O. Kang, J. M. Llinares, V. W. Day and K. Bowman-James, *Chem. Soc. Rev.* **2010**, 39, 3980.
9. V. Amendola, L. Fabbrizzi and L. Mosca, *Chem. Soc. Rev.* **2010**, 39, 3889.
10. R. M. Duke, E. B. Veale, F. M. Pfeffer, P. E. Kruger and T. Gunnlaugsson, *Chem. Soc. Rev.* **2010**, 39, 3936.
11. A.-F. Li, J.-H. Wang, F. Wang and Y.-B. Jiang, *Chem. Soc. Rev.* **2010**, 39, 3729.
12. T. S. Snowden and E. V. Anslyn, *Curr. Opin. Chem. Biol.* **1999**, 3, 740.
13. R. Martinez-Máñez and F. Sancenón, *Chem. Rev.* **2003**, 103, 4419
14. A.-C. C. Carlsson, J. Grafenstein, J.L. Laurila, J. Berquist and M. Erdelyi, *Chem. Commun.* **2012**, 48, 1458.
15. J. L. Sessler, P. A. Gale and W. S. Cho, *Anion Receptor Chemistry*, The Royal Society of Chemistry, Cambridge, **2006**.
16. C. R. Bondy, P. A. Gale and S. J. Loeb, *J. Am. Chem. Soc.* **2004**, 126, 5030.
17. D. R. Turner, E.C. Spencer, J. A. K. Howard, D. A. Tocher and J. W. Steed, *Chem. Commun.* **2004**, 1352.
18. S. O. Kang, M. A. Hossain, D. Powell and K. Bowman-James, *Chem. Commun.* **2005**, 328.
19. K. Bowman-James, *Acc. Chem. Res.* **2005**, 38, 671.
20. R. Custelcean, D. E. Jiang, B. P. Hay, W. S. Luo and B. H. Gu, *Cryst. Growth Des.* **2008**, 8, 1909.
21. K. Uzarevic, I. Dilovic, D. Matkovic-Calogovic, D. Sisak and M. Cindric, *Angew. Chem*. **2008**, 120, 7130.
22. S. O. Kang, V. W. Day and K. Bowman-James, *Org. Lett.* **2008**, 10, 2677.
23. P. Dechambenoit, S. Ferlay, N. Kyritsakas and M. W. Hosseini, *J. Am. Chem. Soc.* **2008**, 130, 17106.
24. M. W. Hosseini, *Acc. Chem. Res.* **2005**, 38, 313.
25. M. W. Hosseini, *Coord. Chem. Rev.* **2003**, 240, 157.
26. J. Keegan, P. E. Kruger, M. Nieuwenhuyzen, J. O'Brien and N. Martin, *Chem. Commun.* **2001**, 2192.

TH-1303_09612216

27. O. A. Gerasimchuk, S.Mason, J. M. Llinares, M. P. Song, N. W. Alcock and K. Bowman-James, *Inorg. Chem.* **2000**, 39, 1371.
28. R. Custelcean and P. Remy, *Cryst. Growth Des.* **2009**, 9, 1985.
29. R. Custelcean, J. P. Bosano, V. Bonnesen, V. Kertesz and B. P. Hay, *Angew. Chem. Int. Ed.* **2009**, 121, 4085.
30. R. Custelcean, P. Remy, P. V. Bonnesen, D. E. Jiang and B. A. Moyer, *Angew. Chem. Int. Ed.* **2008**, 120, 1892.
31. R. Custelcean, *Chem. Commun.* **2008**, 295.
32. T. Wang and X.-P. Yan, *Chem. Eur. J.* **2010**, 16, 4639.
33. H. Maeda and Y. Kusunose, *Chem. Eur. J.* **2005**, 11, 5661.
34. S. J. Brooks, P. A. Gale and M. E. Light, *CrystEngComm* **2005**, 7, 586.
35. H. Juwarker and K. S. Jeong, *Chem. Soc. Rev.* **2010**, 39, 3664.
36. S. Metzger and B. Lippert, *J. Am. Chem. Soc.* **1996**, 118, 12467.
37. P. Auffinger, Lousie S. May and E. Westof, *J. Am. Chem. Soc.* **1996**, 118, 1181.
38. G. R. Desiraju, *Acc. Chem. Res.* **1991**, 24, 290.
39. T. Steiner and W. Saenger, *J. Am. Chem. Soc.* **1992**, 114, 10146.
40. C.V.K. Sharma and G. R. Desiraju, *J. Chem. Soc. PerkinTrans 2*. **1994**, 2345.
41. T. Steiner, *J. Chem. Soc. Perkin Trans.* **1995**, 1315.
42. J. D. Chaney, C. R. Goss, K. Folting, B. D. Santarsiero and M. D. Hollingworth. *J. Am. Chem. Soc.* **1996**, 118, 9432.
43. I. Tabushi, Y. Kuroda and T, Mizutani. *J. Am. Chem. Soc.* **1986**, 108, 4514.
44. Y. Yuan, G. Gao, Z.-L. Jiang, J.-S. You, Z.-Y. Zhou, D.-Q. Yuana and R.-G. Xiea, *Tetrahedron* **2002**, 58, 8993.
45. J. R. Jadhav, M. W. Ahmad and H.-S. Kim, *Bull. Korean Chem. Soc*. **2011**, 32, 2933.
46. (a) W. M. Singh and J. B. Baruah, *Synth. Commun.* **2009**, 39, 1433. (b) M. F. Bazargani, L. Talavat, S. Naderi, H. R. Khavasi, *Acta Crystallographica*, *Section E*: **2011**, 67, o2585. (c) F. Freeman, M. C Keindl, H. N. Po, E. Brinkman, J. A. Masse, *Synthesis* **1989**, 9, 714. (d) J. P. Mahieu, N. M. Gosselet, B. Sebille, M. C. Garel, Y. Beuzard, *Int. J. Bio. Macro*. **1993**, 15, 233. (e) J. P. Mahieu, M. Gosselet, B. Sebille, Y. Beuzard, *Synth. Commun*. **1986**, 16, 1709. (f) H. Werbin and E. T. Strom, *J. Am. Chem. Soc.* **1968**, 90, 7296.
47. A. Caballero, N. G. White and P. D. Beer, *Angew. Chem. Int. Ed.* **2011**, 50, 1845.
48. D.-S. Kim and K. H. Ahn, *J. Org. Chem*. **2008**, 73, 6831.
49. Z. Xu, S. K. Kim and J. Yoon, *Chem. Soc. Rev*. **2010**, 39, 1457.

TH-1303_09612216

50. L. Fabbrizzi, M. Licchelli, G. De Santis, N. Sardone and A. H. Velders, *Chem. Eur. J.* **1996**, 2, 1243.
51. R. Bergonzi, L. Fabbrizzi, N. Licchelli and C. Mangano, *Coord. Chem. Rev*. **1998**, 170, 31.
52. R. A. Illos, E. Harlev and S. Bittner, *Tetrahedron Lett*. **2005**, 46, 8427.
53. T. Iyoda, T. Saika, K. Honda and T. Shimidzu, *Tetrahedron Lett*. **1989**, 30, 5429.
54. M. Arunachalam and P. Ghosh, *Org. Lett.* **2010**, 12, 328.
55. M. Arunachalam and P. Ghosh, *Chem. Commun*. **2009**, 5389.
56. M. Arunachalam and P. Ghosh, *Inorg. Chem*. **2010**, 49, 943.
57. P. S. Lakshminarayanan, I. Ravikumar, E. Suresh and P. Ghosh, *Chem. Commun*. **2007**, 5214.
58. K. M. Armstrong, R. Fairman and R. L. Baldwin, *J. Mol. Biol.* **1993**, 230, 284.
59. G. Kryger, I. Silman and J. L. Sussman, *Structure*, **1999**, 7, 297.
60. G. Parkinson, A. Gunasekera and J. Vijtechovsky, *Nat. Struct. Biol.*, **1996**, 3, 837.
61. S. Liu, X. Ji, G. L. Gilliland, W. J.Stevens and R. N. Armstrong, *J. Am Chem Soc.*, **1993**, 115, 7910.
62. S. Jurado, Z. Abraham, C. Manzano, G. Lopez-Torrejo, L. F. Pacios, J. C. Del Pozoa, *Plant Cell*, **2010**, 22, 3891.
63. N. Phukan and J. B. Baruah, *Cryst. Growth Des.*, **2014**, 14, 2640.
64. S. Saha, A. Ghosh, P. Mahato, S. Mishra, S. K. Mishra, E. Suresh, S. Das, and A. Das, *Org. Lett.* **2010**, 12, 3406.
65. N. Kumari, S. Jha, and S. Bhattacharya, *J. Org. Chem.* **2011**, 72, 8215.
66. J. G. Yu, M. Lei, B. Cheng, X. J. Zhao, *J. Solid State Chem*. **2004**, 177, 681.
67. D. O. Cowan and J. C. Koziar, *J. Am. Chem. Soc.* **1975**, 97, 249.
68. Y. Nakamura, Y. Imakura, T. Kato and Y. Morita, *Chem. Commun*. **1977**, 887.
69. J. M. Nerbonne and R. G. Weiss, *J. Am. Chem. Soc*. **1978**, 100, 2571.
70. P. Mayo, Pure. *Appl. Chem*. **1982**, 54, 1623.
71. H. Mayer and J. Sauer, *Tetrahedron Lett*. **1983**, 24, 4091.
72. V. Ramamurthy, D. R. Corbin, C. V. Kumar and N. J. Turro, *Tetrahedron Lett*. **1990**, 31, 47.

TH-1303_09612216

Chapter 4

Studies on structures of polymorphs and solvates of arylthio-naphthalene-1,2-dione and their photophysical properties

In chapter 2, we have shown conformational polymorphs of thiocarboxylic acid tethered 1,4-naphthoquinones. These conformational polymorphs arise due to conformations arising from the orientation of functional groups attached to the 1,4-naphthoquinone unit. In these polymorphs we have shown that the self-assemblies differ and that they are guided by interplay of various weak interactions such as O-H···O, C-H···O, C-H···π and O-H···π interactions. Analogously, various packing patterns can be generated in assemblies of such 1,2-naphthoquinonoe molecules are shown in figure 4.1a-d. Hence understanding of such assemblies will help to elucidate the physical properties associated with these compounds.

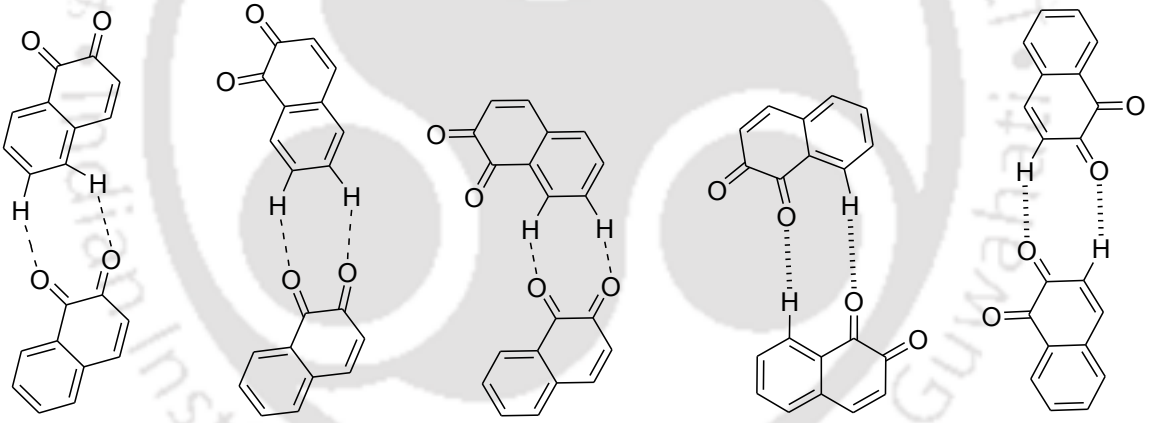

Figure 4.1: Self-assemblies of 1,2-naphthoquinone molecules (a-e).

The stability of such assemblies in the presence of a strongly hydrogen bonding environment would decide the likelihood on formation of polymorphic structures as well as solvates. Phenolic units are important in forming hydrogen bonded structures and the quinone-phenol interaction is a biologically important interaction.[1-2] Thus, building new types of self-assemblies between quinones and phenols would be useful to gather information on structures of different hydrogen bonded motifs.[3-4] Two such ways possible for a phenol to interact with 1,2-naphthoquinone is shown in figure 4.2.

TH-1303_09612216

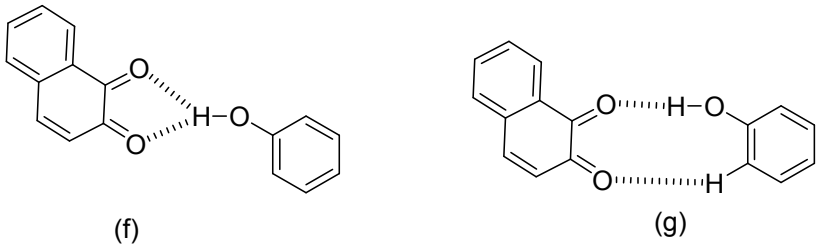

Figure 4.2: Interactions between 1,2-naphthoquinone with phenol.

It would be interesting to attach an phenylthiolato or hydroxy-phenylthiolato units on 1,2-naphthoquinone to study the self-assembled structures. We have synthesized a series of 1,2-naphthoquinone derivatives; namely, 4-(phenylthio)naphthalene-1,2-dione (**4.1**), 4-(4-methylphenylthio)naphthalene-1,2-dione (**4.2**), 4-(4-chlorophenylthio)naphthalene-1,2-dione (**4.3**), 4-(4-bromophenylthio)naphthalene-1,2-dione (**4.4**), 4-(2-hydroxyphenylthio) -naphthalene-1,2-dione (**4.5),** 4-(3-hydroxyphenylthio)naphthalene-1,2-dione (**4.6**), 4-(4-hydroxyphenylthio)naphthalene-1,2-dione (**4.7**) shown in figure 4.3 and studied the structural aspects of their polymorphs, solvates and photophysical properties.

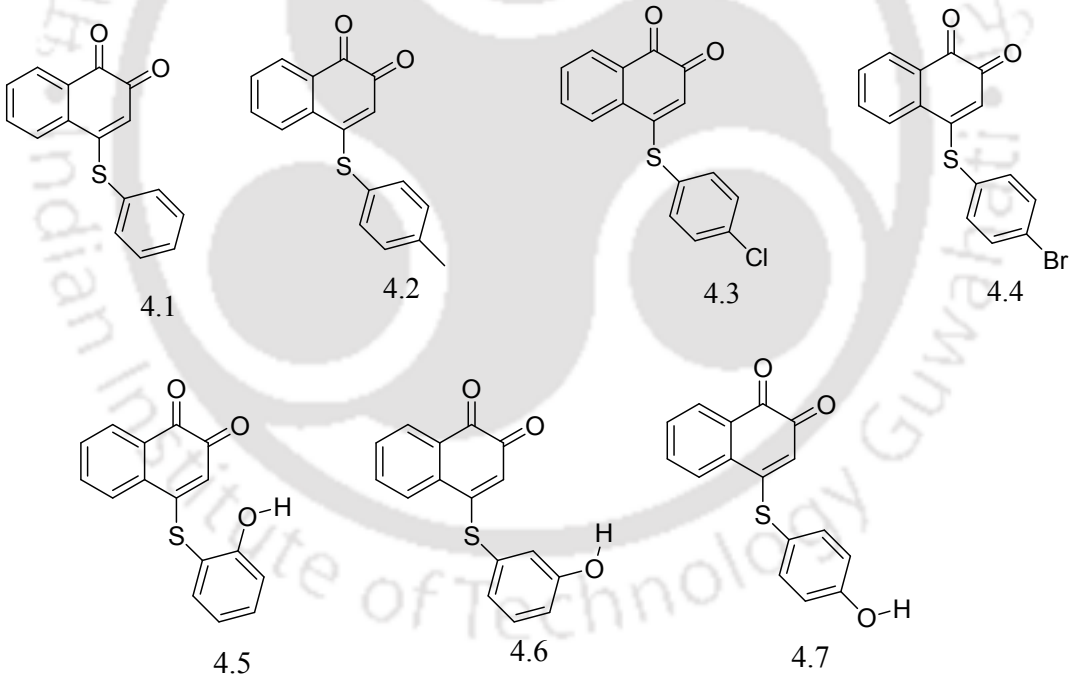

Figure 4.3: Structure of 1,2-naphthoquinone derivatives.

*4.1: Synthesis and characterization of compounds **4.1-4.7***

Reaction of 1,2-naphthoquinone with the corresponding arylthiol following a similar procedure for analogous compounds reported earlier.[5] Compounds **4.1-4.7** are characterized by various spectroscopic techniques such as FT-IR, ^{1}H-NMR, ^{13}C-NMR

TH-1303_09612216

spectroscopy and mass spectrometry. In the ^{1}H-NMR of compound **4.1** we observe two doublet signals at 8.00 ppm and 7.90 ppm for protons a and b, whereas a triplet at 7.80 ppm for proton c and a singlet at 5.5 for d on the other hand a multiplet at 7.62 ppm for hydrogen of phenyl ring (Figure 4.4).

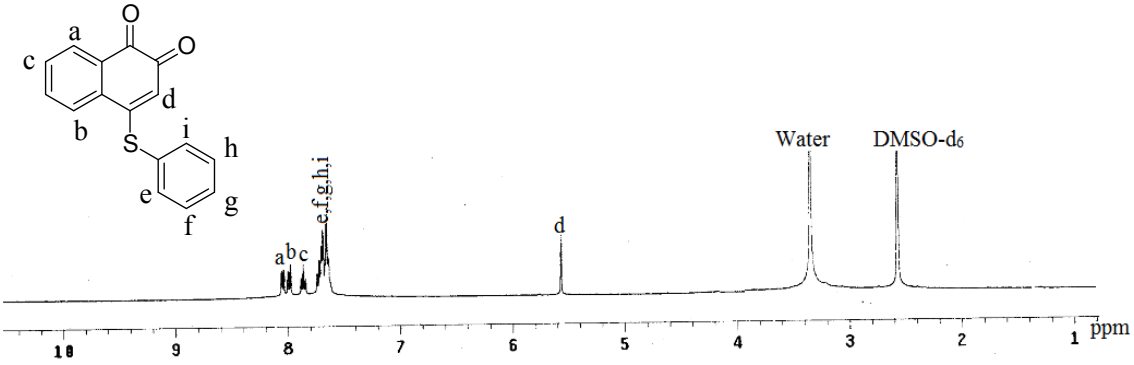

Figure 4.4: ^{1}H-NMR (400MHz, DMSO-d_6) spectra of **4.1**.

Compound **4.1** shows ^{13}C-NMR of carbon signals at 173.2 ppm and 171.0 ppm due to two carbons at two carbonyl groups, whereas the other aromatic carbon of the phenyl unit and part of the ring without carbonyl appear in the range of carbons 162.5-112.9 ppm and the two olefin carbons are at 98.6 and 96.8 ppm. Compound **4.1** shows carbonyl stretching in IR spectra at 1692 cm^{-1} and 1646 cm^{-1}. The other 4-substituted 1,2-naphthoquinones also have matching spectroscopic signals which are listed in the experimental section.

*4.2: Supramolecular assemblies of **4.1-4.7***

With the anticipation of getting different types of self-assemblies leading to polymorphs and also for possible formation of solvate of the compounds **4.1-4.7,** a systematic structural study is carried out. When compound **4.1** was crystallized from methanol or ethanol two types of crystals were obtained. From the spectroscopic and crystallographic analysis they are from two polymorphs. Which are designated as polymorph **I** (**4.1a**) and polymorph **II** (**4.1b**) as shown in Scheme 4.1.

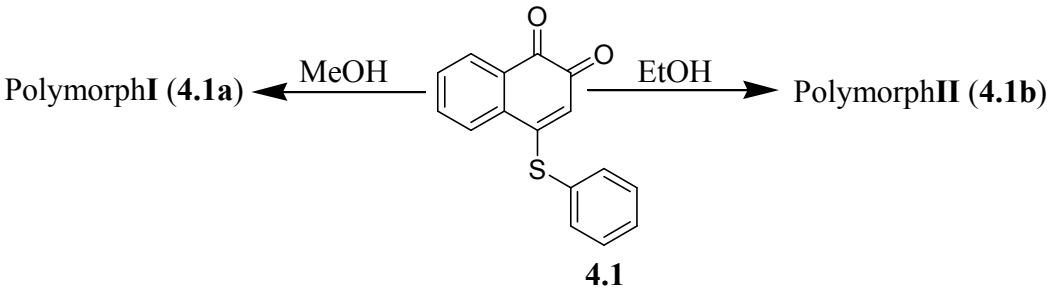

Scheme 4.1: Crystallisation of polymorphs of **4.1**.

TH-1303_09612216

*4.2.1: Polymorphism of 4-(phenylthio)naphthalene-1,2-dione (**4.1**)*

Polymorph **I** (**4.1a**) crystallizes in a triclinic space group P-1 from a solution of **4.1** in methanol solvents. ORTEP diagram of polymorph **I** is shown in figure 4.5a. Analysis of packing of crystal structure showed that molecules of polymorph **I** occur in pairs. These pairs are formed by intermolecular cyclic hydrogen bonded motif as shown in figure 4.5a, whereas the thiophenyl groups are *cis* to each other. Carbonyl groups exhibit C-H···O interactions to form one dimensional structures with dimeric units having cyclic hydrogen bond motifs (Table 4.1). In the packing pattern of polymorph **I**, the naphthoquinone rings are positioned in opposite faces with carbonyl groups, so that the carbonyl groups project away from each other. This happens to compensate the intrinsic polarity (dipole) within the rings so that oppositely polarized diploes are close to each other. Compound 4.1a forms π-stacks in between the naphthoquinone rings which the distance of separation between C1-C8 is 3.39 Å (Figure 4.5c). Although the naphthoquinone rings appears to be placed on top of one another; the effective overlaps are only through C1···C8 interactions as these portions of the rings are geometrically suitable to overlap.

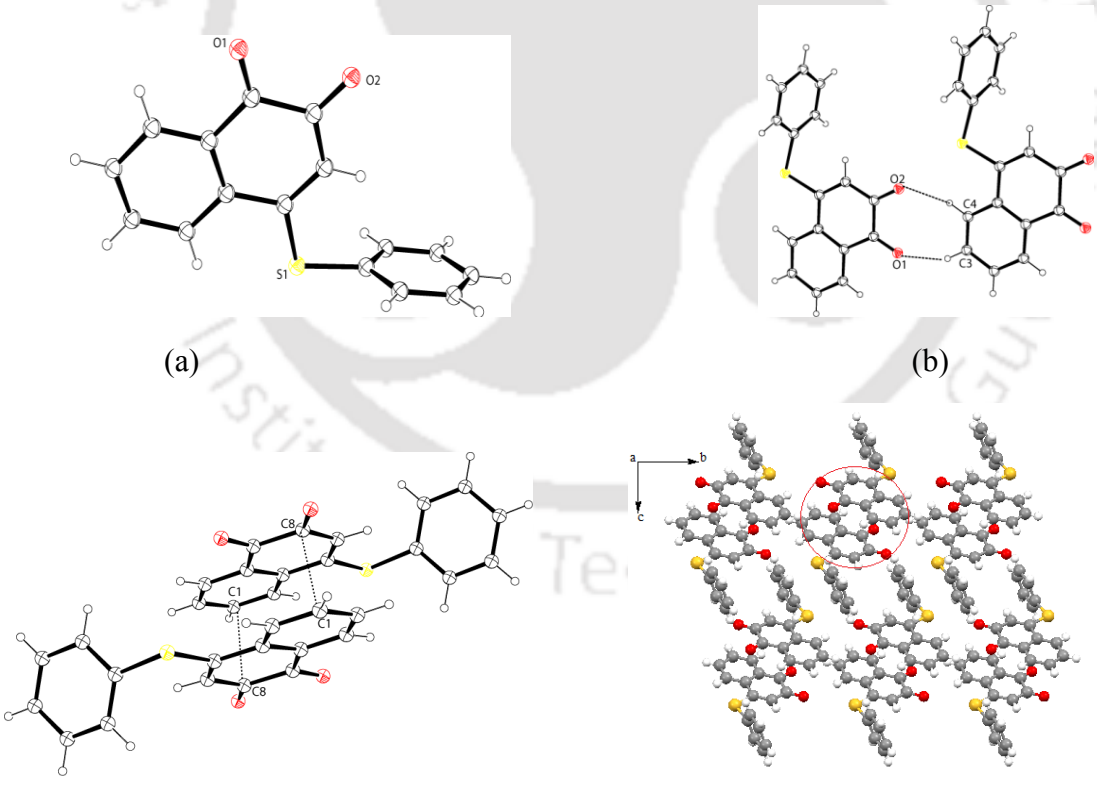

Figure 4.5: (a) ORTEP diagram of polymorph **I** (**4.1a**) (drawn with 30% thermal ellipsoids), (b) Cyclic H-bonding motif, (c) π-π interactions in polymorph **I** and (d) Packing diagram of polymorph **I .**

TH-1303_09612216

Polymorph **II** (**4.1b**) crystallizes in monoclinic space group $P2_1/c$ from a solution of **4.1** in ethanol solvents (Figure 4.6a). In its crystal structure, the molecules are also held together by weak interactions in pairs. These units are formed by an intermolecular cyclic hydrogen bonded motif as shown in figure 4.6b. In these dimeric assemblies thiophenyl groups are *trans* to each other across the cyclic hydrogen bonded motif.

Table **4.1**: Hydrogen bond geometry (Å, °) in polymorph **I** (**4.1a**) and **II** (**4.1b**)

Compound No.	D-H···A	d_{D-H}	$d_{H\cdots A}$	$d_{D\cdots A}$	∠D-H···A
4.1a	C3-H3···O1 [x, 1 + y, z]	0.93	2.55	3.395 (2)	152
	C4-H4···O2 [x, 1 + y, z]	0.93	2.55	3.392 (2)	151
4.1b	C7-H7···O1 [-1+x, 1/2 - y,1/2+ z]	0.93	2.50	3.370 (2)	155
	C8-H8···O2 [-1+x, 1/2-y,1/2+ z]	0.93	2.57	3.366 (18)	143

The dimeric assemblies has C-H···O interactions between the carbonyl group of one molecule of **4.1** with C-H of another molecule. In case of polymorph **II** the naphthoquinone rings of two molecules are stacked parallel; they are eclipsed and each

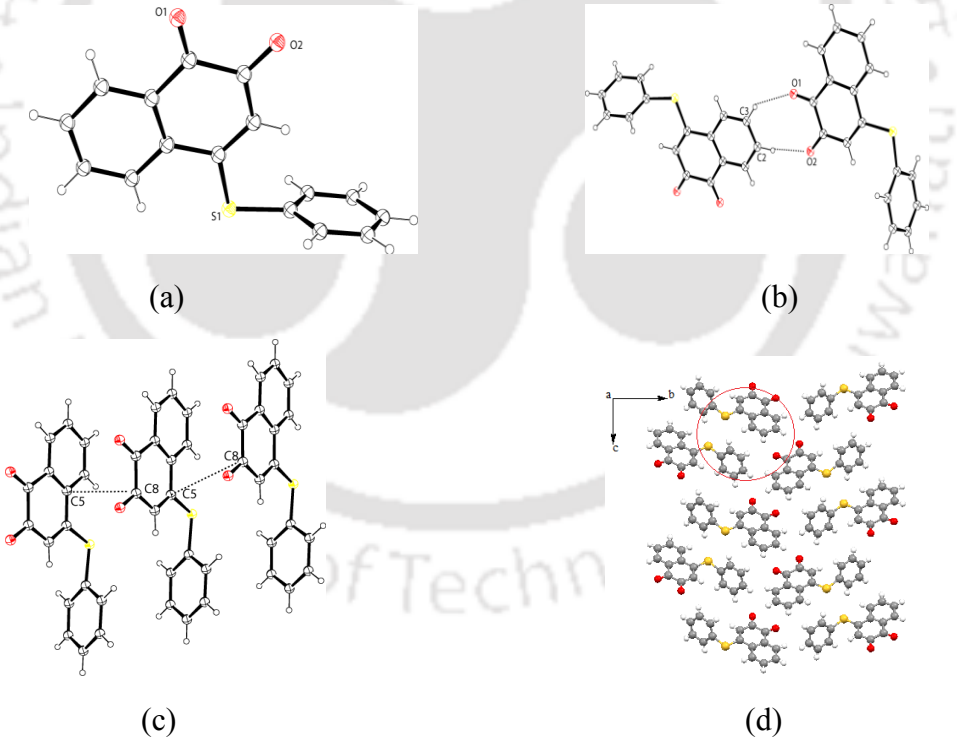

Figure 4.6: (a) ORTEP diagram of polymorph **II** (**4.1b**) (drawn with 30% thermal ellipsoids), (b) Cyclic H-bonding motif, (c) π-π interactions in polymorph **II** and (d) Packing diagram of polymorph **II**.

ring is positioned so that atom C5 of one ring is on top of the atom C8 of another ring with a separation distance of 3.40 Å. Although rings are eclipsed, interactions between

TH-1303_09612216

the rings are compensated by repulsion between rings arising from stacking of similar dipoles placed on top of each other. Thus, stacking interactions become less significant in polymorph **II**. But the dipolar interactions (repulsive as well as attractive) between such stacks cannot be ignored; such interactions contribute to the energy barrier to transform crystals of one polymorphic form to another. From the above structures, it is observed that the torsion angle of C5-C10-S1-C11 and C9-C10-S1-C11 of polymorph **II** (**4.1b**) are 178.25°, -1.98°, whereas in polymorph **I** (**4.1a**) torsion angles of C5-C10-S1-C11 and C9-C10-S1-C11 are -179.84° and 0.36° (Figure 4.7 a-b), respectively, which shows difference between the conformation of the polymorphs **I** and **II**. Torsion angles are shown in table 4.2.

Table **4.2**: Torsion angles of polymorph **I-II**

Polymorph	Dihedral angles (°)
I (**4.1a**)	C5-C10-S1-C11,-179.84°; C9-C10-S1-C11, 0.36°
II (**4.1b**)	C5-C10-S1-C11, 178.25°; C9-C10-S1-C11, -1.98°

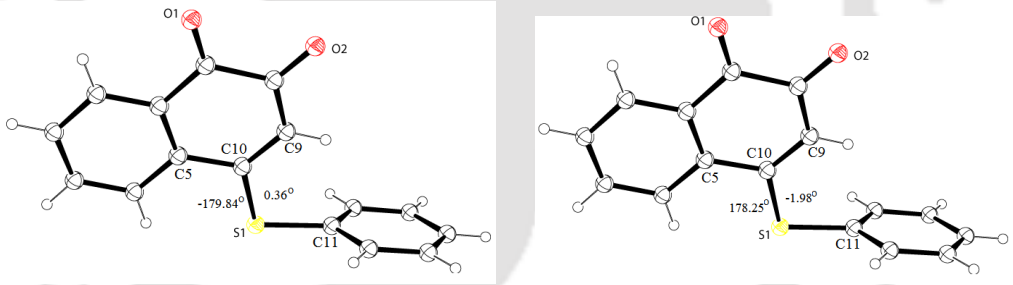

(a) (b)

Figure 4.7: (a) Torsion angle of polymorph **I** (**4.1a**) and (b) Torsion angle of polymorph **II** (**4.1b**) (drawn with 30% thermal ellipsoids).

The presence of C-H···O interactions in the polymorphs can be easily identified from their IR spectra. The C-H frequency in IR has been a useful tool to depict C-H···O interactions.[29] Solid state IR spectra of the two polymorphs in the region of 3000-2000 cm^{-1} in KBr and CCl_4 and found that two polymorphs have different C-H absorption frequencies (Figure 4.8). This clearly supports participation of the C-H in weak interactions and these interactions are distinguishable in polymorphs **I** and **II**.

TH-1303_09612216

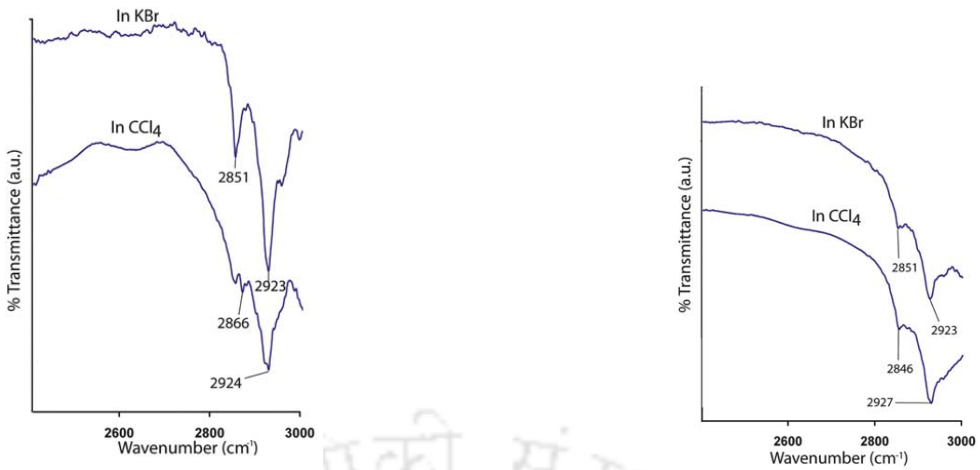

(a) (b)

Figure 4.8: FT-IR of polymorphs in KBr and CCl_4 (a) Polymorph **I** (**4.1a**) and (b) Polymorph **II** (**4.1a**) in the region of 3000-2500 cm^{-1}.

The conformational polymorphs of sulfur containing quinone are well-documented.[7-9] We may suggest that presence of phenylthio group in 1,2-naphthoquinone in different orientations can cause conformational polymorphs, similar to the conformation polymorphs observed in 1,4-naphthoquinone derivatives.[8] It has been recently reported that 2-methyl-1,4-naphthoquinone containing compounds show conformational polymorphism.[9] The primary difference of two polymorphs **I** and **II** arises from their packing patterns. We have compared the phase purity of each polymorph by comparing the powder X-ray diffraction pattern of them with the simulated pattern from the structure determined by single crystal X-ray diffraction. The powder X-ray diffraction patterns of the two polymorphs are distinguishable which are shown in the figure 4.9. We observe that **4.1a** has a crystal density of 1.391 g/cm^3 and **4.1b** has a crystal density of 1.399

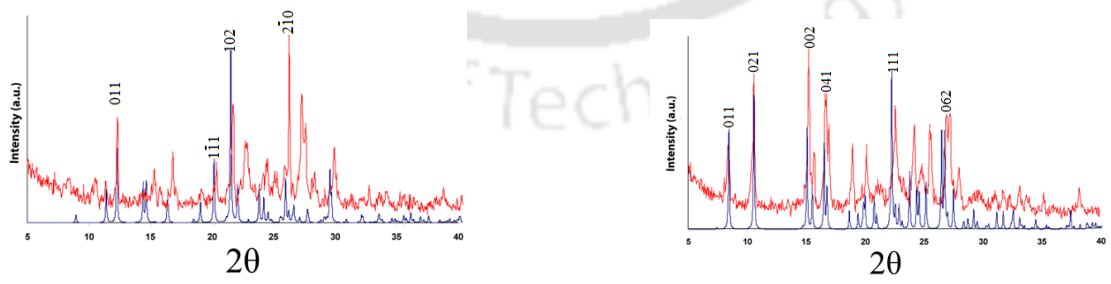

(a) (b)

Figure 4.9: The PXRD of (a) Polymorph **I** (**4.1a**) and (b) polymorph **II** (**4.1**) (at heating rate 5°C per minute).

TH-1303_09612216

g/cm^3. In accordance with the Kitaigorodskii packing principle,[10] the polymorph with larger density should have loose molecular packing. This is an indirect outcome of the Burger-Ramberger density rule,[11] which suggests that at absolute zero, the lower density polymorph has less stability. From differential scanning calorimetry (DSC) with a heating rate of 5 °C per minute, it is found that the polymorph **I** shows endothermic peaks at 177 °C. On the other hand, DSC of polymorph **II** shows melting point at 180 °C.

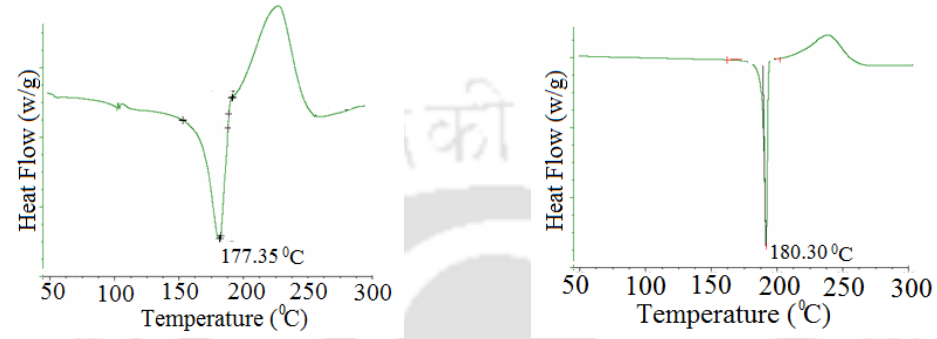

(a) (b)

Figure 4.10: DSC of the (a) Polymorph **I** (**4.1a**) and (b) polymorph **II** (**4.1b**) (at heating rate 5 °C per minute).

*4.2.2: Structural studies of **4.2-4.7***

Compounds **4.2-4.7** resulted in the unsolvated crystals. Interestingly; when compound **4.7** was crystallized from solution in different solvents, different crystals were obtained. The unsolvated form **4.7a** of **4.7** was obtained from dimethylformide (DMF) solvent. The crystal obtained from solution of methanol was methanol solvate **4.7b**, similarly the crystal obtained from dimethylacetamide (DMA) was DMA solvate **4.7c**, and on the other hand the crystal of the **4.7** from aqueous methanol was the hydrate **4.7d** as shown in Scheme 4.2.

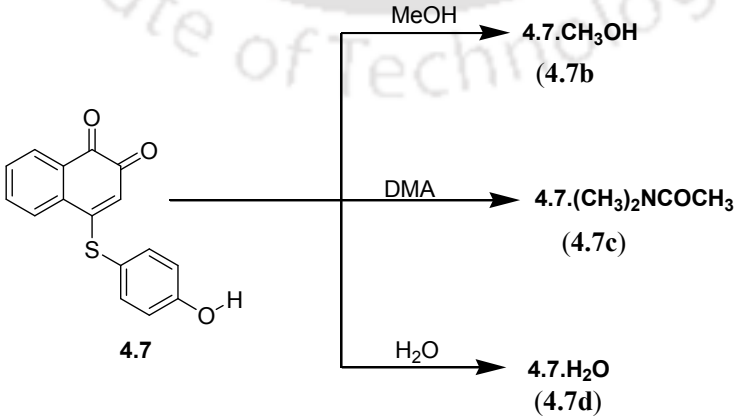

Scheme 4.2: Crystallisation of anhydrous and solvates of **4.7**

TH-1303_09612216

Compound **4.2** crystallizes in monoclinic space group $P2_1/n$. ORTEP diagram of **4.2** is shown in figure 4.11a. In the crystal packing of this compound also dimeric pairs are observed. Such pairs are formed by intermolecular hydrogen bonds as shown in figure 4.11c. Whereas 4-methylthioaryl groups are *cis* to each other across the cyclic hydrogen bonded motifs. Carbonyl groups exhibit C-H···O interactions form a cyclic hydrogen bonded architecture (Table 4.3). Apart from these interactions, more weak interactions such as C-H···π and other C-H···O interactions also contribute to the stability of the crystal.

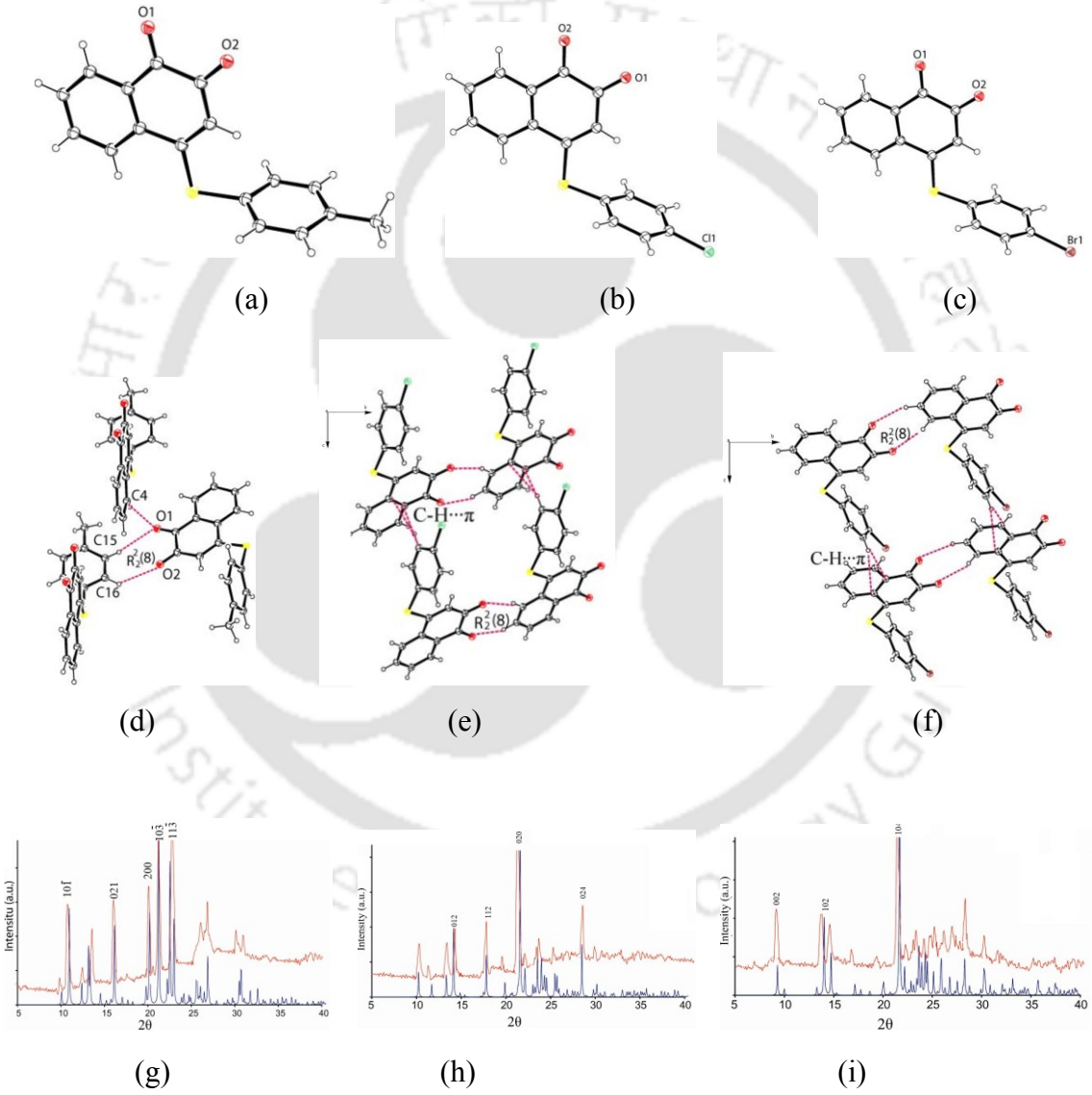

Figure 4.11: (a) ORTEP diagram of compounds (a) **4.2**, (b) **4.3**, (c) **4.4** (drawn with 30% thermal ellipsoids), (d) C-H···O interactions in **4.2**, (e) Hydrogen assemblies of compound **4.3**, (f) hydrogen bonded assembly of compound **4.4**. Powder X-ray diffraction patterns of compounds (g) **4.2**, (h) **4.3** and (i) **4.4**.

TH-1303_09612216

Table **4.3**: Hydrogen bond geometry (Å,°) of compounds **4.2**, **4.3** and **4.4**

Compound	D-H···A	d_{D-H}	$d_{H\cdots A}$	$d_{D\cdots A}$	∠D-H···A
4.2	C4-H4···O1 [1/2-x, 1/2 + y,1/2- z]	0.93	2.56	3.398 (2)	149
	C16-H16···O2[3/2-x, 1/2 + y,1/2- z]	0.93	2.57	3.247 (2)	127
4.3	C3-H3···O2 [x,-1+y, z]	0.93	2.44	3.270 (5)	148
	C4-H4···O1	0.93	2.50	3.403 (5)	162
4.4	C3-H3···O1 [x,1+y, z]	0.93	2.47	3.269 (12)	145
	C4-H4···O2	0.93	2.55	3.459 (12)	165

Compounds **4.3** and **4.4** are isostructural. Both crystallize in monoclinic space group $P2_1/c$. The structures of **4.3** and **4.4** are shown in figure 4.11b-c. They form $R_2^2(8)$ type of cyclic hydrogen bond motifs (Figure 4.11e-f). The carbonyl groups exhibit C-H···O interactions (Table 4.3). The differences between the structures of **4.3** and **4.4** lie in the hydrogen bond parameters. Compound **4.4** has slightly greater distances than the **4.3** because of the greater atomic radius of the bromine atom than chlorine atom. The hydrogen bond parameters of **4.4** are listed in table 4.3.

Compound **4.5** crystallizes in orthorhombic space group $P2_12_12_1$. The structure of **4.5** is shown in figure 4.12a. In its crystal packing, it is observed that the phenolic -OH group form a one-dimensional zigzag O-H···O hydrogen bond with carbonyl groups of 1,2-naphthoquinone moiety along *a*- crystallographic axis. Apart from the hydrogen bond interactions, based on their distance of separations among various bonds there exists weak interactions such as C-H···π and C-H···O interactions also contribute to the stability of the crystal. In the packing there are dimeric units formed between the molecules through O-H···O and C-H···O interactions. This unit is connected through another molecule of **4.5** through C-H···O interactions as shown in figure 4.12c. The arylthiolate groups are *cis* to each other across a $R_2^2(9)$ type hydrogen bond motif as shown in figure 4.12c. The carbonyl groups exhibit C-H···O interactions with a C-H bond on 1,2-naphthoquinone moiety. From the packing pattern of **4.5,** it is seen that 1,2-naphthoquinone molecules are in *head-tail* manner along the crystallographic *a*-axis.

TH-1303_09612216

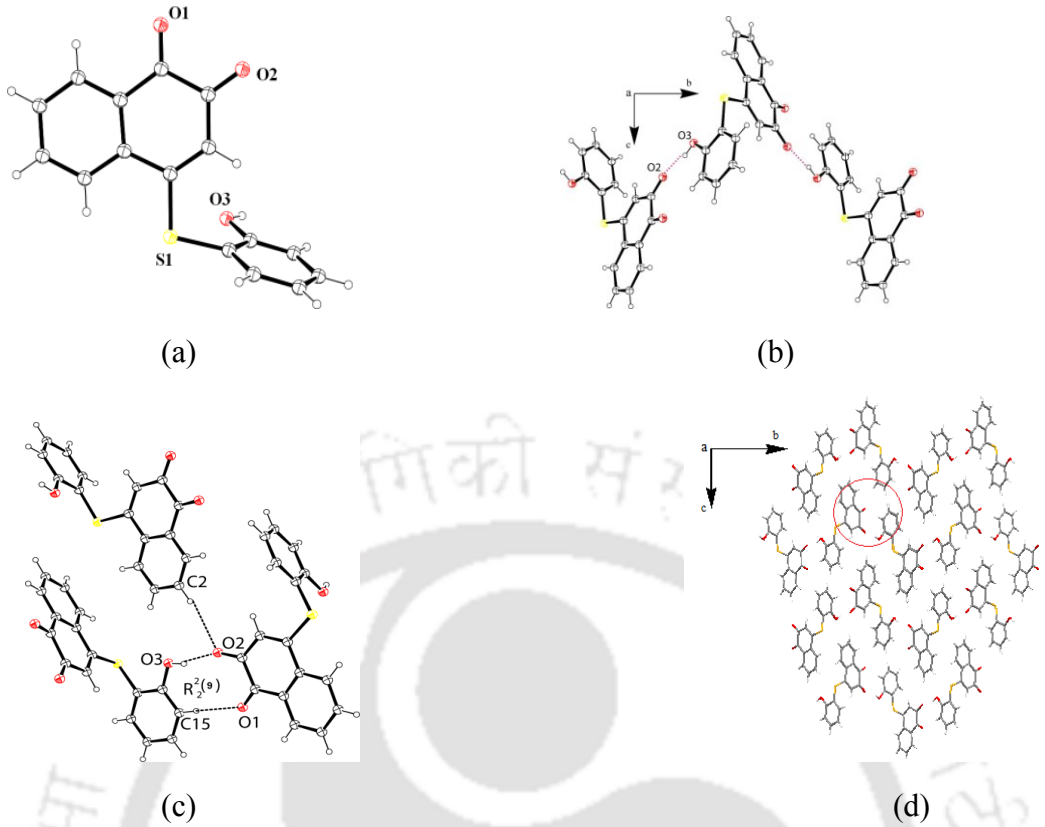

Figure 4.12: (a) ORTEP diagram of **4.5** (drawn with 30% thermal ellipsoids), (b) O-H···O interactions between neighbouring molecules of **4.5**, (c) Self-assemblies of **4.5** and (d) Packing diagram of **4.5** (The red circle indicates that; 1,2-naphthoquinone part is *head* whereas hydroxy-thiophenol part is *tail*).

The compound **4.6** crystallizes in monoclinic space group $P2_1/c$ from a solution **4.6** in methanol solvents. In its crystal structure (Figure 4.13a), it is observed that the phenolic -OH group forms a one-dimensional zigzag O-H···O hydrogen bonds with carbonyl groups of 1,2-naphthoquinone moieties along crystallographic *a*-axis. The carbonyl groups of the naphthoquinone units are involved in bifurcated hydrogen bonds with neighbouring acidic hydrogen atom of the 4-hydroxyphenylthio group of another molecule. This results in formation of cyclic hydrogen bonded motifs having $R^2_1(5)$ geometry.[12-13] The bifurcated hydrogen bonds comprise of two medium strength hydrogen bonds O1···H, O2···H ($d_{D\cdots A}$) distances are 2.42 Å and 2.41 Å forms $R^2_1(5)$ geometry as shown in figure 4.13c. From the packing pattern of **4.6**, it is seen that 1,2-naphthoquinone moieties form *head-head* arrangement along the crystallographic *a*-axis. Apart from the hydrogen bond interactions, weak interactions such as C-H···π and C-H···O interactions present in the lattice as suggested based on distance of separations also contribute to the stability of the crystal.

TH-1303_09612216

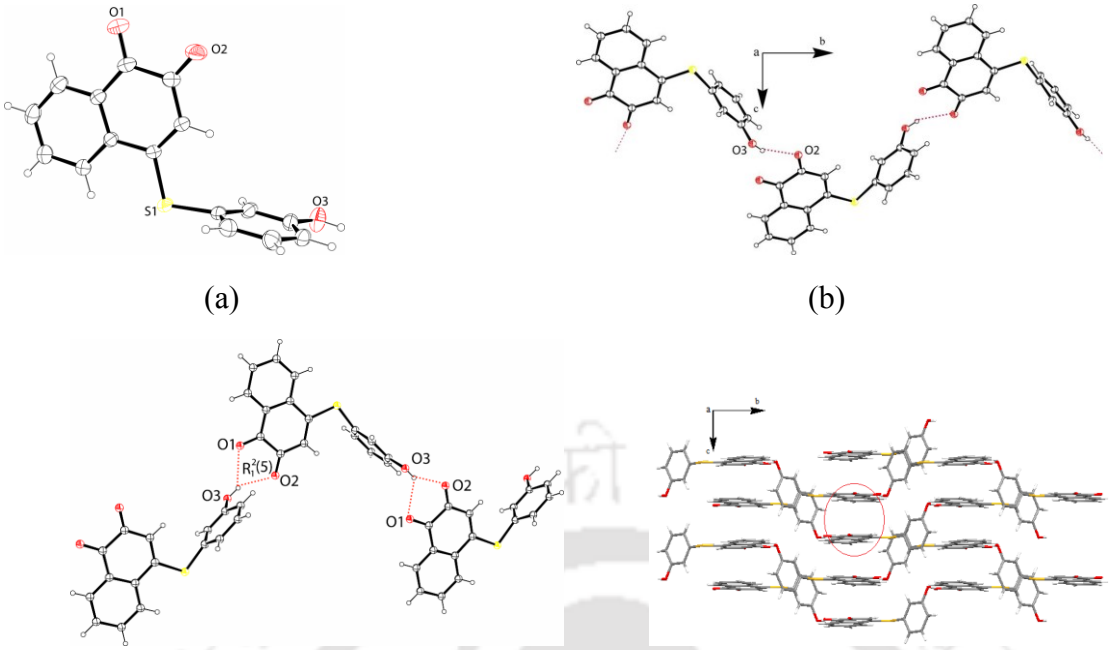

Figure 4.13: (a) ORTEP diagram of **4.6** (30% thermal ellipsoids), (b) The O-H···O interactions in **4.6**, (c) Bifurcated hydrogen bond interactions in **4.6** and (d) Packing diagram of **4.6** (The red circle indicates that; 1,2-naphthoquinone part is *head* whereas hydroxy-thiophenol part is *tail*).

Compound **4.7a** crystallizes in monoclinic space group $P2_1/n$ from a solution of **4.7** in dimethylformamide. In its crystal structure (Figure 4.14a), it is observed that the carbonyl groups of the 1,2-naphthoquinone unit hydrogen bond with a neighbouring hydrogen atom of phenolic unit. This results in the formation of cyclic hydrogen bonded $R^2_1(5)$ geometry as shown in figure 4.14c. The corresponding O1···H, O2···H ($d_{D\cdots A}$) distances are 1.907 Å and 2.639Å respectively; on the other hand, the O3-H distance is 0.820 Å. The salt of ortho-hydoxyquinone derivative form bifurcated hydrogen bond with hydrogen atom of N-H bond.[14] Components of the bifurcated hydrogen bond $d_{D\cdots A}$ distances were found to be 2.987 and 2.584 Å, respectively. Apart from the bifurcated hydrogen bond interactions, weak interactions such as C-H···π and C-H···O interactions also contributed to the stability of the crystal. From the packing pattern of **4.7a,** it is seen that 1,2-naphthoquinone moieties are *head-head* and *head-tail* arrangements along crystallographic *a*-axis.

TH-1303_09612216

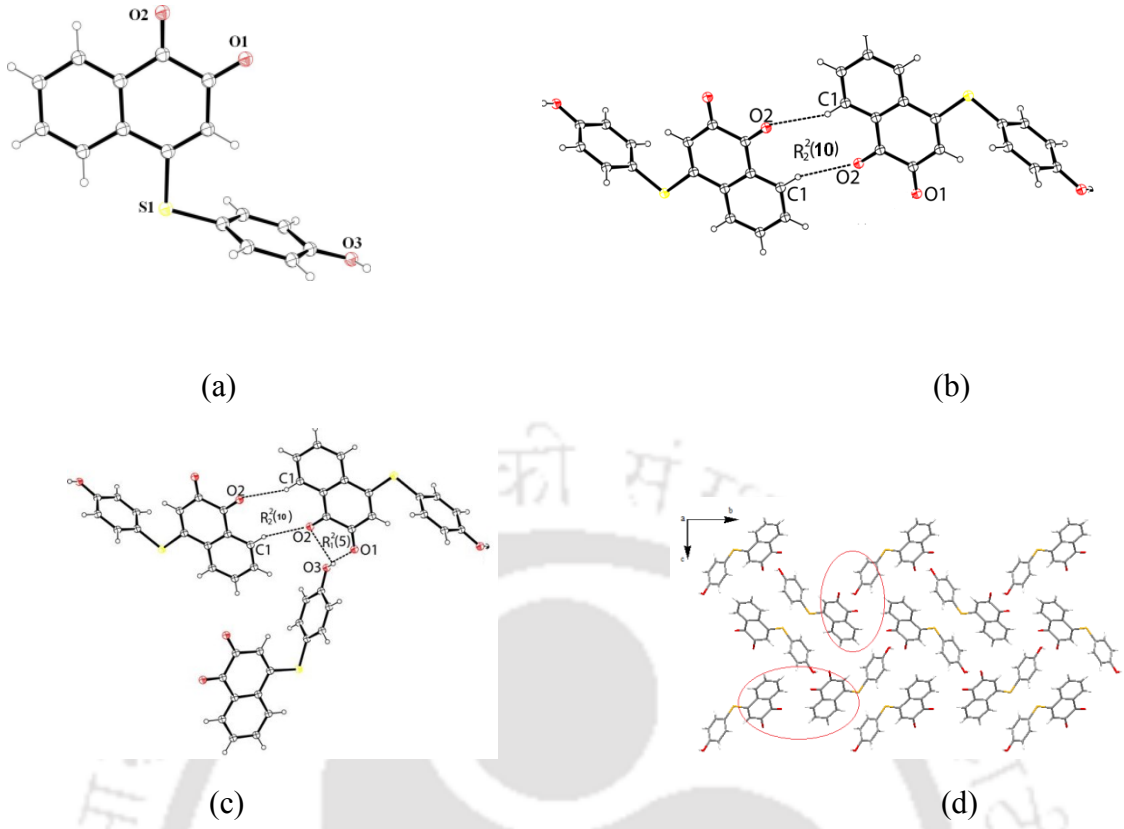

Figure 4.14: (a) ORTEP diagram of **4.7a** (drawn with 30% thermal ellipsoids), (b) C-H···O interactions in a dimeric assembly, (c) Bifurcated hydrogen bond interactions in **4.7a** and (d) Packing diagram of **4.7a** (The red circle indicates that; 1,2-naphthoquinone part is *head* whereas hydroxy-thiophenol part is *tail*).

Bifurcated hydrogen bonds of the compounds **4.6** and **4.7a** are associated with an acidic hydrogen atom as the principal pivote atom. In addition to this the bifurcated hydrogen bond of **4.7a** is associated with one weak and another strong hydrogen bonds, whereas the **4.6** is associated with two equally strong hydrogen bond interactions. Thus, the compound **4.7a** can be manipulated relatively easily by interactions with various solvents to form crystals of solvates (Scheme 4.2). On the other hand, crystal density of the two positional isomeric compounds **4.5** and **4.6** are identical whereas the compound **4.7a** is relatively less dense, the densities are 1.463 g/cm^3, 1.463 g/cm^3 and 1.404 g/cm^3 respectively. Thus, inability to obtain crystalline solvate from **4.6** and **4.5**, are attributed to their self-assembling through strong O-H···O interactions. The primary difference of the three isomeric compounds arises from their packing patterns. The powder X-ray diffraction of the compounds are recorded to ascertain their phase homogeneity. We have found a good agreement of experimental and simulated PXRD data for almost all of these

TH-1303_09612216

compounds, and it suggests the uniformity of the structural features of the bulk materials (Figure 4.15).

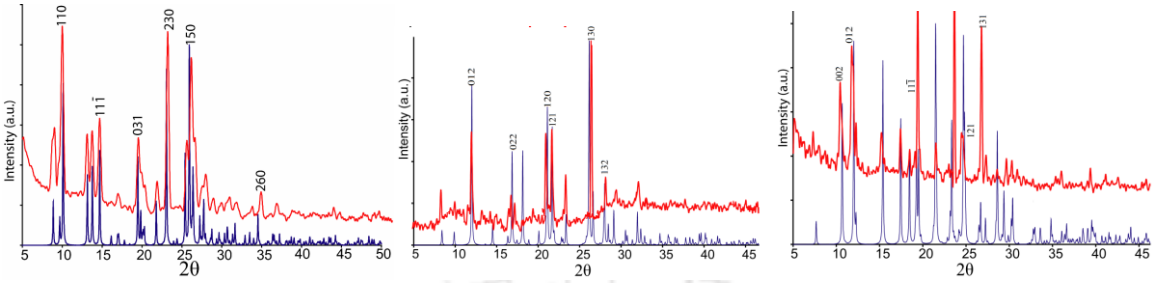

(a) (b) (c)

Figure 4.15: PXRD of compounds (a) **4.5** (b) **4.6** and (c) **4.7a**.

From the IR spectra of **4.5**-**4.7**; it is seen that the C=O stretching frequency for the 1,2-naphthoquinone group for **4.5** appears at 1698 and 1631 cm^{-1}, 1687 and 1633 cm^{-1} for **4.6**. On the other hand C=O stretching frequency for the 1,2-naphthoquinone group for **4.7** appears 1701 and 1632 cm^{-1}. The stretching frequency for -OH groups appears at 3696, 3333, 3316 cm^{-1} respectively. From their IR spectra, it is found the compounds **4.7** and **4.5** have different C-H absorption frequencies, for compound **4.5**, IR stretching frequency for C-H appears 2928, 2850 cm^{-1} and 2967 cm^{-1}, 2926 cm^{-1}, 2851 cm^{-1} for compound **4.7.** Whereas such stretching frequencies are completely absent in case of compound **4.6**. This clearly supports participation of the C-H in weak interactions and these interactions are distinguishable in compounds **4.5**, **4.6** and **4.7** respectively.

The methanol solvate **4.7b** crystallizes in monoclinic space group $P2_1/c$ and its asymmetric unit contains a methanol molecule along with a host molecule of **4.7**. In crystal lattice of **4.7b**, the host molecules are bridged by methanol molecules through strong O-H···O and weak C-H···O interactions. Methanol molecules interact with host molecules by acting donor and oxygen of methanol molecule acts as an acceptor and involves the O-H···O hydrogen bonds with hydroxy group of host molecules, whereas the -OH group of methanol acts as a donor and involves O-H···O interaction with one of carbonyl group of the quinone moieties (host molecule). Both these hydrogen bond interactions led to one dimensional zigzag architecture as shown in figure 4.16b. From its crystal lattice, it is clear that methanol molecules form $R_4^4(10)$ types hydrogen bonded motifs with the host molecules along with the hydroxy group of methanol also forms bifurcated hydrogen bond with carbonyl groups of 1,2-naphthoquinone moieties. The distances between the two O···H (d_D···A) are 2.34 Å and 2.22 Å. Apart from the hydrogen

TH-1303_09612216

bond interactions, weak interactions also contribute to the self-assemblies. From the thermogram (TGA analysis) of the methanol solvate **4.7b**, it is observed that the methanol molecule loses around 130-170 °C (Experimental weight loss 10.2 %, theoretical weight loss 10.3 %). However, there is a sharp weight loss in the region of 150 °C, which occurs due to decomposition of the compound **4.7**.

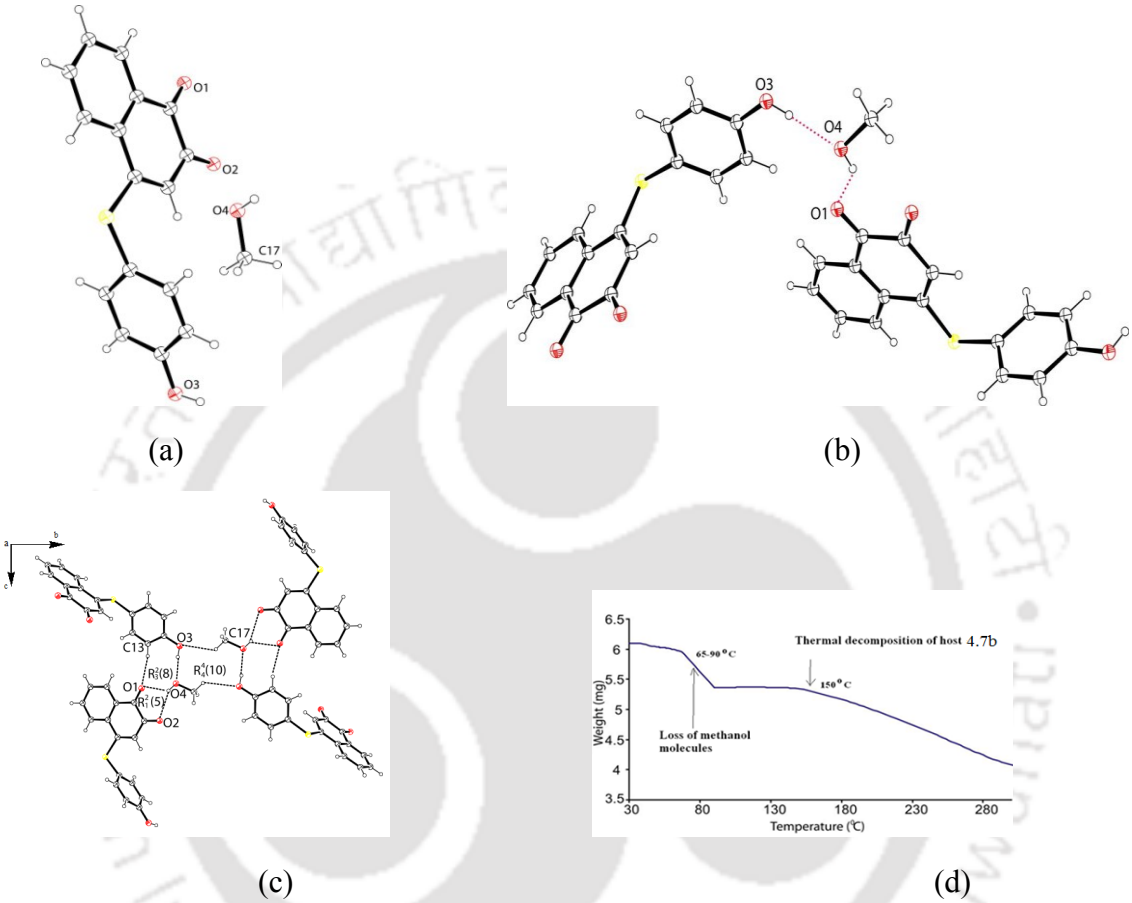

Figure 4.16: (a) ORTEP diagram of methanol solvate **4.7b** (drawn with 30% thermal ellipsoids), (b) Bridging of two molecules of host by methanol, (c) Cyclic and bifurcated hydrogen bonds in the solvate. (d) TGA of methanol solvate **4.7b** (heating rate 5°C per minute).

Table 4.4: Hydrogen bond parameters (Å, °) of **4.5**, **4.6** and **4.7a** and the solvates of **4.7**

Compound No.	D-H···A	$d_{D...H}$	$d_{H...A}$	$d_{D...A}$	∠ D-H···A
4.5	O(3)-H(3a)···O(2) [-x,1/2+y,1/2-z]	0.82	1.97	2.760(4)	163
	C(15)-H(15)···O(1)	0.93	2.29	3.217(4)	173
4.6	O(3)-H(3)···O(1) [1-x,-1/2+y,1/2-z]	0.82	2.42	3.053(2)	135
	O(3)-H(3)···O(2) [-x,1/2+y,1/2-z]	0.82	2.14	2.888(2)	152
	C(16)-H(16)···O(1) [x,1/2-y,-1/2+z]	0.93	2.56	3.319(2)	139
4.7a	O(3)-H(3)···O(1) [3/2-x,1/2+y,1/2-z]	0.82	1.91	2.704(3)	164
	C(1) -H(1) ···O(2) [1-x,-y,-z]	0.93	2.57	3.410(4)	150

TH-1303_09612216

4.7b	O(3)-H(3A)···O(4) [1-x,1-y,1-z]	0.82	1.94	2.747(6)	169
	O(4)-H(4A)···O(2) [1+x,y,z]	0.93(3)	2.03 (3)	2.925(5)	163 (5)
	O(4)-H(4B)···O(4) [2-x,-y,-z]	0.91(5)	2.06(8)	2.766(6)	134(7)
	C(2) -H(2) ···O(2) [x,-1+y,z]	0.93	2.46	3.346(6)	164
	C(12) -H(12) ···O(1) [-x,-y,1-z]	0.93	2.54	3.427(6)	160
4.7c	O(3)-H(3)···O(4) [x,1/2-y,1/2+z]	0.82	1.89	2.686(5)	163
	O(4)-H(4A)···O(1) [-1+x,y,z]	0.82	2.22	2.872(4)	137
	O(4)-H(4B)···O(2)	0.82	2.34	3.081(4)	151
	C(13)-H(13)···O(1)	0.93	2.44	3.0356	171
4.7d	O(1)-H(1)···O(3) [x,1+y,-1+z]	0.82	1.90	2.620(5)	178
	C(12)-H(12)•••O(1) [1/2-x,y,1/2+z]	0.93	2.56	3.231(5)	130
	C(16)-H(16)···O(2) [1/2-x,y,-1/2+z]	0.93	2.49	3.380(5)	160

Dimethylacetamide (DMA) solvate **4.7c** crystallizes in the orthorhombic space group $Pca2_1$ and its asymmetric unit contains a DMA molecule along with a host molecule of **4.7**. There is a strong O-H···O interactions between carbonyl of DMA with the -OH group of phenol (Figure 4.17b). The crystal lattice also has dimers of solvate **4.7c**, which are held altogether different from the dimers found in the other solvates of **4.7** with water or methanol. These dimers are comprised of molecules of **4.7** arranged in head to tail orientations as shown in figure 4.17c. Such arrangements can be explained by considering the 1,2-naphthoquinone part of the molecule **4.7** as the head and the hydroxyphenylthio part as the tail. The tail parts of the two independent molecules of the dimeric assemblies of DMA solvate are oriented in opposite manner. These molecules are interconnected through C-H···O interactions (Table 4.4). Such interactions occur between the carbonyl (O1) of naphthoquinone with C12 of the phenolic unit and of carbonyl O2 with C16 of phenolic unit of another molecule. DMA molecules are crystallographically disordered and are weakly held by C-H···O interactions with host molecules. From the thermogram (TGA analysis) of the DMA solvate, it is observed that the DMA molecule lost around 80 °C (Experimental weight loss 18.5 %, theoretical weight loss 18.0 %). However, there is a sharp weight loss in the region of 225 °C, which occurs due to decomposition of the compound.

TH-1303_09612216

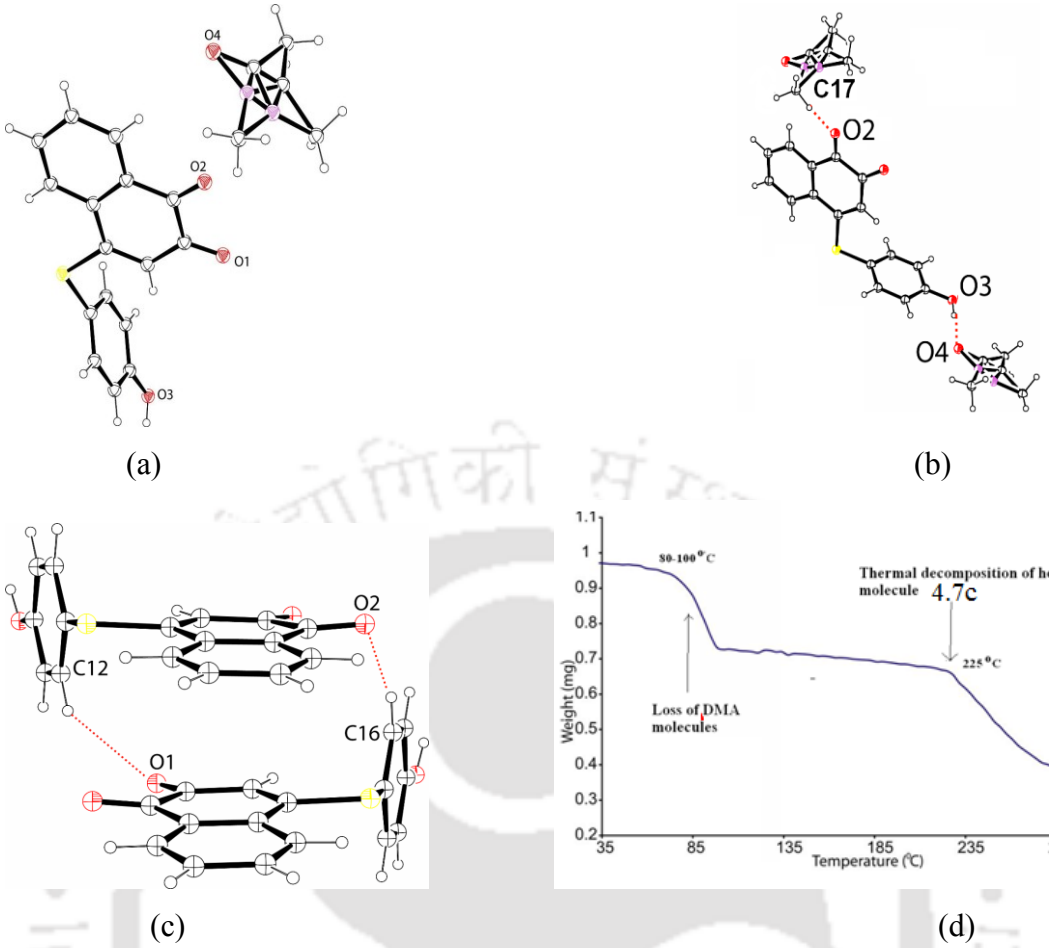

Figure 4.17: (a) ORTEP diagram of DMA solvate **4.7c** (drawn with 30% thermal ellipsoids), (b) Hydrogen bonds in **4.7c**, (c) Dimeric assembly in lattice of **4.7c**, (d) TGA of DMA solvate **4.7c** (heating rate 5°C per minute).

Hydrate **4.7d** crystallizes in triclinic space group P-1 and its asymmetric unit contains a water molecule with a host molecule (Figure 4.18a). The water molecules form a hydrogen bond through one of its hydrogen-atom with two carbonyl groups of the 1,2-naphthoquinone part. It also acts as hydrogen bonded bridge to connect phenolic part to dicarbonyl part of another molecule (Figure 4.18b). There are also strong intermolecular hydrogen bonds involving the intervening water molecules. One prominent hydrogen bond is O(4)-H···O(4) with ($d_{D\cdots A}$) distance 2.766 Å. Two carbonyl groups of the 1,2-naphthoquinone units are involved in strong bifurcated hydrogen bonds forming $R^2_1(5)^{12}$ type motif; in which the O1···H and O2···H distances in the motifs are 2.656 Å and 2.027Å respectively. Further to this, one of the carbonyl groups participating in the $R^2_1(5)$ cyclic hydrogen bonds is involved in weak C-H···O bond interactions with other units. The bond parameters of C-H···O interactions are within the limit where they are generally preffered.[15-17]

TH-1303_09612216

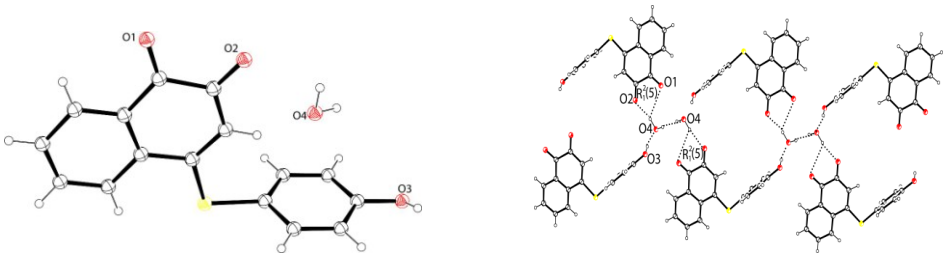

(a) (b)

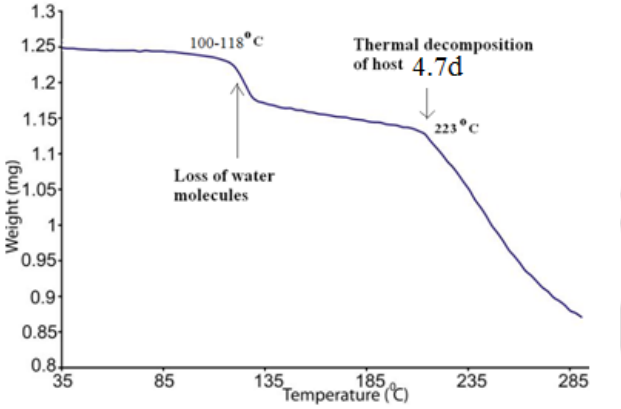

(c)

Figure 4.18: (a) Structure of hydrate **4.7d** (with 30% thermal ellipsoids), (b) Hydrogen bond interactions in hydrate, (c) TGA of hydrate **4.7d** (heating rate 5°C per minute).

From the thermogram (TGA analysis), it is observed that the water molecule are lost around 100-118 °C (Experimental weight loss 5.5 %, theoretical weight loss 6.0 %). However, there is a sharp weight loss in the region of 223°C, which occurs due to decomposition of the compound. Conformational polymorphs and solvates in -OH groups containing compound are well-documented.[18-24] The inclusion of guest molecules by hydroxy compounds is a well known phenomenon where C-H···O interactions play the important role.[22-23] For example, the tetra-hydroxy compound 9,10-bis-(2,5-dihydroxy-1-phenyl)anthracene forms a one dimensional ladder like structure where the anthracene units act as rung and the acetone molecules are incorporated in the ladder, which are stabilized by C-H···O interactions.[24] Primary differences of the three solvates arise from their packing pattern. Powder X-ray diffraction of the three solvates is recorded to ascertain their phase homogeneity. We have found a good agreement of experimental and simulated PXRD data for almost all of these solvates, and it suggests the uniformity of the structural features of the bulk materials (Figure 4.19). IR spectra of compound **4.7a** has strong carbonyl frequency at 1632 cm^{-1}, methanol solvate **4.7b** has strong absorptions at 1635 cm^{-1} and medium absorption at 1689 cm^{-1}. These carbonyl stretching frequencies

TH-1303_09612216

are attributed to quinonic carbonyl groups. DMA solvate **4.7c** shows carbonyl stretching frequencies at 1704 cm^{-1} and 1637 cm^{-1} due to carbonyl group of DMA and carbonyl groups of the 1,2-naphthoquinone respectively. Whereas the hydrate solvate **4.7d** has two strong absorptions at 1626 cm^{-1} and 1635 cm^{-1} respectively.

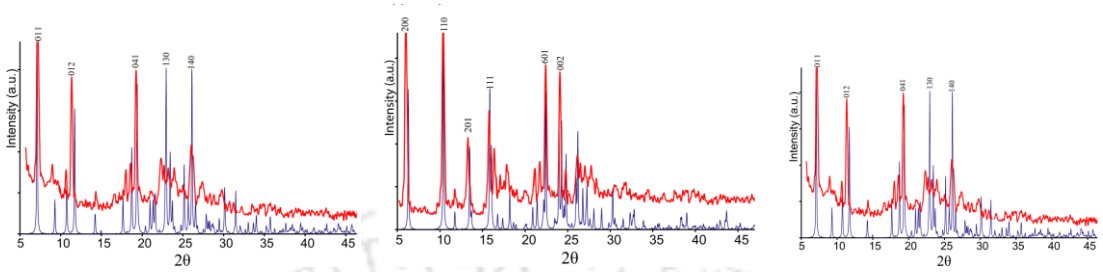

(a) (b) (c)

Figure 4.19: PXRD of the (a) methanol solvate **4.7b**, (b) dimethylacetamide solvate **4.7c** and (c) hydrate **4.7d**.

*4.3: Fluorescence study of compounds **4.5-4.7***

Optical properties of 1,2-quinone derivatives find applications in molecular recognition [25-36] and sensors.[37-43] Quinone derivatives are used for detection of metal ions. [44-57] Compounds **4.5** and **4.7** in methanol or in dimethylacetamide show UV-absorptions from $\pi \rightarrow \pi^*$ transitions at 317 nm whereas the compound **4.6** has absorption at 318 nm. Compound **4.7** shows solvate-emissive property upon excitation at 320 nm, whereas on similar excitation the compound **4.5** and **4.6** do not show any change in emission spectra on different solvent. Compound **4.7** in DMA showed dual fluorescence emission at 421 nm (Φ = 0.026) and 567nm (Φ = 0.032) on excitation at 320 nm and compound **4.5** shows emission peak at 416 nm (Φ = 0.023). On the other hand, compound **4.6** shows emission peak at 418 nm (Φ = 0.012). Dual fluorescence of compound **4.7** can be changed to single emission on addition of methanol as shown in figure 4.20, which shows that the dual fluorescence observed in DMA at higher wavelength emission is quenched; on the other hand the emission at lower wavelength increased. Finally addition of more amounts of methanol to the solution **4.7** in DMA led to single emission peak resembling the emission spectra in the methanol. DMA does not have an exchangeable proton; hence, it does not participate in intermolecular proton transfer. On analysis of fluorescence spectra in different solvents we find that dual fluorescence is obtained in ethanol and n-propanol but at different wavelengths in each case, on the other hand in *t*-butanol single fluorescence is observed. Further, in aprotic solvents such as acetonitrile, THF, DMSO, ethyl acetate,

TH-1303_09612216

hexane and dioxane single emission peak is observed but in chloroform and DMF dual fluorescence is observed.

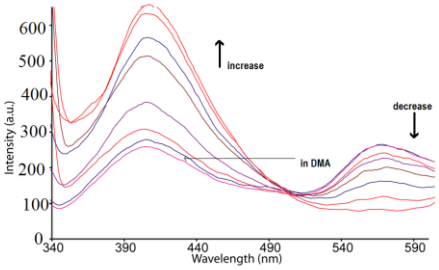

Figure 4.20: (a) Changes in the fluorescence emission of **4.7** (10^{-5} M in 3 mL DMA; λ_{ex} = 320 nm) on addition of methanol in aliquots (10 µL in each aliquot).

The order solvent polarity index[57-58] for the solvents shown in table 4.5 are hexane < n-butanol < n-propanol < THF < chloroform < ethylacetate < dioxane < methanol < ethanol < acetonitrile < DMF < DMA < DMSO.

Table 4.5a: Fluorescence emission of compound **4.7** in different solvents

Solvent	λ_{emi} (nm)	Solvent	λ_{em} (nm)
Ethyl acetate	398	Methanol	410
DCM	381	Ethanol	410, 429
Acetonitrile	398	n-propanol	358, 394
THF	406	n-butanol	419
DMSO	423	Hexane	352
DMF	401, 574	1,4-dioxane	406
DMA	406, 567	Chloroform	360, 377

(10^{-5} M in 3 mLof **4.7** in respective solvent, λ_{ex} 320 nm).

Thus from the irregularities in the trend in the dual fluorescence with respect to solvent polarity, it can be suggested that polarity of solvents contributes less to such phenomenon. On the other hand intramolecular hydrogen bonds in quinones is known to play strong role to cause dual fluorescence in 1,2-dihydroxyanthraquinone.[59] The dual fluorescence emissions from **4.7** observed in DMA solvent can be explained by proposing the formation of stacking arrangement to facilitate exciplex formation. The fluorescence life-time for the compounds **4.5**-**4.7** were recorded, the life times are listed in table 4.6.

TH-1303_09612216

Table 4.5b: Stokes shift and quantum yield for compounds **4.5-4.7**

Compound	λ_{abs} (nm)	λ_{ems} (nm)	Stokes shift (nm)	Quantum Yield (Φ)
4.5	317	416	99	0.023
4.6	318	418	100	0.012
4.7	317	421, 567	104, 250	0.026, 0.032

We observe two life-times in each case for lower wavelength emission peak; whereas single life-time for emission at 567 nm in DMA is observed. The relative quantum yield of the relatively long lived species increases when emissions are monitored above 567 nm (λ_{em} > 567 nm) compared to the one monitored above 420 nm (λ_{em} > 420 nm). It follows that the shorter wavelength emission corresponds to a short-lived species and the longer wavelength emission corresponds to a longer-lived species.

Table 4.6: Fluorescence lifetime of compounds **4.5-4.7**

Fluorescence lifetime data for the compounds upon interaction with aluminium (III)

Compound	λ_{ext} (nm)	λ_{emi} (nm) (Solvent)	τ^1(ns)/(f)%	τ^2 (ns)/(f)%	χ^2
4.7		421 (DMA)	0.754 (64.21)	3.535 (35.79)	1.055
		567 (DMA)	2.787 (100)	-	1.075
4.7 + Al^{3+}	320	405 (MeOH)	0.753 (70.04)	3.586 (29.96)	1.055
4.6		418 (DMA)	0.728 (63.35)	3.501 (36.65)	1.062
4.6 + Al^{3+}		408	0.716 (59.63)	3.596 (40.37)	1.083
4.5		416 (DMA)	0.769 (68.92)	3.567 (31.08)	1.023
4.5 + Al^{3+}		408	0.753 (65.74)	3.675 (34.26)	1.030

On the other hand the fluorescence property of compound **4.7** was explored in the presence of different metal ions. We find that the intensity of fluorescence emission of a solution **4.7** in DMA at 567 nm was higher than the peak at 421 nm. It is observed that the emission peak at 421 nm is significantly enhanced by addition of aluminium (III) ions with a shift of 15 nm towards lower wavelength as shown in figure 4.21a.

To understand the binding interactions and the type of complex formed between these compounds and metal salts, the binding constant values were determined from the fluorescence emission data by using the Benesi-Hildebrand equation.[60] From the increase in the fluorescence with the increase in concentration of

TH-1303_09612216

aluminium (III) ions, the binding constant for a 1:1 complex of **4.7** with aluminium (III) ions is 3.74×10^5 M^{-1}. The fluorescence emission of the compound **4.7** is unaffected by addition of a solution of metal ions such as monovalent or bivalent ions such as lithium, sodium, potassium, beryllium, magnesium, calcium, manganese, iron, cobalt, nickel, copper, zinc, cadmium, and mercury. In each case chloride salt of corresponding metal was used. Aluminium (III) ions are toxic and cause various diseases[61-63], thus selective detection by compound **4.7** is an important result. Selective changes in fluorescence by aluminium (III) ions and silence towards many essential elements in biology is also an important observation due to recent interests in search of aluminium (III) selective fluorescent probes.[64-68] On the other hand, compounds **4.6** and **4.5** in DMA show fluorescence emission at 416 and 420 nm respectively on excitation at 320 nm. Fluorescence emission of compounds **4.6** and **4.5** are unaffected by a solution of

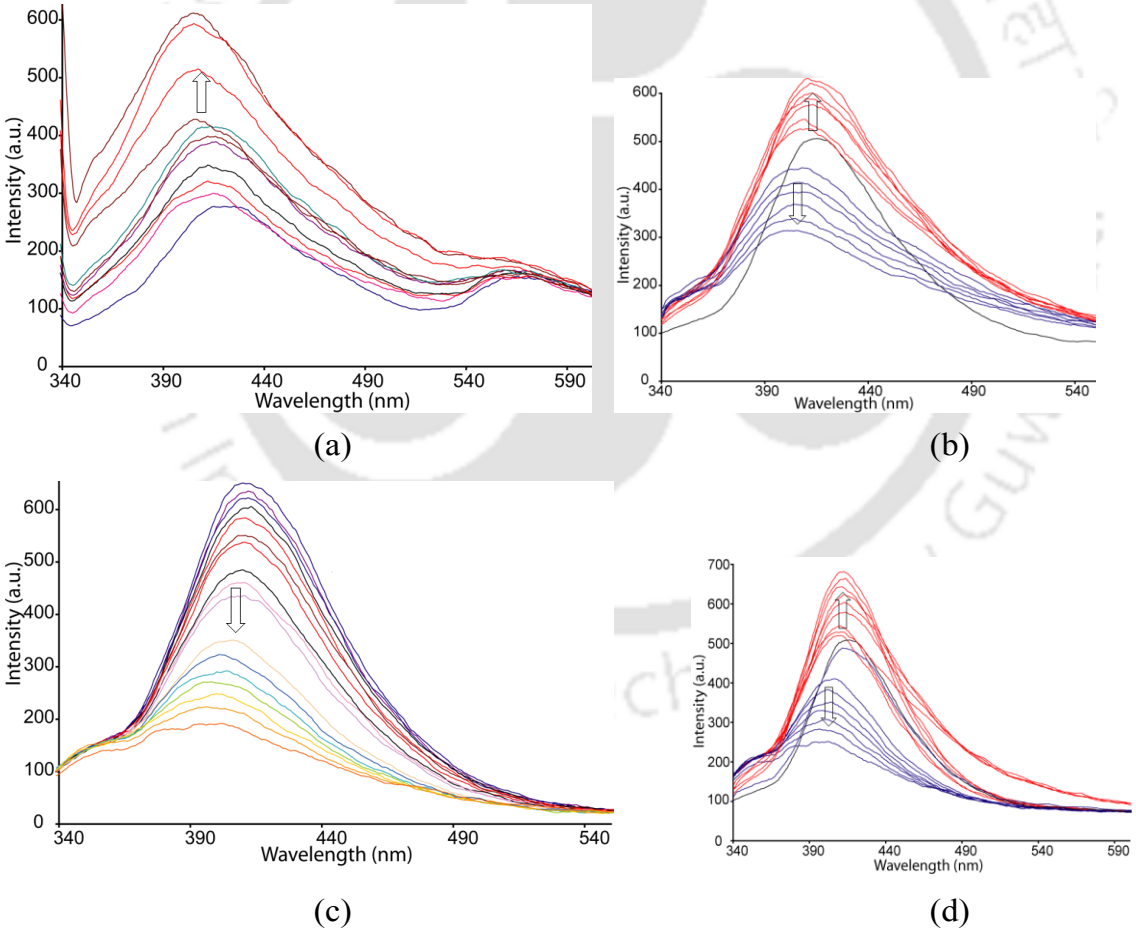

TH-1303_09612216

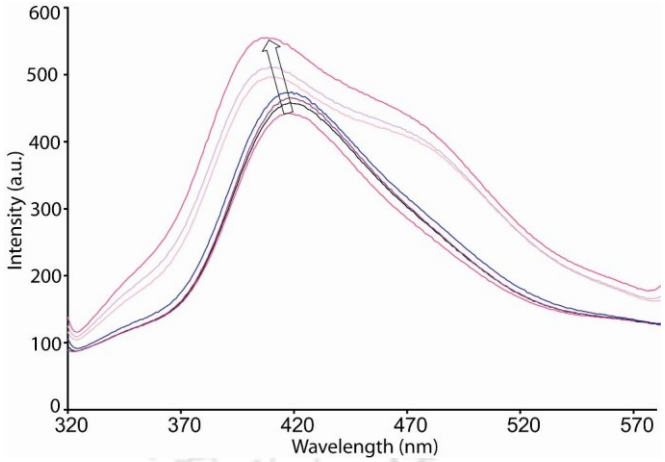

(e)

Figure 4.21: Changes in fluorescence emission (a) **4.7**, (b) **4.5** on addition of solution of aluminium (III) ions. In each case 10^{-5} M of compound in 3 mL DMA was titrated against aluminium (III) ions (10 μL in each aliquot of 10^{-5}M solution in DMA), (c) Changes in fluorescence emission of **4.5** (10^{-5} M in 3 mL DMA) on addition of copper (II) ions (10 μL in each aliquot of 10^{-5}M solution in DMA), (d) Changes in fluorescence emission of **4.5** (10^{-5} M, 3 mL in DMA) on addition of aluminium (III) ions (10 μL in each aliquot of 10^{-5}M in DMA, ten times) followed by addition of copper (II) ions, (10 μL in each aliquot, 10^{-5}M in DMA), (e) Changes in fluorescence emission **4.6** on addition of solution of aluminium (III) ions. In each case 10^{-5} M of compound in 3 mL DMA was titrated against a solution of aluminium (III) ions (10 μL in each aliquot of 10^{-5} M solution in DMA).

other metal salts. The fluorescence emission intensity of a solution of compound **4.5** on addition of aluminium (III) ions show an initial increase in intensity with shift towards lower intensity by 15 nm till 1:1 ligand to metal ion ratio was reached. This change is identical to the response shown by compound **4.7** towards aluminium (III) ions. However, beyond the concentration of metal ion to ligand molar ratio 1:1 the fluorescence intensity starts decreasing until ligand to metal ratio attains 1:2. Thus, two binding constants could be obtained from the two independent slopes observed from linear changes in emission intensities. The binding constants for 1:1 and 1:2 complexes were 4.39×10^5 M^{-1} and 2.85×10^6 M^{-1} respectively. From quenching of fluorescence versus the concentration of copper (II) ions a straight line is obtained and the binding constant for 1:1 copper complex with the compound **4.5** was found to be 5.62×10^5 M^{-1}. It was earlier observed that copper (II) ions caused fluorescence[69] and visible[70] spectral change of 1,4-

TH-1303_09612216

naphthoquinone derivatives. Thus, response in change in intensity of fluorescence emission on interactions with copper (II) ions by compound **4.5** is exactly opposite to that the response aluminium (III) ions. However, 1:1 binding constant in both these cases are comparable. On the other hand, second binding constant of aluminium (III) ions is much larger than these. Thus we could obtain *OFF-ON* as well as *ON-OFF* type of fluorescence by changing the sequence of additions of the ions in a controlled manner. For example, addition of aluminium (III) ions to attain 1:1 ratio of metal ion to ligand ratio. The observed increase in fluorescence intensity by aluminium (III) ions, quenched by addition of copper (II) ions is shown in figure 4.21d. Similarly, the addition of copper (II) ions initially to a solution of compound **4.5** to attain 1:1 metal to ligand ratio followed by addition of aluminium (III) showed an initial decrease in fluorescence followed by increase in fluorescence. Thus, *ON-OFF* as well as *OFF-ON* states of fluorescence could be caused in sequential manner by just changing the sequence of addition of these two ions. From quenching of fluorescence versus the concentration of aluminium (III) ions a straight line was obtained and the binding constant for 1:1 aluminium (III) complex with the compound **4.6** was found to be 7.64×10^5 M^{-1}. The fluorescence lifetimes of the respective fluorescence decay profiles of the **4.5-4.7** in the presence and absence of aluminium (III) ions are listed in table 4.6. The presence of aluminium (III) ions change the fluorescence decay profile of **4.5**, **4.6** as well as that of **4.7** remained biexponential in each case. Life-times indicated that aluminium (III) ions weakly interact with the compounds to form an exciplex. The poor coordination ability of aluminium (III) ions compared with common transition metal ions is the prime reason for relatively less development of selective analytes[71-73] for aluminium (III) ions, but in the present case despite of weak interactions of the ligands with aluminium (III) ions; we could successfully show fluorescence emission changes through weak chelation in by two quinone derivatives.

TH-1303_09612216

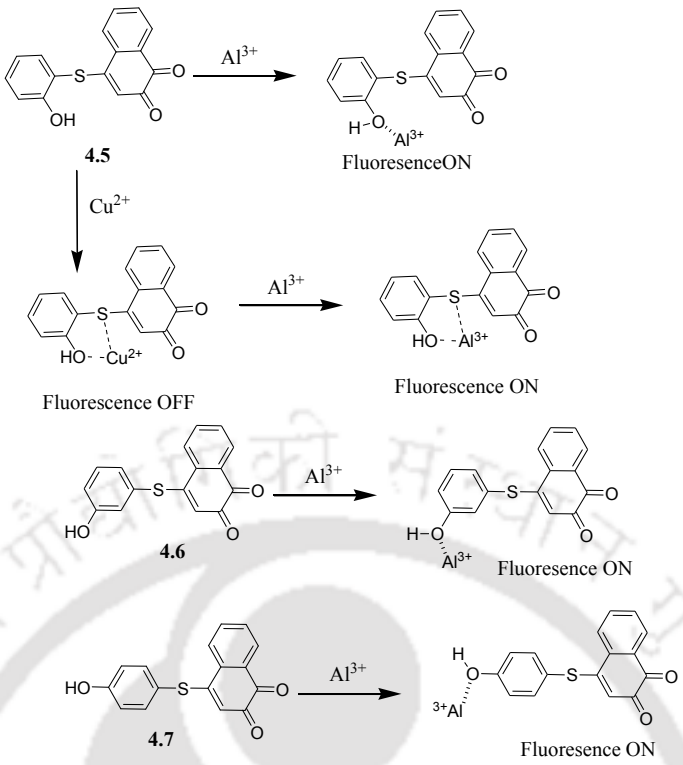

Scheme 4.3: Interactions of aluminium (III) ions with compound **4.5**-**4.7** and interactions of aluminium (III) and copper (II) with compound **4.5**.

From these results, the entire process of fluorescence changes by aluminium (III) ions and copper (II) ions may be explained on the basis of Scheme 4.3. The compound **4.7** interacts with aluminium (III) ions, which increase the acidity of hydrogen and associated proton transfer. Which showed fluorescence enhancement 416 nm and it completely quenched the emission peak at 567 nm. As the excited state charge transfer among the 1,2-dicarbonyl units is inhibited. The compound **4.5** also interacts with aluminium (III) ions through the OH group at the *ortho* position of the phenol ring, thereby; it enhanced the intensity of fluorescence by increasing acidity of the hydrogen for proton transfer. As the concentration of the aluminium (III) ions was increased a 1:2 complex was formed through association. This is proposed on the basis of higher second binding constant of aluminium (III). Secondly, all the three positional isomers have dicarbonyl groups, hence, they are not involved changes hence **4.5** should not be exception. Thus, a two tier process of enhancement followed by quenching of fluorescence in aluminium (III) ions was observed. It is already mentioned that the copper (II) ions showed comparable binding constant with the first binding constant of aluminium (III) ions with compound **4.5**. Thus, when the copper (II) ions were added to a solution of **4.5** containing aluminium (III) ions in 1:1 ratio, the copper (II) ions replaced the aluminium (III) ions causing fluorescence

TH-1303_09612216

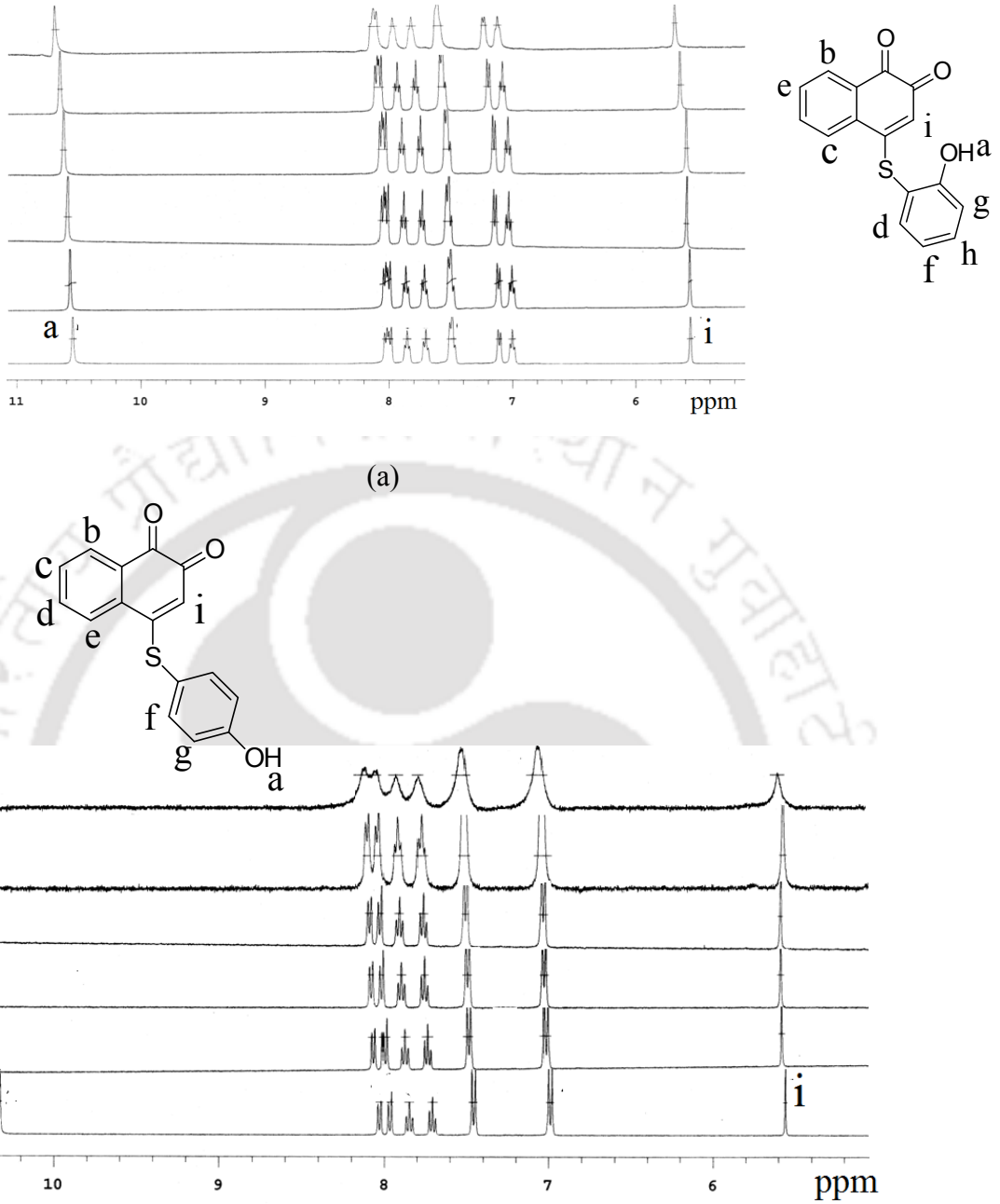

Figure 4.22: ^{1}H-NMR titration with a solution of aluminium (III) in DMSO-d_6 (in the range of 5-11 ppm) of (a) Compound **4.5** and (b) Compound **4.7**.

quenching effect. This caused in the fluorescence intensity of the solution of compound **4.5** containing copper (II) ions when aluminium (III) ions were added. To confirm interactions of aluminium (III) with compounds, we carried out the ^{1}H-NMR titration by adding aluminium (III) ions, to solution of compound **4.6** and **4.7** independently, the spectra at different aluminium concentrations are shown in figure 4.22. In both cases not observe any change in the chemical shifts of protons other than proton of phenolic -OH

TH-1303_09612216

group. It is observed that the aluminium (III) ions affected the chemical shift of the phenolic -OH; this is obvious as the oxygen atom of phenolic group would interact with the aluminium (III) ions.

4.4: Conclusion

This study discerns the different self-assemblies guided by the position of OH group of the phenolic part and by solvents in the solvates in 4-(hydroxyphenylthio) naphthalene-1,2-dione . In solid state solvated form shows differences in packing patterns of the hosts caused by the solvent molecules. Bifurcated hydrogen bonds help in the self-assembling of positional isomers of hydroxyphenyl substituted 1,2-naphthoquonone in different ways. The bifurcated hydrogen bonds involving carbonyls of 1,2-naphthoquinone are absent in positional isomer **4.5**. The nature of hydrogen bonds on the solvates of a particular host differs from system to system. It is also suggested that there is a significant role of position of substituents in a host molecule to form intermolecular bifurcated hydrogen bonds in the solvates or unsolvated form. Compounds **4.5-4.7** are selective in showing enhancement of fluorescent in the presence of aluminium (III) ions. On the other hand, compound **4.7**, shows dual fluorescence in specific solvents.

4.5: Experimental Section

Matrials and physical measurement as described in chapter 2, section 2.4.1, 2.4.2 and chapter 3 section 3.5.1 and 3.5.2.

4.5.1: Physical measurement

The fluorescence life times were measured on a picosecond time-resolved cum steady state luminescence spectrometer of Eddinburg instruments, model: FSP920 and LifeSpecII. The fluorescence emissions were measured in a Perkin-Elmer LS-55 spectrofluorimeter. The fluorescence lifetime were carried out by taking 3 mL solution of compounds (10^{-5} M) in dimethylacetamide and adding 100 µL of the solution of aluminum (III) ions (10^{-5} M).

4.5.2: Quantum yield determination

The quantum yield of fluorescence was determined by using quinine sulphate as a reference in water at room temperature.

$$\textbf{Quantum Yield} = \frac{\textbf{Area of the compound}}{\textbf{Area of Q.S}} \times \frac{\textbf{Absorbance of Q.S}}{\textbf{Absorbance ofCompound}} \times \frac{\textbf{R.I of DMA}}{\textbf{R.I of water}} \times \textbf{0.54}$$

TH-1303_09612216

*4.5.3: General procedure for the synthesis of compounds **4.1-4.7***

4-(Phenylthio)naphthalene-1,2-dione (**4.1**)

To a solution of 1, 2-naphthoquinone (0.474 g, 3 mmol) in methanol (15 mL) thiophenol (0.306 mL, 3 mmol) was added slowly. After addition of thiophenol, the colour of the reaction mixture turns red. The reaction mixture was stirred at room temperature for 8 h. A red precipitate appeared was filtered off and dried in air. Yield: 58%. ^{1}H-NMR (DMSO-d_6, 400 MHz): 8.0 (d, J = 7.6 Hz,1H), 7.9 (d, J = 7.6 Hz, 1H), 7.8 (t, J = 7.6 Hz, 2H), 7.6 (m, 6H), 5.5 (s, 1H), ^{13}C-NMR (100MHz, DMSO-d_6): 173.2, 171.0, 162.5, 161.2, 139.8, 138.7, 133.7, 132.2, 131.2, 129.3, 127.8, 124.1, 120.7, 112.9, 98.6, 96.8. IR (KBr, cm^{-1}): 1692 (m), 1646 (s), 1543 (m), 1384 (w), 1322 (m), 1250 (m), 1168 (w), 932 (m). MS (ESI) m/z: 267.01, m. p. 165 ºC.

4-(4-Methylphenylthio)naphthalene-1,2-Dione (**4.2**)

To a well stirred solution of 1,2-naphthoquinone (0.31 g, 2 mmol) in methanol (20 mL) a solution of 4-methylthiophenol (0.24 g, 2 mol) was added. The reaction mixture was stirred at room temperature for 8 hrs. A red color precipitate was formed. The resulting mixture was filtered and dried in open air. Yield: 65%. ^{1}H-NMR (400 MHz, DMSO-d_6): 8.03 (d, J = 8.0 Hz, 1H), 7.97 (d, J = 8.0 Hz, 1H), 7.85 (t, J = 7.6 Hz, 1H), 7.71 (t, J = 8.0 Hz, 1H), 7.57 (d, J = 6.0 Hz, 2H), 7.43 (d, J = 7.2 Hz, 2H), 5.54 (s, 1H), 2.4 (s, 3H). ^{13}C-NMR (100MHz, DMSO-d_6): 176.2, 174.7, 160.8, 156.4, 146.8, 143.1, 138.6, 135.8, 134.2, 133.7, 130.4, 129.6, 124.3, 118.1, 97.6, 92.3. IR (KBr, cm^{-1}): 3316 (bw), 1687 (m), 1633 (s), 1575 (m), 1525 (s), 1475 (s), 1450 (w), 1325 (s), 1299 (w), 1253 (w), 1226 (s), 1166 (m), 1122 (w), 1019 (m), 955 (w), 937 (s), 886 (m), 860 (w), 782 (w), 763 (m), 702 (w), 674 (w), 595 (w). MS (ESI) m/z: 280.01, m. p. 196 ºC.

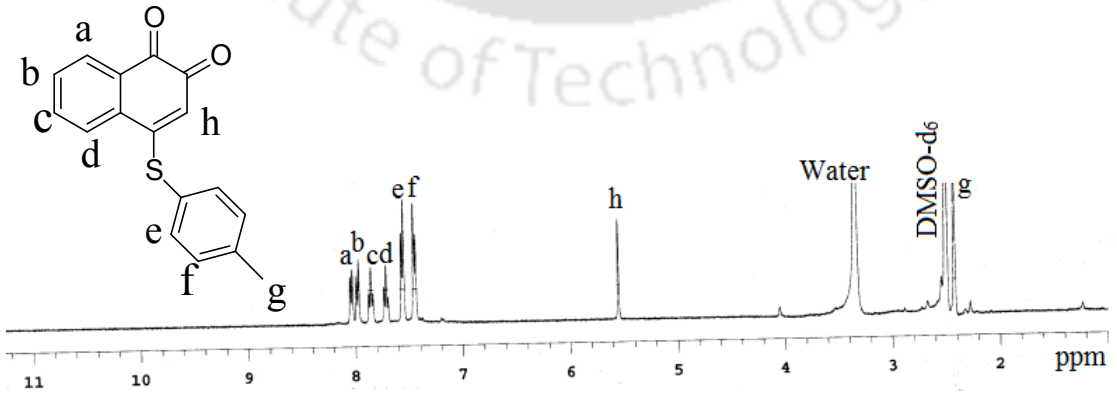

Figure 4.23: ^{1}H-NMR (400MHz, DMSO-d_6) spectra of **4.2**.

4-(4-Chlorophenylthio)naphthalene-1,2-dione (**4.3**)

TH-1303_09612216

To a well stirred solution of 1,2-naphthoquinone (0.31 g, 2 mmol) in methanol (20 mL) a solution of 4-chlorothiotphenol (0.28 g, 2 mol) was added drop wise. The reaction mixture was stirred at room temperature for 8 hrs. A yellow color precipitate was formed. The resulting mixture was filtered and dried in open air. Yield: 76 %. ^{1}H-NMR (400 MHz, DMSO-d_6): 8.04 (d, J = 7.2 Hz, 1H), 7.89 (d, J = 8.0 Hz, 1H), 7.70 (t, J = 7.6 Hz, 1H), 7.67 (d, J = 7.2 Hz, 2H), 7.63 (t, J = 7.2 Hz, 1H), 7.48 (d, J = 7.2 Hz, 2H), 5.67 (s, 1H). ^{13}C-NMR (100 MHz, DMSO-d_6): 178.5, 175.8, 159.4, 137.1, 134.8, 133.1, 132.4, 131.1, 129.8, 128.6, 125.3, 125.2, 124.6, 120.7. IR (KBr, cm^{-1}): 3011 (bw), 1667 (m), 1596 (s), 1567 (m), 1472 (s), 1432 (w), 1378 (m), , 1322 (m), 1262 (w), 1248 (w), 1202 (m), 1146 (m), 1119 (w), 1013 (w), 948 (w), 922 (w), 852 (w), 776 (w), 727 (m), 701 (w), 682 (w), 565 (w). MS (ESI) m/z: 301.06 $[M^{+}+H]^{+}$, m. p. 187 ºC.

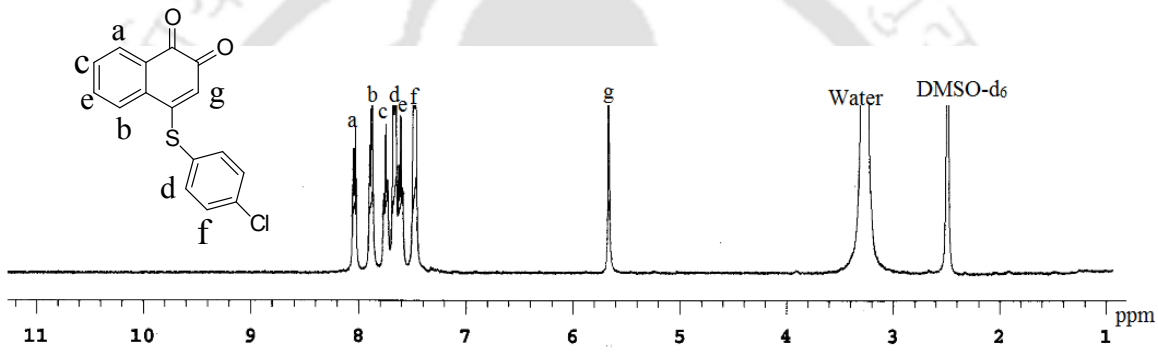

Figure 4.24: ^{1}H-NMR (400MHz, DMSO-d_6) spectra of **4.3**.

4-(4-Bromophenylthio)-naphtha lene-1,2-dione (**4.4**)

To a well stirred solution of 1,2-naphthoquinone (0.31 g, 2 mmol) in methanol (20 mL) a solution of 4-bromothiotphenol (0.37 g, 2 mol) was added drop wise. The reaction mixture was stirred at room temperature for 8 hrs. A dark red color precipitate was formed. The resulting mixture was filtered and dried in open air. Yield: 65 %. ^{1}H-NMR (400 MHz, DMSO-d_6): 8.15 (d, J = 7.2 Hz, 1H), 8.05 (d, J = 6.0 Hz, 1H), 7.80 (t, J = 7.6 Hz, 1H), 7.71 (t, J = 7.2 Hz, 1H), 7.68 (d, J = 6.0 Hz, 2H), 7.61 (d, J = 5.6 Hz, 2H), 5.80 (s, 1H). ^{13}C-NMR (100 MHz, DMSO-d_6): 177.6, 175.0, 158.6, 136.2, 134.0, 132.3, 131.6, 130.2, 129.0, 127.8, 124.4, 124.3, 123.8, 119.9. IR (KBr, cm^{-1}): 3033 (bw), 1679 (m), 1623 (s), 1553 (m), 1511 (m), 1456 (m), 1388 (m), 1352 (m), 1299 (w), 1243 (w), 1231 (s), 1171 (m), 1105 (w), 1054 (w), 976 (w), 942 (m), 887 (w), 845 (w), 776 (w), 753 (m), 701 (w), 645 (w), 525 (w). MS (ESI) m/z: 345.02, $[M^{+}+2H]^{+}$, m. p. 196 ºC.

TH-1303_09612216

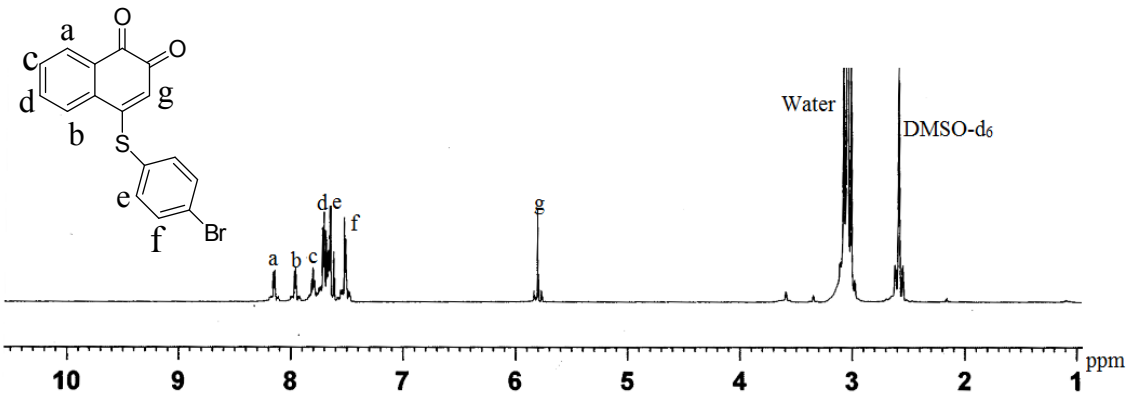

Figure 4.25: ^{1}H-NMR (400MHz, DMSO-d_6) spectra of **4.4**.

4-(2-Hydroxyphenylthio) naphthalene-1,2-dione (**4.5**)

To a well stirred solution of 1, 2-naphthoquinone (0.31 g, 2 mmol) in methanol (20 mL) a solution of 2-mercaptophenol (0.20 mL, 2 mol) was added drop wise. The reaction mixture was stirred at room temperature for 6 hrs. The red precipitate obtained was collected by decanting the solvent and dried in open air. Yield: 85%. ^{1}H-NMR (400MHz, DMSO-d_6): 10.34 (s, 1H), 8.02 (d, J = 7.2 Hz, 1H), 7.93 (d, J = 8 Hz, 1H), 7.73 (d, J = 8 Hz, 1H), 7.57 (t, J = 7.6 Hz, 1H), 7.36 (t, J = 7.6 Hz, 2H), 7.04 (d, J = 8 Hz, 1H), 6.88 (t, J = 7.6 Hz, 1H), 5.70 (s, 1H). ^{13}C-NMR (100MHz, DMSO-d_6): 177.8, 173.6, 162.2, 161.7, 140.1, 138.5, 134.4, 132.9, 131.6, 130.3, 128.5, 125.4, 121.7, 116.1, 99.8, 97.6. IR (KBr, cm^{-1}): 3333 (bm), 2928 (w), 2850 (w), 1698 (m), 1631 (s), 1587 (w), 1578 (w), 1528 (m), 1496 (w), 1450 (m), 1347 (m), 1327 (m), 1305 (w), 1295 (m), 1257 (m), 1218 (w), 1174 (w), 1130 (w), 1116 (w), 1063 (w), 972 (m), 938 (m), 866 (w), 850 (m), 836 (w), 778 (s), 754 (m), 709 (w), 661 (w), 502 (w). MS (ESI) m/z: 283.04, m. p. 172 ºC.

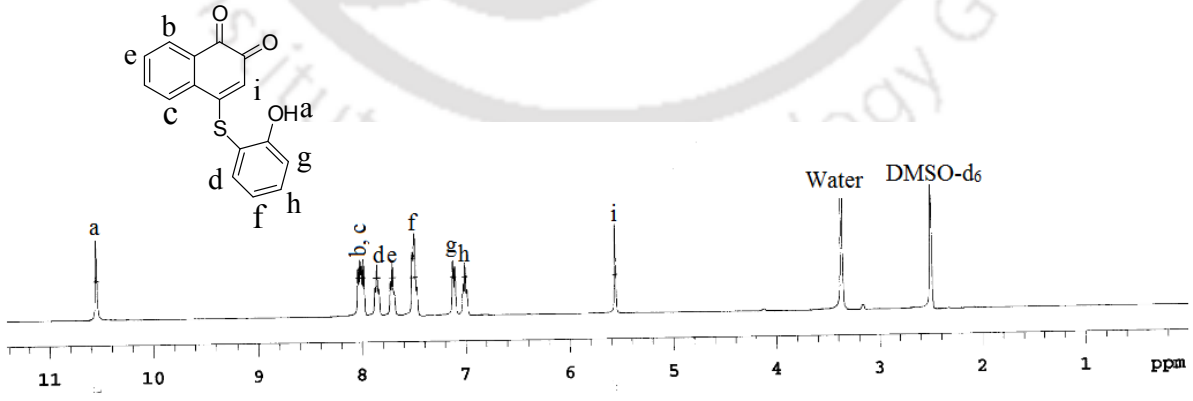

Figure 4.26: ^{1}H-NMR (400MHz, DMSO-d_6) spectra of **4.5**.

4-(3-Hydroxyphenylthio) naphthalene-1, 2-dione (**4.6**)

To a well stirred solution of 1,2-naphthoquinone (0.31 g, 2 mmol) in methanol (20 mL) a solution of 3-mercaptphenol (0.20 mL, 2 mol) was added drop wise. The reaction mixture

TH-1303_09612216

was stirred at room temperature for 8 hrs. A red color precipitate was formed. The resulting mixture was filtered and dried in open air. Yield: 85%. ^{1}H-NMR (400 MHz, DMSO-d_6): 9.55 (s, 1H), 8.05 (d, J = 8.0 Hz, 1H), 7.87 (t, J = 8.0 Hz, 1H), 7.70 (t, J = 7.6 Hz, 1H), 7.56 (d, J = 8.0 Hz, 1H), 7.49 (t, J = 1.6 Hz, 2H), 7.41 (s, 1H), 7.26 (d, J = 8.0 Hz, 1H), 6.96 (d, J = 2.0 Hz, 1H), 5.85 (s, 1H). ^{13}C-NMR (100MHz, DMSO-d_6): 176.2, 174.7, 160.8, 156.4, 146.8, 143.1, 138.6, 135.8, 134.2, 133.7, 130.4, 129.6, 124.3, 118.1, 97.6, 92.3. IR (KBr, cm^{-1}): 3316 (bw), 1687 (m), 1633 (s), 1575 (m), 1525 (s), 1475 (s), 1450 (w), 1325 (s), 1299 (w), 1253 (w), 1226 (s), 1166 (m), 1122 (w), 1019 (m), 955 (w), 937 (s), 886 (m), 860 (w), 782 (w), 763 (m), 702 (w), 674 (w), 595 (w). MS (ESI) m/z: 283.0279, m. p. 167 ºC.

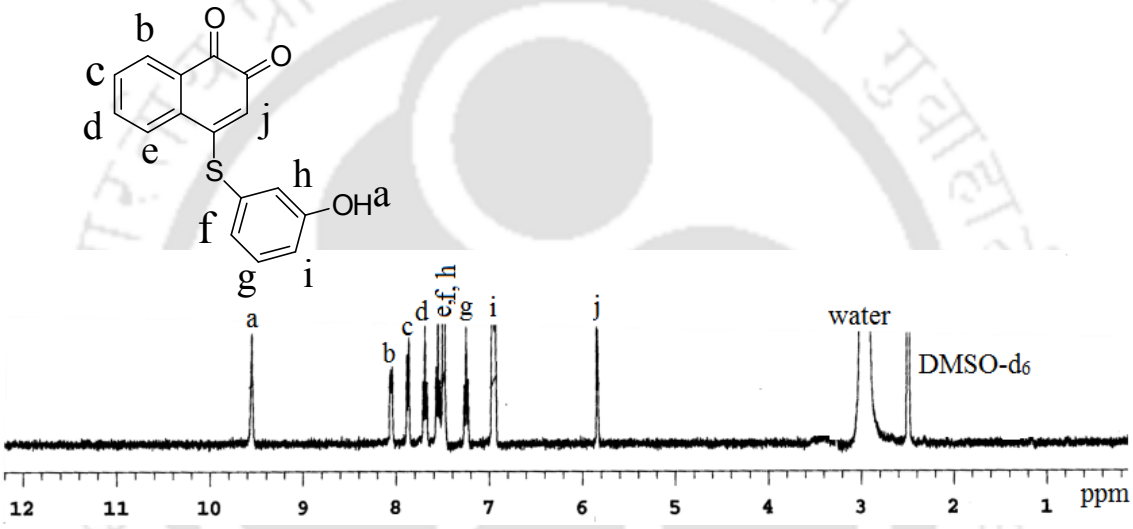

Figure 4.27: ^{1}H-NMR (400MHz, DMSO-d_6) spectra of **4.6**.

4-(4-Hydroxyphenylthio) naphthalene-1,2-dione (**4.7**)

To a well stirred solution of 1,2-naphthoquinone (0.31 g, 2 mmol) in methanol (20 mL) a solution(in methanol 5 mL) of 4-mercaptophenol (0.25 g, 2 mmol) was added drop wise. The reaction mixture was stirred at room temperature for 8 hrs. A red coloured precipitate of **4.4** was obtained. The precipitate was collected and dried in open air. Yield: 92%. ^{1}H-NMR (400 MHz, DMSO-d_6): 10.39 (s, 1H), 8.02 (d, J = 7.6 Hz, 1H), 7.94 (d, J = 7.6 Hz, 1H), 7.82 (t, J = 7.2 Hz, 1H), 7.70 (t, J = 8 Hz, 1H), 7.44 (d, J = 7.2 Hz, 2H), 6.98 (d, J = 6.8 Hz, 2H), 5.55 (s, 1H). ^{13}C-NMR (100 MHz, DMSO-d_6): 178.6, 175.8, 160.5, 160.1, 137.6, 135.2, 132.6, 131.5, 130.4, 128.6, 124.8, 120.5, 117.5, 113.9, 98.1, 97.9. MS (ESI) m/z: 283.05, m. p. 170 ºC.

TH-1303_09612216

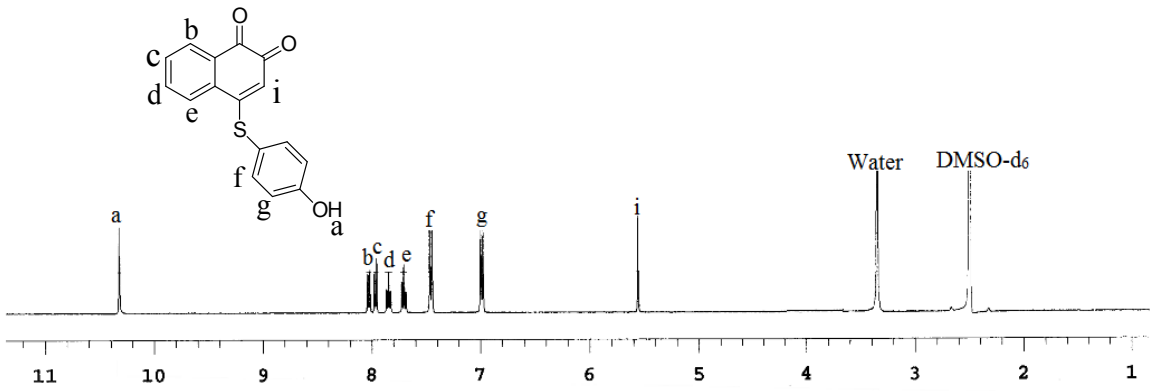

Figure 4.28: ^{1}H-NMR (400MHz, DMSO-d_6) spectra of **4.8**.

Crystal of anhydrous **4.4a** was obtained by slow evaporation of a solution of **4.4** in dry dimethylformamide. IR (KBr, cm^{-1}): 3696 (w), 3502 (bw), 3330 (w), 2967 (w), 2926 (w), 2851 (w), 1701 (w), 1632 (s), 1598 (s), 1577 (m), 1541 (w), 1496 (s), 1480 (m), 1449 (m), 1432 (w), 1345 (s), 1326 (s), 1290 (m), 1257 (m), 1220 (w), 1163 (w), 1115 (w) 1097 (w), 1020 (w), 936 (m), 851 (s), 836 (m), 763 (m), 706 (w), 649 (w), 582 (w).

Solvate **4.4**.$\mathbf{CH_3OH}$ (**4.4b**) was obtained by crystallisation of **4.4** from its solution in methanol. IR (KBr, cm^{-1}): 3494 (bw), 2973 (w), 2925 (w), 2674 (w), 1698 (m), 1635 (s), 1599 (w), 1578 (m), 1540 (s), 1524 (w), 1497 (w), 1450 (m), 1373 (w), 1326 (m), 1294 (w), 1282 (w), 1253 (w), 1172 (w), 1095 (w), 1009 (w) 973 (w), 936 (m), 857 (w), 833 (s), 800 (w), 765 (m), 707 (w), 669 (w), 648 (w), 528 (w).

Solvate **4.4**.$\mathbf{(CH_3)_2NCOCH_3}$ (**4.4c**) was obtained by slow evaporation of a solution of **4.4** in dimethylacetamide solvent. IR (KBr, cm^{-1}): 3463 (bw), 3163 (bw), 2924 (w), 1704 (w), 1637 (s), 1598 (m), 1577 (m), 1541 (m), 1496 (m), 1481 (m), 1481 (w), 1448 (w), 1373 (w), 1326 (m), 1290 (m), 1225 (w), 1226 (m), 1164 (w), 1097 (w), 1019 (w) 936 (m), 836 (m), 782 (w), 762 (m), 706 (w), 594 (w).

4.4.$\mathbf{H_2O}$ (**4.4d**) was obtained by slow evaporation of a solution of **4.4** in ethanol/water mixture. IR (KBr, cm^{-1}): 3541 (w), 3455 (w), 3172 (bw), 2924 (w), 1694 (w), 16358 (s), 1626 (s), 1599 (w), 1579 (s), 1536 (m), 1523 (m), 1496 (w), 1466 (w), 1435 (mw), 1328 (m), 1294 (m), 1257 (m), 1231 (w), 1172 (m), 974 (w), 973 (w), 936 (m), 854 (w), 838 (s), 801 (w), 768 (m), 708 (w), 668 (w), 648 (w), 530 (w).

References:

1. G. Cecchini, E. Maklashina, V. Yankovskaya, T. Iverson and M. S. Iwata, *FEBS Lett.* **2003**, 545, 31.

TH-1303_09612216

2. C. Roy, D. Lancaster, H. Michel, *Structure* **1997**, 5, 1339.
3. T. Hayashi, T. Miyahara, Y. Aoyama, M. Kobayshi and H. Ogoshi, *Pure and Appl. Chem.* **1994,** 66*,* 797.
4. T. Hayash, T. Miyahara, N. Koide, Y. Kato, H. Masuda, and H. Ogoshi, *J. Am. Chem. Soc.* **1997**, 119*,* 7281.
5. A. R. Katritzky, D. Fedoseyenko, P. P. Mohapatra and P. J. Steel, *Synthesis*, **2008**, 05*,* 777.
6. T. Steiner, B. Lutz, J. van der Maas, A. M. M. Schreurs, J. Kroon and M. Tamm, *Chem. Commun*., **1998**, 171.
7. R. P. Kashyap, D. Sun and W. H. Watson, *J. Chem. Crystallogr*., **1995**, 25, 339.
8. W. M. Singh and J. B. Baruah, *J. mol. Struct,* **2009**, 931, 82.
9. Y. Imai, T. Kinuta, K. Nagasaki, T. Harada, T. Sato, N. Tajima, Y. Sasaki, R. Kurodabd and Y.Matsubara, *CrystEngComm*, **2009**, 11, 1223.
10. A. I. Kitaigordoskii, *Molecular Crystals*; Nauka: Moscow, **1971**.
11. A. Burger and R. Ramberger, *Microchim. Acta*, **1979**, II, 259.
12. M. C. Etter, *Acc. Chem. Res.* **1990,** 23, 120.
13. J Bernstein, R. E. Davis, L. Shimoni, N. -L. Chang, *Angew. Chem. Int. Ed. Eng.* 1**995**, 34**,** 1555.
14. A. R. Kennedy, and F. R. N. Waterson, *Acta Crystallogr. Cryst. Struct. Commun.* **2003**, *C59,* 0613-o615.
15. G. A. Jeffrey, *An introduction to hydrogen bonding*; Oxford University Press: Oxford, U.K., **1997**.
16. G. R. Desiraju, T. Steiner, *The weak hydrogen bond in structural chemistry and biology*; Oxford University Press: Oxford, UK, **1999**.
17. M. Nishio, *Weak hydrogen bonds.* In *Encyclopedia of supramolecular chemistry* Atwood, J. L.; Steed, J. W. Eds.; Marcel Dekker Inc.: New York, USA, **2004**
18. J. Chen, J. Wang, J. Ulrich, Q. Yin and L. Xue, *Cryst. Growth Des.* **2008**, 8, 1490.
19. A. Bacchi, M. Carcelli, T. Chiodo, F. Mezzadri, F. Nestola and A. Rossi, *Cryst. Growth Des.* **2009**, 9, 3749.
20. F. C. Pigge, M. K. Dighe and N. P. Rath, *Cryst. Growth Des.* **2006**, 6, 2732.
21. A. Jacobs, N. L. Z. Masuku, L. R. Nassimbeni and J. H. Taljaard, *CrystEngComm*, **2008**, 10, 322.

TH-1303_09612216

22. R. Mondal, J.A. K. Howard, R. Banerjee, and G. R. Desiraju, *Cryst. Growth Des.* 2006, 6, 2507.
23. K. Kasugai, S. Hashimoto, K. Imai, A. Sakon, K. Fujii, H. Uekusa, N. Hayashi, and K. Kobayashi, *Cryst. Growth Des.* **2011**, 11, 4044.
24. K. Tanaka, K. Endo and Y. Aoyama, *Chem. Lett.*, **1999**, 887.
25. P. Nandhikonda, M. P. Begaye, Z. Cao and M. Heagy, *Chem. Commun.* **2009**, 4941.
26. V. Amendola, L. Fabbrizzi, F. Forti, M. Licchelli, C. Mangano, P. Pallavicini, A. Poggi, D. Sacchi and A. Taglieti, *Coord. Chem. Rev*. **2006**, 250, 273.
27. D. Astruc, E. Boisselier and C. Ornelas, *Chem. Rev.* **2010**, 110, 185.
28. M. Formica, V. Fusi, L. Giorgi, M. Micheloni, *Coord. Chem. Rev*. **2012**, 256, 170.
29. A. P. De Silva, H.Q.N. Gunartne, T. Gunnlaugsson, A. J. M. Huxley, C. P. McCoy, J. T. Rademacher and T. E. Rice, *Chem. Rev*. **1997**, 97 1515.
30. V. Amendola, L. Fabbrizzi, F. Forti, M. Licchelli, C. Mangano, P. Pallavicini, A. Poggi, D. Sacchi and A. Taglieti, *Coord. Chem. Rev*. **2006**, 250 273.
31. D. Astruc, E. Boisselier and C. Ornelas, *Chem. Rev*. **2010**, 110 1857.
32. J. Wu, W. Liu, J. Ge, H. Zhang and P. Wang, *Chem. Soc. Rev*. **2011**, 40 3483.
33. X. Chen, S. W. Nam, G. H. Kim, N. Song, Y. Jeong, I. Shin, S. K. Kim, J. Kim, S. Park and J. Yoon, *Chem. Commun*. **2010**, 46, 8953.
34. N. B. Sankaran, S. Banthia and A. Samanta, *Proc. Indian Acad. Sci*. **2002**, 114 539.
35. H. S. Jung, P. S. Kwon, J. W. Lee, J. I. Kim, C. S. Hong, J. W. Kim, S. H. Yan, J. Y. Lee, J. H. Lee, T. Joo and J. S. Kim, *J. Am. Chem. Soc*. **2009**, 131 2008.
36. Q. Zhao, R. F. Li, S. K. Xing, X. M. Liu, T. L. Hu, X. H. Bu, *Inorg. Chem*. **2011**, 50 10041.
37. X. Wan, S. Yao, H. Liu and Y. Yao, *J. Mater. Chem.* A1 **2013**, 10505.
38. S. Banthia and A. Samanta, *J. Phys. Chem B* **2006**, 110 6437.
39. Z. Liu, C. Zhang, X. Wang, W. He and Z. Guo, Org. Lett. **2012**, 14, 4378.
40. C. Gou, S. -H. Qin, H.-Q. Wu, Y. Wang and X.-Y. Liu, *Inorg. Chem. Commun*. **2011**, 14, 1622.
41. B. R. Jali, K. Masud and J. B. Baruah, *Polyhedron* **2013**, 51, 75.
42. S.-P. Wu, R.-Y. Huang and K.-J. Du, *Dalton Trans.* **2009**, 4735.

TH-1303_09612216

43. S. Murali and W. Rettig, *J. Phys. Chem. A* **2006**, 110, 28.

44. S. I. Druzhinin, V. A. Galievsky, T. Yoshihara and K. A. Zachariasse, *J. Phys. Chem.* A **2006**, 110, 12760.

45. J. S. Yang, K. L. Lian, C.Y. Li and M. Y. Chen, *J. Am. Chem. Soc*. **2007**, 129, 13183.

46. J. Dobkowski, J. Wójcik, W. Koźmiński, R. Kołos, J. Waluk, J. Michl, *J. Am. Chem. Soc.* **2002**, 124, 2406.

47. Z. R. Grabowski, K. Rotkiewicz and W. Rettig, *Chem. Rev*. **2003**, 103, 3899.

48. J. S. Yang, K. L. Lian, C.Y. Li and M. Y. Chen, *J. Am. Chem. Soc*. **2007**, 129, 13183.

49. J. Dey and S. K. Dogra, *J. Phys. Chem*. **1994**, 98, 3638.

50. Y.V. Il'ichev, W. Kühnle and K. A. Zachariasse, *J. Phys. Chem*. A **1998**, 102, 5670.

51. W. Schuddeboom, S. A. Jonker, J. M. Warman, U. Leinhos, W. Kuhnle and K. A. Zachariasse, *J. Phys. Chem*. **1992**, 96, 10809.

52. T. Yoshihara, S. I. Druzhinin and K. A. Zachariasse, *J. Am. Chem. Soc*. **2004**, 126, 8535.

53. S. Cogan, S. Zilberg and Y. Haas, *J. Am. Chem. Soc.* **2006**, 128, 3335.

54. Z. R. Grabowski, K. Rotkiewicz and W. Rettig, *Chem. Rev.* **2003**, 103, 3899.

55. K. Bhattacharyya and M. Chowdhury, *Chem. Rev.* **1993**, 93, 507.

56. S. K. Saha, P. Purkayastha and A. B. Das, *J. Photochem. Photobiol*. A **2008**, 195, 368.

57. M. H. Abraham, *Pure Appl. Chem.* **1993,** *65*, 2503.

58. A. A. Oliferenko, P. V. Oliferenko, J. G. Huddleston, R. D. Rogers, V. A. Palyulin, N. S. Zefirov and A. R. Katritzky, *J. Chem. Inf. Comput. Sci*. **2004**, *44*, 1042.

59. V. Sasirekha, M. Umadevi and V. Ramakrishna, *Spectrochem. Acta* A, **2008**, 69, 148.

60. H. A. Benesi and J. H. Hildebrand, *J.* Am. Chem. Soc. **1949**, 71, 2703.

61. M. H. V. Benthem and G. D. Gillispie, *J. Phys*. *Chem.* **1984,** *88*, 2954.

62. C. S. Cronan, W. J. Walker and P. R. Bloom, *Nature* **1986**, 324, 140.

63. G. Berthon, *Coord. Chem. Rev*. **2002**, 228, 319.

TH-1303_09612216

64. D. P. Perl, D. C. Gajdusek, R. M. Garruto, R. T. Yanagihara and f. C. J. Gibbs, *Science* **1982**, 217, 1053.

65. P. D. Darbre, *J. Inorg. Biochem.* **2005**, 99, 1912.

66. S. Kim, J. Y. Noh, K.Y. Kim, J. H. Kim, H.K. Kang, S-W, Nam, S. H. Kim, C. Kim and J. Kim, *Inorg. Chem*. **2012**, 51, 3597.

67. W. Zhong, *Anal. Bioanal Chem*. **2009**, 394, 47.

68. A. Banerjee, A. Sahana, S. Das, S. Lohar, S. Guha, B. Sarkar, S. K. Mukhopadhyay, A. K. Mukherjee and D. Das, *Analyst* **2012**, 137, 2166.

69. T. Kamimura, T. Nishiumi, M. Higuchi and K. Yamaoto, *Electrochem. Solid-State Lett*. **2004**, 7, H9-H11.

70. S.-P. Wu, R. -Y. Huang and K. -J, *Dalton Trans*, **2009**, 4735.

71. K. K. Upadhyay and A. Kumar, *Org. Biomol. Chem*. **2010**, 8, 4892.

72. D. T. Quang and J. S. Kim, *Chem. Rev.* **2010**, 110, 6280.

73. H. Kobayashi, M. Ogawa, R. Alford, P. L. Choyke and Y. Urano, *Chem. Rev.* **2010**, 110, 2620.

74. (a) N. E. Mackenzie, S. Surendrakumar, R. H. Thomson, H. J. Cowe and P. J. Cox, J. Chem. Soc. Perkin Trans1, **1986**, 2233 (b) S. Ukai and K. Hirose, Chem. Pharm. Bull., **1968**, 16, 606.

TH-1303_09612216

Chapter 5

Cytotoxicity and protein binding studies of naphthoquinone derivatives

Serum albumins are the most abundant proteins in the circulatory system of human and they play important roles in transport and deposition of endogenous and exogenous compounds in the human body.[1-2] Human serum albumin is the major protein in blood plasma and plays significant role in transporting several hydrophobic components such as fatty acids, bilirubin, steroids, hormones and drugs by binding them in different pockets protein structures.[3-4] It has an approximate molecular weight 66.5 kD. Bovine serum albumin with similar molecular weight is abundantly found in blood plasma and is often considered as transport proteins. These two proteins belong to most widely studied category of proteins.[5-8] Human serum albumin (HSA) and Bovine serum albumin (BSA) function as carriers for numerous exogenous and endogenous compounds in the body.[1-11] The primary structure of HSA consists of a helical monomer containing three homologous domains (I-III), each is composed of two subdomains called A and B subdomains (Figure 5.1a). Crystallographic studies have revealed that hemin is bound within a narrow D-shaped hydrophobic cavity in subdomain IB with axial coordination of the tyrosine residue Tyr-161 to the central ferric ion and electrostatic interactions between the porphyrin propionates and a triad of basic amino acid residues (Arg-114, His-146, and Lys-190).[12] In terms of the general hydrophilicity of this R-helical heme pocket, subdomain IB of HSA potentially has similar hydrophobic features to the heme binding site of hemoglobin or myoglobin. When HSA-hemin is reduced to form a ferrous complex, it is rapidly oxidized by O_2 at low temperature (-0 °C). This is due to fact that HSA lacks the proximal histidine which enables the prosthetic heme group to bind O_2 and serves to regulate the O_2 binding affinity. Whereas, the primary structure of BSA is composed of 583 amino acid residues and characterized by low tryptophan content along with a high content of cystine, stabilizing a series of nine loops. The secondary structure of serum albumins has 67 % of helix with six turns and 17 disulfide bridges. The tertiary structure is composed of three domains I, II, and III, and each domain is constituted of two subdomains A and B. BSA displays approximately 80 % sequence homology and a

TH-1303_09612216

repeating pattern of disulfides, which are strictly conserved. BSA contains two tryptophan residues, Trp-134 and Trp-213, of which former is located in hydrophilic subdomain IB and latter in hydrophobic subdomain IIA.[13-15]

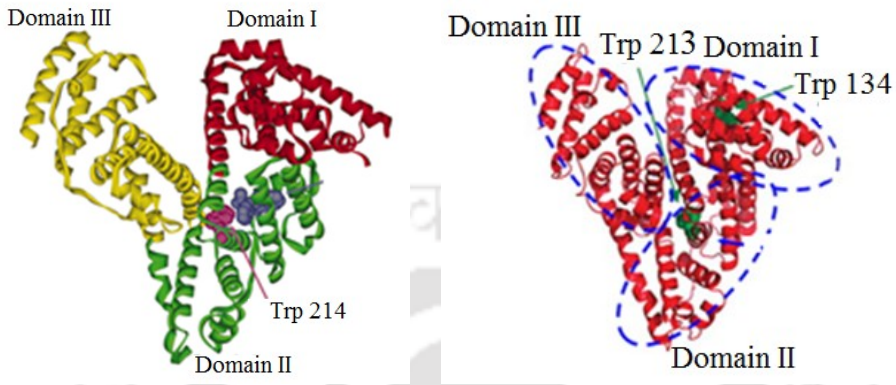

Figure 5.1: Structures of Human serum albumin (HSA) and Bovine serum albumin (BSA).

There are extensive studies on interactions of small molecules with BSA and HSA. Quinone binding with BSA and HAS has provide an understanding on the fluorescence mechanism operative in the interaction of quinines with biological systems. Such study provides information on specific binding action and their utility as probes. Example for quercetin, a quinone derivative, the binding of quercetin to BSA is quantitatively investigated by fluorescence spectroscopy.

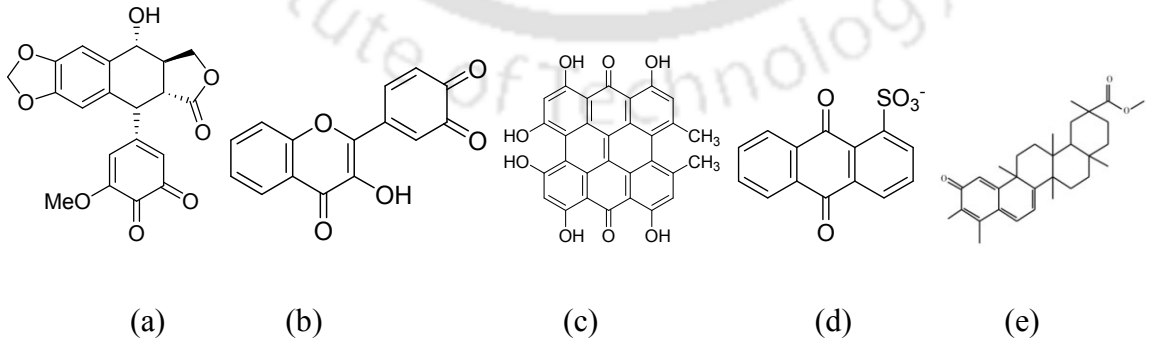

Figure 5.2: Some examples of quinone derivatives which interacts with BSA.

TH-1303_09612216

Fluorescence quenching of tryptophan fluorescence emission of BSA by quercetin suggest its binding occurs in the IIA domain.[16] It is observed from resonance Raman and surface-enhanced Raman spectroscopy that hypericin binds to the subdomain IIA of BSA.[17] From fluorescence and docking analysis, it was observed that 9,10-anthraquinone-1-sulfonate binds to a hydrophobic site in subdomain IIA of HSA.[18] Existing literature suggests that observed binding of BSA and HSA with either a carboxylic acid or a pyridine unit tethered to a quinone are not generalized. Hence, we have taken up studies on interactions of naphthoquinone derivatives (Figure 5.3) with serum albumin proteins.

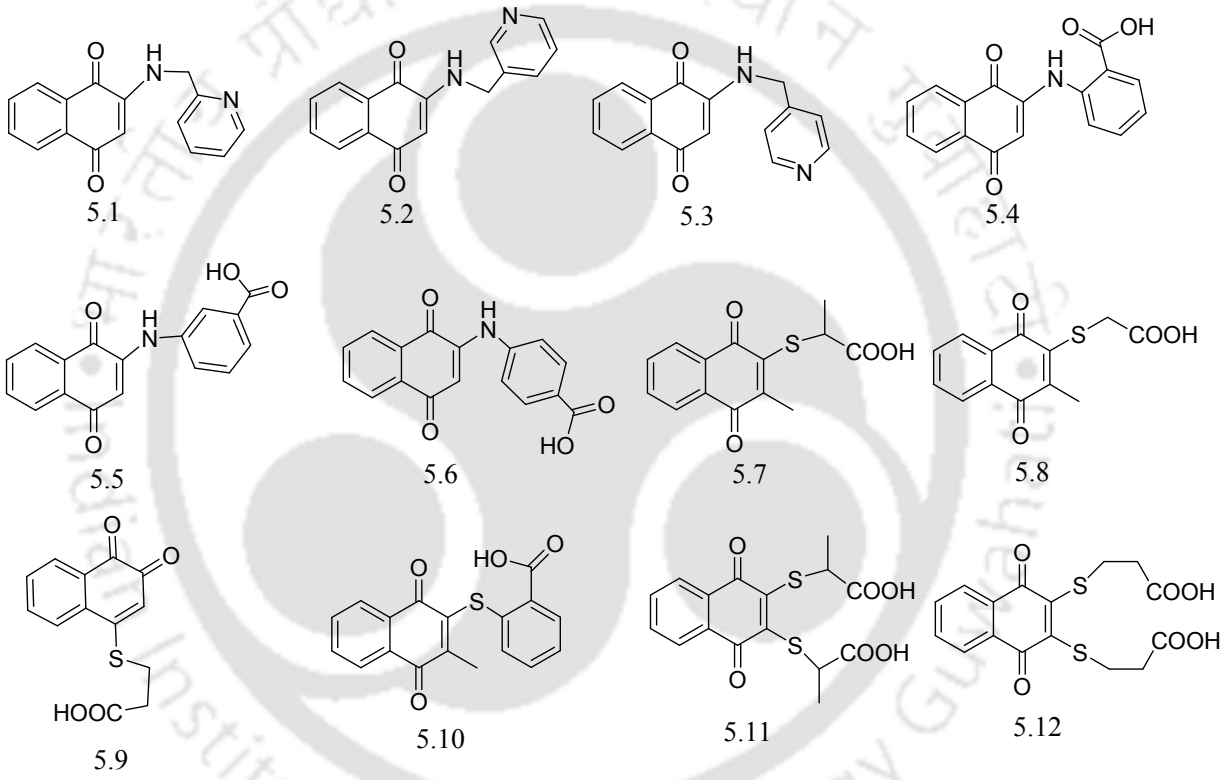

Figure 5.3: Structure of naphthoquinone derivatives.

*5.2: Fluorescence study of BSA and HSA with compounds **5.1-5.12***

Knowledge about the structure of proteins has profited their utility as biomolecules participating in chemical reactions and different biological actions. Molecular interactions of proteins interacting with foreign molecules are often monitored by using optical techniques, namely absorption and emission spectroscopy. These methods are sensitive

TH-1303_09612216

and relatively easy to use. Fluorescence emission spectroscopy is a valuable technique to study binding of different compounds to proteins. Significantly fluorescence spectroscopy is a powerful method to study molecular interactions involving proteins because it is highly sensitive, swift and simple. It has advantages over conventional methods employed for studying drug-protein binding such as affinity or size exclusion chromatography, equilibrium dialysis, ultrafiltration, and ultracentrifugation. These conventional methods suffer from either low sensitivity or lengthy operation time or both. In addition, these methods normally require protein in concentrations far exceeding dissociation constants for the drug-protein complex under investigation. By measuring fluorescence quenching of both BSA and HSA, accessibility of quenchers to fluorophore groups of BSA and HSA can be estimated. This information can help us predict binding mechanisms of drugs to protein molecules. Qualitative analysis of the binding of chemical compounds **5.1-5.12** to BSA and HSA can be detected by examining their fluorescence spectra. Generally, fluorescence of a protein is caused by three intrinsic fluorophore present in the protein, i.e. (1) tryptophan, (2) tyrosine and (3) phenylalanine residues. Actually, intrinsic fluorescence of many proteins is mainly contributed by tryptophan alone. Compounds **5.1-5.12** do not have overlapping fluorescence emission at 352 nm where fluorescence emissions of BSA proteins change. Fluorescence spectrum of BSA presents strong emission maximum at 352 nm, when excited at 295 nm in tris buffer. Excitation wavelength 295 nm is chosen to avoid the contribution from the tyrosine residues in proteins. Gradual addition of compounds to BSA protein leads to a significant change occurs. Fluorescence intensity decreases with increase in concentration of compounds with small blue shift occurs in all cases indicating binding of compounds to BSA. Illustrative cases of fluorescence changes are shown in figure 5.4a-c. Fluorescence spectrum shifts due to change in polarity of the environment, however the change in fluorescence intensity of the flexible molecules depends not the polarity of the medium, but also on the constraint provided by the media.[19] Increasing concentrations of compounds **5.1-5.3** caused a progressive reduction in fluorescence intensity of BSA accompanied by blue shift of 15 nm, 9 nm, and 16 nm upon interactions with compounds **5.1**, **5.2** and **5.3** respectively. On the other hand a similar trend is observed in case of other compounds. The fluorescence intensity of HSA decreases with increase in concentration of added quinone compounds with a small blue shift occurs in all cases

TH-1303_09612216

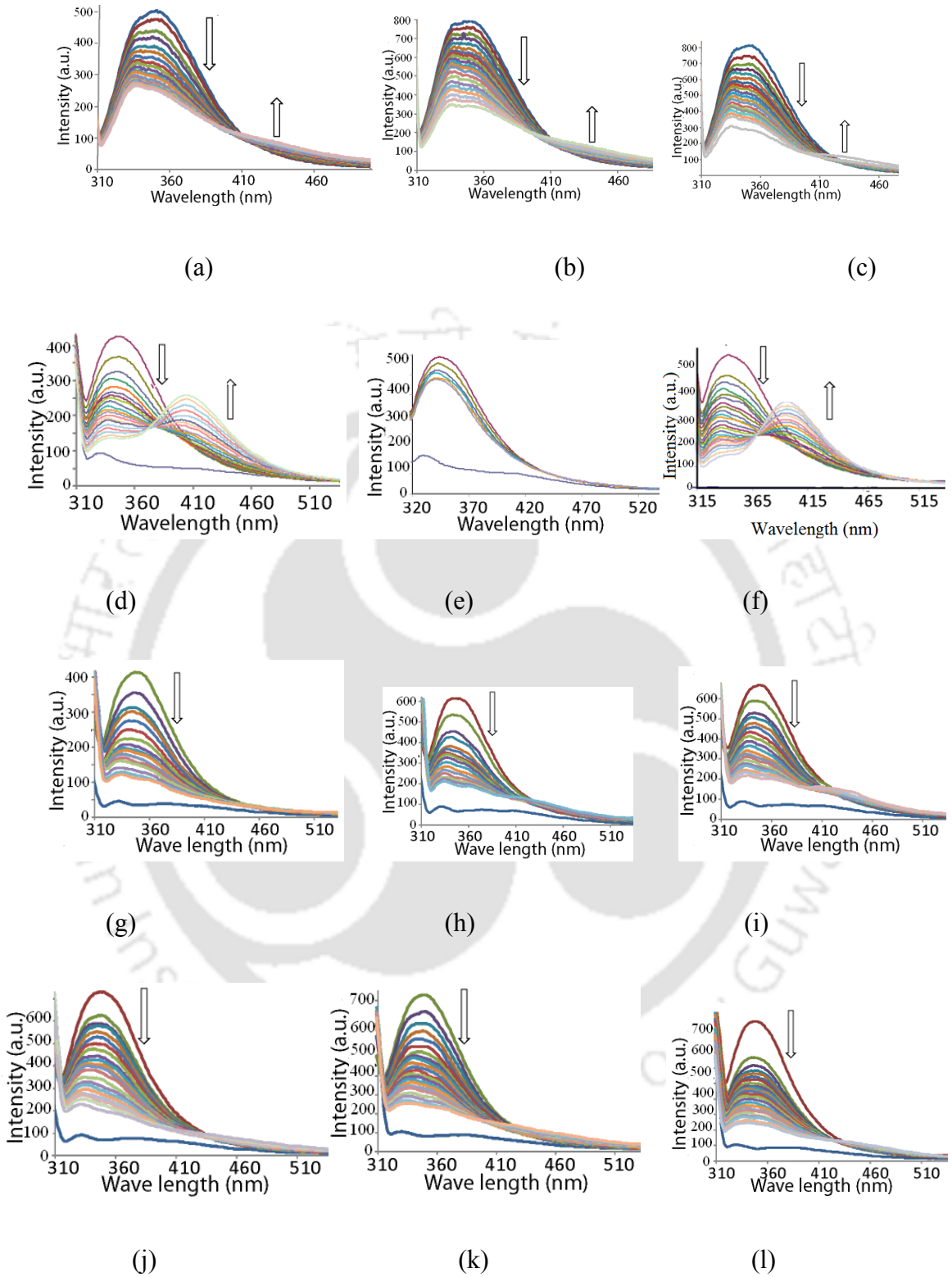

Figure 5.4: Changes in fluorescence emission of BSA with compounds (a) **5.1** (b) **5.2** (c) **5.3** (d) **5.4**, (e) **5.5** (f) **5.6** (g) **5.7** (h) **5.8** (i) **5.9** (j) **5.10** (k) **5.11** and (l) **5.12** (2 µL BSA, in 3 mL tris buffer pH 7.4, to which 10^{-5}M quinoidal compound in 5µL was added)

TH-1303_09612216

indicating binding of all compounds to BSA as shown in figure 5.4 d-l. Increasing concentrations of compounds caused a progressive reduction in fluorescence intensity accompanied by blue shifts in absorption maxima of BSA by 15, 18, 13, 16, 16, 14, 2 and 11 nm upon complexation with compounds **5.4-5.12** except **5.5** respectively. This blue shift of emission peaks along with quenching in fluorescence intensities indicate that interactions of compounds **5.1-5.12** with BSA. Stokes shift calculated from differences in absorption and emission maximum of the samples with and without addition of compounds **5.1-2.12** with BSA are shown in tabular form in table 5.1.

Table 5.1: Fluorescence emission data for compounds **5.1-5.12** with addition of BSA before and after.

BSA/Compound	λ_{abs} (nm)	λ_{ems} (nm)	Stoke shifts (nm)
BSA		352	57
BSA + 5.1		337	42
BSA + 5.2		343	48
BSA + 5.3		336	41
BSA + 5.4		337	42
BSA + 5.5		352	57
BSA + 5.6		334	39
BSA + 5.7	295	335	40
BSA + 5.8		332	37
BSA + 5.9		332	37
BSA + 5.10		330	35
BSA + 5.11		346	51
BSA + 5.12		337	42

Since the emission at 295 nm originates from tryptophan residue in BSA protein, the changes with different Stokes shift infers that BSA protein interacted with different naphthoquinone derivatives in a similar fashions. On the other hand functional group variations have not drastically influence these shifts showing a lesser role in binding interactions. The pyridine containing compounds and carboxylic acid containing compounds effected fluorescence change of BSA in similar manner, suggests that proton transfer between carboxylic acid and tryptophan ratio does not necessarily occur. Tryptophan fluorescence emission was widely used as a tool to monitor changes in protein structures and to make inferences regarding local structure and dynamics.[20-22] There are two tryptophans in native BSA; the Trp-134 is present in domain I of the eighth helix of D129- R144. Trp-213 is located in domain II, in the second helix of E206-F221

TH-1303_09612216

and is buried inside protein structure[23-25] Intrinsic fluorescence of BSA is mainly due to tryptophan residues (Trp-134 and 213) in the hydrophobic cavity of domain I and II. Similarly, HSA shows strong emission maximum at 336 nm, when excited at 290 nm. Gradual addition of compounds **5.1-5.12** to solution of HSA in tris buffer leads to a significant change in emission intensity. The fluorescence emission intensity decreases with increase in concentration of all compounds with small red shift and in a few cases

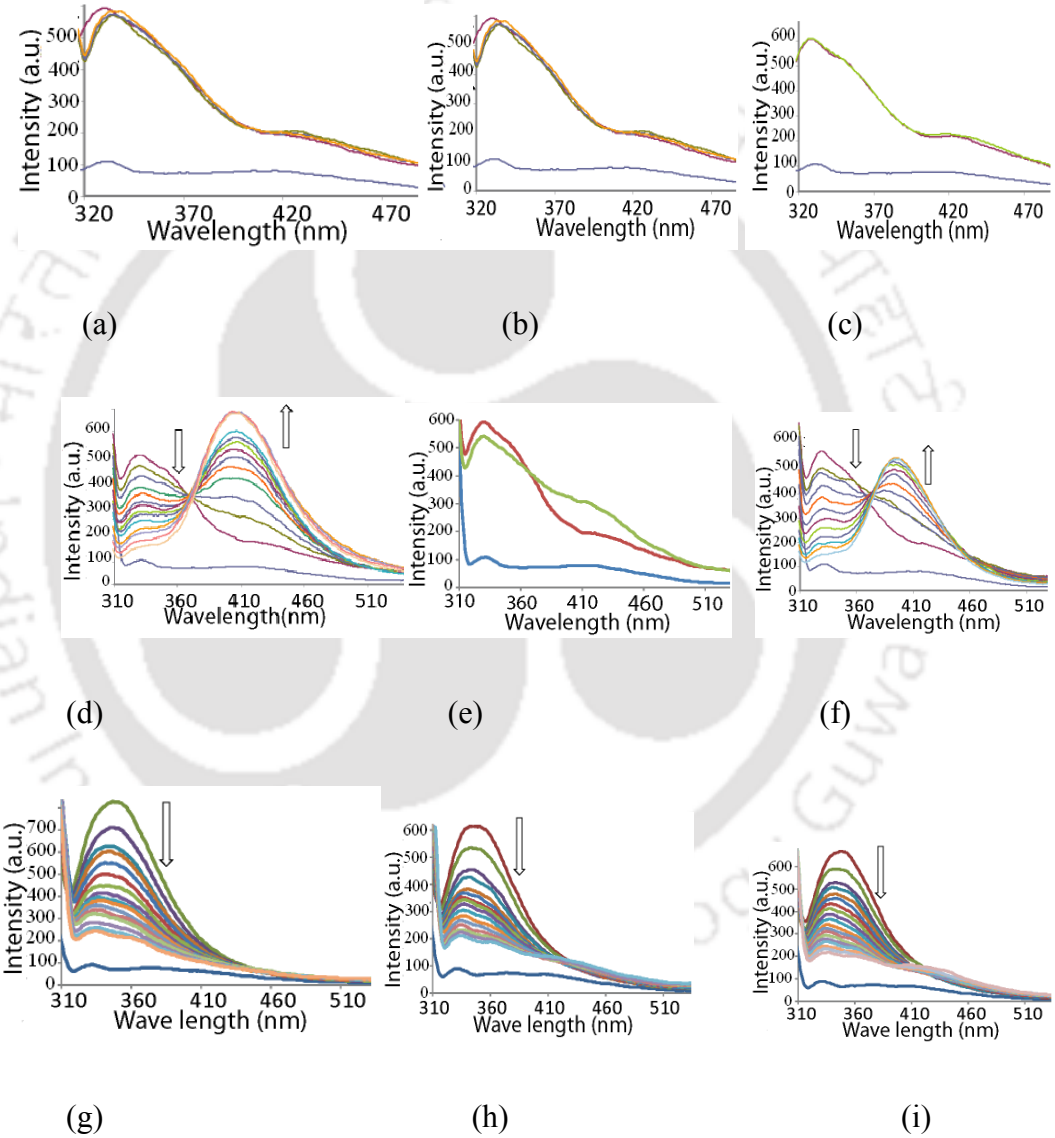

TH-1303_09612216

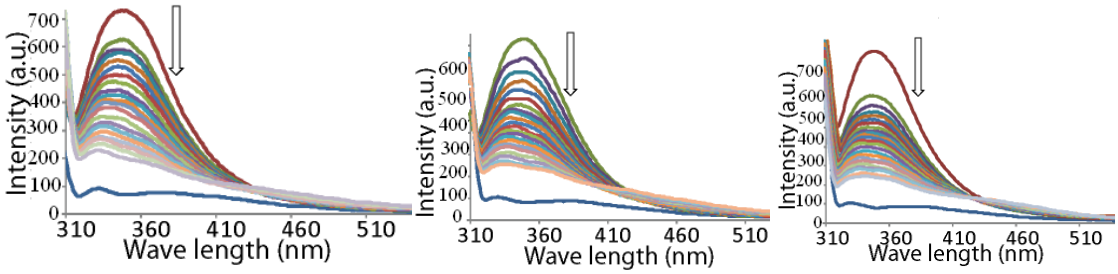

(j) (k) (l)

Figure 5.5: Changes in fluorescence spectra of HSA with compounds (a) **5.1**, (b) **5.2** (c) **5.3** (d) **5.4** (e) **5.5** (f) **5.6** (g) **5.7** (h) **5.8** (i) **5.9** (j) **5.10** (k) **5.11** and (l) **5.12** (2 µL HSA, in 3 mL tris buffer pH 7.4, to which solution of corresponding 10^{-5}M quinoidal compound in DMA were added in 5µL in each aliquot).

there are no detectble changes. For example compunds **5.1-5.3** did not cause significant cahnge in emission of HSA, so is the case with compound **5.5**. This indicated that binding of HSA to napthoquinone derivatives are selective. Fluorescence changes in each case is shown in figure 5.5a-l. Increasing concentrations of these quinoidal compounds caused progressive reductions in fluorescence intensity. The position of emission also changes by very small red shift as compared to the emission peak of parent solution of HSA. This red shift of emission maximum along with reduction in fluorescence intensity indicated that the interactions of HSA with compounds change the environment of tryptophan. The structure of hydrophobic subdomain, where tryptophan does not make sense and the segment of polypeptide changed its conformation to a more extended state after addition of ligands.[26] Shifts in position of emission as well as intensity of tryptophan residues of HSA protein are generally observed upon unfolding. Tryptophan emission of a native protein can be greater or smaller than the emission of free tryptophan in aqueous solution. The emission maximum is usually shifted from shorter to longer wavelengths upon protein unfolding, which corresponds to the fluorescence emission maximum of tryptophan in an aqueous solution. Fluorescence emission maximum of tryptophan of proteins and emission spectra of free tryptophan changes. Emission spectrum of tryptophan HSA reflect the average environment of the tryptophan. Conformational chnages, subunit association, substrate binding or denaturation causes changes in the emission spectra of tryptophan.[27-28] The Stokes shift of observed for the HSA and after

TH-1303_09612216

addition of compounds **5.1-5.12** to HSA are shown in table 5.2. Occurence of new emission peaks at longer wavelength is attributed to denaturation. Accordingly changes in the fluorescence spectra of HSA upon addition of **5.4** and **5.6** suggest that the interactions of **5.4** and **5.6** with HSA modified the environment of tryptophan, which denature HSA and drastically changed the emission.

Table 5.2: Fluorescence emissions of HSA with compounds **5.1-5.12** .

HSA/Compound	λ_{abs} (nm)	λ_{ems} (nm)	Stoke shifts (nm)
HSA		336	46
HSA + 5.1		336	46
HSA + 5.2		336	46
HSA + 5.3		336	46
HSA + 5.4		330	35
HSA + 5.5		336	46
HSA + 5.6	290	329	39
HSA + 5.7		335	40
HSA + 5.8		332	37
HSA + 5.9		332	37
HSA + 5.10		330	35
HSA + 5.11		346	51
HSA + 5.12		33	42

Shift in position of emissions and reduction in fluorescence intensities show that there have been changes in the tryptophan environment. These results are supportive of earlier observations showing that structure of hydrophobic subdomain of tryptophan is flexible.[29] Thus, addition of quinoidal compounds interacting through supramolecular interactions lead to a conformational change in the segment of polypeptide of protein structure. Denaturation of proteins usually results in increased exposure of the protein chromophores (tryptophan, tyrosine, and phenylalanine residues) to water. This results in change in their fluorescence characteristics. Significant change occurs in the fluorescence behaviour of tryptophan on denaturation which usually shifts emission towards longer wavelengths.[30] To understand the binding interaction and the type of complex formed between the compounds and the protein the binding constant values were determined from the fluorescence emission data by using Benesi-Hildebrand equation[31] The BSA binding constants with the compounds **5.1-5.12** are listed in table 5.3.

TH-1303_09612216

Table 5.3: Binding constants and fluorescence anisotropies of BSA and HSA with copmounds **5.1-5.12**.

Compound No.	K × 10^3 (M^{-1}) with BSA	K ×10^3 (M^{-1}) with HSA	Anisotropy with BSA[a]	Anisotropy with HSA[b]
5.1	11.276	c	0.162	d
5.2	9.04 4	c	0.144	d
5.3	26.874	c	0.170	d
5.4	7.77 6	97.918	0.371	0.596
5.5	3.97 2	c	0.267	d
5.6	1460.813	14.959	0.879	0.297
5.7	14.956	20.680	0.144	0.086
5.8	2364 .185	38.003	0.083	0.101
5.9	35.042	21.427	0.072	0.089
5.10	6.449	1019.707	0.109	0.134
5.11	103.392	7.592	0.077	0.069
5.12	15.253	25.615	0.098	0.099

[a]Anisotropy for BSA = 0.05203. [b] Anisotropy for HSA = 0.0388. [c] Did not change the fluorescence of HSA, hence not determined. [d]No change in fluorescence of HSA by the substrates hence anisotropies were not measured.

The relative magnitude of the BSA binding constants with different quinoidal compounds are **5.8** > **5.6** > **5.11** > **5.9** > **5.3** > **5.12** > **5.7** > **5.1** > **5.2** > **5.4** > **5.10** > **5.5**. Binding constants of BSA with compound **5.8** and **5.6** are exceptionally high. On the other hand, compound **5.5** has the least binding constant with BSA. Besides, compound **5.8** has ~594 times and **5.6** has ~367 times higher binding constant with respect to **5.5**. Thus, it may be concluded that these two compounds are selectively recognised by BSA. For HSA binding constants are in the order **5.10** > **5.4** > **5.8** > **5.12** > **5.9** > **5.7** > **5.6** > **5.11**. Compound **5.10** showed relatively high binding constant with HSA. For comparison, binding constant of HSA with compound **5.10** was 134 times higher than the HSA binding constant with compound **5.11**. Compound **5.5** did not change fluorescence emission of a solution of HSA, suggesting no binding of HSA with this compound. From these binding constant experiments it is observed that BSA binds with three structural isomers **5.1-5.3** and magnitude of BSA binding constants with them followed the order **5.3** > **5.1** > **5.2**. On the other hand, HSA does not bind to these three isomers. Binding of BSA with compounds **5.1-5.3** are due to supramolecular interactions to recognise these molecules. No binding observed for the HSA with **5.1-5.3**, but their weak binding with BSA, may be understood from the location of the tryptophan residues present in BSA or HSA. BSA has two tryptophan residues TRP-134 and TRP-213. These two residues are

TH-1303_09612216

responsible for fluorescence emission of BSA. In BSA the TRP-134 is located in a well exposed part of the protein structure and the domain in which the TRP-213 residue is located is well beneath the protein structure. On the other hand, the HSA has one tryptophan residue, namely the TRP-213 residue. This residue is located in the hydrophobic pocket of HSA; it is buried inside the protein structure. Difference in binding with HSA compared to that of BSA by compounds **5.1**-**5.3** and **5.5** meant that these molecules has specific interactions at the well exposed TRP-213 residue of the BSA. In comparison to other compounds changes in the intensity of the fluorescence emission shown by **5.1**-**5.3** and **5.5** were also less. Alternatively, these four compounds affected the fluorescence of TRP-134 without affecting the fluorescence of TRP-213 residue of BSA. To gain more information about compounds-BSA or HSA protein interactions, we performed steady-state fluorescence anisotropy measurements of the BSA and HSA in either the absence or presence of the all compounds. All anisotropy values of the proteins in the absence or presence of compounds are the mean values of their individual determinations.

$$r = (I_{VV}\text{-}GI_{VH}/I_{VV}+2GI_{VH}) \qquad \text{Equation } \mathbf{5.1}$$

Degree (*r)* of anisotropy in the tryptophan fluorescence of the proteins was calculated using equation 5.1, at peak of the protein fluorescence spectrum, where I_{VV} and I_{VH} are the fluorescence intensities of the emitted light polarized parallel and perpendicular to the excited light, respectively, and $G = I_{VH}/I_{HH}$ is the instrumental grating factor. Increase in anisotropy values of the BSA proteins in the presence of ligands support their ligand binding are shown in (Table 5.3). BSA and HSA are globular proteins.[32] Shape of a globular protein can change on substrate binding or by denaturation. Relative change in globular protein structure caused by a substrate can be examined by measuring fluorescence anisotropy.[33] It is observed that the fluorescence anisotropy of the substrate bound BSA or HSA by each substrate **5.1**-**5.12** are different, the values are listed in table 5.3. Fluorescence anisotropy value for native state of BSA was found to be close to zero.[34-35] From table 5.3 it is clear that the highest anisotropy of BSA is obtained in case of BSA interacting with compound **5.6**. From anisotropy obtained from HSA interaction, it was shown that the highest anisotropy value arose on interaction of HSA with compound **5.4**. Interaction of BSA or HSA with compound **5.9** shows small but similar anisotropic values as that of BSA or HSA respectively. It suggests that **5.9** caused small

TH-1303_09612216

deformation on the globular structures of BSA or HSA. A docking experiment on compound **5.3** shows that it is held inside the hydrophobic pocket of BSA *via* N-H···O interactions of Val-481 and Ser-453

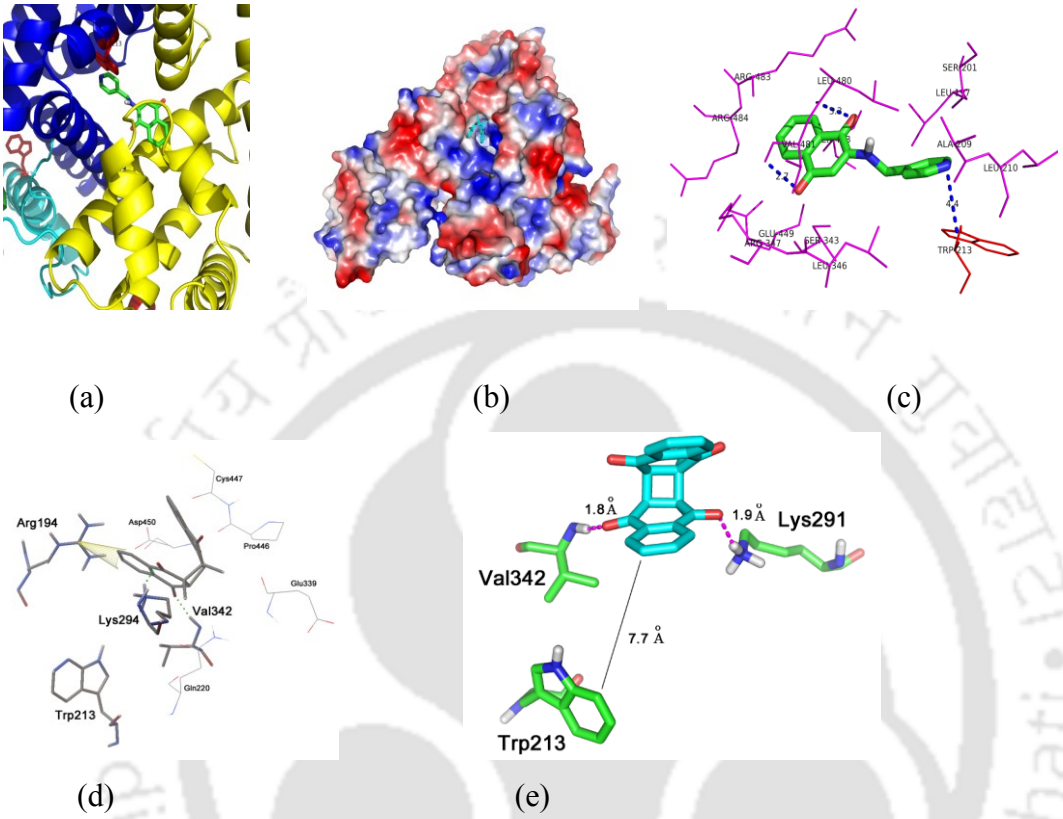

Figure 5.6: Molecular docking analysis showing (a) Compound **5.3** inside the hydrophobic pocket of BSA. (b) Molecule of bmq inside hydrophobic pocket of BSA, (c) Hydrogen bonding interactions of compound **5.3**. (d) Hydrogen bond interactions of dmq with amino acid residues of BSA protein. (e) Interactions of dmq with BSA.

as shown in figure 5.6, and docking analysis BSA with 2+2 cycloadduct of 2-methyl-1,4-naphthoquinone, it is observed that, it is held inside the hydrophobic pocket of BSA *via* N-H···O interactions of Val-342 (N-H···O, 1.8 Å) and Lys-291 (N-H···O, 1.9 Å) residues of BSA with two carbonyl groups on one ring of the naphthoquinone and the TRP-213 is located in the near vicinity of the naphthoquinone at a distance 7 Å to cause fluorescence quenching of BSA through space interactions. This also supports that intrinsic acidity or basicity associated with naphthoquinone derivatives is due to carboxylic acid or pyridine functionality do not contribute directly to the fluorescence quenching of BSA but

TH-1303_09612216

effective binding of these functional groups with different residues in the BSA causes the differences in fluorescence emissions.

5.2.1: Fluorescence lifetime study

There are large numbers of studies devoted to measurement of fluorescence lifetimes of BSA and HSA under different conditions.[36-40] Fluorescence emission decay profiles of BSA at 352 nm showed two different decay exponentials; one has lifetime 0.12 ± 0.2 ns (τ^1) contributed 21 % of total fluorescence; the remaining fluorescence emission has a life time 5.58 ± 0.2 ns (τ^2). Such decay profiles corresponded to characteristic decay profile of the tryptophan residue.[41] So changes in fluorescence lifetimes on addition of naphthoquinone derivatives occur from interaction of tryptophan residue of BSA. Observed fluorescence life times are listed in table 5.4. It was observed that fluorescence lifetimes of BSA nominally decreased by interactions with compounds **5.1-5.3**. On the other hand, the presence of carboxylic acid derivatives **5.4-5.6** significantly affected the fluorescence lifetimes of BSA. The extent of changes in decay profiles suggested distingishable interactions with proteins of these two classes with quinoidal compounds. Similar changes were observed in other compounds which binds to BSA.[42-43] Differences between these two classes of compounds are obvious from their functional groups; carboxylic acids have strong acid-base type of interactions with tryptophan, whereas nitrogen atom of pyridine derivatives interacted via weak hydrogen bonds of N-H bond of tryptophan residue.We observe three lifetimes for HSA as best fit decay profile is obtained from three exponential plots rather than the plots of two exponential functions. While interactions of compounds **5.4** and **5.6** with HSA changes these life times significantly. Drastic change in first lifetime (τ^1) suggests strong interactions of tryptophan residue of HSA with quinoidal compounds. This occurs as this lifetime is characteristic of a free tryptophan.[44-45] Nitrogen heterocyclic containing quinoidal compounds bind to BSA only, while the carboxylic acid containing quinoidal compounds **5.4-5.6** showed differences in selectivity towards binding to BSA or HSA. Since several naphthoquinone derivatives studied here have carboxylic acid as functional group. It was essential to compare the binding of serum albumin proteins to related carboxylic acids.

TH-1303_09612216

Table 5.4: Flourescence lifetime of BSA with compounds **5.1-5.6** and HSA with **5.4-5.6**

Samples	λ_{em} (nm)	τ (ns)/ (f %)	χ^2
BSA[a]	352	τ^1 = 0.12 (21.07); τ^2=5.58 (78.93)	1.096
BSA+ **5.1**	337	τ^1=0.11 (26.12); τ^2=5.36 (73.88)	1.076
BSA+ **5.2**	343	τ^1=0.09 (32.94); τ^2=5.28 (67.06)	1.031
BSA+ **5.3**	336	τ^1=0.07 (38.20); τ^2=5.14 (61.80)	1.024
BSA+ **5.4**	337	τ^1 = 0.69 (34.53); τ^2=7.25 (65.47)	1.063
BSA+ **5.5**	352	τ^1 = 0.44 (32.32); τ^2 = 4.40 (67.38)	1.060
BSA+ **5.6**	334	τ^1 = 0.46 (44.62); τ^2 = 4.42(55.38)	1.016
HSA[b]	332	τ^1 = 0.51 (27.67); τ^2 = 1.38 (16.32); τ^3 = 4.86 (56.01)	1.046
HSA+ **5.4**	406	τ^1 = 0.03 (1.32); τ^2 = 0.68 (26.37); τ^3 = 4.88 (72.31)	1.069
HSA+ **5.6**	396	τ^1 = 0.54 (8.64); τ^2 = 0.55 (41.11); τ^3= 3.10 (50.24)	1.038

[a] Data for BSA(14 μM) in buffer (20 mM Tris, 160 mM NaCl, 50 μM $ZnSO_4$, pH 7.4) with compounds **5.1-5.6** concentration 41 *n*M in each cases in presence/ absence of compounds. [b] Data for HSA(14 μM, 3 mL) in buffer (20 mM Tris, 160 mM NaCl, 50 μM $ZnSO_4$, pH 7.4) with compound **5.4** and **5.6** concentration 42 μM in each cases in presence/ absence of compounds.

It is also a known fact that the long-chain carboxylic acids interact with BSA or HSA and their interactions increase with the length of the attached hydrophobic chain.[45] However, there is no comparative study on interactions of serum albumin proteins with hydroxybenzoic (**5.13-5.14**) or mercaptobenzoic acids (**5.15-5.16**). Thus, we studied the interactions of BSA and HSA with positional isomers of hydroxybenzoic and mercaptobenzoic acids **5.13-5.16** as shown in figure 5.7.

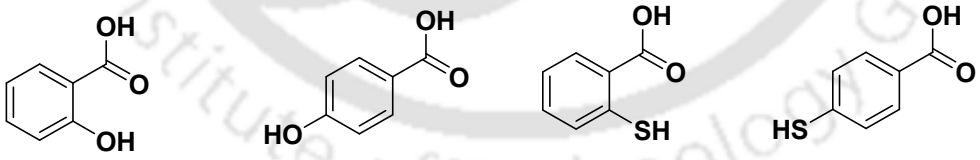

5.13 5.14 5.15 5.16

Figure 5.7: Positional isomers of hydroxybenzoic acid (**5.13-5.14**) and mercaptobenzoic acid (**5.15-5.16**).

Changes in fluorescence emission of HSA and BSA by these compounds were investigated and changes in each case are shown in figure 5.8. Changes in fluorescence emission caused by compounds **5.13-5.16** on the emission spectra of HSA did not follow a predictable trend based on the orientations or nature of the functional groups. We

TH-1303_09612216

observed that compound **5.13** interacted with BSA and caused quenching of fluorescence at 352 nm without generating new emission peak.

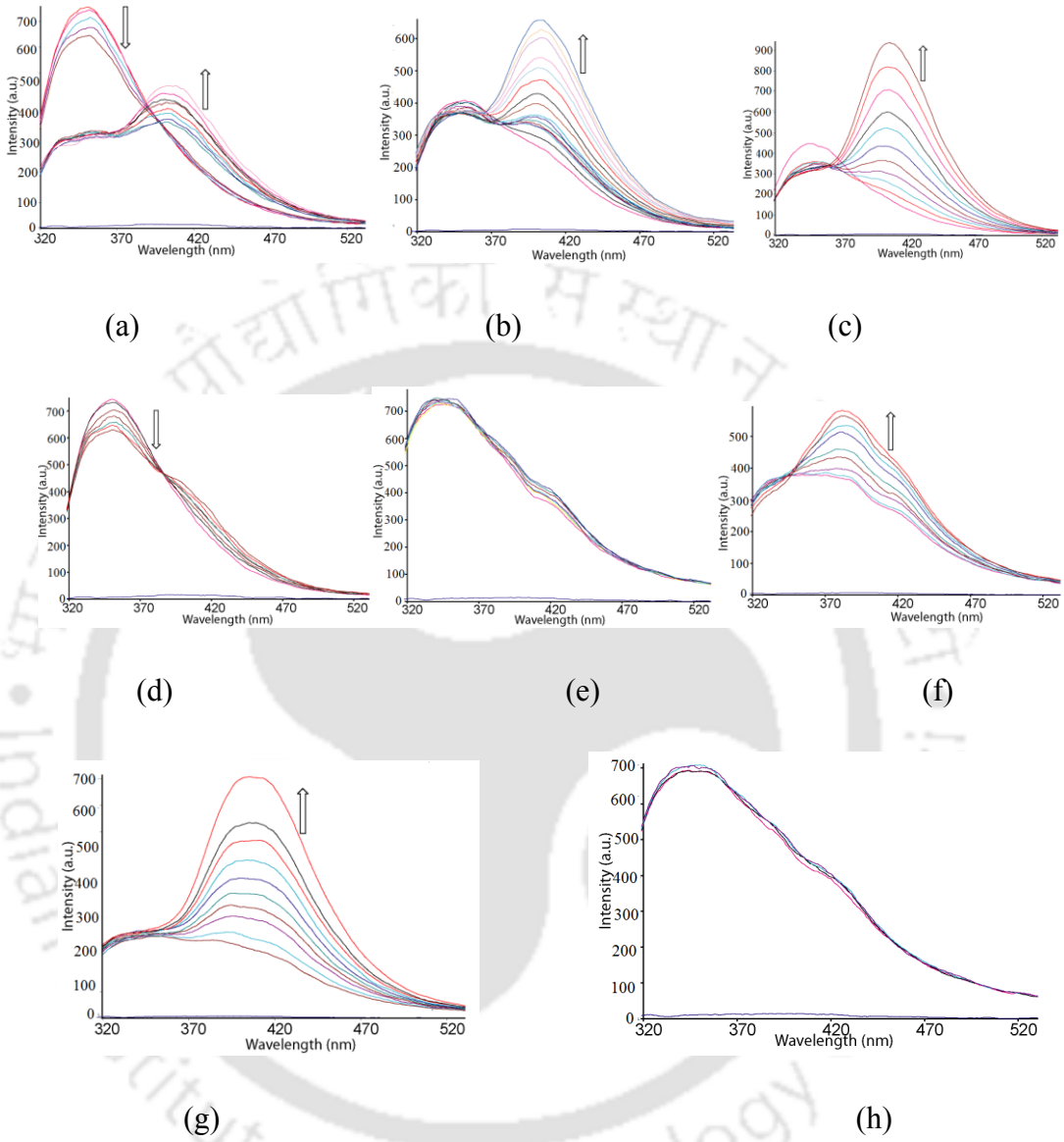

Figure 5.8: Fluorescence emission spectra of HSA (4μM; 3 ml Tris buffer pH 7.4 10^{-5}M in 5μL aliquots) on gradual addition of compounds (a) **5.13**, (b) **5.14**, (c) **5.15**, (d) **5.16**. Fluorescence emission spectra of BSA (2 μM, in 3 ml Tris buffer pH 7.4 on addition of acid 10^{-5}M in 5μL aliquots) on gradual addition compounds (e) **5.13**, (f) **5.14**, (g) **5.15** and (h) **5.16**.

Compounds **5.14** and **5.15** are silent in interacting with BSA. HSA had negligible interactions with compound **5.14**. Compounds **5.13** or **5.16** interact with HSA leading to

TH-1303_09612216

new fluorescence emission peak at longer but identical wavelength at 410 nm. These two compounds do not have individual emission peak at 410 nm, thus this peak occur due to their interactions with HSA. This peak is attributed to denaturated HSA, it corresponds to denatured HSA.[37] On the other hand, HSA interacts with the compound **5.15**, at very low concentration, but as concentration of **5.15** was increased, it caused denaturation of HSA. All these compounds belong to the family of carboxylic acid; results on specific binding of particular compound by BSA or HSA were clear indication of molecular recognition by serum albumin proteins. These provided evidences on the importance of supramolecular interactions over intrinsic acidity as guiding factor for binding to serum albumin proteins. Compound **5.13** and **5.15** strongly binds to BSA while binding of BSA with compounds **5.14** or **5.16** are insignificant. This opens a new dimension to explore BSA and HAS as receptor for molecular recognition study.

5.3: Cytotoxicity study

Human serum albumin and bovine serum albumin are indispensible proteins in measurement of cytotoxicity. Thus, prior understanding on substrate binding with HSA and BSA would help to ascertain the cytotoxic action of a drug. Generally naphthoquinone derivatives are cytotoxic.[46-60] Several naphthoquinone derivatives are used as anti-cancer drugs. β-Lapachone is a 1,2-napthoquinone derivative which is a inhibitor for DNA topoisomerase I and II[31-32], it causes apoptotic cell death.[61-68] Juglone induces apoptosis and prevents mitotic exit and plumbagin inhibits cell proliferation and induces apoptosis[69-72], plumbagin shows enhancement of autophagy in breast cancer cell lines.[73] Cell proliferations caused by 5-hydroxy-2-methyl-1,4 naphthoquinone were found to be concentration dependent[74], this makes avenue to systematically study the cytotoxicity of various naphthoquinone compounds and their actions in presence of proteins, as latter can bind and effect cytotoxicity.[75-78]

5.3.1: Cytotoxicity of napthoquinone derivatives

Cytotoxicity of compounds **5.1-5.12** were determined in four cancer cell lines representing pancreatic ductal adenocarcinoma (Mia Paca-2, BxPC-3, Panc-1) and colorectal carcinoma (HCT 116). Cytotoxicity of these compounds varied in different cell lines. In 3-(4,5-dimethylthiazol-2-yl)-2,5-diphenyltetrazolium bromide (MTT) assay,

TH-1303_09612216

compounds **5.1-5.12** showed cytotoxicity in the six cancer cell lines, IC_{50} values were ranging from 12 μM to 36 μM. The six cell lines showed similar sensitivity to the naphthoquinone derivatives. In Mia paca-2 cell line cytotoxicity sequence was **5.9** > **5.7** > **5.6** > **5.8** > **5.1** > **5.2** > **5.5** > **5.3** ≈ **5.4** ≈ **5.11** > **5.12** > **5.10**. Similarly, other cell lines also differentiated cytotoxicity of the individual compound **5.1-5.12**. From cytotoxicity experiments, it was observed that compound **5.9** showed low IC_{50} value. On the other hand, in HCT 116 cell line compound **5.6** and compound **5.9** showed superior cytotoxicity. IC_{50} value shown by the compound **5.9**. was consistently low in all cell lines in comparision to other compounds as shown in table 5.5. Cytotoxicity in different cancer cell lines suggested that the compounds **5.1-5.12** have therapeutic potentials as anticancer agents. Comparing the trends of cytotoxicity with serum albumin binding with the corresponding quinoidal compound, no linear correlation between cytotoxicity and HSA or BSA binding in this class of compounds was observed.

Table 5.5: Cytotoxicity of compounds **5.1-5.12** in MTT assay expressed as IC_{50} (μM)[a]

Compound No.	Mia Paca-2	BxPC-3	Panc-1	HCT 116 (p53 +/+)	Mia Paca-2	HCT-116 (p53 +/+)
	10% FBS				2% FBS	
5.1	19.3 ± 1.7[b]	32.0 ± 1.2	16.1 ± 0.8	14.4 ± 1.6	17.8 ± 1.5	12.2 ± 1.4
5.2	21.6 ± 2.2	12.6 ± 1.4	14.7 ± 1.3	24.3 ± 2.3	7.5 ± 0.6	20.8 ± 0.8
5.3	26.6 ± 2.4	24.2 ± 1.5	16.5 ± 1.7	36.3 ± 2.1	7.4 ± 0.7	29.7 ± 1.6
5.4	26.6 ± 0.9	24.1 ± 2.1	25.8 ± 0.4	13.1 ± 1.0	20.2 ± 0.7	8.7 ± 0.2
5.5	23.0 ± 2.1	15.5 ± 2.4	25.5 ± 1.5	13.5 ± 1.9	18.7 ± 1.3	11.3 ± 1.4
5.6	12.0 ± 1.6	14.0 ± 1.8	18.1 ± 0.6	12.0 ± 0.9	9.9 ± 1.1	7.5 ± 0.3
5.7	9.4 ± 1.1	17.9 ± 1.5	11.6 ± 1.0	16.5 ± 1.1	c	c
5.8	16.5 ± 1.7	23.4 ± 1.7	13.5 ± 1.2	19.5 ± 3.4	c	c
5.9	2.7 ± 0.6	7.6 ± 1.0	3.0 ± 0.1	4.9 ± 0.1	c	c
5.10	32.0 ± 2.7	34.4 ± 3.2	21.6 ± 0.7	27.8 ± 2.5	c	c
5.11	26.9 ± 0.6	68.9 ± 3.4	17.4 ± 0.4	43.2 ± 2.5	c	c
5.12	28.7 ± 0.8	55.7 ± 4.2	25.8 ± 2.7	35.6 ± 2.1	c	c

[a] IC_{50} is defined as drug concentration causing a 50% decrease in cell population. [b] Mean ± SD were calculated from three independent experiments.[c]not determined.

5.3.2: Effect of BSA on cytotoxicity of naphthoquinone derivatives

To understand effect of BSA on cytotoxicity, we evaluated the effect of BSA of on the anti-proliferative activity by increasing concentration of each naphthoquinone derivative. For such studies, matching concentrations of fetal bovine serum (FBS) resembling the concentration of human plasma albumin level were maintained.[79-80] FBS is a source of

TH-1303_09612216

growth factor and is used with other nutrients in *in vitro* cell culture. On the other hand BSA is a major component of commercially available FBS. With consideration of BSA binding properties with the naphthoquinone derivatives, we looked for perspective influence of FBS used in cell culture media on anti-cancer activities together with quinoidal compounds. We observed that on reducing the concentration of FBS to 2 %, IC_{50} values of the naphthoquinone derivatives were improved. Cytotoxicities of compounds **5.1** and **5.6** decreased as concentrations of the FBS in

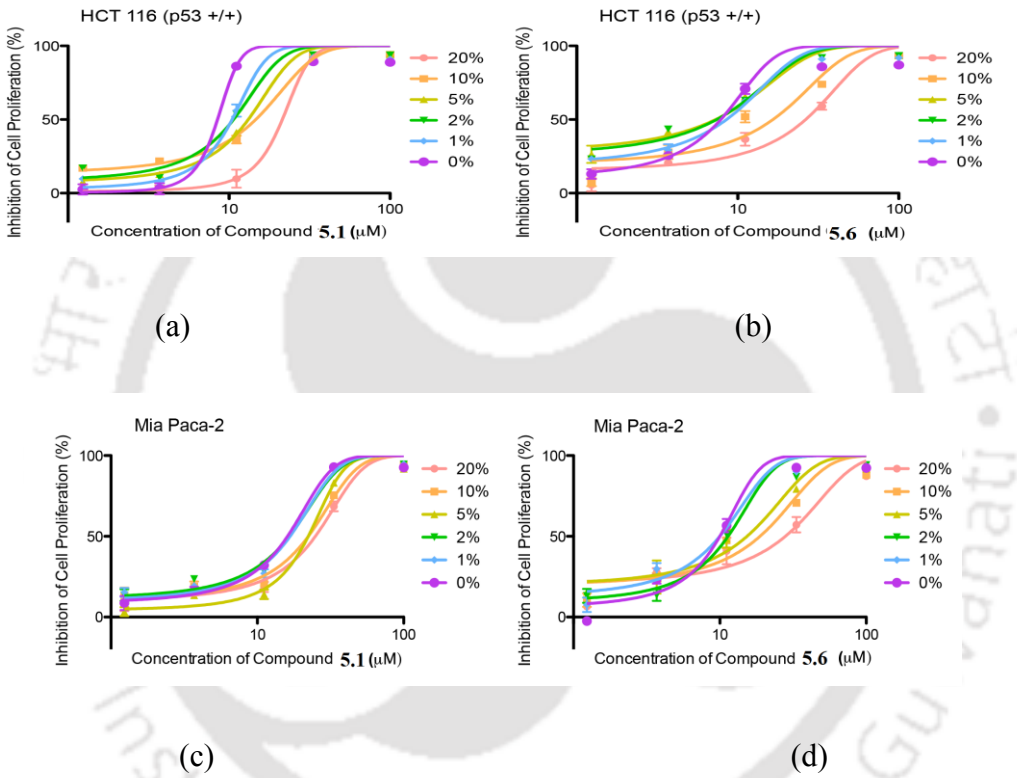

Figure 5.9: The effect of concentration of FBS in cell culture media on cytotoxicity of compound **5.1** and **5.6**. (a) **5.1** in HCT 116 p53 (+/+), (b) **5.6** in HCT 116 p53 (+/+), (c) **5.1** in Mia Paca-2 and (d) **5.6** in Mia Paca-2. (e) Structure of quinone methide pentacyclic triterpenoid derivative.

media were increased (Figure 5.9). This suggests interactions of compounds **5.1** and **5.6** with FBS. We also performed cell proliferation assays in the presence of additional amounts of BSA (Figure 5.10). For such study a matching concentration of FBS that resembles human plasma albumin level were mantained.[81] *Cis*-platin was used in this study as positive control, as it was known to bind to BSA in vitro.[82] In identical

TH-1303_09612216

conditions, reduced cytotoxic effects were observed with both compounds **5.1** and **5.6** (Figure 5.11).

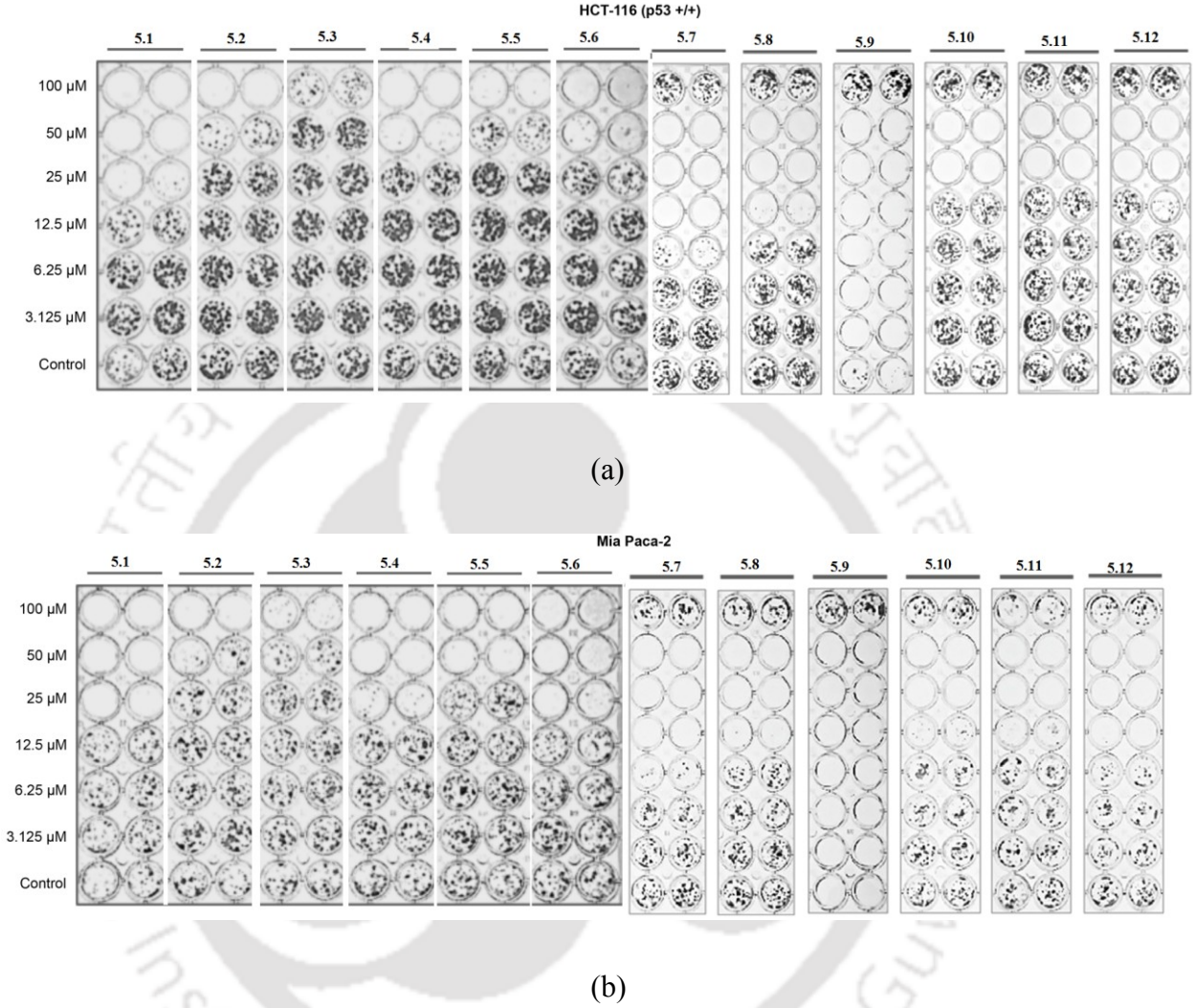

Figure 5.10: Colony formation assays in (a) HCT 116 (p53 +/+) cells and (b) Mia Paca-2 cells. Cells were treated with compounds **5.1-5.12** (3.125-100 µM) for 24 hrs and left in culture in fresh media until colonies were formed.

Cytotoxicity of compound **5.6** was significantly changed in presence of BSA, suggesting its superior BSA binding activity helping in decrement in drug activity. This effect is comparable to protein binding inhibiting drug action of platinum containing drugs. Similar studies on effect of inhibition on cell proliferation with increase in concentrations of compounds **5.7**, **5.9** and **5.10** at different concentrtations of FBS were carried out (Figure 5.12). Trend of changes in cytotoxicity in each case was found to be similar. Cytotoxic activities and characterization of quinone methide pentacyclic triterpenoid

TH-1303_09612216

derivative (Figure 5.2e) was reported earlier.[83] It was found that compound exhibited both in vitro a cytotoxic effect on murine P388 leukemia cells with IC_{50} value of (0.041±0.020) µg/mL and an antiplasmodial activity against the chloroquine-resistant strain FC29 of plasmodium falciparum with IC_{50} value of (0.052±0.030) µg/mL. Some quinone derivatives and their cytotoxicity against human cancer cell lines have also evaluated in vitro.[84]

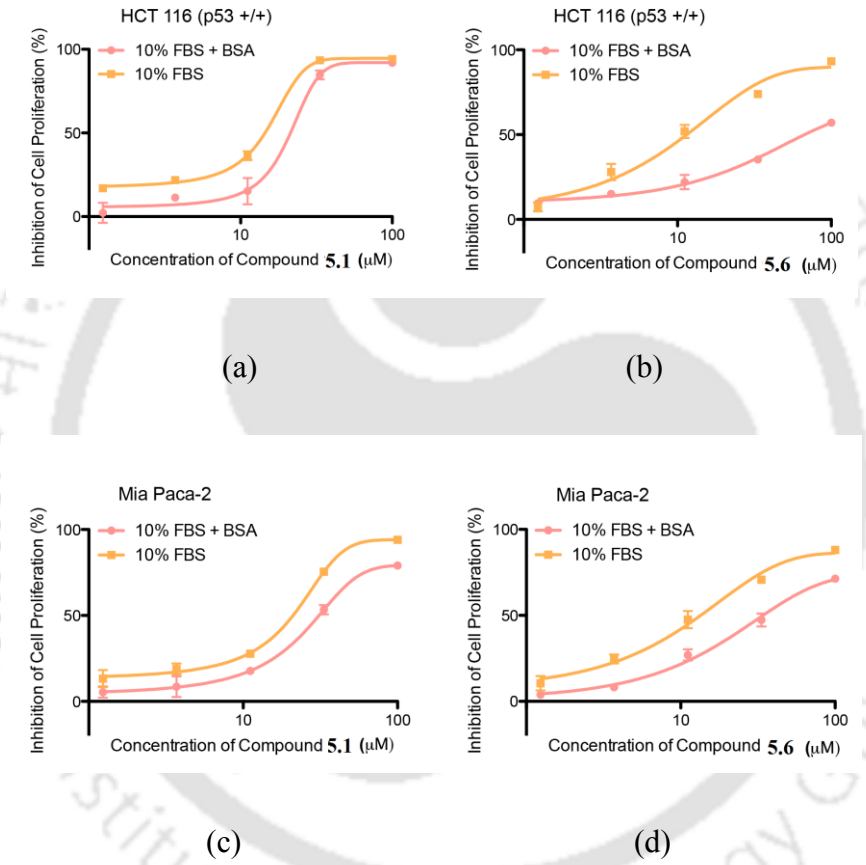

Figure 5.11: Plots showing that presence of excess BSA decreased cytotoxicity of compounds **5.1** and **5.6.** (a) **5.1** in HCT 116 p53 (+/+), (b) **5.6** in HCT 116 p53 (+/+), (c) **5.1** in Mia Paca-2 and (d) **5.6** in Mia Paca-2.

Naphthoquinone derivatives studied here showed cytotoxicity with IC_{50} value 17.59- 6.91 µg/mL. When the compounds concentrations were increased in the range of 1 to 10 µM there were sharp increase in inhibition in cell proliferation. However, when similar studies were carried out by adding BSA, there were lowering on percentage inhibition of cell proliferation in this region. Cell proliferation inhibition caused by the compounds

TH-1303_09612216

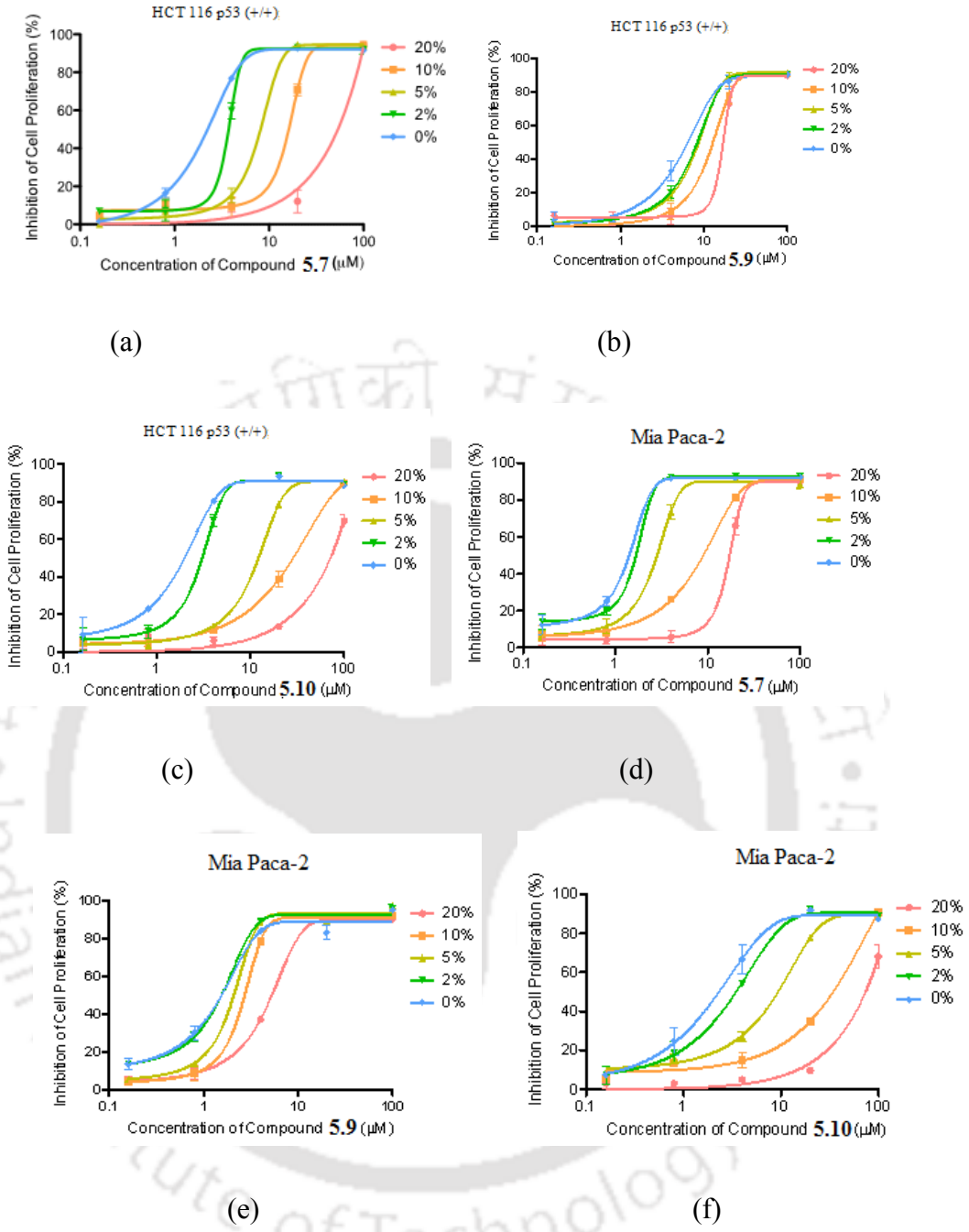

Figure 5.12: Plots showing effect of concentration of FBS in cell culture media effecting cytotoxicity of compounds **5.7**, **5.9** and **5.10** (a) **5.7** in HCT 116 p53 (+/+), (b) **5.9** in HCT 116 p53 (+/+), (c) **5.10** in HCT 116 p53 (+/+), (d) **5.7** in Mia Paca-2, (e) **5.9** in Mia Paca-2 and (f) **5.10** in Mia Paca-2.

could be controlled by adding amount of BSA. This implied that binding of BSA allows slow delivery of the drug to interact with FBS. Critical concentration required to complete cell proliferation inhibition by these compounds could be increased by 5-10 fold by

TH-1303_09612216

adding suitable amount of BSA. Such changes were dependent on the amounts of BSA used, this observation adds advantages to make use of proteins in delivery of quinoidal compounds. Thus, it may be concluded that protein binding to naphthoquinone derivatives reduced their cytotoxicity. Experiments carried out by adding extra BSA, showed lowering of percentage inhibition of cell proliferation. These results showed a possible control of cell proliferation inhibition by adequate amount of BSA. This also implied that BSA binding to substrates control the cell proliferation. From differences in cytotoxicity, it can be suggested that cell proliferation inhibition by the naphthoquinone derivatives **5.7**, **5.9** and **5.10** can be increased 5 to 10 times by adding extra BSA. Such BSA dependent changes added advantages to make use of BSA protien to control cytotoxicity.

5.4: Conclusions

In conclusion, we have shown the systematic study on the effect of BSA binding and also determined cytotoxicity of naphthoquinone derivatives. Pyridine tethered naphthoquinone causes change in the fluorescence emission of BSA; whereas these derivatives did not change in fluorescence emission HSA. This is a new observation on molecular recognition by HSA. Compounds **5.6** and **5.8** have relatively higher binding constants with BSA with respect to the other 1,4-naphthoquinone derivatives, they have comparable cytotoxicities to the rest of the 1,4-naphthoquinone derivatives. On the other hand **5.9** is identified as an efficient cytotoxic substrate which has low binding constants with BSA and HSA. Compound **5.9** also has a relatively small anisotropic value with BSA or HSA suggesting that it causes a minimum distortion of BSA and HSA proteins. Naphthoquinone derivatives with smaller binding constants with BSA or having no binding to HSA show cytotoxicity. Increase of concentration of BSA reduces cytotoxicity. Choice of suitable aromatic skeleton and functional groups on naphthoquinone derivatives has prominent role in cytotoxicity measurements carried out in a medium having BSA or HSA. Study on variations of cytotoxicity with concentration of BSA points out that an optimum amount of BSA can improve cytotoxicity of naphthoquinone derivatives.

5.5: Experimental section

TH-1303_09612216

Materials and physical measurements are used as described in chapter 2, section 2.4.1, 2.4.2 and chapter 3 section 3.5.1 and 3.5.2, chapter 4 section 4.5.1.
Synthesis and details of spectroscopic data of compound **5.10** is given in the chapter 2. we renumbered the compound as **5.10** = **2.1**. Compounds **5.1**, **5.2** and **5.3** were prepared by our reported procedures.[85]

5.5.1: Preparation of solution of BSA and HSA protein in buffer

Tris buffer of pH 7.4 was prepared in double-distilled water for all the protein binding experiments. A stock solution of BSA and HSA (14 μM) was prepared in buffer (20 mM Tris, 160 mM NaCl, 50 μM $ZnSO_4$, pH 7.4), while stock solutions of naphthoquinone compounds were prepared in DMSO because of their lower solubility in water.

5.5.2: Calculation of binding constants and anisotropy

Binding constants of BSA and HSA with substrates were determined using the Benesi-Hildebrand equation by the fluorescence method.

$$\frac{1}{[I - {}_0]} = \frac{1}{\lfloor I_1 - {}_0]} + \frac{1}{\lfloor I_1 - {}_0]K[BSA/HSA]}$$

where I_0, I and I_1 are the emission intensities in absence of BSA and HAS, in presence of BSA and HSA and when the molecule is completely solubilized in BSA and HSA respectively. The anisotropy values of the proteins in the absence or presence of compounds are the mean values of their individual determinations.

$$r = (I_{VV}\text{-}GI_{VH}/I_{VV}+2GI_{VH}) \quad ...5.1$$

The degree (*r)* of anisotropy in the tryptophan fluorescence of the proteins was calculated using equation 5.2 , at the peak of the protein fluorescence spectrum, where I_{VV} and I_{VH} are the fluorescence intensities of the emitted light polarized parallel and perpendicular to the excited light, respectively, and $G = I_{VH}/I_{HH}$ is the instrumental grating facto.r

5.5.3: Cell culture

TH-1303_09612216

Mia Paca-2, BxPC-3, Panc-1 cells (pancreatic adenocarcinoma) were obtained from the laboratory of Dr. Alan L. Epstein, Keck School of Medicine, University of Southern California. Cell lines HCT-116 (p53+/+) (colorectal carcinoma), Jurkat (acute T cell leukemia), HL-60 (acute promyelocytic leukemia) were purchased from ATCC. All cell lines were cultured as monolayer and maintained in RPMI1640 supplemented with 10 % fetal bovine serum (FBS) in a humidified atmosphere with 5% CO_2 at 37° C.

5.5.4: MTT assay

3-(4,5-Dimethylthiazol-2-yl)-2,5-diphenyltetrazolium bromide (MTT) assay was used to determine cytotoxic effect of the compounds. The cells were seeded in 96-well tissue culture plates at the concentration of 2,000-8,000 cells/well dependent on doubling time of specific cell lines. After overnight attachment, cells were treated with a continuous exposure to studied compounds for 72 hrs. MTT solution was then added to each well for a final concentration of 0.3 mg/mL MTT. After 4h incubation at 37 °C, media from each well was removed and DMSO was added to dissolve the formazan crystals formed by live cells. Absorbance was measured at 570 nm using a microplate reader (Molecular devices, Sunnyvale, CA). Cytotoxicities of compounds were calculated as percentage inhibition of cell proliferation against untreated controls. IC_{50} values for cytotoxic compounds were then determined from a plot of percentage inhibition of cell proliferation versus log of compound concentration in Prism 5.0 Software (GraphPad, La Jolla, CA, USA).

5.5.5: Colony formation assay

Cells were seeded in 96-well tissue culture plates at the concentration of 150 cells / well. After overnight attachment, cells were treated with studied compounds for 24 hrs, and left in culture in fresh media typically for 5-7 days after removal of compounds until colonies were formed. Colonies were then fixed and stained with crystal violet solution (1 % formaldehyde, 0.05 % crystal violet, 1% methanol in distilled water).

*5.5.6: General procedure for synthesis of compounds **5.1-5.12***

2-(1, 4-Dioxo-1,4-dihydro-naphthalen-2-yl-amino)benzoic acid (**5.4**)

To a well stirred solution of 1,4-naphthoquinone (0.32 g, 2 mmol) in methanol (20 mL) a solution of 2-amino benzoic acid (0.27 g, 2 mmol) in methanol (10 mL) was dropwise

TH-1303_09612216

added. Reaction mixture was stirred overnight. Then it was kept at room temperature to evaporate the solvent. A dark red precipitate was formed. Yield: 65%. ^{1}H-NMR (400MHz, DMSO-d_6): 13.23 (s, 1H), 10.83 (s. 1H), 8.25-7.56 (m, 8H), 6.56 (s, 1H). ^{13}C-NMR (100MHz, DMSO-d_6): 181.9, 178.4, 169.4, 144.3, 139.4, 135.7, 134.9, 133.7, 132.7, 131.8 127.0, 126.5, 126.0, 123.9, 121.2, 117.0, 105.6. IR (KBr, cm^{-1}): 3370 (m), 3236 (m), 3060 (w), 2917(w), 1673 (s), 1611 (s), 1584 (s), 1572 (s), 1528 (s), 1453(m), 1412 (w), 1357 (m), 1296 (s), 1262 (s), 1215 (m), 1151 (m), 1124 (w), 1083 (w), 991 (w), 753 (w), 719 (w). MS (ESI) m/z: 292.00 [M^{+}-H], 293.01 [M^{+}]. m. p. 287 ^{o}C.

3-(1,4-Dioxo-1,4-dihydro-naphthalen-2-yl-amino)benzoic acid (**5.5**)

To a well stirred solution of 1,4-naphthoquinone (0.32 g, 2 mmol) in methanol (20 mL) a solution of 3-aminobenzoic acid (0.27 g, 2 mmol) in methanol (10 mL) was added drop wise. The reaction mixture was stirred overnight to obtain an orange precipitate. The solid was filtered to get the product. Yield: 81%. ^{1}H-NMR (400MHz, DMSO-d_6): 13.50 (bs, 1H), 9.39 (s, 1H), 7.94-7.79 (m, 8H), 6.12 (s, 1H). ^{13}C-NMR (100MHz, DMSO-d_6): 182.8, 181.4, 172.3, 166.8, 146.1, 138.5, 134.9, 132.7, 131.9, 130.4, 129.7, 127.9, 126.2, 125.8, 125.3, 124.0, 102.3. IR (KBr, cm^{-1}): 3288 (s), 2664 (w) 2554 (w), 1681 (s), 1614 (s), 1598 (s), 1571 (s), 1523 (s), 1459 (m), 1480 (m), 1304 (s), 1355 (m), 1333 (m), 1273 (m), 1247 (m), 1088(w), 1003 (w), 807 (w), 753 (m), 719 (m). MS (ESI) m/z: 292.97, m. p. 283 ^{o}C

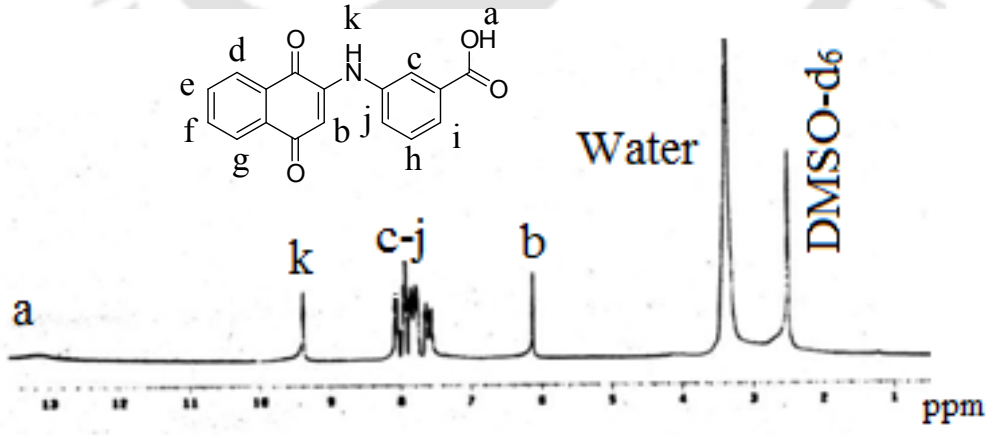

Figure 5.13: 1H-NMR (400 MHz, DMSO-d6) spectra of **5.5**.

4-(1, 4-Dioxo-1,4-dihydro-naphthalen-2-yl-amino)benzoic acid (**5.6**)

TH-1303_09612216

To a well stirred solution of 1, 4-naphthoquinone (0.32 g, 2 mmol) in methanol (20 mL) a solution of 4-aminobenzoic acid (0.27 g, 2 mmol) in methanol (10 mL) was added drop-wise. The reaction mixture was stirred overnight. A red colored solid product separated. Yield: 72%. ^{1}H-NMR (400 MHz, DMSO-d_6): 9.27 (s, 1H), 8.06 (d, J = 8.0Hz, 2H), 7.96 (d, J = 8.0Hz, 2H), 7.80 (t, J = 7.4Hz, 1H), 7.73 (t, J = 7.6Hz, 1H), 7.46 (d, J = 8.4Hz, 2H), 6.37 (s, 1H). ^{13}C-NMR (400MHz, DMSO-d_6): 182.9, 181.4, 172.6, 166.8, 145.1, 142.5, 136.4, 134.9, 132.9, 132.4, 130.6, 126.2, 125.3, 122.2, 112.6, 104.1. IR (KBr, cm^{-1}): 3460 (m), 3363 (m), 3229 (w), 2968 (w), 2547 (w), 2670 (w), 1625 (s), 1666 (s), 1600 (s), 1574 (s), 1441 (m), 1309 (s), 1291 (s), 1173 (s), 1128(w), 843 (w) 771(w). MS (ESI) m/z: 292.95. Melting point: 317 ^{o}C.

2-(1,4-Dihydro-2-methyl-1,4-dioxonaphthalen-3yl-thio)propanoic acid (**5.7**)

To a solution of 2-methyl-1,4-naphthoquinone (0.34 g, 2 mmol) in methanol (15 mL), thiolactic acid (0.18 mL, 2 mmol) was added drop wise. After complete addition of thiolactic acid, the color of the reaction mixture turned yellow. The reaction mixture was further stirred at room temperature for 2 hrs. A yellow precipitate of **5.7** appeared, was filtered, and dried in air. Yellow crystals were obtained upon crystallisation of a solution in methanol. Yield: 95%. ^{1}H-NMR (DMSO-d_6, 400MHz): 12.80 (bs, 1H), 8.0 (dd, J = 2.8 Hz, 2H), 7.85 (dd, J =2.8 Hz, 2H), 4.35 (m, 1H), 2.25 (s, 3H), 1.41 (d, J = 11.2 Hz, 3H). ^{13}C-NMR (100MHz, DMSO-d_6): 182.6, 181.1, 173.5, 148.5, 145.2, 134.8, 134.6, 132.9, 132.1, 127.1, 126.9, 44.1, 17.9, 15.9. IR (KBr, cm^{-1}) : 3414 (bw), 2908 (w), 2582 (w), 1716 (s), 1662 (s), 1589 (m), 1474 (m), 1550 (m), 1424 (m), 1317 (m), 1286 (s), 1212 (m), 1181 (m), 1141 (w), 1028 (w), 944 (m), 840 (w), 702 (m). MS (ESI) m/z: 276.05, m.p. 168 ºC.

2-(1,4-Dihydro-2-methyl-1,4-dioxonaphthalen-3yl-thio)acetic acid (**5.8**)

To a solution of 2-methyl-1,4-naphthoquinone (0.34 g, 2 mmol) in methanol (15 mL), 2-mercaptoacetic acid (0.12 mL, 2 mmol) was added drop wise. After complete addition of 3-mercaptopropionic acid, the color of the reaction mixture turned yellow. The reaction mixture was further stirred at room temperature for 6 hrs. A yellow precipitate appeared, was filtered, and dried in air. Yield: 75%, ^{1}H-NMR ($CDCl_3$, 400 MHz): 8.08 (dd, J = 7.2, 3.2 Hz, 2H), 7.54 (dd, J = 7.2, 3.2 Hz, 2H), 3.98 (s, 2H), 2.37 (s, 3H); ^{13}C-NMR ($CDCl_3$,

TH-1303_09612216

100 MHz): 182.05, 181.09, 170.96, 146.38, 145.26, 133.78, 133.49, 132.82, 131.97, 126.75, 126.52, 35.57, 15.09. IR (KBr, cm^{-1}): 3445 (bw), 2925 (w), 1716 (s), 1662 (s), 1589 (m), 1551 (m), 1424 (m), 1375 (w), 1318 (s), 1287 (s), 1212 (m), 1177 (m), 1113 (w), 1026 (w), 946 (m), 840 (w), 702 (s). MS (ESI) m/z: 263.05 $[M^+ + H]^+$, m. p. 155 ºC.

3-(1,2-Dihydro-1,2-dioxonaphthalen-4-ylthio) propanoic acid (**5.9**)

To a solution of 1,2-naphthoquinone (0.31 g, 2 mmol) in methanol (15 mL) thiopropanoic acid (0.17 ml, 2 mmol) was added drop wise. The solution was stirred at room temperature for 8 hrs. On standing, the reaction mixture resulted in the formation of a red colour precipitate, which was filtered and dried in air. Yield: 82%. ^{1}H-NMR (DMSO-d_6, 400MHz) : 8.00 (d, J = 7.6 Hz, 1H), 7.80 (t, J = 4.4 Hz, 1H), 7.78 (d, J = 7.2 Hz , 1H), 7.66 (t, J = 7.2 Hz, 1H), 6.44 (s,1H), 3.16 (t, J = 2.0 Hz, 2H), 2.78 (t, J = 6.8 Hz, 2H). ^{13}C-NMR (100MHz, DMSO-d_6): 178.7, 175.8, 172.3, 156.8, 135.1, 131.2, 130.6, 128.3, 124.9, 120.1, 32.1, 26.0. IR (KBr, cm^{-1}): 3434 (bw), 2924 (m), 1694 (s), 1654 (m), 1589 (w), 1456 (m), 1295 (w), 1276 (s), 1231 (w), 1204 (m), 1158 (w), 1140 (m), 812 (w), 701 (m), 637 (w). MS (ESI) m/z: 263.01 $[M+H]^+$, m. p. 162 ºC.

2,2'-(1,4-Dihydro-1,4-dioxo-naphthalen-2,3-diylthio)dipropanoic acid (**5.11**)

To a solution of 1,4-naphthoquinone (0.31 g, 2 mmol) in methanol (15 mL) thiolactic acid (0.35 mL, 4 mmol) was added drop wise. The colour of the reaction mixture became colorless after complete addition of thiolactic acid. The solution was stirred at room temperature for 2 hrs. On standing, the reaction mixture resulted in formation of a precipitate, which was filtered and dried in air. Yield: 90%. ^{1}H-NMR (DMSO-d_6 , 400MHz) : 8.91 (s, 2H), 8.13 (dd, J = 2.8 Hz, 2H), 7.59 (dd, J = 2.8 Hz , 2H), 3.88 (q, J = 7.2Hz, 2H), 1.34 (d, J = 7.2Hz, 6H). ^{13}C-NMR (100MHz, DMSO-d_6): 174.1, 150.0, 149.5, 119.8, 119.1, 116.1, 115.8, 42.8, 17.6. IR (KBr, cm^{-1}): 3542 (bw), 3409 (m), 2932 (w), 1694 (s), 1566 (m), 1455 (m), 1427 (m), 1398 (m), 1258 (m), 1231 (w), 1165 (w), 1084 (w), 1059 (w), 889 (m), 765 (m), 656 (m). MS (ESI) m/z: 366.04. m.p. 195 ºC.

3,3'-(1,4-Dihydro-1,4-dioxo-naphthalen-2,3-diylthio) dipropanoic acid (**5.12**)

To a solution of 1,4-naphthoquinone (0.31 g, 2 mmol) in methanol (15 mL) 3-mercaptopropionic acid (0.42 mL, 4 mmol) was added drop wise. The colour of the reaction mixture became red after complete addition of 3-mercaptopropionic acid. The

TH-1303_09612216

solution was stirred at room temperature for 8 hrs. On standing, the reaction mixture resulted in formation of red precipitate, which was filtered and dried in air. Yield: 95%. ^{1}H-NMR (DMSO-d_6, 400MHz): 12.37 (s, 2H), 7.98 (dd, J = 1.6 Hz, 2H), 7.81 (dd, J = 1.6 Hz, 2H), 2.67 (t, J = 7.2Hz, 4H), 2.57 (t, J = 7.2 Hz, 4H). IR (KBr, cm^{-1}) : 3441 (bw), 2924 (m), 1694 (s), 1654 (s), 1589 (m), 1456 (m), 1432 (w), 1405 (w), 1347 (w), 1295 (w), 1276 (s), 1204 (m), 1158 (m), 1140 (m), 942 (w), 864 (w), 812 (w), 797 (w) 701 (m) 660 (w). MS (ESI) m/z: 366.07. m. p. 186 ºC.

References:

1. T. Peters Jr., All about albumin: Biochemistry, genetics and medical applications, *Academic Press, Inc. Orlando, FL* **1996**.
2. D. C. Carter and J. X. Ho, *Adv. Protein Chem.* **1994**, 4, 153.
3. X. M. He and D. C. Carter, *Nature* **1992**, 358, 209.
4. S. Curry, H. Madelkow, P. Brick and N. Franks, *Nat. Struct. Biol.* **1998**, 5, 827.
5. J. R. Brown, *Albumin Structure, Function and Uses;* V. M. Rosenoer, M. Oratz, M. A. Rothschild, *Eds.; Pergamon: Oxford, U.K.*, **1977**; *Vol. 27*.
6. A. A. Bhattacharya, T. Grune and S. Curry, *J. Mol. Biol.* **2000**, 303, 721.
7. S. Curry, Plasma Albumin as a Fatty Acid Carrier. In *Ad*v. *Mol. Cell. Biol.*; G. van der Vusse, Ed.; Elsevier: **2003**; Vol. 33, pp 29.
8. I. Petitpas, C. E. Petersen, C.-E. Ha, A. A. Bhattacharya, P. A. Zunszain, J. Ghuman, N. V. Bhagavan and S. Curry, *Proc. Natl. Acad. Sci. U.S.A.* **2003**, 100, 6440.
9. E. Tolosano and F. Altruda, *DNA Cell Biol.* **2002**, 21, 297.
10. U. Kragh-Hansen, *Pharmacol. Re*V. **1981**, 33, 17.
11. T. Peters, *Ad*V. *Protein Chem.* **1985**, 37, 61.

TH-1303_09612216

12. P. A. Zunszain, J. Ghuman, T. Komatsu, E. Tsuchida and S. Curry, *BMC. Struct. Biol.* **2003**, 3, 6.

13. M. Wardell, Z. Wang, J. X. Ho, J. Robert, F. Ruker, J. Rubel, D. C. Carter, *Biochem.Biophys. Res. Commun.* **2002**, 291, 813.

14. O. K. Abou-Zied, O. I. K. Al-Shihi, *J. Am. Chem. Soc*. **2008**, 130, 10793.

15. O. K. Abou-Zied, *J. Phys. Chem. B* **2007**, 111, 9879.

16. A. E. Alegria, P .S. Cruz, A. Kumar, C. Garcia, F A. Gonzalez, A. orellano, B. Zayas and M. Gordaliza, *Free Radic Res*. **2008**, 42, 70.

17. O. Dangles, C. Dufour and S. Bret, *J. Chem. Soc*., *Perkin Trans.* **1999**, 2,737.

18. P. Misˇkovsky´, D. Jancura, S. Sa´nchez-Corte´s, E. Kocˇisˇova´, and L.Chinsky, *J. Am. Chem. Soc.* **1998,** 120*,* 6374.

19. B. Bhattacharya, S. Nakka, L. Guruprasad and A. Samanta, *J. Phys. Chem.* B , **2009**, 113, 2143.

20. J. Tian, J. Liu, X. Tian, Z. Hu and X. Chen, *J. Mol. Struct.* **2004**, 69, 1197.

21. Y. Chen and M. Barkley, *Biochemistry* **1998**, 37, 9976.

22. P. L Gentili, *J. Phys. Chem. B* **2008**, 112, 16793.

23. T. Gensch, *Photochem. Photobiol. Sci.* **2004**, 3, 531.

24. C. Sun and J. Yang, *Biophys. J.* **2005**, *88*, 3518.

25. J. M. Vanderkooi, D. B. Calhoun and S. W. Englander, *Science* **1987**, 236, 568.

26. T. Yuan, A. M. Weljie and H. J. Vogel, *Biochemistry* **1998**, 37, 3187.

27. M. R. Eftink, *Methods Biochem. Anal.* **1990**, 35, 117.

28. E. A. Burstein, Luminescence of protein chromophores. In *Model Studies: Science and Technology Results*; Biophysics, VINITI: Moscow, **1976**; Vol. 6.

29. O. K. Abou-Zied and O. I. K. Al-Shihi, *J. Am. Chem. Soc*. **2008**, 130, 10793.

30. F. L. Cui, J. Fan, J. P. Li and Z. Hu, *Bioorg. Med. Chem*. **2004**, 12 151.

31. H. A. Benesi and J. H. Hildebrand, *J.* Am. Chem. Soc. **1949**, 71, 2703.

32. S. Hamai, *J.* Phys. Chem. **1989**, 93, 2074.

33. J. W. Hawkins and A. Dugaiczyk, The human serum albumin gene: structure of a unique locus. Gene, **1982**, 19 55.

34. M. E. Harper, A. *Am. J. Hum. Genet*., **1983**, 35 565

TH-1303_09612216

35. F. L. G. Flecha and V. Levi, *Biochem. Mole. Bio. Edu*., **2003**, 31319.
36. F. L. G. Flecha and V. Levi, *Biochem. Mole. Bio. Edu*., **2003**, 31, 319.
37. M. Amiri, K. Jankeje and J. R. Albani, *J. Pharm Biomed Anal*., **2010**, 51, 1097.
38. C. N. Pace, F. Vajdos, L. Fee, G. Grimsley and T. Gray, *Protein Sci*., **1995**, 4, 2411
39. M. K. Helms, C. E. Petersen, N. V. Bhagavan and D. M. Jameson, *FEBS Lett*., **1997**, 408, 67.
40. D. M. Davis, D. McLoskey, D. J. S. Brich, P. R. Gellert, R. S. Kittlety and R. M. Swart, *Biophys. Chem*., **1996**, 60, 63.
41. P. Marzola and E. Gratton, *J. Phys. Chem*., **1991**, 95, 9488.
42. F. L. Cui, J. Fan, L. J. Ping and Z. Hu, *Bioorg. Med. Chem*., **2004**, 12, 151.
43. J. R. Albani, *J. Fluoresc*., **2009**, 19, 1061.
44. N. Tayeh, T. Rungassamy and J. R. Albani, *J. Pharm. Biomed. Anal.* **2009**, 50, 107
45. A. B. Patel, S. Srivastava and R. S. Phadke, *J. Biol. Chem*., **1999**, **274**, 21755.
46. S. Banerjee, S. Padhye, A. Azmi, Z. Wang, P. A. Phillp, O. Kucuk, F. H. Sarkar and R.M. Mohammad, *Nutr. Cancer*, **2010**, 62, 938.
47. R. P. Verma, *Anti-cancer Agents Med. Chem*., **2006**, 6, 489.
48. K. Ngampong, P. R. Narathip, H. A. Komkrit and K. Boonsong, *Biosci. Biotechnol. Biochem*. **2010**, 74, 1205.
49. G. J. Kapadia, V. Balasubramanian, H. Tokuda, T. Konoshima, M. Takasaki, J. Koyama, K. Tagahaya and H. Nishino, *Cancer Lett.,* **1997**, 113 47.
50. V. Kuete, H. K. Wabo, K.O. Eyong, M. T. Feussi, B. Krusche, P. Tane, G. N. Folefoc and T. Efferth, *PLOSone*, **2011**, 6, e21762.
51. Y. Shung, J. K. Im, S. Lee and H. Cho, *Bull Korean Chem. Soc.,* **2004**, 25, 1408.
52. S. Shukla, C.-P. Wu, K. Nandigama and S. V. Ambudkar, *Mol. Cancer Ther*., **2007**, 6 3279.
53. C. V. Kumar and E. H. Asuncion, *J. Am. Chem. Soc*., **1993**, 115, 8547.
54. A. M. Pizarro, A. Habtemariam and P. J. Sadler, *Organomet. Chem*., **2010**, 32, 21.

TH-1303_09612216

55. P. Scharf and J. Muller, *Chem Plus Chem,* **2013**, 78, 20.

56. L. Ronconi and P. J. Sadler, *Coord. Chem. Rev.,* **2007**, 251, 1633.

57. C. V. Kumar and E. H. Asuncion, *J. Chem. Soc. Chem. Commun*., **1992**, 470.

58. P. Pandya, Md. M. Islam, G. Sureshkumar, B. Jayaram and S. Kumar, *J. Chem. Sci.*, **2010**, 122, 247.

59. M. Coll, J. Aymami, G. A. van der Marel, J. H. vanBoom, A. Rich and A. H. J. Wang, *Biochem*., **1989**, 28, 310.

60. J. L. Dimicoli and C. Helene, *Biochem*., **1974**, 13, 714.

61. P. Krishnan, K. F. Bastow, *Biochem. Pharmacol*., **2000**, 60, 1367.

62. C. J. Li, L. Averboukh and A. B. Pardee, *J. Biol. Chem*., **1993**, 268, 22463.

63. B.T. Choi, J. Cheong andY. H. Choi, *Anticancer Drugs*, **2003**, 14, 845.

64. Y. Li, X. Sun, J.T. LaMont, A. B. Pardee and C. J. Li, *Proc. Natl. Acad. Sci. USA*, 2003, 100, 2674.

65. K. V. Rao, T. J. McBride and J. J. Oleson, *Cancer Res*., **1968**, 28, 1952.

66. L. L. Bennett Jr, D. Smithers, L. M. Rose, D. J. Adamson and H. J. Thomas. *Cancer Res.*, **1979**, 39, 4868.

67. W. Knecht and M. Loffler, FEBS Lett., **2000**, 467, 27.

68. A. J. Kemp, S. D. Lyons and R. I. Christopherson, *J. Biol. Chem*., **1986**, 261, 14891.

69. Y. L. Hsu, C. Y. Cho, P. L. Kuo, Y. T. Huang and C. C. Lin, *J. Pharmacol. Exp. Ther*., **2006**, 318, 484.

70. P. L. Kuo, Y. L. Hsu and C. Y. Cho, *Mol. Cancer Ther*., **2006**, 5, 3209.

71. Y. Luo, M. R. Mughal, T. G. Ouyang, H. Jiang, W. Luo, Q.-S. Yu, N. H. Greig and M. P. Mattson, *J. Neurochem*., **2010**, 115, 1337.

TH-1303_09612216

72. J. Xu, J. Wang, J. C. Luft, S. Tian, G. Owens, A. A. Pandya, P. Berglund, P. Pohlhaus, B. W. Maynor, J. Smith, B. Hubby, M. E. Napier and J. M. DeSimone, *J. Am. Chem. Soc*., **2012**, 134, 8774.

73. M. Delgado, K. J. Lee, L. Altobell III, C. Spanka, P. Wentworth and K. D. Janda, *J. Am. Chem. Soc*., **2002**, 124, 4946.

74. F. J. -J. Toublan, S. Boppart and K. S. Suslick, *J. Am. Chem. Soc*., 2006, 128, 3472.

75. C. D. Walkey, J. B. Olsen, H. Guo, A. Emili and W. C. W. Chan, *J. Am. Chem. Soc.,* **2012**, 134, 2139.

76. S. Roy, S. Saha, R. Majumdar, R. R. Dighe and A. R. Chakravarty, *Inorg. Chem*., **2009**, 48, 9501.

77. T. Sen, K. K. Haldar, A. Patra, *J. Phys. Chem., 112C,* **2008** 17945.

78. J. K. Pokorski, K. Breitenkamp, L. O. Liepold, S. Qazi and M. G. Finn, *J. Am. Chem. Soc*., **2011**, 133, 9242.

79. Y. Kobori, and M. Fuki, *J. Am. Chem. Soc*. **2011**, 133, 16770.

80. M. Guelden, S. Moerchel, H. Seibert, *Toxicology Lett*., **2003**, 137, 159.

81. A. Boitano, J. A. Ellman, G. D. Glick and A. W. Opipari Jr., *Cancer Res*., **2003**, 63, 6870.

82. W. C. Cole and W. Wolf, *Chem. Biol. Interact*., **1980**, 30, 223.

83. F. P. Ruphin, R, Baholy, A, Emmanue, R, Amelie, M. T. Martin and N. Koto-te-Nyiwa, *Asian Pac J Trop Biomed*. **2013**, 3, 780.

84. S. Y. Lee, E. Moon, S. Y. Kim, S. U. Choi and K. R. Lee, *Biosci. Biotechnol. Biochem.*, **2013**, 77, 276.

85. B. R. Jali, K. Masud and J. B. Baruah, *Polyhedron,* **2013**, 51, 75.

TH-1303_09612216

Conclusion

Supramolecular assemblies present in a series of thioarylcarboxylic acid, thioimidazole, hydroxyarylthio-tethered 1,2- and 1,4-napthoquinone derivatives are established. Structural studies are extended to find utility of the naphthoquinone derivatives in anion and cation recognition, protein binding and cytotoxicity.

Effects of carbonyl groups on naphthoquinone of thiophenylcarboxylic acid tethered naphthquinones on cyclic dimeric hydrogen bonded motif of carboxylic acid part are established. Carbonyl groups of naphthoquinone participate in supramolecular interactions, but retain hydrogen bonded dimeric motifs. Such carbonyl groups of naphthoquinone contribute to form self-assemblies. Differences in such self-assemblies lead to polymorphs, which are also associated with conformational differences of quinone derivatives. Unit cell of acetonitrile solvate of a thiophenylcarboxylic acid tethered 1,4-naphthoquinone showed three host quinoidal molecules of independent symmetry associated with one acetonitrile molecule. This point out that solvated species could be signature of assemblies formed in solution, which guides different conformations while crystallization. Packing patterns of conformational polymorphs differs in arrangement of molecules in *head-head* and *head to tail* arrangements. It has been shown that large structural variations can be brought about in thioarylcraboxylic acid tethered naphthoquinone by attaching hydroxy group on naphthoquinone ring. Strong hydrogen bond forming ability of OH group disrupts dimeric hydrogen bonded assembly formed between carboxylic acid parts.

Various self-assemblies formed in the salts of thioimidazole tethered 2-methyl-1,4-naphthoquinone derivatives are guided by the type of anions present. Methyl group attached on one nitrogen atom of imidazole ring drastically changes packing patterns from the unsubstituted one. Substitution also causes change in physical properties. Fluorescence emissions of such derivatives also differ. Recognition of bromide ion through a *keto-enol* tautomerism process is established by thioimidazole tethered 2-methyl-1,4-naphthoquinone. Among different acids, phosphoric acid is found to cleave C-S bond thioimidazole tethered 2-methyl-1,4-naphthoquinone. This is considered as an indirect means to recognize phosphoric acid by thioimidazole tethered 2-methyl-1,4-naphthoquinone derivatives.

TH-1303_09612216

Structural studies on positional isomers of hydroxypenenylthio tethered 1,2-naphthoquinones have shown that depending on orientations of hydroxyphenylthio units attached on the quinoidal moiety, bifurcated hydrogen bonds between a 1,2-naphthoquinone and a phenolic OH group occurs. Specifically positional isomer having 4-hydroxyphenylthio group tethered to 1,2-naphthoquinone forms various solvates. In each solvate self-assembling pattern and stacking patterns differ. Analysis of their structures revealed that presence and absence of bifurcated hydrogen bonds in positional isomers are decided by appropriate position of the hydroxy group on hydroxyphenylthio unit and in solvates by hydrogen bond nature of solvent molecules. 4-Hydroxyphenylthio tethered 1,2-naphthoquinone shows dual fluorescence in certain solvents. All the position isomers are specifically responsive to enhance their fluorescence by aluminum (III) ions.

It has been also showed that BSA and HSA interact with various naphthoquinone derivatives to cause fluorescence changes of these proteins. Binding constants of various naphthoquinone derivatives are determined; which shows that presence of acid or aromatic nitrogen base on quinoidal molecules cause similar effect to the changes in fluorescence. Positional isomers having pyridine or carboxylic acid units tethered to naphthoquinones cause change fluorescence emissions of BSA and HSA in characteristic manner. Based on the change on emission caused by naphthoquinone derivatives molecular recognition of selected compounds is shown. Cytotoxicity of several naphthoquinone derivatives are studied and shown that these compounds show anticancer activities and such activities are controlled by presence of serum albumin proteins.

TH-1303_09612216

Appendix

Details of the analytical instruments

X-Ray Diffractions

Single crystal X-ray diffraction data were collected on Bruker 3-circle diffractometers with CCD area detectors ProteumM APEX or SMART 6000 or Bruker Nonius Apex 2, using graphite-monochromated Mo-$K\alpha$ radiation (λ = 0.71073 Å) from a 60W microfocus Bede Microsource with glass polycapillary optics or a sealed tube.

X-ray diffraction data for all crystals were collected using Bruker SMART software. This software was also used for indexing and determination of the unit cell parameters. The structures were solved by direct methods and refined by full-matrix least squares against F^2 of all data, using SHELXTL software. The CIF of all the compounds characterized by single crystal X-ray structure are included in the soft copy.

All non-H atom were refined by full-matrix least squares in anisotropic, all H atoms in isotropic approximation, against F^2 of all reflections. All non-H atoms were refined by full-matrix least squares in the anisotropic approximation and the hydrogen atoms attached to these atoms were treated as 'riding' in calculated positions and in some of the cases the hydrogen atoms have been located on the difference Fourier maps. In all cases the hydrogen atoms attached to polar atoms such as O and N were located on the difference Fourier maps and refined in the final structure in isotropic approximation. The crystallographic tables for all the compounds are given at the end of this section, which includes the crystal parameters and the refinement factors.

Powder X-ray Diffraction data were collected on a Bruker D8 diffractometer in Bragg-Brentano θ-θ geometry with Cu Kα radiation (λ = 1.5418 Å) on a glass surface of an air-dried sample using a secondary curved graphite monochromator. Diffraction patterns were collected over a 2θ range of 5-50^0 at a scan rate of 5 ^{0} min^{-1}.

TH-1303_09612216

UV-visible spectroscopy, Fluorescence spectroscopy and IR Spectroscopy

UV-vis absorption spectra were recorded using Perkin-Elmer Lambda 750 spectrophotometer equipped with double cell compartments. All the chemicals and solvents used were as obtained from the standard suppliers such as E.Merck Germany, Sigma Aldrich USA, Ranbaxy India. The solvents for optical spectroscopy were of HPLC grade (Aldrich or Merck) and used as obtained. The fluorescence spectra were recorded using a Perkin-Elmer LS 55 spectrofluorometer. The fluorescence life times were measured on a picosecond time-resolved cum steady state luminescence spectrometer of Edinburgh instruments, model: FSP920 and Life SpecII. The fluorescence emissions were measured in a Perkin-Elmer LS-55 spectrofluorometer. The FT-IR spectra were recorded on Perkin-Elmer spectrum one spectrometer in the range 4000-400 cm^{-1}.

NMR and Mass Spectroscopy

The ^{1}HNMR and ^{13}CNMR spectra were recorded in a Bruker 400 MHz spectrometer. The chemical shifts in the NMR spectra are all given in ppm and tetramethylsilane as the internal standard. Electrospray ionization mass (ESI-MS) spectra were recorded on a Waters (Micromass MS Technologies) Q-Tof Premier mass spectrometer.

Thermogravimetric Studies

The thermogravimetric studies were performed using a Mettler Toledo TGA/ STDA 851^{e} and Mettler Toledo DSC^{e} thermal analyser. Typically about 5-7 mg of the samples were mounted on platinum crucibles and the TG/DSC profiles recorded at the heating rate of 10 °C/min and under nitrogen atmosphere.

TH-1303_09612216

Crystallographic data and refinement parameters for the compounds

Compound No.	**2.1a**	**2.1b**	**2.1c**
Formula	$C_{18}H_{12}O_4S$	$C_{18}H_{12}O_4S$	$C_{18}H_{12}O_4S$
Formula wt.	324.25	324.25	324.25
Crystal system	Triclinic	Monoclinic	Orthorhombic
Space group	P-1	P 2_1/c	$P2_12_12_1$
a /Å	4.781(4)	4.941(2)	4.903(3)
b /Å	7.930(5)	10.113(5)	22.146(12)
c /Å	20.853(15)	30.621(14)	27.486(14)
α/°	89.025(4)	90.00	90.00
β/°	83.942(4)	93.72(3)	90.00
γ/°	73.130(4)	90.00	90.00
V/ $Å^3$	752.43(10)	1527.0(12)	2985.0(3)
Z	2	4	8
Density/Mgm^{-3}	1.432	1.411	1.444
Abs. Coeff. /mm^{-1}	0.233	0.230	0.235
F(000)	336	672	1344
Total no. of reflections	2666	2596	3160
Reflections, $I > 2\sigma(I)$	1635	1822	2595
Max. 2θ/°	50.00	49.66	50.50
Ranges (h, k, l)	$-5 \le h \le 5$ $-9 \le k \le 9$ $-24 \le l \le 24$	$-5 \le h \le 5$ $-11 \le k \le 11$ $-36 \le l \le 36$	$-5 \le h \le 5$ $-26 \le k \le 26$ $-32 \le l \le 32$
Complete to 2θ (%)	100.0	98.6	100.0
Data/ Restraints/Parameters	2666 / 0 / 210	2596 / 0 / 210	3160 / 0 / 419
Goof (F^2)	1.161	1.090	1.044
R indices [$I > 2\sigma(I)$]	0.0330	0.1023	0.0296
R indices (all data)	0.0431	0.2140	0.0357

TH-1303_09612216

Compound No.	**2.1d**	**2.2**	**2.3**
Formula	$C_{56}H_{39}NO_{12}S_3$	$C_{20}H_{17}NO_6S$	$C_{19}H_{14}O_4S$
Formula wt.	462.44	399.42	338.37
Crystal system	Triclinic	Monoclinic	Monoclinic
Space group	P-1	P 2_1	C 2/c
a /Å	7.739(3)	7.756(9)	22.352(6)
b /Å	13.469(6)	12.845(17)	7.184(2)
c /Å	24.012(12)	9.599(12)	21.329(7)
α/°	103.506(4)	90.00	90.00
β/°	99.067(3)	98.119(7)	109.070(3)
γ/°	96.329(3)	90.00	90.00
V/ $Å^3$	2375.18(18)	946.9(2)	3237.37(16)
Z	2	2	8
Density/Mgm^{-3}	1.418	1.401	1.338
Abs. Coeff. /mm^{-1}	0.225	0.209	0.220
F(000)	1052	416	1408
Total no. of reflections	7652	2000	2911
Reflections, $I > 2\sigma(I)$	5286	1921	2240
Max. 2θ/°	48.46	52.46	50.48
Ranges (h, k, l)	$-8 \le h \le 8$ $-15 \le k \le 15$ $-27 \le l \le 27$	$-9 \le h \le 9$ $-15 \le k \le 15$ $-11 \le l \le 11$	$-26 \le h \le 26$ $-8 \le k \le 8$ $-25 \le l \le 25$
Complete to 2θ (%)	100.0	100.0	99.6
Data/ Restraints/Parameters	7652 / 0 / 656	2000 / 1 / 257	2911 / 0 / 219
Goof (F^2)	1.007	1.561	1.081
R indices [$I > 2\sigma(I)$]	0.0452	0.1120	0.0710
R indices (all data)	0.0697	0.1165	0.0849

TH-1303_09612216

Compound No.	**3.2a**	**3.2b**	**3.2c**
Formulae	$C_{14}H_{11}ClN_2O_2S$	$C_{14}H_{11}BrN_2O_2S$	$C_{14}H_{11}N_3O_5S$
Formula. wt.	306.77	351.22	333.33
Crystal system	Monoclinic	Monoclinic	Monoclinic
Space group	$P2_1/c$	$P2_1/c$	$P2_1/c$
a (Å)	11.569(7)	11.723(4)	8.399(4)
b (Å)	11.897(8)	11.842(4)	11.323(5)
c (Å)	10.735(7)	11.149(4)	15.590(7)
α(°)	90.00	90.00	90.00
β(°)	106.906(4)	108.626(2)	99.382(3)
γ(°)	90.00	90.00	90.00
V/ $Å^3$	1413.87(16)	1466.94(9)	1463.04(12)
Z	4	4	4
Density/Mgm^{-3}	1.441	1.581	1.513
Abs. Coeff. /mm^{-1}	0.419	2.946	0.252
F(000)	632	704	688
Total no. of reflections	2490	4210	3615
Reflections, $I > 2\sigma(I)$	1656	3104	2402
Max. 2θ/°	49.98	59.68	57.02
Ranges (h, k, l)	$-13 \le h \le 13$ $-14 \le k \le 14$ $-12 \le l \le 12$	$-16 \le h \le 16$ $-16 \le k \le 16$ $-15 \le l \le 15$	$-11 \le h \le 11$ $-15 \le k \le 15$ $-20 \le l \le 20$
Complete to 2θ (%)	100	99.8	97.4
Data/ Restraints/Parameters	2490 / 0 /182	4210 / 0 / 182	3615 / 0 / 209
Goof (F^2)	0.977	1.001	1.027
R indices [$I > 2\sigma(I)$]	0.0519	0.0435	0.0415
R indices (all data)	0.0810	0.1077	0.0622

TH-1303_09612216

Compound No.	**3.2d**	**3.2e**	**3.3a**
Formulae	$C_{14}H_{11}ClN_2O_6S$	$C_{14}H_{11}BF_4N_2O_2S$	$C_{15}H_{13}ClN_2O_2S$
Formula. wt.	370.77	358.12	320.79
Crystal system	Monoclinic	Monoclinic	Monoclinic
Space group	C2/c	C2/c	$P2_1/c$
a (Å)	14.404(5)	14.240(10)	10.209(5)
b (Å)	10.886(4)	10.927(9)	8.992(4)
c (Å)	20.422(8)	20.245(18)	16.555(7)
α(°)	90.00	90.00	90.00
β(°)	104.851(13)	104.374(5)	101.725(2)
γ(°)	90.00	90.00	90.00
V/ $Å^3$	3095(2)	3051.8(4)	1488.17(12)
Z	8	8	4
Density/Mgm^{-3}	1.591	1.559	1.432
Abs. Coeff. /mm^{-1}	0.417	0.267	0.402
F(000)	1520	1456	664
Total no. of reflections	2730	2636	3249
Reflections, $I > 2\sigma(I)$	1041	981	2561
Max. 2θ/°	50.00	49.66	54.20
Ranges (h, k, l)	$-17 \le h \le 17$ $-12 \le k \le 12$ $-24 \le l \le 24$	$-16 \le h \le 16$ $-12 \le k \le 12$ $-23 \le l \le 23$	$-13 \le h \le 12$ $-11 \le k \le 11$ $-20 \le l \le 20$
Complete to 2θ (%)	100	100	98.5
Data/ Restraints/Parameters	2730 / 0 / 218	2636/0/218	3249/ 0/192
Goof (F^2)	1.170	1.516	1.151
R indices [$I > 2\sigma(I)$]	0.0759	0.0902	0.0402
R indices (all data)	0.0903	0.0951	0.0529

TH-1303_09612216

Compound No.	**3.3b**	**3.4**	**4.1a**
Formulae	$C_{15}H_{13}N_3O_5S$	$C_{26}H_{16}O4$	$C_{16}H_{10}O_2S$
Formula. wt.	344.35	344.35	266.30
Crystal system	Triclinic	Monoclinic	Triclinic
Space group	P-1	C_2/c	P-1
a (Å)	8.011(18)	10.833 (4)	7.757(9)
b (Å)	9.152(2)	11.646 (4)	8.335(8)
c (Å)	11.943(3)	26.939 (11)	10.196(11)
α(°)	84.028(13)	90.00	75.158(7)
β(°)	75.263(12)	97.474(3)	89.963(7)
γ(°)	65.280(12)	90.00	86.091(7)
V/ Å3	769.3(3)	3369.9(2)	635.76(12)
Z	2	8	2
Density/Mgm-3	1.500	1.357	1.391
Abs. Coeff. /mm-1	0.243	0.093	0.248
F(000)	360	1440	276
Total no. of reflections	3558	2999	2279
Reflections, I > 2σ(I)	2069	2275	1879
Max. 2θ/°	55.54	50.50	50.48
Ranges (h, k, l)	-10 ≤ h ≤ 10 -11 ≤ k ≤ 11 -15 ≤ l ≤ 15	-12 ≤ h ≤ 12 -13 ≤ k ≤ 13 -32≤ l ≤ 32	-9 ≤ h ≤ 9 -9 ≤ k ≤ 9 -12 ≤ l ≤ 11
Complete to 2θ (%)	98.2	98.2	99.0
Data/ Restraints/Parameters	3558 / 0 / 219	2999/0/237	2279/ 0/172
Goof (F^2)	1.025	1.075	1.084
R indices [I > 2σ(I)]	0.0410	0.0746	0.0402
R indices (all data)	0.0613	0.0833	0.0491

TH-1303_09612216

Compound No.	**4.1b**	**4.2**	**4.3**
Formulae	$C_{16}H_{10}O_2S$	$C_{17}H_{12}O_2S$	$C_{16}H_9O_3SCl$
Mol. wt.	266.30	280.34	300.75
Crystal system	Monoclinic	Monoclinic	Monoclinic
Space group	$P2_1/c$	$P2_1/n$	$P2_1/c$
a /Å	4.569(4)	9.0116(7)	8.656(8)
b /Å	23.812(2)	12.169(10)	8.208(5)
c /Å	11.774(9)	12.972(11)	19.343(19)
α/°	90.00	90.00	90.00
β/°	99.299(6)	101.986(5)	93.351(10)
γ/°	90.00	90.00	90.00
V/ $Å^3$	1264.31(19)	1391.6(2)	1372.1(2)
Z	4	4	4
Density/g.cm^{-3}	1.399	1.338	1.456
Abs. Coeff. /mm^{-1}	0.249	0.230	0.427
F(000)	552	584	616
Total no. of reflections	2252	2516	2756
Reflections, $I > 2\sigma(I)$	1457	2011	1314
Max. 2θ/°	50.48	50.50	52.54
Ranges (h, k, l)	$-5 \leq h \leq 5$	$-10 \leq h \leq 10$	$-10 \leq h \leq 10$
	$-28 \leq k \leq 25$	$-14 \leq k \leq 14$	$-10 \leq k \leq 10$
	$-13 \leq l \leq 14$	$-15 \leq l \leq 15$	$-22 \leq l \leq 24$
Complete to 2θ (%)	98.30	100.00	99.60
Data/ Restraints/Parameters	2252/ 0/ 172	2516/0/182	2756/0/181
Goof (F^2)	0.969	1.040	0.741
R indices [$I > 2\sigma(I)$]	0.0528	0.0381	0.0509
R indices (all data)	0.0887	0.0497	0.0931

TH-1303_09612216

Compound No.	**4.4**	**4.5**	**4.6**	**4.7b**
Formulae	$C_{16}H_9O_3SBr$	$C_{16}H_{10}O_3S_1$	$C_{16}H_{10}O_3S_1$	$C_{17}H_{12}O_4S_1$
Mol. wt.	345.20	282.31	282.31	314.35
Crystal system	Monoclinic	Orthorhombic	Monoclinic	Monoclinic
Space group	$P2_1/c$	$P2_12_12_1$	$P2_1/c$	$P2_1/c$
a /Å	8.855(15)	5.519(2)	10.230(4)	4.892(5)
b /Å	8.189(11)	12.977(6)	18.245(6)	19.036(16)
c /Å	19.034(4)	17.890(11)	7.054(4)	16.438(14)
α/°	90.00	90.00	90.00	90.00
β/°	93.102(19)	90.00	103.238(5)	91.829(9)
γ/°	90.00	90.00	90.00	90.00
V/ $Å^3$	1378.4(4)	1281.35(11)	1281.88(10)	1530.1(2)
Z	4	4	4	4
Density/$g.cm^{-3}$	1.664	1.463	1.463	1.365
Abs. Coeff. /mm^{-1}	3.130	0.256	0.256	0.226
F(000)	688	584	584	656
Total no. of reflections	2498	1921	3299	2760
Reflections, $I > 2\sigma(I)$	1331	1900	1948	1787
Max. 2θ/°	50.50	57.26	57.32	50.50
Ranges (h, k, l)	$-10 \leq h \leq 10$	$-7 \leq h \leq 7$	$-13 \leq h \leq 13$	$-5 \leq h \leq 5$
	$-9 \leq k \leq 9$	$-17 \leq k \leq 17$	$-24 \leq k \leq 24$	$-21 \leq k \leq 22$
	$-22 \leq l \leq 22$	$-24 \leq l \leq 24$	$-9 \leq l \leq 9$	$-19 \leq l \leq 19$
Complete to 2θ (%)	99.70	100.00	99.80	99.80
Data/ Restraints/Parameters	2498/ 0/ 181	1921/0/182	3299/0/181	2760/ 0/ 202
Goof (F^2)	1.023	0.927	1.430	1.035
R indices [$I > 2\sigma(I)$]	0.0677	0.0420	0.0512	0.0571
R indices (all data)	0.0995	0.0548	0.0828	0.0936

TH-1303_09612216

Compound No.	**4.7a**	**4.7c**	**4.7d**
Formulae	$C_{16}H_{10}O_3S_1$	$C_{20}H_{19}NO_4S_1$	$C_{16}H_{12}O_4S_1$
Mol. wt.	282.31	369.43	300.33
Crystal system	Monoclinic	Orthorhombic	Triclinic
Space group	$P2_1/n$	Pca 2_1	P-1
a /Å	5.038(3)	28.109(2)	8.034(2)
b /Å	16.002(9)	8.912(8)	9.146(3)
c /Å	16.562(11)	7.416(6)	10.893(3)
α/°	90.00	90.00	103.101(10)
β/°	89.209(6)	90.00	94.202(10)
γ/°	90.00	90.00	114.164(10)
V/ $Å^3$	1335.26(14)	1857.8(3)	698.85(3)
Z	4	4	2
Density/$g.cm^{-3}$	1.404	1.321	1.427
Abs. Coeff. /mm^{-1}	0.246	0.199	0.244
F(000)	584	776	312
Total no. of reflections	2401	2590	2499
Reflections, $I > 2\sigma(I)$	1774	2295	2099
Max. θ/°	50.50	57.74	50.50
Ranges (h, k, l)	$-6 \le h \le 6$	$-38 \le h \le 38$	$-9 \le h \le 9$
	$-19 \le k \le 19$	$-12 \le k \le 12$	$-12 \le k \le 12$
	$-19 \le l \le 18$	$-10 \le l \le 10$	$-12 \le l \le 12$
Complete to 2θ (%)	99.80	100.00	98.60
Data/ Restraints/Parameters	2401/ 0/ 182	2590/4/257	2499/15/199
Goof (F^2)	1.261	1.240	0.974
R indices [$I > 2\sigma(I)$]	0.0533	0.0556	0.0384
R indices (all data)	0.0725	0.0976	0.0498

TH-1303_09612216

List of publication

1. **B. R. Jali**, Y.Kuang, N. Neamati, J. B. Baruah, Substrate selective protein binding of isomers of aromatic carboxylic acid or pyridine tethered-naphthoquinone and their cytotoxicity.
   Chemico-Biological Interactions, **2014**, 214C, 10-17.
2. **B. R. Jali**, J. B. Baruah, Fluorescence properties of positional isomers of hydroxyphenylthio naphthalene-1,2-diones and cation recognition. *Dyes and Pigments* **2014**, 110, 56-66.
3. **B. R. Jali,** J. B. Baruah, Recognition of bromide ion by protonated form of 2-(1H-imidazol-2- ylthio)-3-methylnaphthalene-1,4-dione. *Chempluschem,* **2013** 78, 589-597.
4. **B. R. Jali**, K. Masud, J. B. Baruah, Selectivity in changes of fluorescence emission of 1,4-naphthoquinone derivatives by manganese and cadmium ions.
   Polyhedron, **2013**, 51, 75-81.
5. **B. R. Jali**, J. B. Baruah, Quinone tethered silylethers: protein binding and film forming abilities.
   Book chapter in Silicones and Silicone-Modified Materials VI. ACS Symposium Series. **2013**, 1154, 177-183.
6. **B. R. Jali**, J. B. Baruah,Polymorphs and solvates of 2-(1,4-dihydro-1,4-dioxonaphthalen-3-ylthio)benzoic acid.
   Crystal Growth and Design, **2012**, 12, 3114-3122
7. **B. R. Jali**, W.M. Singh, J. B. Baruah, Polymorphs of aromatic thiolato 1, 2 or 1,4-naphthoquinones.
   CrystEngComm, **2011** 13, 763-767.

TH-1303_09612216